JAERI-M
85-205

ANNUAL REPORT OF THE FUSION RESEARCH CENTER FOR THE PERIOD OF APRIL 1, 1984 TO MARCH 31, 1985

January 1986

Fusion Research Center

日本原子力研究所
Japan Atomic Energy Research Institute

JAERI-Mレポートは，日本原子力研究所が不定期に公刊している研究報告書です。
入手の問合わせは，日本原子力研究所技術情報部情報資料課（〒319-11茨城県那珂郡東海村）あて，お申しこしください。なお，このほかに財団法人原子力弘済会資料センター（〒319-11 茨城県那珂郡東海村日本原子力研究所内）で複写による実費頒布をおこなっております。

JAERI-M reports are issued irregularly.
Inquiries about availability of the reports should be addressed to Information Division Department of Technical Information, Japan Atomic Energy Research Institute, Tokai-mura, Naka-gun, Ibaraki-ken 319-11, Japan.

編集兼発行　日本原子力研究所
印　　刷　いばらき印刷㈱

JAERI-M 85-205

Annual Report of the Fusion Research Center for the period of April 1, 1984 to March 31, 1985

Fusion Research Center
Tokai Research Establishment, JAERI+

(Received November 25, 1985)

Research and development activities of the Fusion Research Center (Department of Large Tokamak Development and Department of Thermonuclear Fusion Research) from April 1984 to March 1985 are described.

The JT-60 program progressed as scheduled. Commissioning of the JT-60 tokamak was completed by the end of the period under review. In parallel with installation and test of the tokamak machine, installation of basic diagnostic instruments and examination of the procedure for experiment had been made to meet the first phase Joule heating experiment. (The first plasma discharge was recorded on April 8, 1985). Construction of auxiliary heating systems had continued.

A medium-sized tokamak, JFT-2M, had been operated for high-power ICRF heating and ECH assisted LH current drive experiments. Installation of a power supply for plasma shaping in JFT-2M was completed. In the field of plasma theory, detailed analysis had been made on nonlinear kink/tearing modes in a plasma with free boundary and also on ICRF heating.

Development of a high-voltage, high-current He ion source for JT-60 plasma diagnostics had proceeded successfully, and tests of JT-60 LH and ICRF luanchers as well. Surface erosion of a new ceramics, SiC with BeO addition by proton bombardment was studied.

In IEA's Large Coil Task, three coil test was made at ORNL. A 11 T experiment of TMC-1, a large-bore Nb_3Sn coil was completed. Commissioning tests of tritium handling facilities had proceeded in the

---

+ at present, Naka Fusion Research Establishment, JAERI

Tritium Process Laboratory.

Design studies of the Fusion Experimental Reactor (FER) and INTOR had been advanced.

Keywords: Annual Report, Activities, Fusion Research, JT-60, Commissioning, Joule Heating Experiment, JFT-2M, Plasma Diagnostics, Plasma Dischange, ICRF Heating, Design Stadies, Fusion Experimental Reactor, INTOR

JAERI －M 85－205

核融合研究センター年報（昭和 59 年度）

日本原子力研究所東海研究所
核融合研究センター[+]

（1985 年 11 月 25 日受理）

昭和 59 年度における核融合研究センターの研究開発の現状と成果を述べる。

ＪＴ－60 計画は，順調に進められ，ＪＴ－60 の試験運転を，今年度末に完了した。トカマク装置の据付および試験と並行して，第一期ジュール加熱実験に向けて，基本的計測装置の据付および試験が行われた。（最初のプラズマ放電は，昭和 60 年４月８日に行われた。） 追加熱装置の建設は，現在進行中である。

中型トカマク装置ＪＦＴ－２Ｍにおいて，高出力ＩＣＲＦ加熱実験・ＥＣＨ加熱されたプラズマにおけるＬＨ電流駆動実験を行った。またプラズマ断面制御用電源の据付も完了した。理論面では，自由境界条件の非線形キンク／ティアリングモードの詳細な解析を行うとともに，ＩＣＲＦ加熱の解析を行った。

ＪＴ－60 計測用高電圧，大電流 He イオン源の開発が順調に完了し，ＪＴ－60 用ＬＨ およびＩＣＲＦ加熱装置の開発も順調に進んでいる。新しいセラミックであるＢｅＯを添加したＳｉＣに対するプロトンによる表面侵食が研究された。

国際エネルギー機関による大型コイル事業において，３コイルのテストが米国オークリッジ研究所において行われた。大口径 Nb_3Sn コイル ＴＭＣ－１の発生磁場 11Ｔの実験も完了した。トリチウムプロセス研究棟において，トリチウム取扱い施設の試験運転が進められた。

実験炉（ＦＥＲ）および INTOR の設計検討も進められている。

＋　現在，日本原子力研究所那珂研究所

CONTENTS

目　　次

I. PLASMA THEORY AND COMPUTATION

1. Introduction

During the period from April 1 1984 to March 31 1985, emphases of the theoretical works are put on analyses of (1) the beta limit and related problems, (2) the disruptions, (3) the rf heating, and (4) the divertor plasma.

As for the beta limit analyses a remarkable result is establishment of the practical beta scaling laws applicable to a standard tokamak with a moderate noncircular cross section. An effort to clarify the mechanism which limits maximum beta in a realistic tokamak plasma is also made by solving a nonlinear model equations and analyzing the saturation state of ballooning modes. "Pseudo-vacuum" model is found effective to carry out a nonlinear simulation of a resistive MHD system with a free boundary, which will be a powerful computational method for the disruption analyses. Several new features of a surface tearing mode and magnetic bubble formation process are being clarified. By using the previously developed numerical codes a lot of analyses on the rf heating are carried out. Some basic processes concerning the rf heating are also studied. Divertor plasma analyses are mainly carried out on the basis of the particle model simulation. Basic processes in the divertor plasma are discussed and problems concerning applicability of the fluid model are commented.

Some physics codes in the TRITON system are under improvement and standardization. By these refinement of the codes they are widely usable as basic codes of the new codes developed for application to a new problem. Development and improvement of the supporting codes in the TRITON system are now being continued. Some of the codes are published and used for various purposes.

2. Transport and Heating Studies

2.1 Introduction

It is important to know the role of ballooning mode and other kinds of high-mode-number instabilities on transport and beta limitation of a tokamak plasma. From this viewpoint motion of electrons due to high-mode-number electrostatic waves is extensively studied. In order to clarify the relations between the plasma beta and the magnetic fluctuation nonlinear behavior of the ballooning mode is also examined on the basis of simplified model equations. Diffusion flux across disrupted magnetic surfaces is estimated in relation with the rapid density decrease observed at the major disruption.

Studies on a divertor plasma are carried out by using a particle simulation technique and several features of the plasma are clarified.

As for the analyses of the rf heating excitation of the ICRF waves by a waveguide launcher and origin of impurities during the heating process are studied extensively. And some basic processes relating the rf heating are investigated.

2.2 Transport

2.2.1 Motion of electrons due to high-mode-number electro static waves in tokamak[1)]

Guiding-center motion of electrons due to a high-mode-number electrostatic wave (poloidal mode number is m) in a tokamak is studied. Effects of the toroidicity and magnetic shear are considered. Radial displacement by $E\times B$ drift is investigated. Motions of untrapped electrons are almost periodic. Motions of trapped electrons are also perodic if the amplitude φ is small enough. The island width Δ_t of trapped electrons is independent of φ, but Δ_u of untrapped electrons is proportional to $\sqrt{\varphi}$. When φ is so large that conditions, $(\kappa R v_{\parallel}/v)(mqR/r)(\rho/r)(me\varphi/E)>0.25$ and $\kappa\Delta_t<2(r/R)(E/me\varphi)$, are satisfied, stochastic motions of trapped electrons are observed, ($\kappa=q^{-1}dq/dr$; q: safety factor, R: major radius, r: minor radius, ρ: Larmor radius, E: energy). The radial flow, $r\sim\sqrt{t}$ (t: time), can be induced when φ becomes much larger $\kappa\Delta_t>2(r/R)(E/me\varphi)$.

2.2.2 Simulation of ballooning instabilities

Nonlinear evolution of ballooning modes in tokamaks is examined by the two-fluids model with resistivity in two-dimensional geometry. All the purterbed quantities are assumed to be localized along the field line with the scale length of order Rq (R is the major radius and q the safety factor of the tokamak). Time evolution of density, electrostatic potential and the parallel component of the vector potential is solved numerically.

At low beta region, drift waves become unstable due to the toroidal curvature and the system becomes weakly turbulent, in which each mode has a frequency spectrum with a peak at the druft frequency. As beta value increases, large scale magnetic fluctuation appears and at high beta region ($\beta > a/Rq^2$, a: minor radius) the eddy of the largest scale becomes dominant.

2.2.3 Cross field particle diffusion in plasma disruption[2)]

A mechanism of cross field diffusion of plasma particles induced by the parallel electron heat flow is discussed. The diffusion coefficient in the disrupted magnetic field in tokamaks is estimated to have the Bohm-like dependence. Particle can diffuse much faster than streaming along field lines.

2.2.4 Particle simulation of divertor plasma[3)]

Characteristics of divertor plasmas are studied by using a one-dimensional electrostatic particle simulation code with a binary collision model. Dependence of plasma parameters, such as temperature, flow speed, pre-sheath potential, etc., on the collisionality is investigated in detail. Collisions play an important role in supplying electrons with large velocity parallel to the magnetic field, which can pass through the sheath potential barrier near the divertor plate. The pre-sheath with the scale length of the system size is formed by the collisional relaxation of the velocity distribution as well as by the particle source. The flow speed is increased by this potential and exceeds the sound speed.

2.2.5 Thermal conductivity in divertor plasma

We investigate the property of divertor plasmas by particle simulations. The cold particle source near the divertor plate is

introduced in the simulation as well as the hot particle source. We perform simulation runs for the wide range of R_C and l_{mfp}/L (R_C: ratio of cold particle flux to hot particle flux, l_{mfp}/L: ratio of electron collision mean free path to system size). Thermal conductivity parallel to the magnetic field is studied in detail. Electron thermal conductivity obtained by particle simulations is almost the same as that given by Braginskii, while ion thermal conductivity is much different from that by Braginskii, especially, when $R_C \gg 1$ and the flow speed is much smaller than the sound speed.

2.2.6 Alfvén loss cone instability driven by thermonuclear alpha particles

The Alfvén loss cone instability by α-particles produced by D-T reactions is investigated. The instability is caused by anisotropy in the α-particle distribution which is obtained numerically by solving the Fokker-Planck equation without the use of the Legendre expansion with respect to the pitch angle variable. The time evolution of the instability growth rate is calculated, and the relation between the growth rate and the energy anisotropy is studied.

2.3 Heating

2.3.1 Excitation of ICRF waves in tokamaks by waveguide launcher[4)]

Excitation of ICRF (ion cyclotron range of frequencies) waves in tokamak plasmas by using the waveguide antenna is investigated. In order to obtain the surface impedance of the plasma, the wave propagation equation for the fast wave is solved. The reflection/transmission coefficient is calculated for the parallel plates launcher which simulates a ridged waveguide. Dependences of the transmission coefficient on geometrical and plasma parameters are studied. It is found that the transmission coefficient can be of the order of 10 %. comparable to that of the loop antenna. Non-plasma loss of the launcher is also discussed.

2.3.2 A possible origin of metal impurities in ICRF heating experiments[5)]

A model of possible origin of metal impurities in ICRF heating

experiments of tokamaks is presented. Scrape-off ions are directly accelerated by the reactive electric field of the radio frequency (rf) wave near the antenna and cause the sputtering of impurities. Using the wave form which is obtained by solving the wave equation, the threshold power for the onset of rf-induced sputtering is estimated.

2.3.3 Radio frequency conductivity of plasma in inhomogeneous magnetic field[6)]

Nonlocal conductivity tensor is obtained to study the kinetic effects on propagation and absorption of rf waves in dispersive plasma. Generalized linear propagator in the presence of the inhomogeneity of magnetic field strength along the field line is calculated. The influence of the inhomogeneity to the rf-energy deposition is found to be appreciable. Application to toroidal plasmas is shown.

2.3.4 Differential form of wave propagation equation in inhomogeneous plasma[7)]

Differential formulation of the wave propagation equation in the inhomogeneous and dispersive plasma is derived by employing the nonlocal and kinetic conductivity tensor. The expressions of the associated power deposition and wave energy flux are also presented.

References

1) Takizuka, T., Itoh, K., Azumi, M., Comments Plasma Phys. Controlled Fusion 9 (1984) 1.
2) Itoh, K., Itoh, S.-I., Phys. Letters 109A (1985) 31.
3) Takizuka, T., Tani, K., Azumi, M., Shimizu, K., J. Nuclear Materials 128 & 129 (1984) 104.
4) Itoh, K., Itoh, S.-I., Fukuyama, A., Excitation of ICRF waves in tokamaks by waveguide launcher, HIFT-94 (Research Report of Hiroshima University) (July 1984).
5) Itoh, K., Fukuyama, A., Itoh, S.-I., A possible origin of metal impurities in ICRF heating experiments, HIFT-93 (Research Report of Hiroshima University) (July 1984).
6) Itoh, S.-I., Fukuyama, A., Itoh, K., Radio frequenct conductivity of plasma in inhomogeneous magnetic field, HIFT-91 (Research Report of

Hiroshima University) (July 1984).
7) Itoh, S.-I., Fukuyama, A., Itoh, K., Differential form of wave propagation equation in inhomogeneous plasma, HIFT-92 (Research Report of Hiroshima University) (July 1984).

3. Equilibrium and Stability Analysis

3.1 Introduction

In the computational MHD studies of a tokamak plasma we have made effort to develop highly accurate computational method of equilibrium, derive reliable beta scaling according to the high-n ballooning and n=1 external kink modes, and study new disruption scenario based on the magnetic bubble formation in the vicinity of the resonant value of safety factor.

In order to attain accurate equilibria for linear stability analysis we are developing an inverse FCT equilibrium code with high beta tokamak ordering. We obtained practical beta scaling laws which are represented by the proportionality with a normalized plasma current. The results are almost consistent with experiments and also with theoretical results by other authors. To analyze the disruption process we made an extensive study by the numerical simulation of the nonlinear MHD model based on the "pseudo-vacuum" model. From the results we found the importance of the surface tearing mode and the consequently obtained magnetic bubbles.

3.2 Equilibrium analysis

3.2.1 High beta tokamak ordering FCT equilibria

For an accurate MHD stability analysis an inverse solution of the Grad-Shafranov equilibrium equation is an attractive method because by the method positions of the magnetic surfaces are determined as $R=R(\psi,\theta)$, and $Z=Z(\psi,\theta)$ and the metric quantities necessary for the stability analysis are obtained on the determined magnetic surfaces with high accuracy. When we calculate a series of equilibria under the FCT (flux conserving

tokamak) condition, however, we encounter a difficulty due to highly nonlinear feature of the FCT condition and the fact that the boundary condition on R and Z are only given implicitly in the inverse solution with the FCT condition.

In order to cope with the difficulty we use the approximate method known as the high beta tokamak ordering: $\beta=O(\varepsilon)$, $\varepsilon\beta_p=O(\varepsilon)$, $q=O(1)$, instead of using the exact equation of the FCT equilibrium. Then the FCT condition is transformed to a constraint on Jacobian and it gives the boundary conditions on R and Z in an explicit form. The partial differential equations obtained by the high beta bokamak ordering are reduced to two-points boundary value (TPBV) problems for the nonlinear ordinary differential equation for $O(1)$ approximation and a linear one for $O(\varepsilon)$. They are much easier to solve and we can solve these TPBV problems for nonlinear ordinary differential equation by using Newton's method (the method of quasilinearization).

3.2.2 Equilibrium database CLIO-V2

We have updated the equilibrium database CLIO-V1 and developed a new database CLIO-V2. Both the databases are usable under a new version of database supervising code GAEA-MT. The CLIO-series database is a kind of an encyclopedia of the tokamak plasma equilibria and one can consult it how much are the values of parameters to calculate a desired equilibrium.

3.3 Linear MHD instabilities

3.3.1 Scaling of beta limit[1)]

The scaling of the beta limit was obtained for $n=\infty$ ballooning mode and $n=1$ external kink mode, where n is the toroidal mode number. For the ballooning mode analysis, the profile of the safety factor was fixed as $q(\psi)=q_0(1-\psi)^{\alpha}$, and the pressure profile was optimized to the ballooning instability in FCT sequence of equilibria. The optimized pressure profile was multiplied by a constant for the analysis of the external kink mode. The obtained scaling laws (Fig. I.3.1) are

$\beta(\%) = 4\ I_N$ for ballooning mode,

$\beta(\%) = 3.2\ I_N$ for kink mode,

where I_N is the normalized toroidal current defined by

$I_N = I(MA)/a(m)B(T)$.

3.3.2 Linear stability analysis of a free boundary system with a "pseudo-vacuum"[2)]

In order to simulate a nonlinear MHD behavior of a free boundary plasma we studied a resistive MHD model with a "pseudo-vacuum". The "pseudo-vacuum" model essentially consists of combination of a main plasma with a high conductivity and a "pseudo-vacuum" region simulated by an extremely highly resistive plasma. Before the nonlinear calculation applicability of the "pseudo-vacuum" model to the study of a free boundary kink mode was carefully investigated by the linear stability analyses. Some features of the newly found surface tearing mode have been also clarified through the series of linear stability analyses.

3.4 Nonlinear MHD instabilities

3.4.1 Magnetic bubble formation due to surface tearing mode[2)]

Nonlinear calculation of a free boundary mode in a cylindrical tokamak plasma with finite conductivity is carried out by using the conventional reduced set of resistive MHD equations with the "pseudo-vacuum" model. In Fig. I.3.2 we show the stability diagram for kink, surface tearing and tearing modes (m/n=2/1 and m/n=3/1 modes) in the shear strength (q_a/q_0) versus q_a plane with the equilibrium currend profiles corresponding to the shear strength and the saturation states obtained by the nonlinear calculations. The other parameters are the ratio of the position of plasma surface to that of shell a/b=0.66 and the equilibium plasma resistivity profiles $\eta(r) \propto J(r)^{-1}$ with $\eta(0)=10^{-6}$. In the figures of the saturation state, the bold lines denote the plasma surfaces, which are chosen to be circle in the initial states.

By this figure, we can see that the vacuum bubbles are formed due to surface tearing mode as well as free boundary kink mode for the condition that the safety factor at the plasma surface, q_a, is around 2. This bubble formation is a candidate of the major disruptions in the tokamak discharge with q_a nearly equal to 2.

3.4.2 Numerical study of m=1 resistive internal kink mode in a cylindrical tokamak[3)]

A numerical analysis of nonlinear behavior of m=1 resistive internal kink instability in a tokamak is presented in a cylindrical approximation. A two-dimensional nonlinear code which solves incompressible resistive MHD equations with helical symmetry has been developed. For the case of small longitudinal wave number k, the magnetic axis moves outwards until it reaches the critical surface where the value of helical magnetic flux has the same value as the one at the magnetic axis. On the other hand, as k is increased, the shift of the magnetic axis saturates before touching this critical surface. This result gives a possible explanation of suppression of internal disruptions observed in high power neutral beam injection experiment of tokamaks.

References

1) Tuda, T., Azumi, M., Itoh, K., Kurita, G., Takeda, T., Takizuka, T., Tokuda, S., Tsunematsu, T., Adachi, M., Tanaka, Y., Watanabe, M., Itoh, S.-I., Accessible beta value of takamaks, in *Plasma Physics and Controlled Nuclear Fusion Research*, (IAEA, Vienna, 1985) Vol.2, p.173.

2) Kurita, G., Azumi, M., Tuda, T., Tsunematsu, T., Takizuka, T., Tanaka, Y., Takeda, T., Bubble formation due to surface tearing mode, Proc. US-Japan Workshop on Magnetic Reconnection, December 10-13, 1984, Austin, Texas, DOE/ET/53088-182, (IFSR 182) p.325.

3) Tanaka, Y., Azumi, M., Kurita, G., Takeda, T., Plasma Phys. and Controlled Fusion, 27 (1985) 579.

4. TRITON System

4.1 Introduction

As for the physics codes in the TRITIN system improvements and standardizations are made. According to these changes the codes become inteligible and can be easily benchmarked. Several extensions of the

codes to new problems are attempted, which is more easily carried out by an appropriate standardization. Many supporting codes are developed. Some of them are the improved version of previously developed codes and the others are newly developed ones. They are being effectively used to development of codes and analyses of physics problems.

4.2 Physics codes

4.2.1 Standard version of ERATO-J code, ERATOS

A standard version of the ERATO-J code (ERATOS) has been developed for general use. It is compiled after the preprocess by EOS77 and outputs automatically a detailed user's mannual. The code ERATOS has reference data to helpful for updating the code for user's own purpose.

4.2.2 Linear resistive MHD code NOTUS-C1

The primitive set of resistive MHD equations was solved in the cylindrical model. In this calculation, asymmetric eigenvalue equation was solved by using EISPAC package, and the mesh points, N_r, was limited up to about 30 (matrix size 360×360) in usual computations. A new eigenvalue solver was developed by using the inverse iteration method. The mesh point available becomes $N_r \leqq 1000$ by using this solver.

4.2.3 Standard version of nonlinear resistive MHD code AEOLUS-RT

A standard version of nonlinear resistive MHD code AEOLUS-RT has been developed for general use. This code is based on the conventional reduced set of resistive MHD equations. As a benchmark test of the code a disruption scenario due to nonlinear destabilization of tearing modes by an island overlapping is well recovered by this code.

4.3 Supporting codes

4.3.1 Eigenvalue solver of an asymmetric matrix for resistive MHD analysis

A matrix method to solve a reduced set of linear resistive MHD equations of a tokamak plasma has been developed. A complex eigenvalue of an asymmetric block tridiagonal matrix derived from the equations is

calculated by the inverse iteration method. Combination of determinant method and bisection method is sometimes effectively used to determine initial guess of the eigenvalue.

Several applications of the subroutine to analyze the resistive MHD problems are considered and tested.

4.3.2 Versatile preprocessor system for inclusion and extraction of Fortran statements, EOS77

The extended OLYMPUS preprocessor system (EOS) has been updated so as to generate a FORTRAN77 source program (EOS77). EOS77 preprocessor has several new functions: it handles character variables, it changes the name of variables in common blocks into the specified name and users can use the parameter statement and the include statement in the EOS77 source program.

4.3.3 Integrative graphic subroutine package ARGUS-V4[1)]

Development of an integrative graphic subroutine package ARGUS-V4 is completed and the concept of the package has been published. The basic idea is that any single graphic procedure is composed of three elementary processes, i.e., registration of a graphic data set, processing of the data to matchwith the required graphic format and plotting of the graph. The package based upon the concept contained various subroutines clearly classified according to the above elementary processes. By using the package graphic procedures in a scientific or engineering programs can be coded very easily and the program becomes intelligible. As the package ARGUS-V4 is written in the standard FORTRAN77 language and uses only basic plotting subroutines in the CALCOMP library, it can be installed with a few alterations in various computer systems.

4.3.4 Three dimensional graphic system ARGUS-V5

Basic system for interactive 3D graphics was developed. This system is composed of two modules. One is for the management of the data structure bases on GKS (Graphic Kernel System) and another is the "driver" to manage the graphic terminals. By using this system, users can interactively edit their numerical data by watching 3D pictures.

4.3.5 Interfacing routines for graphic terminals

The common interfacing routines, JGSP, for the graphic terminals in the nuclear fusion research center in JAERI were developed for plotting two dimensional objects. The three dimensional version with interactive commands are being developed.

4.3.6 Database supervising code GAEA-MT for numerical results of simulation

We have designed the improved version of GAEA-MT. The structure of data was reconsidered in such a way that the amount of the necessary key data files can be reduced substantially and the locality of key data can be kept.

4.3.7 Software information sorting code PLUTO-R[2)]

A software information sorting code PLUTO-R is developed as one of the supporting codes of the TRITON system for the fusion plasma analyses. The objective of the PLUTO-R code is to sort reference materials of the codes in the TRITON code system. The easiness in the registration of information is especially persued. As experience and skill in the data registration are not required, this code is usable for construction of general small scale private information system.

References

1) Takeda, T., Tsunematsu, T., Tokuda, S, Comput. Phys. Commun. 34 (1984) 15.
2) Tsunematsu, T., Naraoka, K., Adachi, M., Takeda, T., Software information sorting code "PLUTO-R", JAERI-M 84-185 (September 1984) in Japanese.

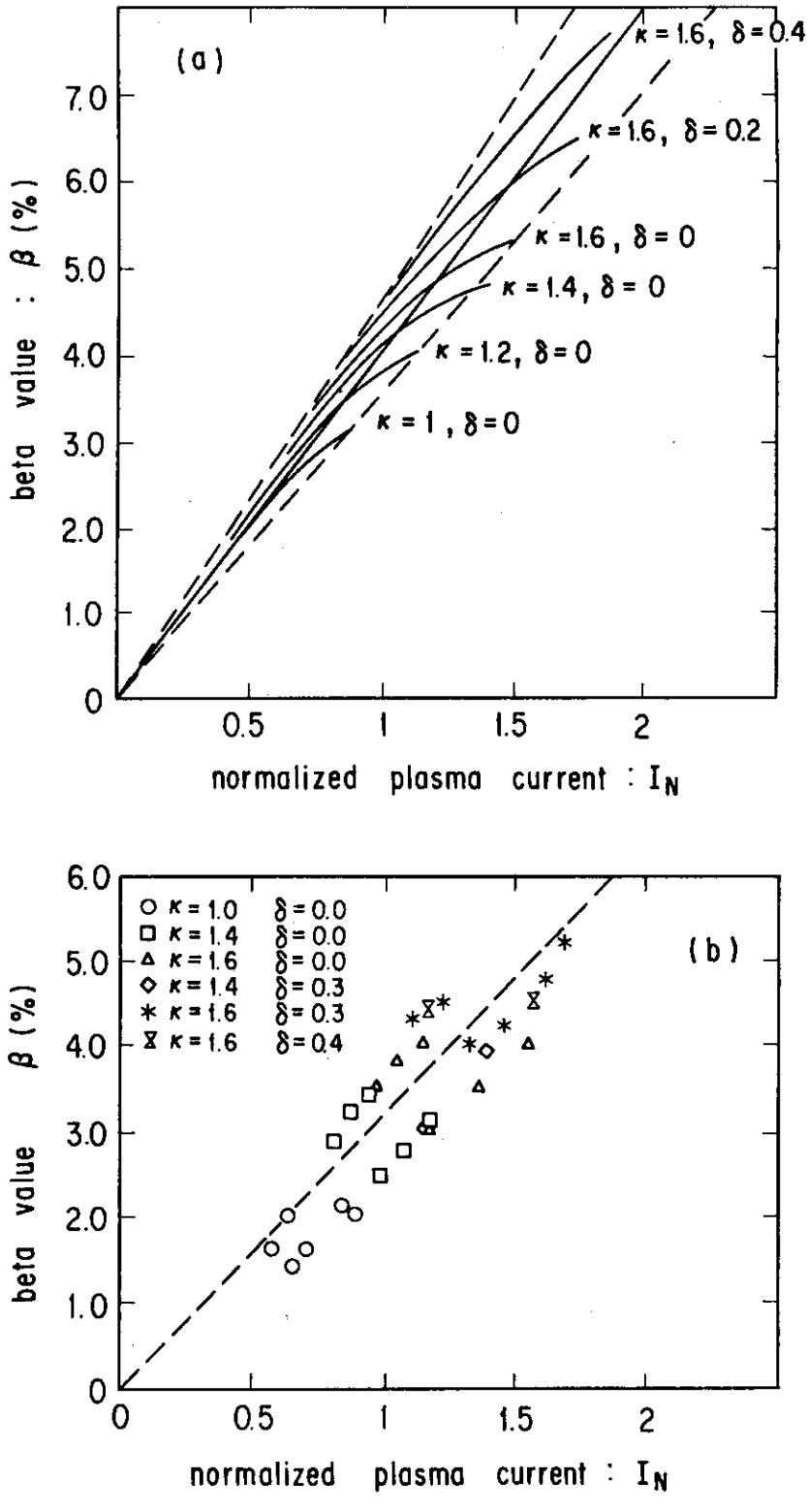

Fig. I.3-1 Scaling laws of beta limit, (a) for $n=\infty$ ballooning mode and (b) $n=1$ external kink mode.

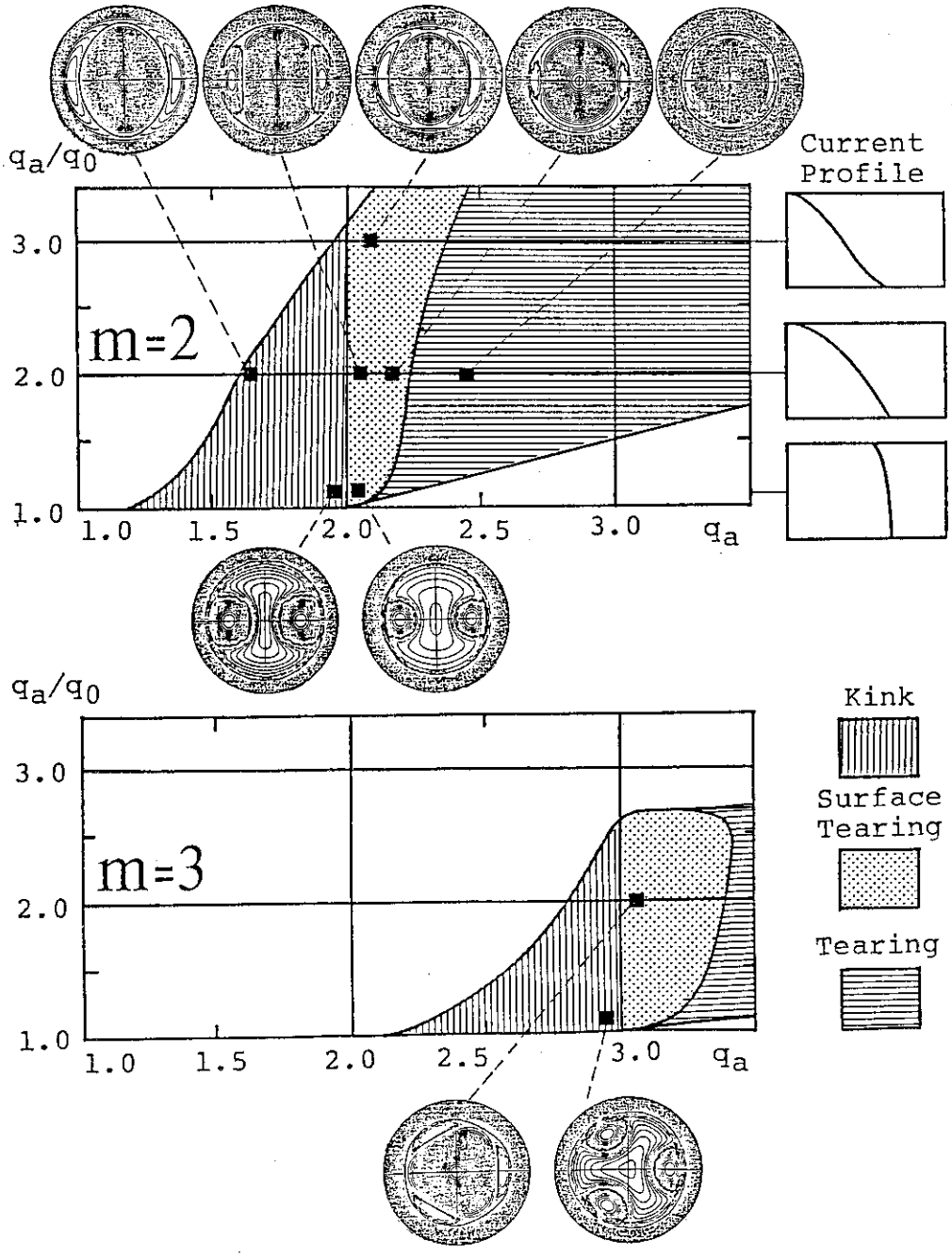

Fig. I.3-2 Stability diagram of the external kink modes, surface tearing modes, and fixed boundary tearing modes for mode numbers of $(m,n)=(2,1)$ and $(3,1)$. In contour plots above and below the diagram the plasma surfaces at the saturation states are indicated by bold lines. Subfigures on the right hand side are current profiles corresponding to the shear parameter q_a/q_0=1.1, 2.0, and 3.0.

II. TOROIDAL CONFINEMENT EXPERIMENT JFT-2M

1. Introduction

The commissioning of a medium sized D-shaped tokamak JFT-2M was completed in April, 1983, with a neutral beam injection (NBI) system of 2 MW, a second ion cyclotron range of frequency (ICRF) heating system of 800 kW, and a lower hybrid (LH) wave heating/current drive system of 600 kW. After a typical ohmically heated circular-discharge of plasma current 300 kA was obtained in June 1983, experiments on second harmonic ICRF heating, combination heating of NBI and ICRF, and current drive with LH wave (LHCD) were done until March 1984.

Installation of a new high power ICRF (4.5 MW, 14 to 38 MHz) system began in March 1984. Heating experiments with mainly the ICRF system were conducted from April to September. Key results of the ICRF experiment are the successful increase of plasma stored energy with the heating power and the reduction of impurity release by controlling of incident ICRF waves. Experimental results of the ICRF heating are described in Subsection II.2. Plasma heating using Multi-Short-Pulse neutral beams was also studied, whose results are described in Subsections II. 3 and 4.

After installation of a 60-GHz gyrotron (200 kW) system for electron cyclotron resonance heating (ECRH) in September, RF current drive and electron heating experiments were done with the gyrotron system and the lower hybrid wave system. It was demonstrated that high energy electrons generated by LH wave coupled with simultaneously injected ECRH wave, and that then the LH wave-sustained plasma current was significantly increased by the ECRH wave. Subsection II. 5 describes results on these experiments.

During the present reporting period, improvements on diagnostics went on steadily. Subsection II. 6 decribes two examples of them; calibration of Thomson scattering measurement and FIR interferometry.

The development of pneumatic pellet acceleration technology was also done in collaboration with Mitsubishi Heavy Industries Co., and a pellet speed of 600 to 800 m/s for a pellet size of 1 mm dia. × 1 mm length was confirmed.

For three months from the end of December, JFT-2M experiments were

stopped by installation of the poloidal power supply for D-shaped plasma discharges and magnetic limiter operation. Testing on generation of D-shaped 500 kA plasmas has been successfully made. A full rating D-shape experiment of 500 kA plasma current is now in progress.

2. High Power ICRF Heating Experiments in the JFT-2M Tokamak[1)]

2.1 Apparatus

In the present ICRF heating experiment, target plasma has a D-shaped cross section with the elongation ratio of about 1.2. Plasma surface is determined by graphite limiters, and the vessel wall is gettered by titanium.

The rf generator with 4.5 MW maximum power is operated at 15.2 MHz in order to perform heating experiments in two-ion-hybrid regime. An array of three loop antennae on the high field side is used. The length of radiative part is 50 cm and the width of the center conductor is 7 cm. The Faraday shield is made of titanium[2)]. In order to perform the electron heating experiments in a mode conversion regime, the density ratio of hydrogen to deuterium n_H/n_D is about 40 %, which is determined by the spectroscopic measurement and the mass-separated charge exchange neutral analysis. The toroidal magnetic field of 1.15T is determined so as to obtain the maximum heating efficiency and the minimum increase of the radiation loss power.

2.2 Effects of $k_{//}$ spectrum

The ICRF heating experiments on $k_{//}$ spectrum have been carried out by changing the phase relation of rf currents among the three antennae. When all of the rf currents are applied in-phase (in-phase operation), there is a peak of the $k_{//}$ spectrum at $k_{//}=0$. On the contrary, when the rf current of the middle antenna is applied almost out of phase (out-of-phase operation), $k_{//}$ spectrum has a peak at about $k_{//}=8\ m^{-1}$.

In both operations, the temporal evolutions of plasma parameters with the net input power P_{RF} of 300 kW are shown in Fig. 1. In these

experiments the plasma current I_p is fixed to 150 kA. In the case of the in-phase operation, the electron density increased during the ICRF heating. On the other hand in the case of out-of-phase operation, the density decreased. So the gas puffing is controlled to obtain the nearly same density.

The solid lines and the broken lines in the figure correspond to the out-of-phase operation and the in-phase operation, respectively. The increments of the central deuterium ion temperature, whose energy spectrum has no high energy tail, are almost the same in both cases. Main difference appears in impurity behavior between two operations. The increase of the radiation loss power P_R in the in-phase operation is larger than that in the out-of-phase operation by a factor of 1.6. The increases of the line radiations of impurities in the in-phase operation are also larger than those in out-of phase operation. Though the loop voltage decreases with the heating in both cases, the decrement is smaller in the in-phase operation. Furthermore, the loop voltage increases gradually from 60 ms after the initiation of ICRF pulse in the case of in-phase operation. The central electron temperature obtained by soft X-ray spectrum analysis and the poloidal beta determined by magnetic measurement increase and are sustained during the ICRF heating in the out-of-phase operation. On the other hand, in the in-phase operation the electron temperature and the poloidal beta increase in the initial stage, but thery begin to decrease at 60 ms after the initiation of ICRF pulse. The $2\omega_{ce}$ emission I_{ECE} at r=20 cm indicates that the electron temperature in the peripheral region increases and holds in the out-of-phase operation, but it decreases gradually in the in-phase operation.

These experimental results indicate that the in-phase operation of the loop antennae causes the impurity increase and then the radiation cooling. In the out-of-phase operation, however, the increase of the radiation loss power is reduced by a factor of 1.6 and the radiation cooling seems not to deteriorate the plasma parameters in this power level. Therefore, the high power heating experiment is performed in the out-of-phase operation.

2.3 High power heating experiment

The density limit is raised from about 4×10^{13} cm^{-3} in the Ohmic heating to 5-6 $\times 10^{13}$ cm^{-3} with the 1.6 MW ICRF heating.

The temporal evolution of plasma parameters with 1.2 MW ICRF heating are shown in Fig. 2. The plasma current is 228 kA, and the ICRF heating is started at 600 ms. The line averaged electron density has been raised from 3.1×10^{13} cm^{-3} to 5.0×10^{13} cm^{-3} during ICRF heating by the gas puffing. The loop voltage decreases from 1.7 V to 0.8 V. The central electron temperature measured by Thomson scattering increases from 0.8 keV at 600 ms to 1.9 keV at 640 ms and then decreases gradually. The poloidal beta, however, continues to increase during the ICRF heating. Therefore, the decay of the electron temperature is considered as the result of the rapid increase of the electron density. The central deuterium temperature obtained by charge exchange neutral analysis increases from 0.5 keV to 0.9 keV. Strong electron heating is observed in $n_H/n_D = 40$ % plasma as expected with the mode conversion theory[3].

The profiles of the electron density, temperature measured by Thomson scattering, and the ion temperatures obtained by the charge exchange neutral analysis, the neutron emission and Doppler broadening of the spectral line (CV) at 720 ms are shown in Fig. 3. In this case, the poloidal beta determined by the magnetic measurement increases from 0.35 to 0.9 in the ICRF heating, and then the averaged toroidal beta reaches 1.1 %. The poloidal beta deduced from the profile data increases from 0.31 to 0.89, where $(n_H+n_D)/n_e$ of 0.8 is assumed. Therefore, both of the poloidal beta are in good agreement within the experimental accuracy.

In the case of ICRF heating of 1.6 MW, the poloidal beta of 1.0 has been obtained. So the averaged toroidal beta of 1.2 % has been achieved by only ICRF heating.

2.4 Scaling of confinement

The density dependence of the gross energy confinement time is shown in Fig. 4(a). The gross energy confinement time and the total input power are defined by $\tau_{EG}=W/P_{tot}$, where $P_{tot}=P_{RF}+P_{OH}$ and W is

the stored energy of the plasma. In Ohmic heating, τ_{EG} has a linear dependence on the line averaged electron density up to 2.5×10^{13} cm^{-3}, and then deviates a little. There is the same tendency also in the case of ICRF heating. Here, the density dependence of the gross energy confinement time can be represented approximately by $n_{e13}(1-0.083\ n_{e13})$ with n_{e13} in 10^{13} cm^{-3}.

The power dependence of the stored energy is shown in Fig. 4(b). In order to eliminate the density dependence of the confinement time, we define the normalized stored energy W* by $W^* = W/[n_{e13}(1-0.083\ n_{e13})]$. The figure indicates the degradation of τ_{EG} with the power in the ICRF heating, but the degradation is not so large as in the NBI heating case. We can not conclude that the deterioration of the energy transport or the radiation cooling by the impurities causes this degradation of τ_{EG}. Because there is another possibility that a part of the rf power is absorbed in the peripheral region of the plasma[4].

References

1) MORI, M., HASEGAWA, K., HONDA, A., et al., in Plasma Physics and Controlled Nuclear Fusion Research (Proc. 10th Int. Conf. in London, 1984), Vol.1, IAEA, Vienna (1985) 445.
2) ODAJIMA, K., MATSUMOTO, H., KIMURA, H., et al., in Heating in Toroidal Plasma (Proc. 4th Int. Symposium Rome, 1984), Vol.1 (1984) 243.
3) ITOH, S.I., FUKUYAMA, A., ITOH, K., in Heating in Toroidal Plasma (Proc. 4th Int. Symposium Rome, 1984), Vol.1 (1984) 399.
4) COTSAFTIS, M., ibid., Vol.1 (1984) 357.

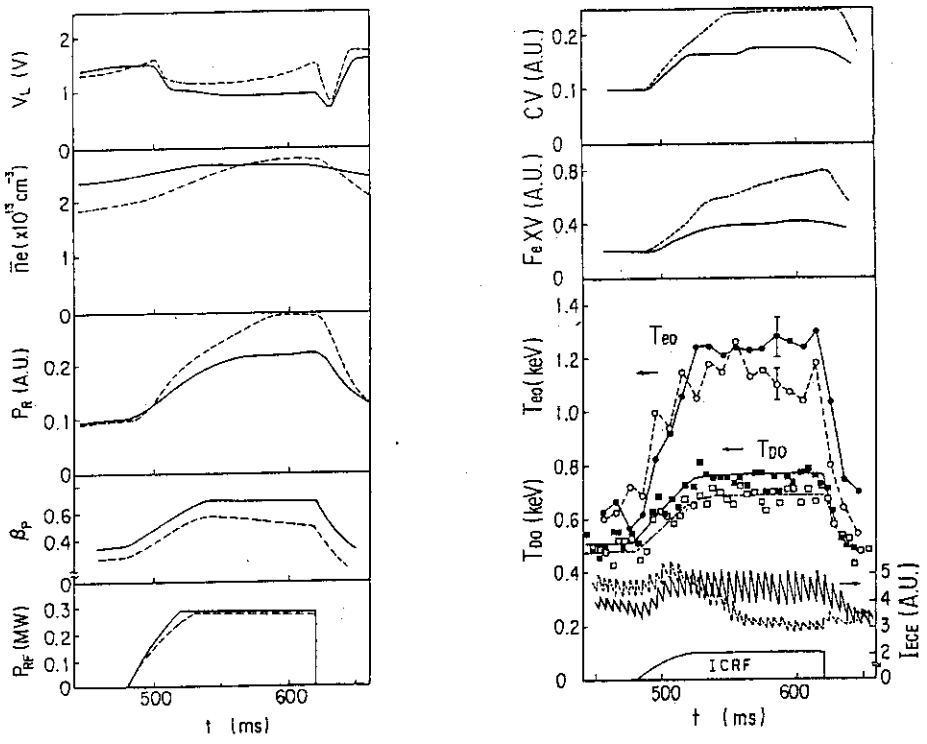

Fig. II.2-1 Temporal evolution of the plasma parameters in the ICRF heating of 300kW with an array of three loop antennae. The solid lines and the dotted lines correspond to the out-of-phase operation and the in-phase operation, respectively. In this experiment, the toroidal magnetic field B_T is 1.15T and the plasma current I_P is 150kA.

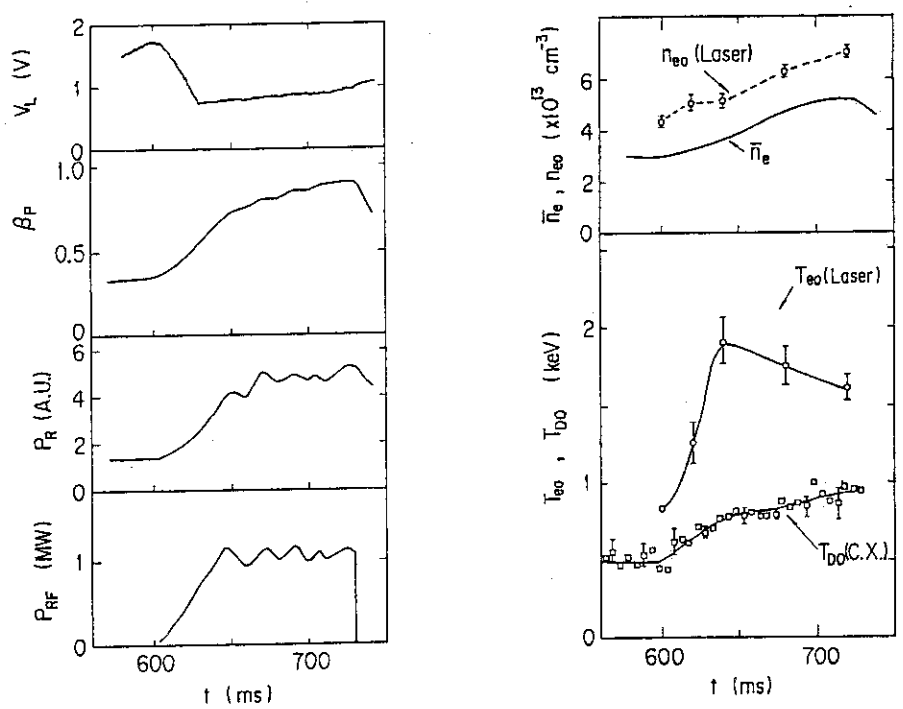

Fig. II.2-2 Temporal evolution of the plasma parameters in the out-of-phase operation with 1.2MW ICRF power. The ICRF power is radiated during 600-730ms. Here, I_P=228kA and B_T=1.15T.

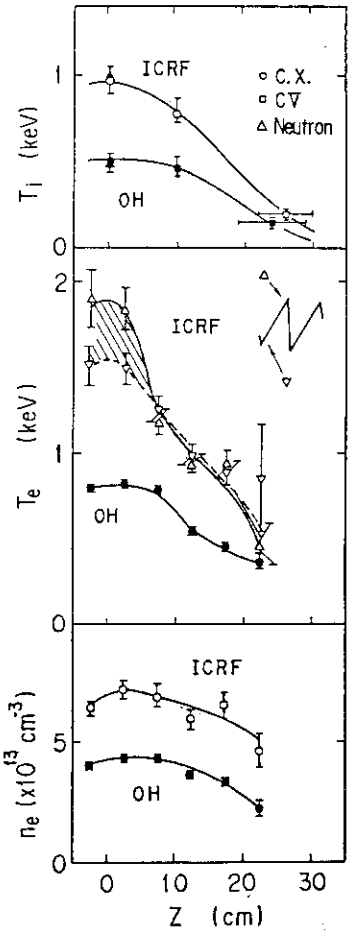

Fig. II.2-3

The profiles of the ion temperature, the electron temperature and the electron density at t=600ms (the Ohmic heating) and t=720ms (the ICRF heating). The ion temperatures are measured by the charge exchange neutral analysis, the Doppler broadening of CV line and the neutron emission. The electron temperature and the electron density are measured by Thomson scattering. The electron temperatures at the top and the bottom of the sawtooth oscillation are distinguished by Δ and ∇, respectively. The experimental conditions are the same as those of Fig. II.2-2.

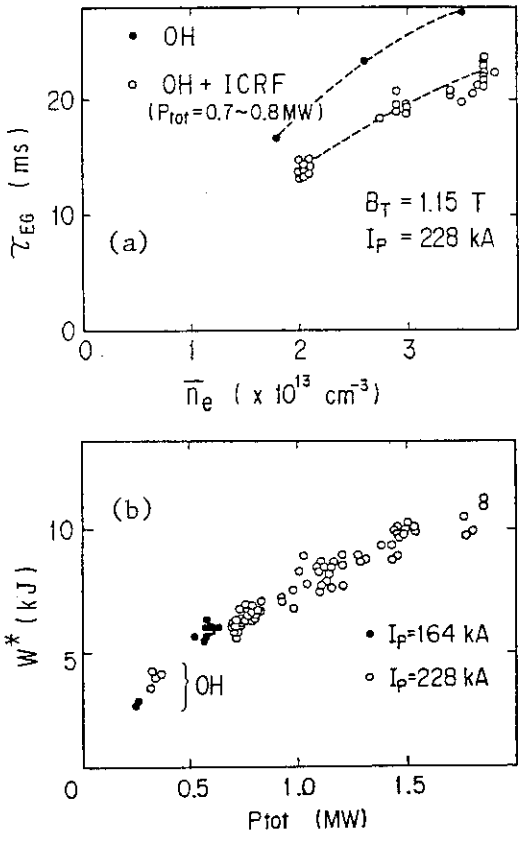

Fig. II.2-4

(a) The density dependence of the gross energy confinement time $\tau_{EG}=W/P_{tot}$ is shown in Fig. II.2-4(a), where W is the stored energy of the plasma and P_{tot} is the total input power of the Ohmic heating power and the net input power of the ICRF. The density dependence of τ_{EG} can be represented approximately by $n_{e13}(1-0.083n_{e13})$ with n_{e13} in 10^{13}cm^{-3}.

(b) The power dependence of the normalized stored energy $W^*=W/[n_{e13}(1-0.083n_{e13})]$ is shown in Fig. 4(b) in the cases of I_p=288kA and I_p=164kA.

3. Plasma Heating by Multiple-Short-Pulse Neutral Beams[1)]

A neutral-beam injection (NBI) method has been developed to control the averaged and maximum input power independently. The method, multiple-short-pulse (MSP) injection method, is characterized by the repetition period t_r and pulse length t_l, and is expected to be a useful tool for the investigation of NBI effects on plasma confinement. The method is also used to modify the velocity distribution function of injected beam particles. In the JFT-2M tokamak, we have excited waves with this method in the ion-cyclotron range of frequencies (ICRF) due to beam-plasma interactions in a controllable manner as shown in Fig. 1. The excited wave qualitatively agrees with the Alfven wave eigenmode in ICRF and may contribute to the nonclassical energy transfer from the beam ions to the bulk ions. We compared the charge-exchange spectra during the MSP injection with those of ordinary continuous injection in the low density regime.

Reference

1) S. Yamamoto et al., in Plasma Physics and Controlled Nuclear Fusion Research (Proc. 10th Inb. Conf. London, 1984), Vol.1, IAEA, Vienna (1985) 665.

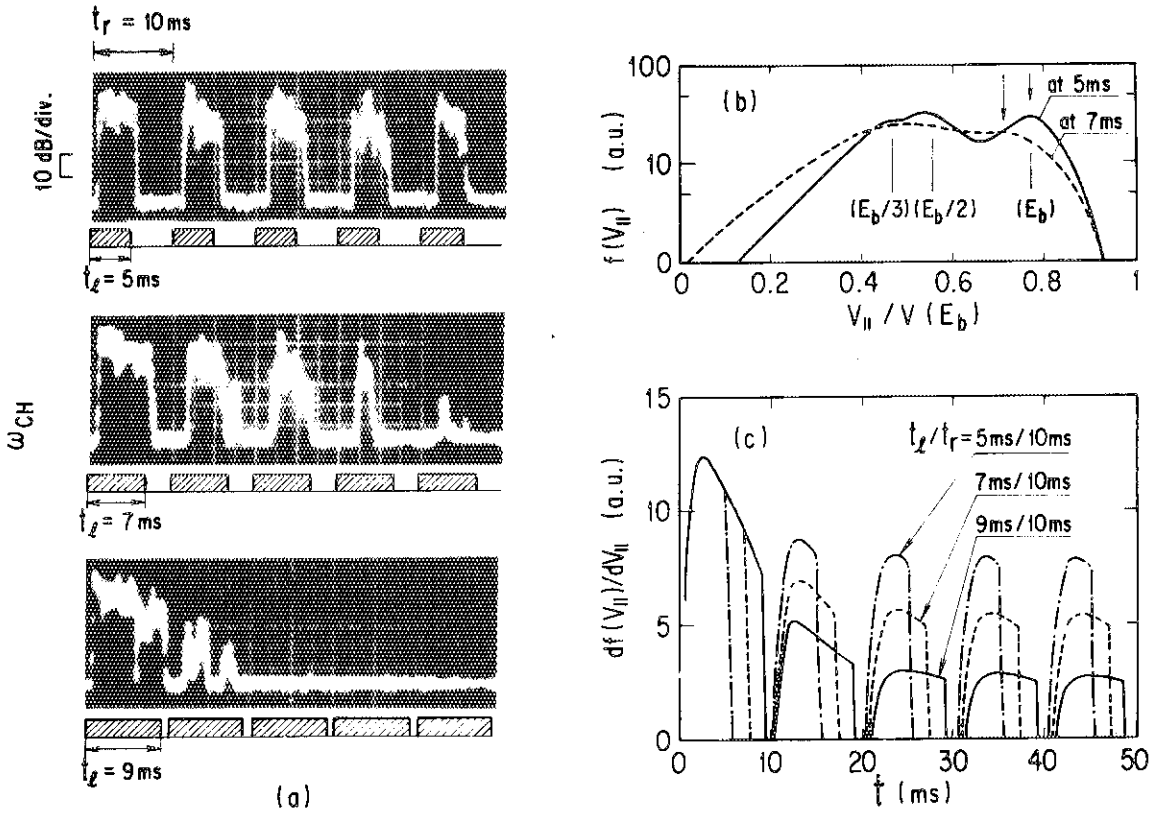

Fig. II.3-1(a) Relation between rf-oscillation amplitude ($\omega/2\pi$=19MHz) and beam pulse length (t_l=5ms, 7ms and 9ms) when the pulse repetition period is fixed (t_r=10ms). B_T=1.25T, I_p=150kA, n_e=$1.5\times10^{13}cm^{-3}$, n_H/n_D=0.3∿0.5, E_b=35keV, and I_b=50A (0.75MW co-injection).

(b) Calculated parallel velocity distribution function $f(v_{||})$ at the plasma center. In this case, beam is shut off at t=5ms. Calculation parameters are as follows: T_e=800eV, T_i=600eV, $n_e(0)=2.25\times10^{13}cm^{-3}$, E_b=35kV, I_b=50A and beam power fraction P(E):P(E/2):P(E/3)=6:3:1.

(c) Time behavior of slope of parallel velocity distribution function defined between two points denoted by arrows in (b) for MSP cases (t_l=5ms, 7ms and 9ms) and t_r=10ms.

4. Observation of ICRF Oscillation in the Tokamak Plasma during NBI

4.1 Discovery of beam driven ICRF oscillations

Oscillations in ion cyclotron range of frequencies (ICRF) have been observed in the JFT-2M plasma during neutral beam injection. Observation was made by using Langmuir probes and an ordinary spectrum analyzer.

Figure II.4-1 shows an example of the frequency spectrum obtained under the condition that hydrogen beam in the codirection was injected into the deuterium plasma. It can be found that peaks at 19 MHz and 38 MHz manifest, which are the ion cyclotron frequency of protons just at the center of the plasma and its second hamronics. Another one can be found at 32 MHz. In the following, characteristics of these oscillations are described briefly.

4.2 Oscillations in a transient manner

Figure II.4-2 shows the time variation of the intensity of the 19 MHz/38 MHz oscillations. The most distinctive feature of this type of oscillation is that it only appears at the initial phase of the beam injection (hence, we called it "transient mode"). Other noteworthy aspects of this mode are as follows;

1) The oscillation appears when the target plasma is deuterium but hardly appears when the target is hydrogen plasma;
2) The second harmonics appears with the diminishing of the fundamental as can bee seen in Fig. II.4-2;
3) The plasma density affects the duration of the oscillation: the lowering of the density lengthens the duration;
4) The frequency is definitly determined by the cyclotron frequency at the center of the plasma;
5) The beam of counter injection less excites the oscillation than that of co-injection;
6) Preliminary measurement of the wave length showed that the parallel wave length is about 1 m. Thus the phase velocity roughly agrees with the Alfven velosity.

4.3 Oscillation in the steady state

Figure II.4-3 shows the time behavior of the intensity of the 32 MHz oscillation. In contrast with the transient mode, the figure exhibits rather gradual and continuous behavior (We would like to call this "steady-state mode"). Furthermore, this mode appears although the target plasma is hydrogen. Being summarized, this mode shows sharp contrasts to that mode in all aspects observed (i.e. frequency, time behavior, plasma species).

4.4 Remarks

Excitation of ICRF oscillation at the beginning of NBI has been predicted by Stix[1] long time ago. However, experimental evidence of such oscillation has not been reported in the literature as yet. So, the transient mode is the first evidence for Stix's prediction. The mode identification and the effects to the energy transport was discussed in Sec. II.3.

Oscillations in ICRF during NBI has already been observed at the TFR tokamak.[2] This oscillation seems to correspond to our steady-state mode because, although somewhat different, the oscillogram signals showed rather continuous behavior.

References

1) T.H. Stix, Phys. Fluids 16, 1922 (1973).
2) Equipe TFR, in Plasma Physics and Controlled Nuclear Fusion Research (IAEA, Vienna, 1980) Vol.2, p.547.

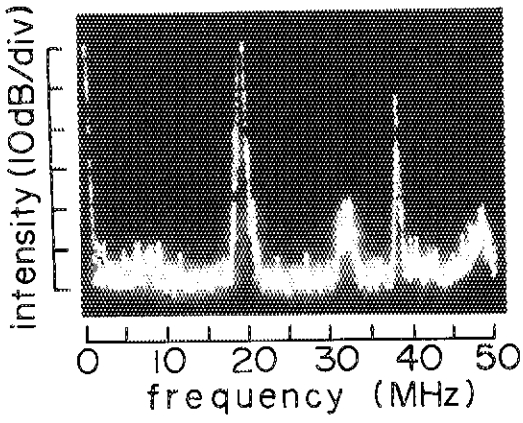

Fig.II.4-1 Frequency spectrum at the biginning of neutral beam injection.

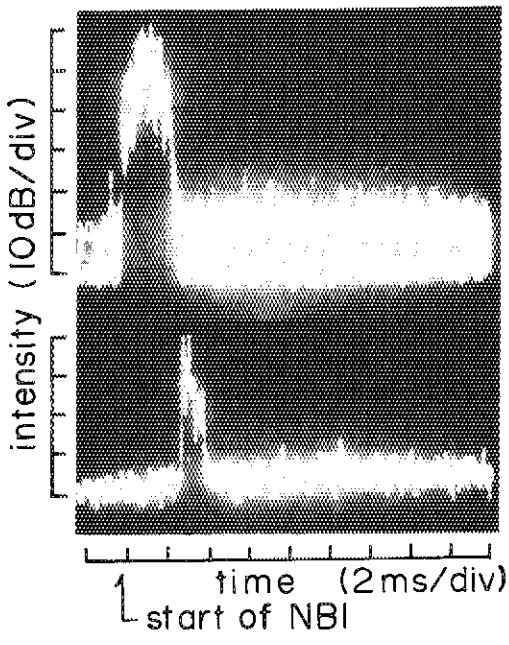

Fig.II.4-2 Time variation of the intensity of the oscillations; upper: at the cyclotron frequency of protons; lower: at the second harmonics.

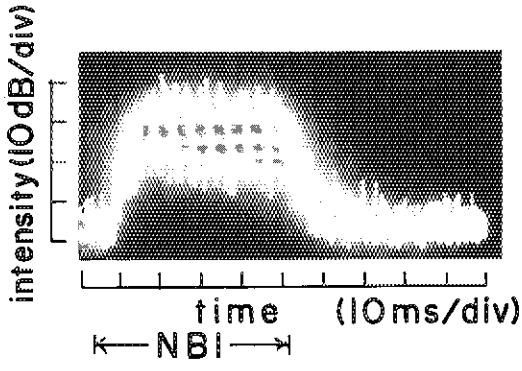

Fig.II.4-3 Time variation of the oscillation at 32 MHz found in Fig.II.4-1.

5. RE Current-Drive (LHH + ECH) and Electron Cyclotron Heating Experiments on JFT-2M Tokamak

5.1 Introduction

The rf current drive using the ECW seems to have several attractive features. First, it is possible to place the antenna far away from the plasma without the coupling problem. Second, the penetration of the ECW in the high density plasma is possible by choosing the frequency above the cutoff frequency. Third, as the resonant coupling of the ECW to the electrons occurs in the parameter space in which the electron cyclotron resonance (ECR) condition is satisfied, the power deposition (or the current) can be controlled by choosing the ECR condition appropriately. Fourth, the theoretical current drive efficiency by the ECW is as large as 3/4 of that by the LHW[1]. Fifth, the threshold power of the ECW parametric decay instability is relatively large, which means that high power density can be transmitted to the plasma core region to maintain the current.

The difficulty higherto encountered to obtain the ECH driven current by the bulk heating of the plasma lies in that the large single path absorption sufficient for the energy absorption to occur in one side of the ECR layer[2] is needed. And there is a possibility that the drive efficiency may deteriorate by the tranpped particle effect by the bulk heating.

But by using the relativistically down shifted ECR of the high energy electrons, these difficulties are avoided. The reflection at the vessel wall may increase the power deposition at the shifted ECR layer even if the absorption in single path is not large. Moreover, it was revealed that the current drive efficiency J/Pd is improved by the wave coupling to the high energy electrons[1),2)].

The combined effects of LHH + ECH are studied on the JFT-2M tokamak ($R = 1.31$ m, $a = 0.35$ m) experimentally. The frequency of the LHW is 750 MHz, and the spectrum of the parallel refractive index is controlled by four waveguides[4]. The launcher spectrum concentrates dominantly around $n_{//} = 1 \sim 3$ when the phase difference is -90°. The frequency of the ECW is 60 GHz. The second harmonic X-mode with $n_{//} = -0.17$ of the narrow beam divergence is launched in almost linear TE_{11} mode from the low field side of the torus.

5.2 LHH + ECH Current drive

Time evolutions are depicted in Fig. II.5-1(a). The toroidal electric field is applied by the primary OH circuit in the initial 100 ms for the production of the target plasma, and then the primary voltage is shut down and held zero (AVR operation). The application of the LHW of pulse length ∿400 ms and power 70 kW starts before the shut down of the primary voltage. In this way, the quick ramp-up of the plasma current I_p by the LHW is obtained. Ramp-up only by the LHW without the initial OH field takes longer time with less stability to reach 10 kA level of the driven current.

A saturation of the LHW driven current around $I_p \simeq 18$ kA with the efficiency 0.26 A/W is observed. The ECH pulse is applied for 100 ms during the saturation phase. A significant ramp-up of the current occurs almost linearly in time as shown in the figure. During the ECH pulse, the loop voltage drops and the plasma density changes. In this case, the 2nd harmonic ECR layer locates at $r_o = 0.1$ m outside and the plasma displacement is held inside of the center of the vacuum vessel with $B_{t0} = 1.15$ T.

The time rate of the current rise $(d/dt)\ I_p$ as a function of B_{t0} is given in Fig. II.5-1(b). I_p has two peaks. A peak around $B_{t0} = 1.0$ T corresponds to the location of the ECR layer around the plasma core which is shifted inside, and indicates the contribution of the current rise. The second peak in $B_{t0} = 1.15 \sim 1.30$ T seems to be due to the coupling of the ECW to the LH sustained tail electrons. The drive mechanisms are different between the two cases, namely, the coupling to the bulk electrons causes an increase in the bulk electron temperature which enhances the damping of the LHW and then the plasma current. The drive efficiency, however, stays constant. On the other hand, the second case is due to the coupling of the ECW to the LH sustained tail. There are marked different results between the two cases. In the former case, the increased current does not decrease after the ECH pulse, which implies that a new saturation level is set for the LHW current drive by the effect of bulk ECH, for instance, by increase in the bulk electron temperature. On the other hand, in the latter case, the current decrease after the end of the ECH pulse, indicating that the increased current is attributed to the ECW. The time behaviour of the density is also different between the two cases as shown in the figure. The

density drop of $B_{t0} = 1.0$ T case is larger than that of $B_{t0} > 1.1$ T case in which a gradual increase in density occurs after the small density drop at the beginning of the ECW pulse. The ECW coupling to the trapped electrons at the ECR layer in the low field side may affect the particle transport.

The resonant energy of an electron is obtained as shown in Fig. II.5-1(c) by the relativistic ECR condition

$$1-s\omega_{ce}/\omega - n_{//}v_{//}/c = 0 \qquad (s = 1, 2, 3, \ldots).$$

A divergence of the microwave beam from the horn antenna gives a spread of $-0.26 < n_{//} < -0.09$. Owing to the 2nd harmonic resonance ($s = 2$), ECW couples to the tail electrons at the center of the vessel which have the energy of $12 \sim 27$ keV in $B_{t0} = 1.15$ T ($r_0 = .10$ m) cese, $20 \sim 45$ keV in $B_{t0} = 1.20$ T ($r_0 = .16$ m) case and $45 \sim 85$ keV in $B_{t0} = 1.30$ T ($r_0 = .28$ m) case. The resonant energy of the plasma core shifted inside is even higher. The energy spectrum analysis of the soft X-ray radiation shows that an increase of the photon counts of energy up to 80 keV occurs and the increment is a few times as large as the radiation from the LH sustained plasma. The contribution from the $s = 3$ resonance seems to be small which is derived from the negligible I_p in $B_{t0} < 0.8$ T cases. The soft X-ray measurement shows also that the emission region is highly localized inside of the center of the chamber during the ECH pulse, implying that the current channel is localized inside. In the $B_{t0} = 1.40$ T case in which no bulk ECR layer exists in the plasma column, the coupling to the tail electrons is detected by the ECE measurement in spite of no increase in the current. The increase in I_p decreases as the plasma density increases because of the decrease of the LH tail.

These observations show the coupling of the ECW to the high energy tail electrons satisfying the resonance condition, and resulting localized current channel. It brings the possibility of the formation of the hot electron channel in the high temperature tokamak plasmas which is proposed to stabilize the high beta tokamak plasmas[5].

5.3 Bulk electron heating by the second harmonic X-mode ECH

Bulk ECH by a 28 GHz fundametal ($s = 1$) wave was investigated on

the JFT-2 tokamak by launching three different modes[6]. In the JFT-2M, the bulk ECH by the 60 GHz 2nd harmonic (s = 2) X-mode is studied. The calculated absorption in single path is given in Fig. II.5-2(a). The absorption rate increases with plasma density n_e and electron temperature T_e of the ECR layer. More than 80 % of the wave power is absorbed in the parameter region of $T_e > 500$ eV and $n_e > 1.0 \times 10^{19}$ m^{-3}. Therefore the local core heating by ECH is expected in the JFT-2M.

The experimental result of the density dependence of the increase of the center electron temperature ΔT_{eo} and the value $\Delta\Lambda \equiv \Delta(\beta_p + l_i/2)$, where β_p denotes poloidal beta value and l_i denotes the internal inductance, are plotted in Fig. II.5-2(b). Calculated cutoff density of X-made and O-mode is expressed by arrows in the abscissa. It is shown that the wave cutoff occurs above the right hand cutoff density. The ΔT_{eo} which is linear in rf power in $r_o = 0$ m case, depends much on r_o as shown in Fig. II.5-2(c). In the off-center heating in which $r_o = -0.13$ m, +0.18 m, no increase in T_{eo} is observed. However, a drop in the loop voltage and increase of the laser electron temperature around the ECR layer are obtained. Namely, the temperature profile becomes broad. The change in l_i affects $\Delta\Lambda$ and the effect is not negligible, because the increase in β_p is small due to the decrease of the joule power during the ECH pulse the power of which is less than the jould power. The density drop by ECH was large in the off-center heating and was proportional to the plasma density as were observed in the 28 GHz ECH on the JFT-2. A comparison with the fundamental ECH shows almost the same core heating efficiency $\eta \equiv \Delta T_{eo}\, \bar{n}_e / P_{rf}/R = 5 \times 10^{19}$ eV/kW/m^4.

These observations show the local heating and the possibility of the profile control by the 2nd harmonic X-mode ECH. No impurity problem is observed up to the power level of 80 kW, which is one of the advantages of ECH.

References

1) N.J. Fisch and A.H. Boozer, Phys. Rev. Lett., 45, 720 (1980).
2) O.C. Eldridge, ORNL/TM-7503 (1980).
3) I. Fidone, G. Giruzzi, G. Granata et al., Phys. Fluids, 27, 2468 (1984).

4) Y. Uesugi, K. Hoshino, T. Yamamoto et al., submitted to Nucl. Fusion.
5) J.Y. Hsu, C.S. Liu, R. Prater et al., GA-A 17731 (1984).
6) K. Hoshino, T. Yamamoti, A. Funahashi et al., J. Phys. Soc. Jpan., 54, 2507 (1985).

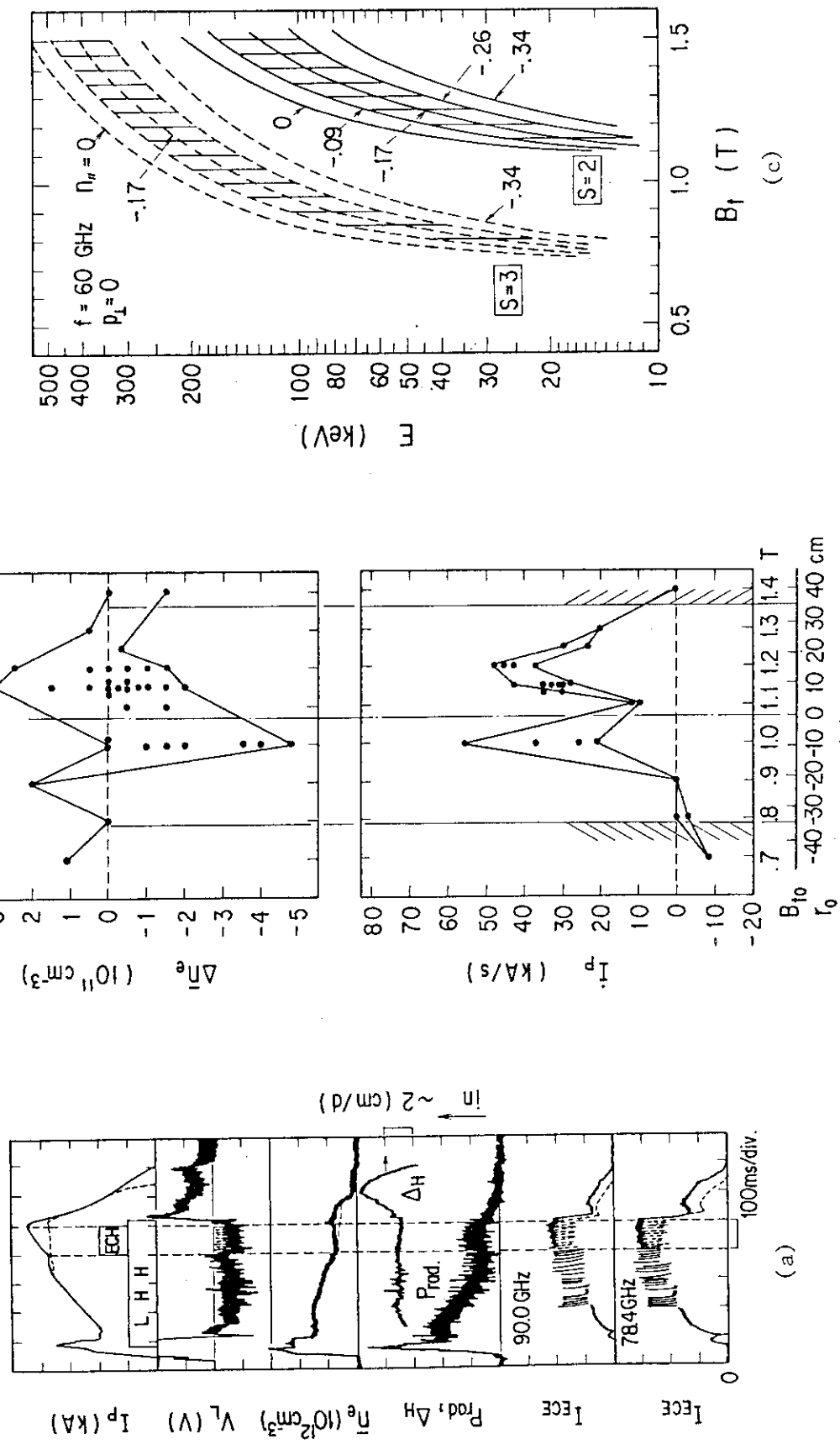

Fig. II.5-1(a) Time evolutions. B_{t0}=1.15T, P_{LH}=P_{ECH}=70kW. Δ_H denotes the displacement of the plasma column.
(b) I_p and $\Delta\bar{n}_e$ during the ECH pulse. r_0 denotes the minor position of the bulk ECR layer (s=2).
(c) Resonant energy v.s. the local magnetic field B_t. s denotes the harmonic number of the ECR.

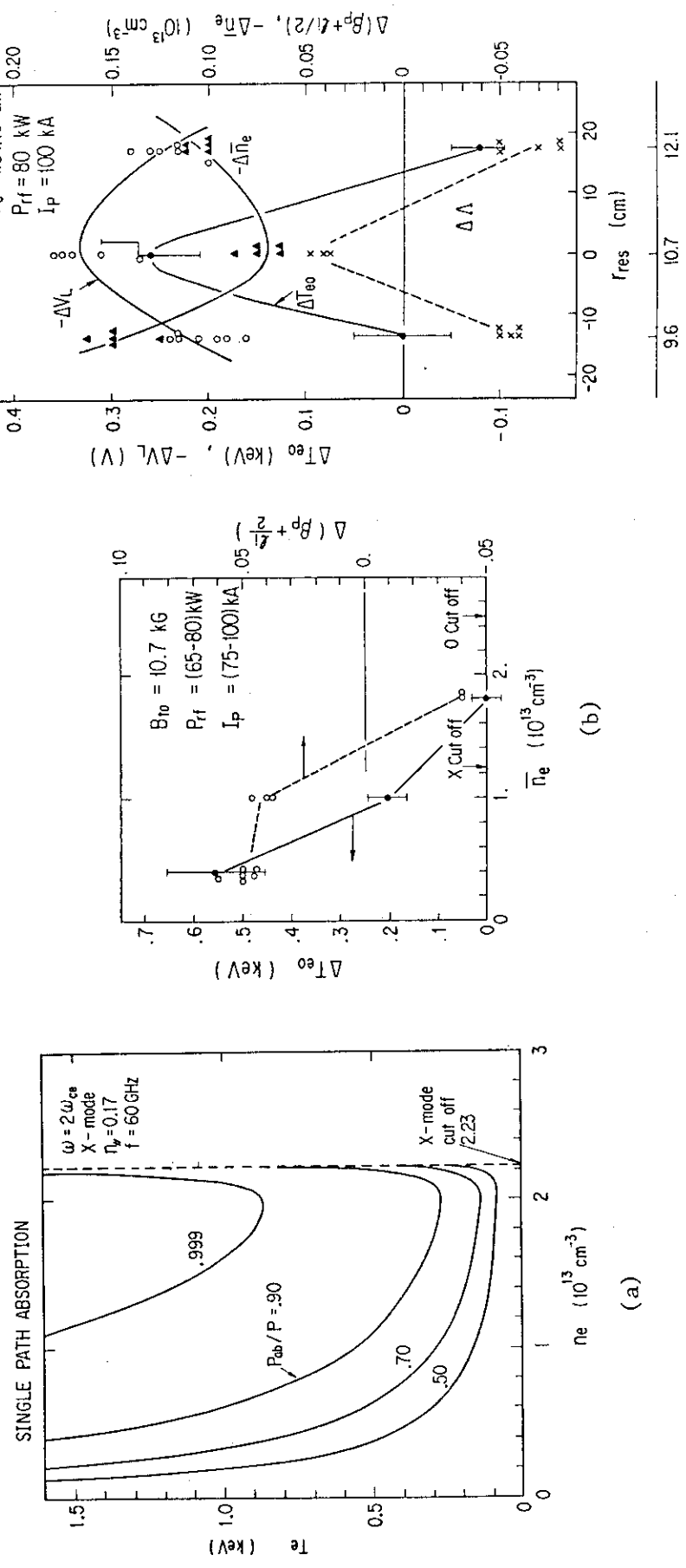

Fig. II.5-2(a) Calculated power absorption rate P_{ab}/P_{rf} at the 2nd harmonic ECR layer. f=60GHz, $n_{//}$=0.17. Cutoff of the X-mode occurs at $n_e=2.23\times10^{19}m^{-3}$ which is the right hand cutoff density.

(b) Density dependence of the increase in the center electron temperature ΔT_{eo} and the value $\Delta\Lambda\equiv\Delta(\beta p+l_i/2)$. Position of the ECR layer is at the center of the chamber r_o=0m. Base $T_{eo}\simeq700$eV (low density case) and $T_{eo}\simeq600$eV (higher density cases).

(c) Dependence on the minor position of the ECR layer. $\bar{n}_e=1.0\times10^{19}m^{-3}$, P_{rf}=80kW, I_p=100kA.

6. Diagnostics in JFT-2M

6.1 Rotational raman scattering of hydrogen for calibrating a thomson scattering device

6.1.1 Raman Scattering[1),2)]

Hydrogen gas fills the JFT-2M tokamak, whose pressure is changed from 60 to 200 Torr. Six different pressures in between are selected for the Raman scattering calibration. The rotational anti-Stokes Raman lines (6776 and 6671 Å) of hydrogen are used for the calibration. The physical characteristics of these lines are tabulated in Table II.6. The 6776-Å Raman line passes through the first spectral channel at the four positions of scattering angle 80°, 84°, 88°, and 92°, and the first and second spectral channels at the two positions of scattering angle 90° and 100°; another Raman line 6671 Å passes through the second spectral channel at the four positions and the second and third spectral channels at the two positions. Therefore, the 6776-Å Raman line is more important for the electron density calibration.

The Raman scattered signal is

$$S_K^R(\theta) = n_{H2}(J) I_R \frac{d\sigma_R}{d\Omega} \Delta\Omega_\theta \ell_\theta \gamma_\theta \left(\frac{S_{k,\theta}}{N_{k,\theta}} \right) \eta_{k,\theta} \rho_{k,\theta}(\lambda_R) T_{k,\theta} / h\nu_R. \quad (1)$$

Substituting $n_{H2} = 0.114$, $I_R = 8 \times 10^6$ erg, $d\sigma_R/d\Omega = (2.26 \text{ and } 2.86) \times 10^{-31}$ cm^2·sr^{-1}, $\Delta\Omega_\theta = 2.07 \times 10^{-2}$ sr, $\ell_\theta = 1.67$ cm, $\gamma_\theta = 0.96$, $(S_{k,\theta}/N_{k,\theta}) = 1.5$ count, $\eta_{k,\theta} = 0.08$, $\rho_{k,\theta}(\lambda_R = 6776 \text{ Å}) = 0.72$, $T_{k,\theta} = 0.06$, and $h\nu_R = 2.97 \times 10^{-12}$ erg into Eq. (1), the theoretical value at the scattering angle 80° is

$$S_{k=1}^R(80) = (0.41 \text{ and } 0.52) N_{H_2} \text{ count}. \quad (2)$$

The theoretical value of Eq. (2) is shown in Fig. II.6.1 with the thin solid straight line and the broken line corresponding to cases A and B in Table II.6.1, respectively; the theoretical value $(0.74 \text{ and } 0.94) N_{H_2}$ at the scattering angle of 100° is shown in Fig. II.6.1. The difference below 10% between experiment and theory is due to the uncertainty of each Raman scattering cross section ±3 % which is derived from the quoted value of γ_{00}, and the signal per photoelectron ±3 % and the error of the vignetting or plasma spillage ±2 %, the transmittance of

observation window and light collection optics ±10 %, and the gas filling pressure ±2 % in Eq. (2). The uncertainty of laser power is negligible. The resulting uncertainty in theory is ±11 %. The representative error in the experimental value in Fig. II.6.1 is due to the photoelectron statistics. This agreement between experimental and theoretical values in Fig. II.6.1 shows the evidence that signals from hydrogen gas are caused by the Raman effect. The Raman scattered signals are proportional to the relative laser energy as shown in Fig. II.6.2, which also shows that the signals are caused by the Raman effect.

6.1.2 Calibration constant and estimation of electron temperature and density

In the calibration experiment for a simultaneous six-position Thomson scattering device, the closely related two light sources, namely, Raman scattered light and LED light, are available to get the calibration constants for all channels: A detailed report of calibration constant $K_{i,\theta}$ was published recently[5]. This calibration experiment is performed simultaneously at six positions with six LED lights, whose incident light intensity is changed by the neutral density filter. The wavelength intensity of the LED light source is calibrated by a W-standard lamp. The experimental results of the normalized sensitivity $K_{i,\theta}$ and the signal per one photoelectron created at the PM tube photocathode are described in refs. 1-2).

Next, we discuss the calibration constant $C_{R,\theta}$ obtained from the Raman scattering.

Substituting total Thomson cross section $\sigma_T = (8\pi/3)\ 7.94 \times 10^{-26}$ cm^2, $S^R_{k=1}(80)/n_{H_2}(2) = 3.60$ count $\times$ Torr^{-1} from Fig. II.6.1, $E_R = 140$ counts and total Raman cross section σ_0 from Table II.6.1 into the following equation:

$$D_{R,\theta} = \frac{d\sigma_T}{d\Omega} S^R_k(\theta)/[n_{H_2}(J)E_R \frac{d\sigma_R}{d\Omega} \rho_{k,\theta}(\lambda_R)] \qquad (3)$$

the Raman constant $C_{R,\theta}$ at the position of scattering angle $\theta = 80$ is given by

$$C_{R,\theta} = 1.9 \times 10^{-13}\ \text{cm}^3. \qquad (4)$$

The uncertainty based on Photoelectron statistics is ±4 %. The resulting

uncertainty in the Raman constant is given by

$$\frac{\Delta C_{R,\theta}}{C_{R,\theta}} \simeq \pm\sqrt{\left(\frac{\Delta S_k^R(\theta)}{S_k^R(\theta)}\right)^2 + \left(\frac{\Delta n_{H_2}(J)}{n_{H_2}(J)}\right)^2 + \left(\frac{\Delta\sigma_0}{\sigma_0}\right)^2} \simeq \pm 0.08, \qquad (5)$$

where the Raman cross section and the number density of hydrogen occupying th J_{th} rotational level in one gas filling pressure are constant since the room temperature is almost constant during the Raman scattering experiment.

In the JFT-2M plasma with additional heating, both neutral beam injection heating (NBI) of 500 kW from 350 to 450 msec and ion cyclotron range frequency heating (ICRF) of 500 kW from 380 to 430 msec, typical electron temperature and density profiles are measured at the top and bottom of the sawtooth oscillation as shown in Fig. II.6.3. During all the additional heating shown in Fig. II.6.3, one can find large sawtooth oscillation with a 300-eV change in electron temperature, a sharp electron-temperature profile at the top of the sawtooth oscillation compared with that of NBI heating only, and an increase in electron density during the ICRF heating.

Explanation of symbols:

$n_{H_2}(J)$: the number density of hydrogen occupying the J_{th} rotational level

I_R : the laser energy

$\frac{d\sigma_R}{d\Omega}$: the differential Raman cross section for anti-Stokes radiation

$\Delta\Omega$: the effective solid angle of scattering light collection

ℓ_θ : the effective length of scattered light

γ_θ : the loss ratio due to vignetting or plasma spillage into the vessel observation window

$S_{k,\theta}/N_{k,\theta}$: the output signal per one photoelectron

$\eta_{k,\theta}$: the quantum efficiency of the PM tube

$\rho_{k,\theta}(\lambda_R)$: the k_{th} channel response normalized to the integrated Raman line

$T_{k,\theta}$: the transmittance of the k_{th} spectral channel

$h\nu_R$: the photon energy

N_{H_2} : the number density of hydrogen moleculars

E_R : the relative laser energy for the Raman scattering measurement

n : the principal quantum number

J : the rotational level

γ_{00} : the anisotropic polarizability for the initial and final states in the ground vibrational level

$\Delta\nu$: the frequency shift

σ_0 : the total cross section for the pure rotational lines in terms of the number of photons scattered for unit incident photon flux

B_0 : the rotational constant for H_2 gas

F : the rotation partition function

I : the nuclear-spin quantum number

g_J : the statistical weight factor dependent on the nuclear spin

θ : the scattering angle

References

1) T. Yamauchi and I. Yanagisawa : Appl. Opt. 24 (1985) 700.

2) T. Yamauchi, I. Yanagisawa and H. Kawashima : Jpn. J. Appl. Phys 23 (1984) 1389.

3) R.W. Carlson and W.R. Fenner : Astrophys. J. 178 (1972) 551.

4) N.J. Bridge and A.D. Buckingham : Proc. R. Soc. London Ser. A295 (1966) 334.

5) I. Yanagisawa and T. Yamauchi : JAERI-M84-186 (1984) (in Japanese).

Table II.6-1 Physical characteristics of two Raman lines (Case A is derived from the experiment of Carlson and Fenner[3] and case B is derived from the experiment of Bridge and Buckingham.[4])

	Raman line(Å)	n	J	$\Delta\nu(cm^{-1})$	$\gamma_{oo}(cm^3)$	$\sigma_o(cm^2)$	$n_{H2}(J)/N_{H2}$	$Bo(cm^{-1})$	Q	I	g_J
A	6776	0	2 → 0	354.6	$0.353\cdot10^{-24}$	$3.43\cdot10^{-30}$	0.114	59.3	6.89	1/2	1
	6671	0	3 → 1	587.3	$0.373\cdot10^{-24}$	$5.24\cdot10^{-30}$	0.082	59.3	6.89	1/2	3
B	6776	0	2 → 0	354.6	$0.314\cdot10^{-24}$	$2.71\cdot10^{-30}$	0.114	59.3	6.89	1/2	1
	6671	0	3 → 1	587.3		$3.71\cdot10^{-30}$	0.082	59.3	6.89	1/2	3

(at 293 K)

Table II.6-2 Calibration constant $C_{R,\theta}$ by the Raman scattering experiment.

Position	$C_{R,\theta}$ (cm^3)
1	$1.98 \cdot 10^{-13}$
2	$1.68 \cdot 10^{-13}$
3	$1.78 \cdot 10^{-13}$
4	$1.93 \cdot 10^{-13}$
5	$1.48 \cdot 10^{-13}$
6	$3.44 \cdot 10^{-13}$

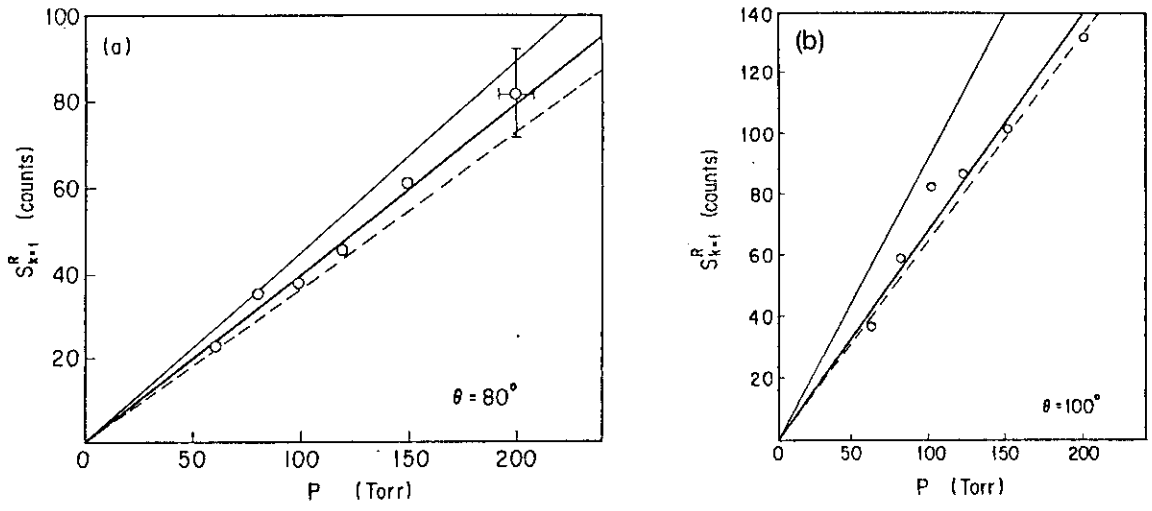

Fig. II.6-1 Raman scattered signals of hydrogen gas pressures 0-200 Torr at the scattering angles 80°. The thin solid straight line and the broken line show the theoretical values which depend on cases A and B in Table I, respectively. (a) Scattering angle θ=80° and first chnnel, (b) θ=100° and first channel.

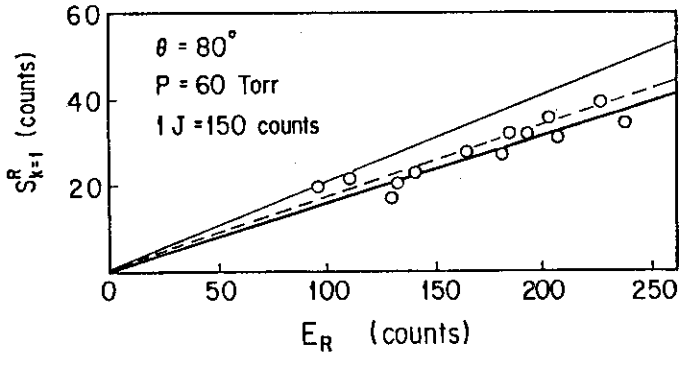

Fig. II.6-2 Raman scattered signals proportional to the relative laser energy. The hydrogen gas pressure is 60 Torr and the scattering angle is 80°. The thin solid straight line and the broken line show the theoretical values which depend on cases A and B in Table I, respectively.

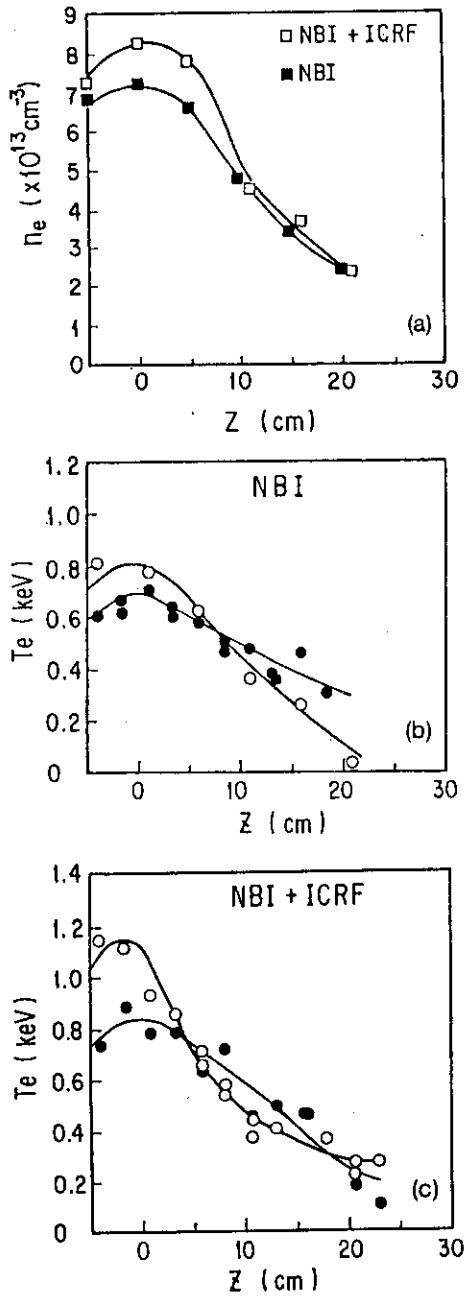

Fig. II.6-3 Electron temperature Te and density n_e profiles in the NBI (500 kW) and NBI+ICRF (1 MW) heating plasma. The o and ● represent the top and bottom of the sawtooth oscillation (Te figure), the □ and ■ represent the NBI+ICRF and NBI heating plasma (n_e figure), respectively. (a) Electron density profiles, (b) electron temperature profiles in NBI, and (c) electron temperature profiles in NBI+ICRF.

6.2 Far infrared laser interferometer in the JFT-2M tokamak[1)]

6.2.1 Introduction

A HCN laser interferometer with three vertical chords was installed in the JFT-2M tokamak for electron density measurement. The optical arrangement of the interferometer is a Mach-Zehnder type and mechanically independent of the JFT-2M in order to suppress the mechanical vibrations. Two HCN lasers are employed for direct reading of the electron density by means of the beat modulation method. The beat frequency of two lasers is stabilized around 500 kHz by adjusting the cavity length. Transmission characteristics of a dielectric waveguide are investigated and the optimum configuration of the waveguide and TPX lens for compensation of the refraction and divergence of the laser beam is obtained.

6.2.2 HCN laser interferometer

The optical arrangement of the interferometer is shown in Fig. II.6-4. A probe laser beam is splitted into three vertical beams. Two matching concave and convex mirrors are used to transform a divergent beam into a convergent one with its beam waist at the meridian plane of the plasma. The diameter of the beam waist is 17 mm. Crystal quartz plates are employed for vacuum windows. A combination of the Pyrex waveguides and TPX lenses are employed to compensate the refraction and divergence of the beams. TPX lenses are designed to place the crossing point between the optical axis and the laser beam at the center of the waveguide mouth.

The HCN laser is a waveguide laser with a cavity length of 2.5 m and a discharge length of 2 m. To avoid thermal expansion of the cavity, mirror mounts are fixed by four invar rods and connected with the laser tybe by bellows. The axial discharge is maintained by a DC power supply of 5 kV, 1.5 A. The output power of the laser is about 40 mW. The Schottky barrier diode*) is employed for detection of the beat singals. The output beat signals of three channels and the reference beat signal are introduced to the counter circuit to convert the phase modulated beat signals to the time variation of the electron density.

6.2.3 Characteristics of the waveguide[2)]

In this interferometer, the waveguides of Pyrex glass are used to compensate the refraction and divergence of the laser beam. It is

expected that TPX lens bends the refracted beam to the optical axis and the waveguide compensates the inclination between the beam axis and optical one, and suppresses the beam divergence. The transmission coefficient of the waveguide as a function of the distance between the beam waiste and the waveguide mouth is shown in Fig. II.6-5. The incident beam is Gaussian and the incident angle is 0°. The transmission has a weak dependence on Z since the beam diameter (d) at the waveguide mouth is much smaller than the waveguide diameter (D). The beam profiles are shown in Fig. II.6-6, taking the incident angle as a parameter. In the present experiments, the plane of the polarization is parallel to the incident plane. The beam profile near the waveguide exit ($\ell = 2$ cm) show complex patterns caused by the higher modes of the waveguide. When the incident angle is oblique to the guide axis, the peak moves toward the beam axis as shown in Fig. II.6-6. However, the beam profiles at $\ell = 70$ cm apart from the waveguide exit show that the peak comes close to the guide axis. From these observations, it is concluded that the waveguide compensates the deviation of the beam from the optical axis. The transmission of 75 % is obtained within the incident angle of 1°.

6.2.4 Summary

HCN laser interferometer was installed in the JFT-2M tokamak. The main features of the present experiments are as follows;

(1) The interferometer has a simple structure of Mach-Zehnder type and is not affected by mechanical vibrations.

(2) The compensation of the refraction and divergence of the laser beams can be done by a combination of TPX lens and dielectric waveguide.

References

1) Conf. Digest of the 9th Int. Conf. on Infrared and Millimeter Waves, Takarazuka, Japan, 1984, W-5-7.

2) J.P. Crenn, Trans. on Microwave Theory and Techniques, MTT-27 (1979) 573.

*) Development of the schootky barrier diode is supported by the Ministry of Education, Science and Culture by a grant for energy research (fusion).

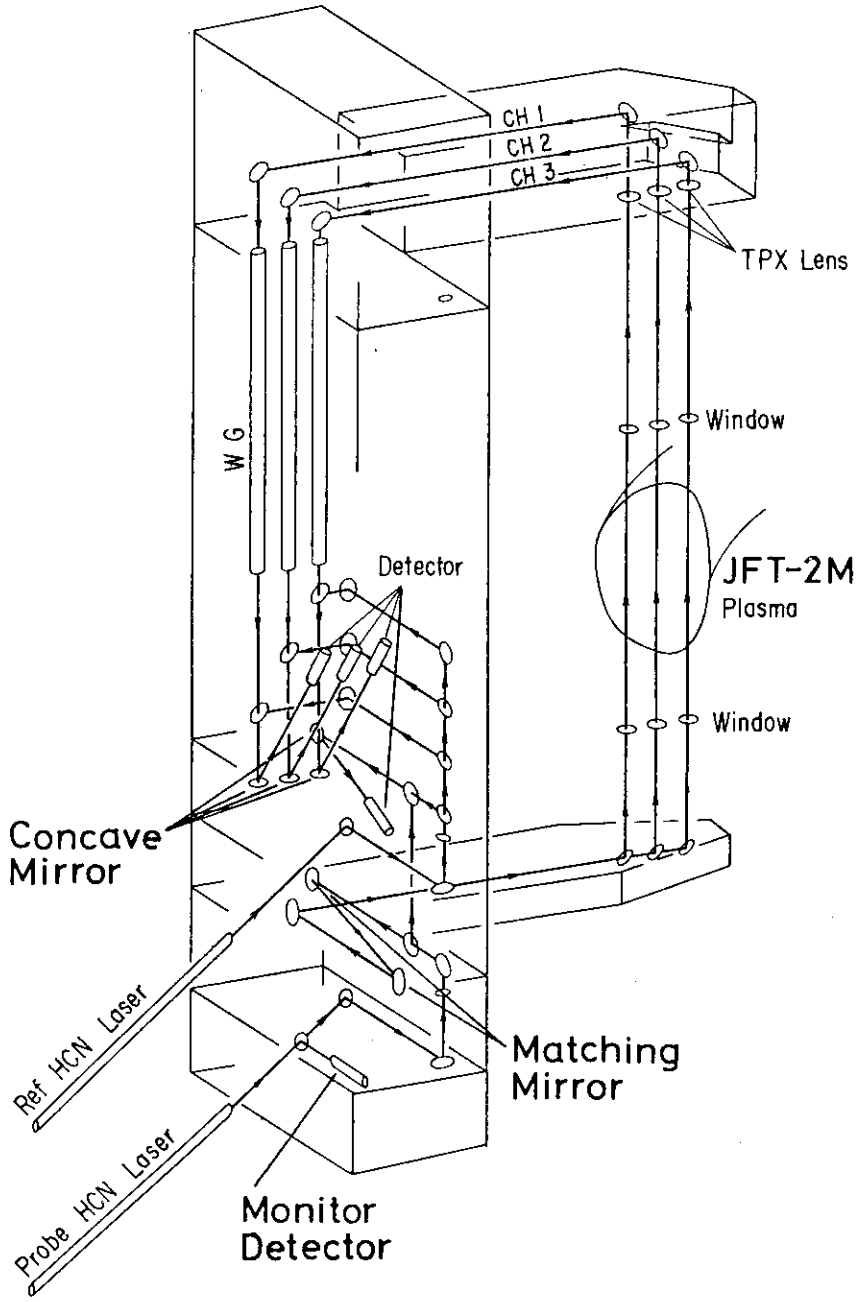

Fig.II.6-4 Schematic diagram of the HCN laser interferometer.

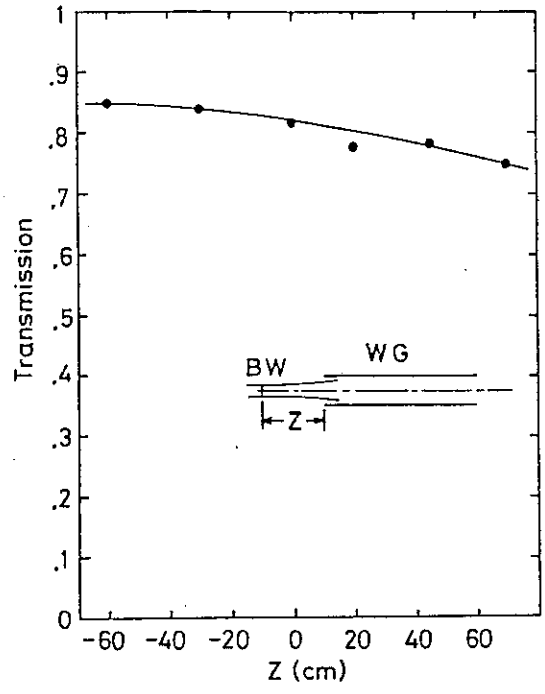

Fig. II.6-5 Transmission coefficient as a function of the distance between the beam waist and the guide entrance, The distance Z has a plus value when the beam waist is located outside the guide.

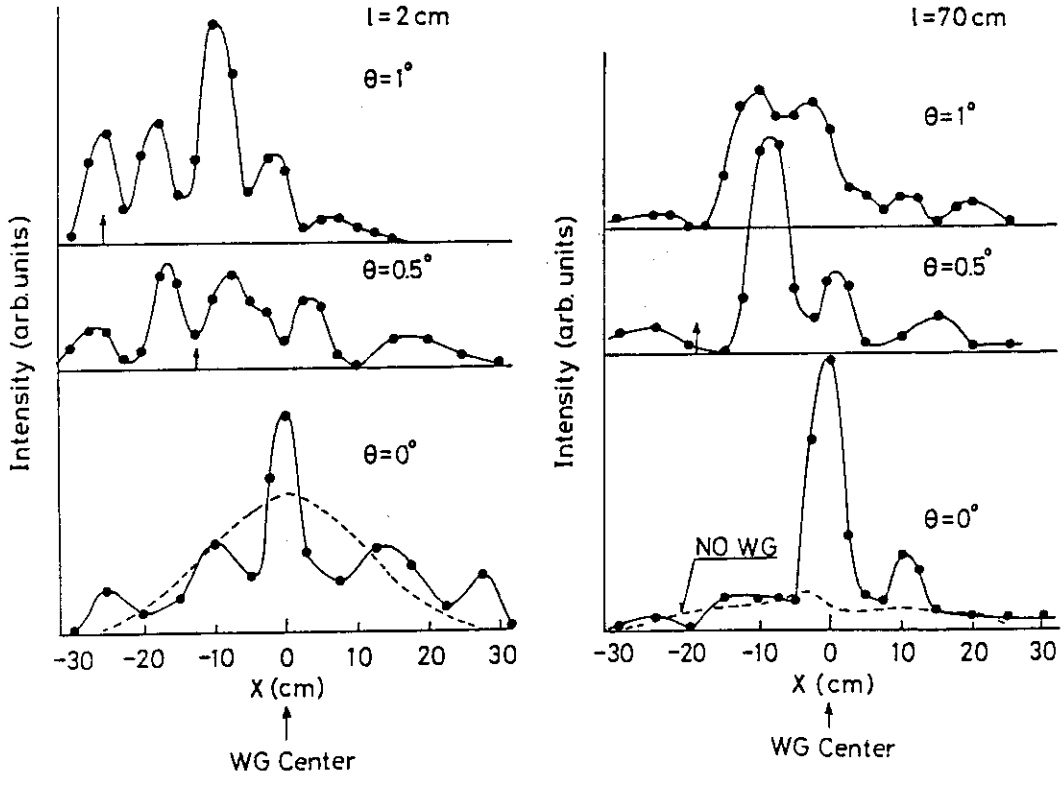

Fig. II.6-6 Intensity profile of the beams through the waveguide, where ℓ is the distance between the guide exit and the detector. Arrows show the center of the beam without the guide. The dooted line in the left hand shows the theoretical profile of the Gaussian beam.

III. OPERATION AND MAINTENANCE

1. Introduction

Facility Operation and Engineering Division has been engaged in operation and maintenance of JFT-2M tokamak, Neutral Beam Injection (NBI) system, Lower Hybrid Heating (LHH) device and flywheel motor-generator (MG), and development of auxiliary equipments and instruments. NBI, LHH and MG have been operated smoothly on schedule and also done the maintenance of those devices.

2. Operation and Maintenance

JFT-2M tokamak was operated on schedule in spite of a few troubles on a toroidal field coil, vacuum system and poloidal field power supply owing to the suitable treatment of members. Modes of operation were that in the first half ICRF and/or NBI heating experiments were done and in the latter half current drive experiment used by LHH and ECH were accomplished.

NBI system was operated smoothly on experimental schedule and has been remodelled in gas injection system for reliable beam injection.

Power supply of LHH device was remodelled in the crowbar circuit for protecting klystron tube from spike voltages and in the control circuit for obtaining the long duration (0.5 s) of oscillation, and the device was operated on schedule. The operation schedule of JFT-2M, NBI, LHH and MG is shown in Table III. 2-1.

3. Development of Equipments and Instruments

3.1 Pellet injection system

Pellet injector of which speed was 600 ∿ 800 m/s and diameter and length were 1 mmϕ and 1 mm, respectively, adjusted and operated, and a

fuelling experiment in JFT-2M was performed. Its results were as follows that a mean electron density increased to $5 \sim 7 \times 10^{12}$ cm^{-3} and judging from the observation of H_α intensity the pellet arrived into a half diameter of the plasma. For increasing the pellet volume the diameter and length of the pellet carrier have been increased to 1.65 mmϕ and 1.65 mm, respectively.

3.2 TV monitoring of plasma

High speed video (color) and optical system which can record and play 200 field per second and can shorten its exposure time at 20 μs has been installed. It was able to show a cross section of noncircular plasma as shown in Fig. III.3.2-1.

3.3 Electron cyclotron resonance discharge cleaning (ECR-DC)

Reducing light impurities (carbon, oxygen, etc.) on the first wall is very important in tokamak for producing the better plasma, and a baking and a discharge cleaning have been usually employed for the procedures. As discharge cleaning Taylor-type discharge cleaning (TDC) has been used usually, however, has some demerits which are bad access to the tokamak device for generating X-ray and expensive power supply. For improvement of these demerits ECR-DC method has been developed and the equipment was installed in JFT-2M, of which main parts are RF power supply (2.45 GHz, 5 kW CW) and two launchers with helical antenas.

Effects of ECR-DC were experimented as observing volatile gases-water vapour, methane and carbon menoxide-produced by chemical reactions of hydrogen atoms and metal oxide on the wall, and the result was the very effective producing of water vapour. In-situ observation of the surface on Mo sample used by Auger electron spectroscopy was performed, and the resultant figure as shown in Fig. III.3.3-1 showed that oxygen reduced and disappeared for an hour and Mo substrate was exposured. The experiment indicated moreover that ECR-DC was the same effect as TDC on producing the tokamak plasma.

3.4 Monitoring of NBI power

A calorimeter as shown in Fig. III.3.4-1 was settled in JFT-2M for measuring real injection power into the plasma, which was also able to measure the spatial distribution of the beam by only one injection, and the result is showed in Fig. III.3.4-2.

Table III.2-1 Operation of JET-2M, NBI, LHH and MG.

(Month)	1984 4 5 6 7 8 9 10 11 12	1985 1 2 3
JFT-2M	— operation and maintenance	construc-tion / operation and maintenance
NBI	operation and maintenance	
M-G	operation and maintenance	
LHH	operation and maintenance	

Detail of the operation (JFT2M, NBI, M-G and LHH)

	(Fiscal year)	1983	1984 APR-JUN	1984 JUL-SEP	1984 OCT-DEC	1985 JAN-MAR	TOTAL
SFT -2M	Total days of operation (days)	128	29	38	45	20	132
	Times of discahrge (shots)	7657	1694	3428	2935	1238	9288
	Baking (times)	6	3	1	1	1	6
	Discharge Cleaning (hours)	219.3	72.3	54.8	45.1	17.6	189.8
	Vent. of vacuum chamber (times)	5	2	2	0	2	6
NBI	Total days of operation (days)	85	17	14	0	14	45
	Flashing and Injection (shots)	A: 3614 B:13169	A:2460 B:2406	809 1172	0 0	1815 148	A:5084 B:3722
	Conditioning (shots)	A:16151 B:21982	A:2464 B:2483	910 2662	0 0	2218 1758	A:5592 B:6309
	Vent. of vacuum tank (times)	2	3	1	0	1	5
	Change of filament (time)	A: 2 B: 1	1 1	0 1	0 0	1 0	A: 2 B: 2
M-G	M-G (#1) (hours)	1115	257	348	307	192	1104
	M-G (#2) (hours)	1104	255	345	304	192	1096
LHH	Total days of operation (days)	20	0	0	34	5	39
	Times of power injection (times)	1454	0	0	2397	0	2397

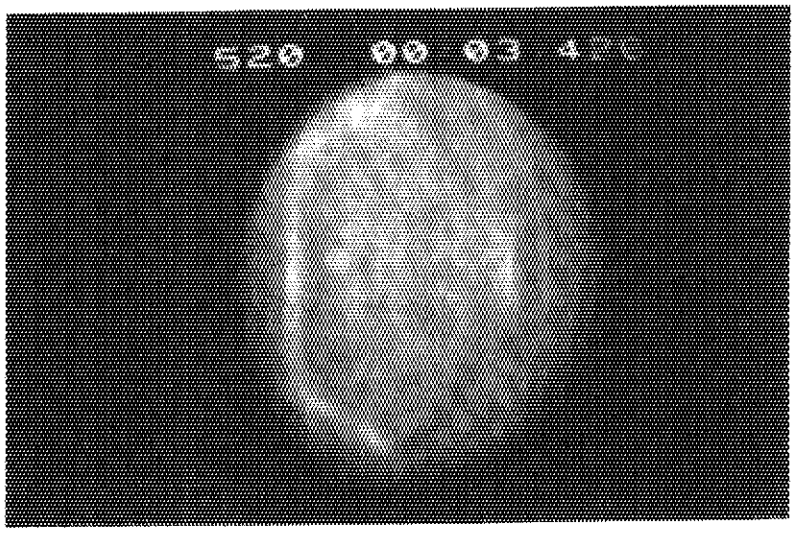

Fig. III.3.2-1 Photograph of cross section of plasma by TV monitoring.

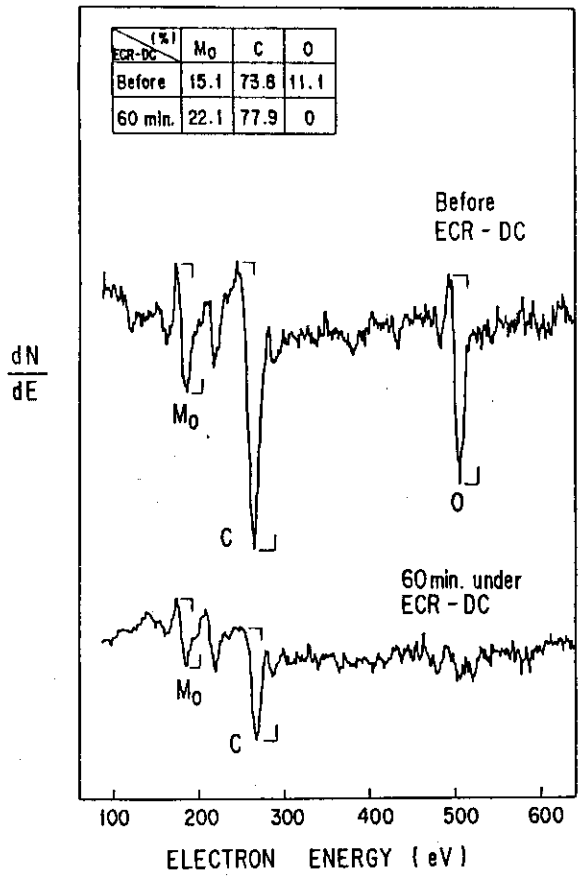

Fig. III.3.3-1 Auger electron spectra in ECR-DC

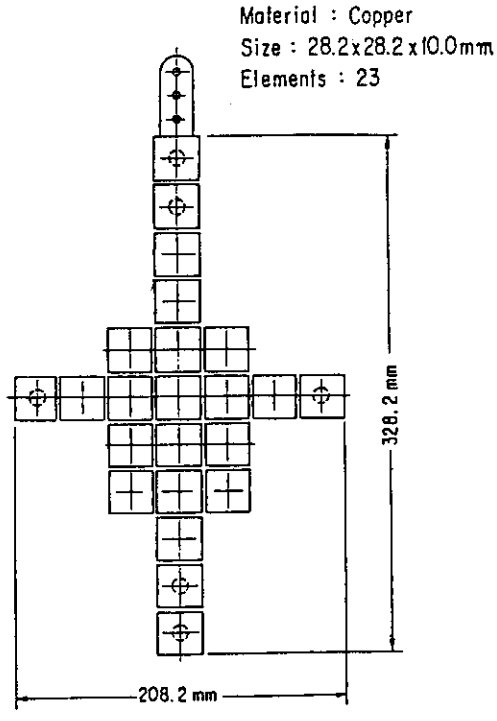

Fig. III.3.4-1 A schematic view of calorimeter's sensors

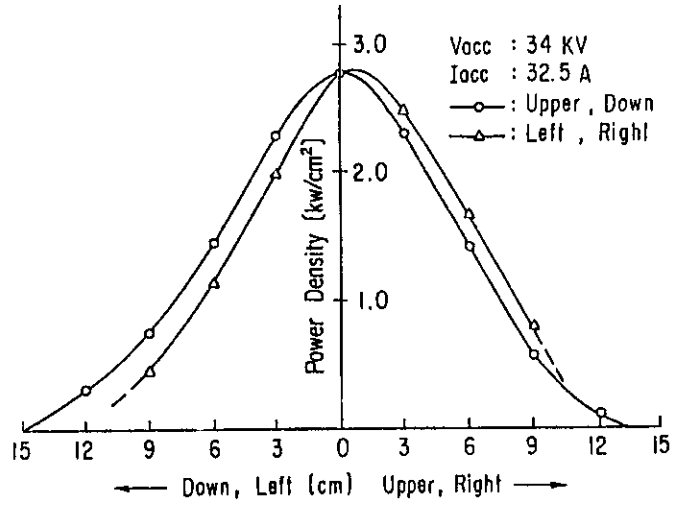

Fig. III.3.4-2 A spatial distribution of injection beam in the vacuum chamber of JFT-2M

IV. DEVELOPMENT OF PLASMA HEATING SYSTEM

1. Neutral Beam Injection System

1.1 Ion source development

1.1.1 Improvements of the ion source for JT-60

The ion source for JT-60 NBI is designed to produce ion beams of 40 A at 100 keV for 10 sec. The maximum rated ion beam was extractred in March 1983. Based on the test performed so far, we tried further improvements of the ion source. The effect of the magnetic field on the uniformity of the source plasma is reported.

Influences of an external magnetic field and a field produced by the filament current on the performance of a magnetic multipole ion source were experimentally studied. In the central region of the source plasma, there is a residual field of 10 to 20 Gauss generated by many permanent magnets. When directions of the filament currents were arranged to produce an axial field which directed opposite to the residual field, the ion production efficiency of the source was higher (good direction case). For the reversed direction of the current, the efficiency became lower (bad direction case). When the external field generated by a set of additional coils was imposed to the source and the field strength was changed step by step, the arc efficiency varied as shown in Fig. IV.1-1. Measurements of ion saturation current density profile near the plasma grid surface showed that the more uniform the density profile, the higher the arc efficiency becomes.

1.1.2 Development of a 200 keV, 3.5 A ion source for the helium beam injector

A 200 keV, 3.5 A helium beam injector will form part of a diagnostic system to measure the central ion temperature for JT-60. The required performance characteristics of the ion source for this injector are tabulated in Table IV.1-1. The energy level of this system is of interest since it enables us to foresee the high-voltage problems associated with future plasma heating injectors. The injector beam line was installed in a test bay to facilitate ion source development prior to install on JT-60 on Sept. 1985. A schematic figure of injector is shown

in Fig. IV.1-2. As a result of extraction-grid improvement and power-supply debugging, ion beams of 3.5 A at 200 keV was obtained for 100 ms. Ion beams with 1/e divergence of 0.25 was also obtained at 140 keV. The improvement of the ion source are still now being continued to obtain sharper beam for raising the accuracy of the temperature measurement/1/.

1.1.3 Development of negative ion source

The negative ion based neutral beam system will be required for future fusion reactors in order to achive an acceptable injection efficiency at beam energy higher than 200 keV. Out of sevaral methods of producing negative ion beam, volume production is the most attractive because of no cesium handling and very good extracted beam quality.

The volume production ion source now under study is a tandem multicusp plasma source. This source is composed of piled short chambers so that the chamber depth and the magnetic filter position are variable. This chamber enabled us a systematic survey of ion current density dependence of the depth, filter position, and mean electron temperature. The survey indicated that the negative ion current density increased with the chamber depth in the case of no magnetic filter, but it increased with a decrease in the depth in the case of the filter configuration. Results obtained with 15 cm deep chamber is shown in Fig. IV.1-3. The current density with magnetic filter (dashed line) reached as high as 12 mA/cm^2, but the density without filter (solid line) stays low. When the depth was increased, the dashed line decreased while the solid line increased, reaching nearly equal conditions in the case of 30 cm deep chamber. Ion current density of 15 mA/cm^2 was obtained further reducing the depth to 13 cm.

A temporal variation in the negative ion current density was also observed during the arc pulse. The current density is considerably high for the beginning of the arc discharge of several mili-seconds. This phenomenon is now under investigarion/2/.

1.2 Performance test of JT-60 neutral beam injector

In order to deliver neutral beams of 20 MW into JT-60 plasma, the neutral beam system consists of 14 injector units with 28 ion sources and other systems of power supply, water, vacuum, and control. This

system is so large and complicated that careful inspections as well as ion beam conditioning of every injector unit are necessary for favorable start of the system for the tokamak experiment. The inspection started on April 1985 followed by ion beam extraction test on June, mounting the first unit on the test stand to which the proto-type injector facility was converted. The test was conducted at a rate of a injector per four weeks. Within this period the ion sources were operated approximately 5000 shots and conditioned to the standard operation level of 70 A at 75 keV, 10 s. Extracted beam characteristics were also tested using the optical beam monitor system, the power flow monitor system, and movable calorimeters. The test results indicated that the performance of the injector is satisfactory. Nine injectors were tested and conditioned in this fiscal year. The last unit is scheduled to be performed on August 1985.

1.3 Development of optical beam monitor

In neutral beam injectors, measurement of the spatial and energy distribution of the neutral beams is important to optimize the injection performances. Such a measurement has been done calorimetrically or electrically with probes that are inserted into the beams. As the beam power and the pulse length increase, however, it becomes difficult to use such methods because of thermal destruction. Therefore, optical beam monitoring system has been developed for JT-60 NBI.

The system is composed of a beam profile monitor and a spectroscopic monitor. The beam profile monitor /3/, which aims to monitor the beam divergence and the beam axis deflection angle, employs a charge coupled device (CCD) image sensor as a detector. The beam is imaged by f/2.4 lens on the CCD sensor, which has 384×389 picture elements within the area of 12.7×9.7 mm. As the camera is placed so that the scanning direction is perpendicular to the beam axis, the intensity profile of the electric signal of the scanning lines corresponds to the beam profile. The image information is stored in a digital video memory with a time interval of 1/60 s and the stored information is analyzed by a computer system. In JT-60 NBI, two CCD cameras for horizontal and vertical profiles are installed at the entrance of the beam drift tube. On the opposite side of the camera, a blackened plate with honeycomb board is installed to suppress the reflected light. On the center of

the board, a marker light is guided with a optical fiber cable to indicate the geometrical center of the beam axis.

The neutral beam contains three dominant energy components (H(E), H(E/2) and H(H/3)) and relatively low energy components such as H(E/18) which result from the fragmentation of impurities such as H_2O+. In order to monitor the ratio of these energy components, the spectroscopic monitor with a optical fiber has been developed for JT-60 NBI. The doppler-shifted Balmer alpha light from the fast hydrogen atoms is focused by a telescopic lens and introduced to a optical fiber. The diameter of the core of the fiber is as large as 0.8 mm. The fiber is guided to the accessible room about 100 m from the beamline, where the light is introduced to the spectrometer.

These optical beam montiors have been tested in the test bed of the JT-60 NBI and demonstrated high sensitivity, high resolving power and good reliability.

References

/1/ T. Itoh et al., 4th Int. Sympo. on Heating in Toroidal Plasmas, Rome, Italy, 1984.

/2/ T. Shibata et al., IAEA Technical Committee Meeting on Negative Ion beam Heating, Grenoble, France 1985.
Y. Okumura et al., JAERI-M 84-098 1984.

/3/ Y. Okumura, M. Akiba and K. Mizuhashi, Rev. Sci. Instrum. 55 (1984) 2027.

Table IV.1-1 Specification of ion source for 200 keV He beam injector.

BEAM	He
BEAM ENERGY	40 ~ 200 keV
BEAM CURRENT	3.5 A
BEAM DIVERGENCE	0.4° (1/e)
PULSE LENGTH	0.1 sec
DUTY	1/200

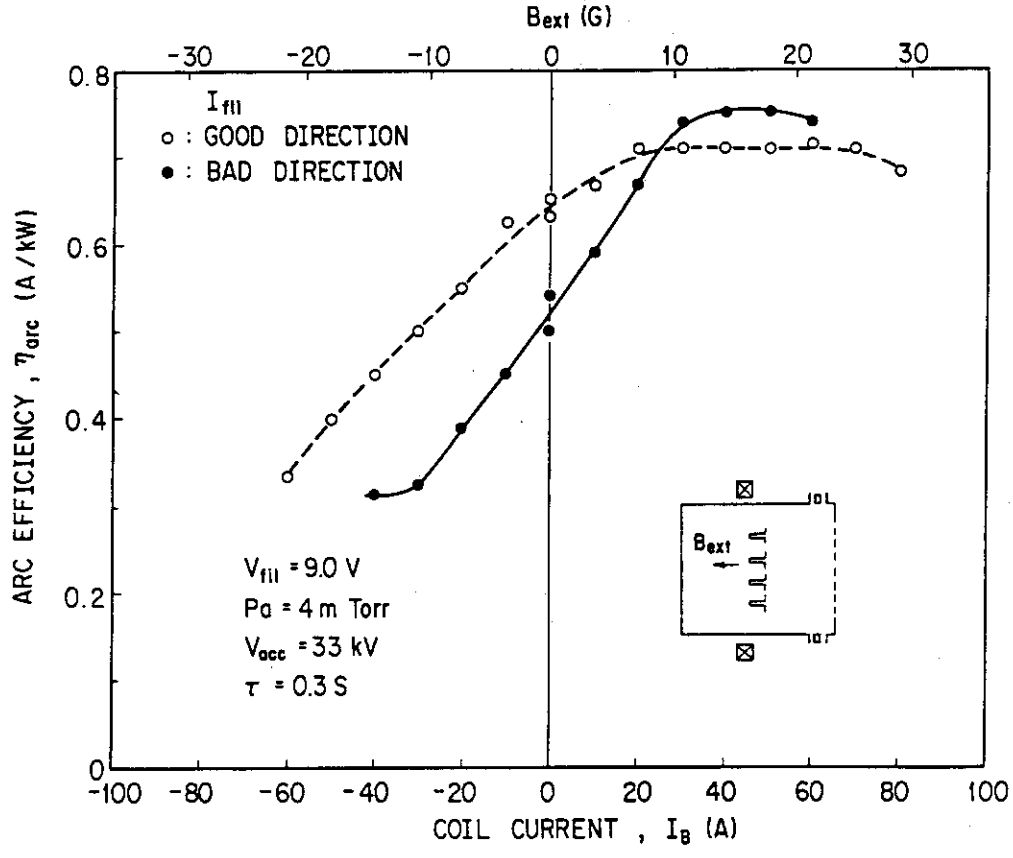

Fig.IV.1-1 Arc efficiency vs external field for both good and bad directions of the filament current.

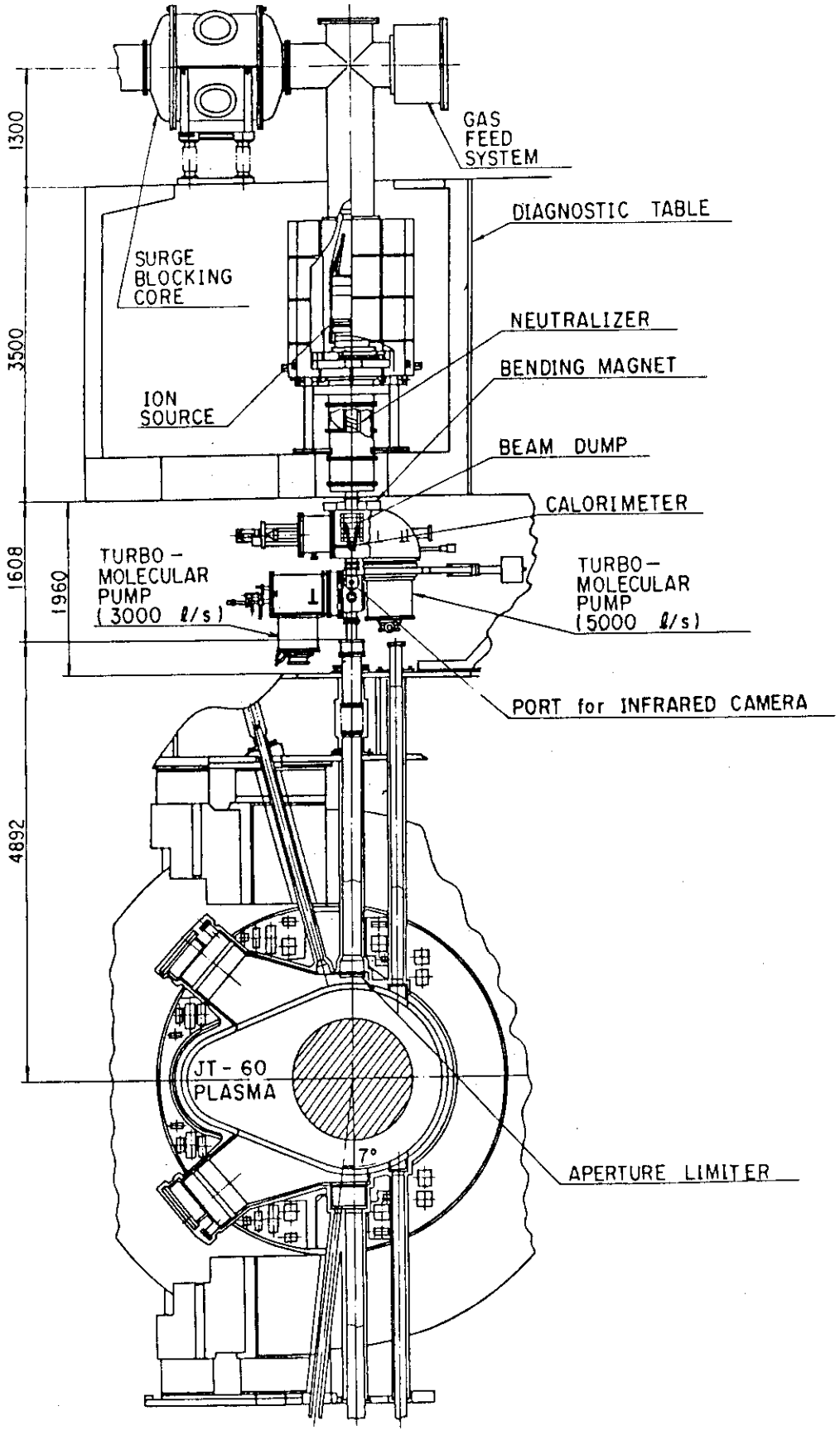

Fig.IV.1-2 Schematic figure of the Helium beam injector.

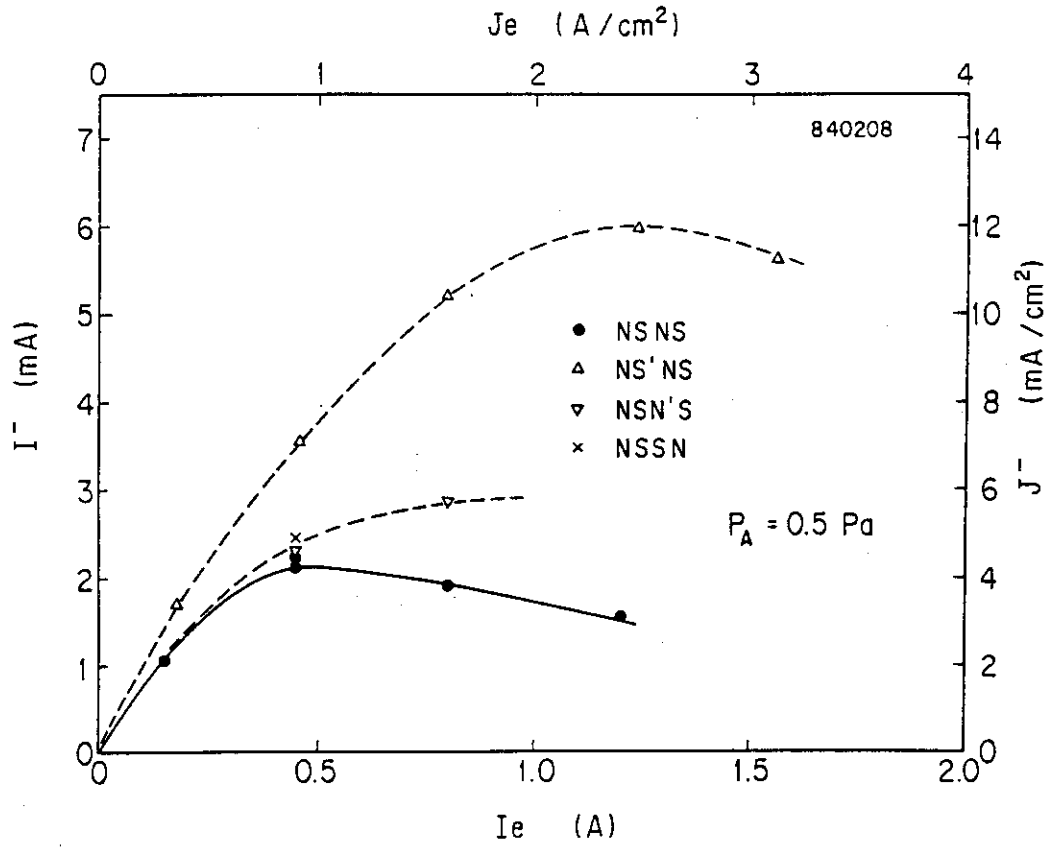

Fig.IV.1-3 H^- current for various magnetic filter configurations for 15 cm high chamber.

2. RF Heating System

2.1 Introduction

The RF heating is a very promising method for high temperature and high density tokamaks. In JT-60, three units of lower hybrid range of frequencies (LHRF: at ∿2 GHz) heating and one unit of ion cyclotron range of frequencies (ICRF: at ∿120 MHz) heating are planned. There are many items to be researched and developed to establish the efficient plasma heating. Above all, the launcher and high power RF source at 2 GHz for LHRF heating (klystron) are the most important components. As for the klystron, we had finished the R&D successfully in 1983.[1),2)] However, we need further studies about the conditioning technique and the reliability of the klystron. In this year, the R&D works of the launchers for lower hybrid range of frequencies (LHRF) heating and ion cyclotron range of frequencies (ICRF) heating and the conditioning experiment of the klystron had been continued.

2.2 LHRF launcher

The phased array waveguide launcher of 8 columns × 4 rows is adopted for LHRF heating on JT-60. It was demanded that the transmitted RF power power density in the launcher of more than 4.5 kW/cm^2, pulse duration of 10 sec in ouder to attain the 10 MW RF power injection into the plasma. We have been carrying out the RF power transmission experiment since 1981. Until March 1983, the power transimission density of 5.0 kW/cm^2, 10 sec was achieved in vacuum with dummy load termination. In 1984, the study has been done laying stress on the affection of the residual magnetic field from the tokamak on the RF power transmission. The experiment was performed using the evacuated test waveguide of RF test stand (RFTS-II)[1)] on which the magnetic field was superimposed. When the strength of the magnetic field satisfies the condition $f = f_{ce}$, where f is RF frequency and f_{ce} is a cyclotron frequency, and H_2 gas was filled up to 1×10^{-4} torr, the discharge in the waveguide due to the electron cyclotron frequency (ECR) has occurred. ECR breakdown caused an increase in the reflected power. However, this discharge had been suppressed after several shot of RF conditioning, and finally,

the RF power transmission of 10.0 kW/cm^2 with 10 sec was attained without any discharge up to 2×10^{-4} torr of H_2 gas. This result shows that the ECR in the launcher will not be a serious problem if the pressure in the launcher is kept less than about 1×10^{-4} torr.

On the other hand, an unipole multipactoring discharge[3] had been observed around $f = 2\ f_{ce}$. The unipole multipactoring is a resonant type discharge which occurs on a single electric plate in the presence of RF electric field when the magnetic field of about $f = 2\ f_{ce}$ is imposed. The experimental result is shown in Fig. IV.2-1 as ratio of RF power absorption in the waveguide against the strength of the magnetic field. About 25 % of the incident power is absorbed at $f_{ce}/f = 0.5$. This power deposited into the waveguide wall so that the temperature of the waveguide wall is increased drastically. The maximum increase rate of the temperature at $P_{in} = 200$ kW was 100 °C/0.1 sec, which is very dangerous for waveguide because it is far beyond the cooling capability of the launcher, so the waveguide wall will melt by the long pulse RF injection like in JT-60. To suppress the unipole multipactoring discharge, we tested the carbon coating having the low secondary emission ratio since the multipactoring depends on the secondary emission ratio strongly. Then, no increase in the temperature of the waveguide wall nor absorption of the incident RF power occurred. The carbon coating method is relatively easy to apply to the launcher and gives little affection on the RF power transmission. Therefore, the adoption of the carbon coating on the launcher of LHRF heating in JT-60 has been decided.

2.3 ICRF launcher

For the coupling system of ICRF heating on JT-60, the launcher of 2 columns × 2 rows-loop antenna is adopted. The configuration of the launcher is so complicated that we need to understand a radiation pattern of the launcher experimentally. Therefore, we constructed a test launcher of 2-looped antenna having the same size with JT-60, i.e. the loop size is 23 cm × 8 cm, and studied about it. The figure of the launcher is illustrated in Fig. IV.2-2. This antenna is short in length compared with a conventional one. Moreover, a Faracay shield attached in front of the launcher is single layer type (open Faraday shield) because it suffers from a large heat load from a plasma and

ohmic loss of the RF furthermore it receives a large electromagnetic force during plasma disruption. At first the launcher was baked up to 250 °C with high temperature air for two days with no trouble and its mechanical reliability was assumed. Next, we measured the electromagnetic field pattern inside/outside of the Faraday shield with a static electric probe and a magnetic probe. RF power loss at the Faraday shield is mainly determined by the magnetic field in the axis direction of the launcher B_X. The value of B_X is compressed at gaps of the Faraday shield. Compression ratio B_X/B_{XO} is in proportion to the ratio of the total length of the gaps to the whole length of the Faraday shield in the poloidal direction. Magnetic field in poloidal direction B_Y is also modulated significantly with the current flowing on the Faraday shield. However, Faraday shield gives no significant modulation to the magnetic field in toroidal drection B_Z. On the other hand, the RF electric field in toroidal direction E_Z is fully cancelled even for the open Fraday shield. Moreove, thermal distribution due to the RF loss on the Faraday shield was directly observed by infrared camera.

2.4 Conditioning of 1 MW klystron for JT-60

The specification of the klystron is shown in Table IV.2-1. In 1984, we have continued its quality test and conditioning experiment. In the process of conditioning, it was found that a ceramic window for the power output is the most important section since the crack of the ceramic window sometimes occurred. Also, it was found crack of the ceramic window occurs when the temperature of the ceramic increased abruptly. Therefore, we monitored its temperature directly with an infrared camera during conditioning to study the phenomena of temperature increase.

References

1) T. Nagashima, et al., in Proc. of 10th Symp. of Engineering, Philadelphia, U.S.A. (1983).
2) S. Miyake, et al., in Proc. of 1984 IEEE Inter. Electron Devices Meeting, San Fransisco, U.S.A.
3) K. Sakamoto, et al., to be published.

Table IV.2.1 Typical performances of 1 MW class klystrons.

Frequency	2.01 GHz
Output Power	1 MW
Pulse Width	10 sec
Beam Voltage	83.0 kV
Beam Current	26.5 A
Power Gain	53 dB

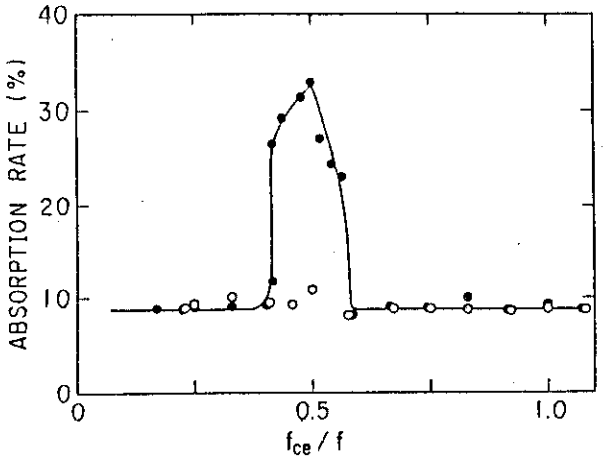

Fig.IV.2-1 RF power absorption rate by the unipole multipactoring discharge v.s. f_{ce}/f in the case of input power P_{in}=200kW and pulse duration of 1sec are shown. The symbols (●) and (○) are the data with and without unipole multipactoring discharge respectively.

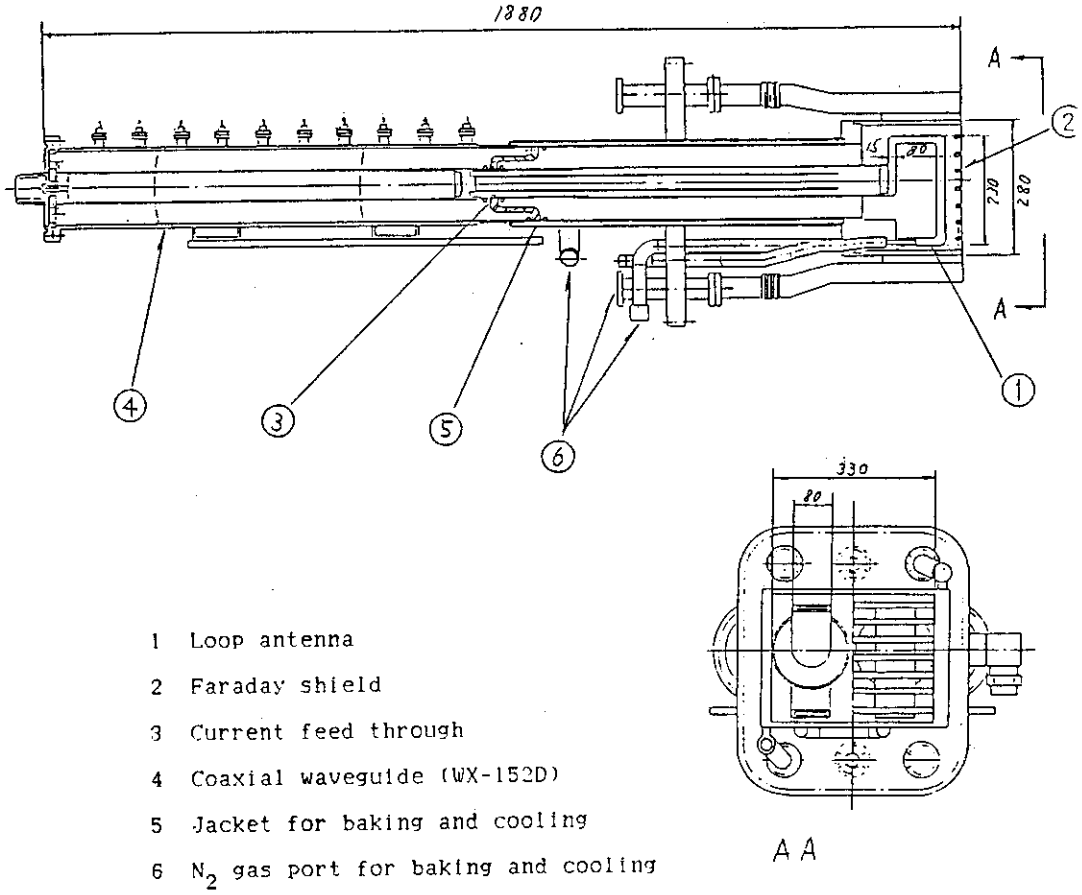

1 Loop antenna
2 Faraday shield
3 Current feed through
4 Coaxial waveguide (WX-152D)
5 Jacket for baking and cooling
6 N_2 gas port for baking and cooling

Fig.IV.2-2 2-looped launcher for ICRF heating.

V. SURFACE PHYSICS AND VACUUM TECHNOLOGY

1. Surface Physics

1.1 Intoduction

Surface physics studies which are related to plasma surface interactions have been continued in close connection with the JT-60 project, the design study of the next step tokamaks and the tokamak experiments in JFT-2M. Especially in this fiscal year, international cooperation was made in the TEXTOR (KFA Jülich, F.R. of Germany) programme. The primary objective of these studies is to investigate the interaction of the plasma with wall and limiter materials using ion accelerators and tokamak machines to find out conditions which minimize impurity production and control hydrogen recycling rate.

In this fiscal year, progress was made with measurement of the sputtering yield of silicon carbide by low energy light ions, measurement of the effect of oxygen exposure on sputtering by light ion irradiation of molybdenum, and new finding of plasma-limiter interaction, tion, i.e. limiter induced convection, in the JFT-2M.

1.2 Measurement of the sputtering yield of SiC by low energy light ions[1)]

New silicon carbide with high thermal conductivity is a promising candidate material for the first wall of fusion devices. Sputtering yield measurement for this material has been made by the bombardment with hydrogen, deuterium, and helium ions in a low energy region (350 eV - 2.5 keV) at room temperature. The present results are illustrated in Fig. V.1-1 together with other experimental data by Bohdansky and Roth[2)] and Sone et al.[3)] The silicon carbide material used here was made by sintering with BeO addition of 2 wt%[4)]. The present results except for helium ions show very low sputtering yield compared to the German data. The ratio of our data to them ranges between 1/2 and 2/3. The reason of this big difference has not been clarified up to now, but it is obvious from the deuteron sputtering yield data for various

concentrations of the BeO addition that there exists no relationship between the sputtering yield and the BeO content (see Fig. V.1-2). This means that the addition of BeO does not decrease the deuteron sputtering yield of SiC matrix within an experimental accuracy. Thus, the big difference may be due to the difference of the matreials used, e.g. stoichiometry/non-stoichiometry, or atomic structure, and to the difference of the target temperature. It should be noted in Fig. V.1-1 that there exists no difference between the present data and the German ones in the helium ion sputtering yield. It is thought that both silicon carbides have different chemical reactivities with hydrogen isotopes. But the details are still unknown at present.

1.3 Oxygen exposure effect on sputtering yield for light ion irradiation of molybdenum[5)]

Sputtering yield of molybdenum and angular distribution of sputtered molybdenum under oxygen exposure have been measured for D^+- and $^4He^+$-ion irradiation in the energy range of 2.5 to 6 keV at ambient room temperature (150 °C or less). The deuterium and helium irradiations were performed with high current ion irradiation facilities EVITA in KFA-Jülich and 10 kV accelerator in Garching, respectively. Sputtering yields were determined from the weight loss of the targets. The angular distributions were measured by collecting the sputtered material on a hemi-cylindrical carbon collector (Papyex), which in turn was analyzed by Rutherford backscattering of 1 MeV He^+ ions. The measured sputtering yields are shown in Fig. V.1-3 as a function of the impinging oxygen-to-projectile flux together with the previous argon data[6)] for comparison. It is clearly seen that for helium bombardment with both the normal and oblique incidence, the sputtering yield decreases with increasing oxygen-to-helium flux ratio as observed in argon bombardment, while the sputtering yield for deuterium bombardment show almost a constant value not depending on the oxygen-to-deuterium flux ratio. The possible explanation of the constant yields for deuterium can be due to that the implanted deuterium could react with the adsorbed oxygen at the surface to form D_2O which easily desorbs from the target in the present condition resulting in the reduction of the oxygen exposure effect on the yield so that the critical value could shift

towards higher values.

In Fig. V.1-4 the angular distribution of molybdenum bombarded at an angle of incidence of 70° obtained at room temperature are shown for two typical oxygen partial pressures, 5×10^{-8} Torr and 2×10^{-5} Torr. For oxygen partial pressure of 2×10^{-5} Torr the angular distribution of oxygen is also shown in the figure. For the light-ion bombardment at oblique angle of incidence the angular distribution generally shows a strong anisotropy with a preferred emission in forward direction with respect to the beam, which is mainly due to direct ejection of primary recoils by incoming projectiles. The present results that the oxygen exposure does not influence the angular emission distribution shape but only reduces the emission yield indicate strongly that the main sputtering process under oxygen exposure at room temperature is due to the physical collision process not to the chemically assisted process, because the latter leads to a more isotropic distribution.

1.4 Plasma wall interaction studies on JFT-2M

A new type of plasma-limiter interaction, "limiter-induced convection" has been found in the JFT-2M tokamak. The observation was made for a Ohmically heated plasma by taking photographs around an inside rail limiter and by monitoring the plasma near the limiter with Langmuir probes.

Figure V.1-5 shows photographs of plasma light around the limiter (L), where the difference of the condition between (a) and (b) is the direction of the toroidal magnetic field B_t. It can be seen in the figure that the light emission takes place anti-symmetrically with respect to the center of the limiter. Furthermore, the pattern of the light emission reverses with the reversal of B_t. The probe measurement is shown in Fig. V.1-6 where (a) and (b) correspond to those Fig. V.1-5. The probes were located on the right hand side of the limiter and on upper/lower side of the median plane (designated by U/L): that is, each probe monitored bright or dark region of the light emission. Figure V.1-6 exhibits that the plasma density at the bright region is about 2 orders of magnitude larger than that at the dark region. These results indicates that radial convection takes place near the limiter.

The convection can be explained by "obstacle-induced convection"

known in the multipole experiments; depletion or blockage of drift motions of charged particles by the limiter induces cross-field electric fields and, then plasma convection. An important consequence of the present observation is that the mechanism we dicussed can be extended to a cause of the deterioration of the confinement during NBI (L-mode). This model can demonstrate agreements with all experimental results known at the L-mode. Further studies on the limiter-induced convection during radio frequency heating as well as NBI are planned on JFT-2M experiments.

References

1) Sone K. and Yamada R. : to be published.
2) Bohdansky J. and Roth J. : J. Nucl. Mater. 122&123 (1984) 1417.
3) Sone K., et al. : J. Nucl. Mater. 98 (1981) 270.
4) Takeda Y., et al. : Advances in Ceramics 7 (1983) 253.
5) Saidoh M., et al. : Presented at 11th Intern. Conf. Atomic Collisions in Solids, Washington, Aug. 4-9, 1985.
6) Saidoh M. : J. Nucl. Mater., 128&129 (1984) 540.

2. Vacuum Technology

2.1 Introduction

The operation and experiment of JT-60 and the design study of the next generation device create a necessity for solving new problems in the vacuum and surface technological area. They include research and development of wall preparation processes suited for plasma generation and confinement, leak locating systems applicable to large and complicated vacuum vessels, and key vacuum components such as novel pumps and valves.

In the fiscal year 1984, significat progress has been made on the development of an in-situ coating device for JT-60 and the study on microwave-wall interaction. The development of leak locating techniques is also continued. A feasibility study has been initiated for develop-

ing turbomechanical pumps for fusion applications.

2.2 Fabrication and performance tests of the prototype in-situ coating device for JT-60

The development plan to invent an in-situ coating device was started in FY 1981. The device is intended to use for the repair of TiC-coated walls of JT-60 which will be eroded or damaged by plasma particle irradiation and/or heat shock. At first, the coating method was determined to be a kind of reactive evaporation, i.e., evaporating titanium in a low pressure acetylene atmosphere. Then, performance tests were carried out for different types of titanium evaporators.

In FY's 1983 and 84, a prototype coating device was designed and fabricated in cooperation with Mitsubishi Electric Corporation. It basically consists of an ohmically-heated titanium evaporator and a vacuum manipulator to be mounted in one of four vertical ports about 20 cm in diameter of the JT-60 vacuum vessel. Movement is introduced into the vacuum vessel through rotary motion seals using a low vapor pressure magnetic fluid seal. The major engineering issues come across in the R & D phase were solid lubrication of movable parts at elevated temperatures (up to 300 °C) in high vacuum and mitigation of outgassing from construction materials. Figure V. 2-1 shows the prototype in-situ coating device installed in the JVX-II vacuum vessel. The performance tests of the device were successfully carried out by the end of FY 1984.

2.3 Microwave-wall interaction study

The understanding of the interactions between RF wave and wall surface becomes increasingly important as the additional RF heating power increases. On the other hand, it is very interesting to know the mechanisms of gas desorption from wall surface through the interactions because they might be utilized to obtain low outgassing rate of wall materials without high temperature baking. An outgassing rate measurement has been made for Inconel 625 and TiC walls with and without microwave (2.45 GHz) power introduction into a vacuum vessel (JVX-I). Figure V. 2-2 shows variation in total pressure and mass filter signals

of H_2, H_2O and CO, which occurs by the microwave-wall interaction. It can be seen that the gases desorbe intermittently. This may be due to the impact desorption by charged particles locally produced and accelerated in the strong electromagnetic field.

In this connection, an Auger electron spectrometer has been employed to determine the secondary electron emission coefficient of various wall materials. The coefficient of a material relates closely to the surface composition which is modified by surface treatments including baking, argon ion etching and methane glow discharge.

Based on these results, some measures have been taken to reduce outgassing rate and secondary electron emission coefficient of the walls of vacuum vessels and RF components.

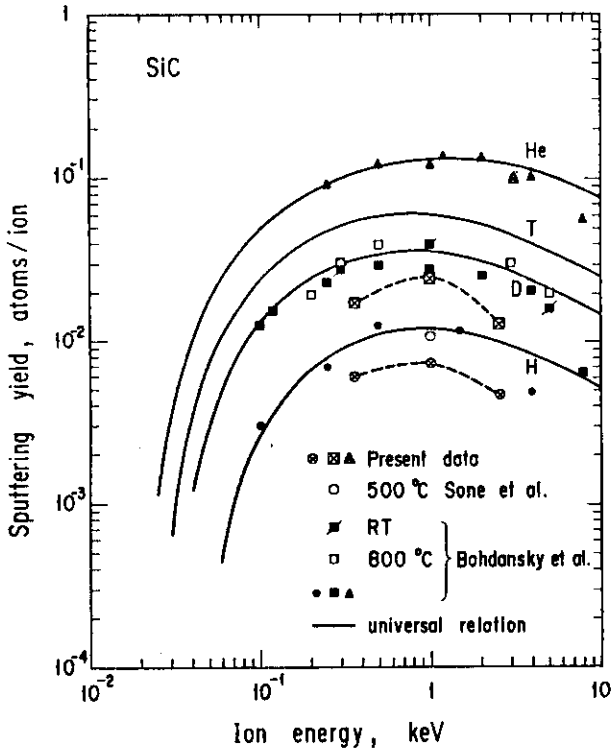

Fig. V.1-1 Energy dependence of the sputtering yield of SiC with H, D, ^{4}He. The universal relation by Bohdansky and Roth[2] is given by solid lines. Note the big difference between the present data and the German ones.

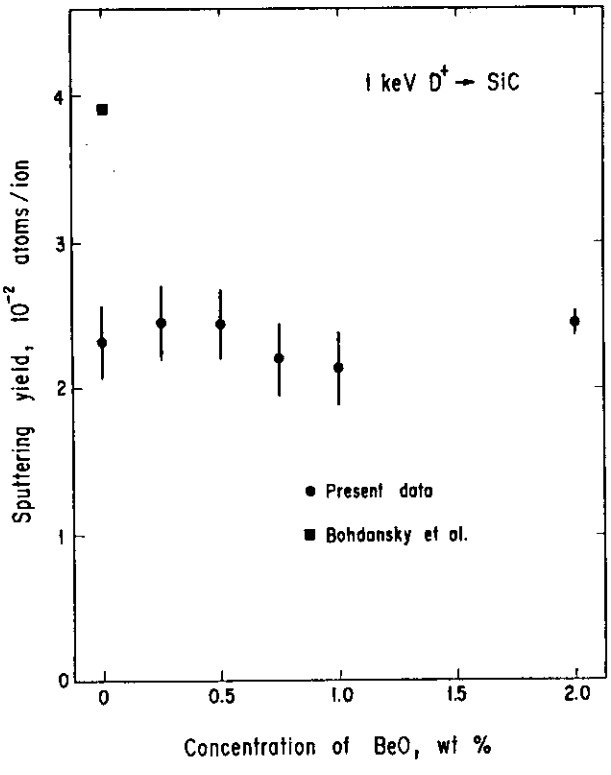

Fig. V.1-2 Deuteron sputtering yield as a function of the concentration of BeO addition in wt%.

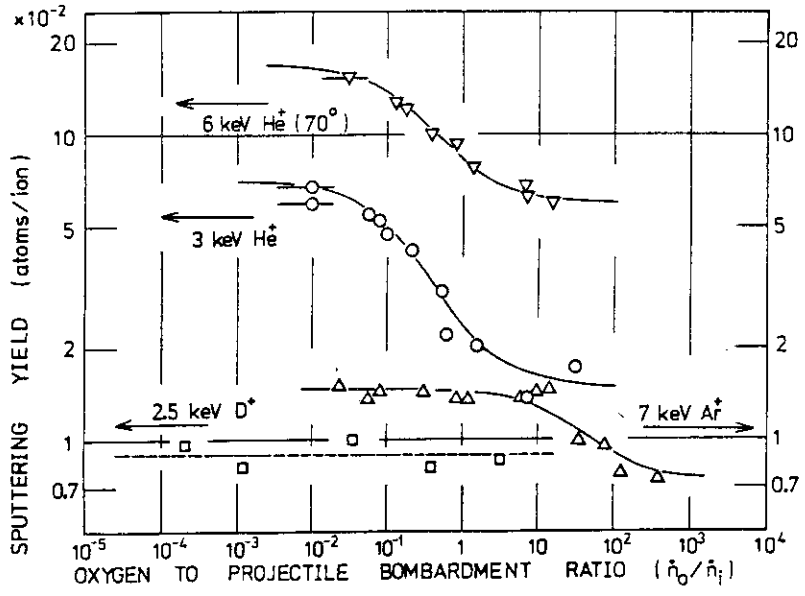

Fig. V.1-3 Sputtering yields for different ion bombardments under oxygen exposure as a function of oxygen-to-projectile flux ratio. The bombarding angles to the target are the surface normal for 2.5keV D^+ 3keV He^+ and 7keV Ar^+ and 70° from the surface normal for 6keV He^+, respectively.

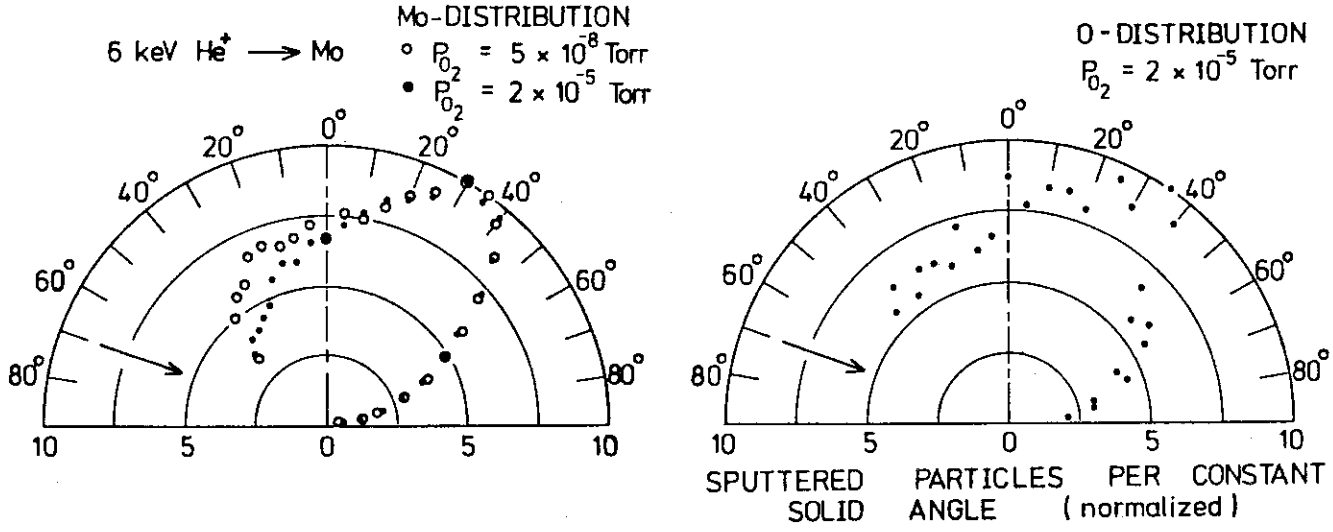

Fig. V.1-4 Angular distributions of the sputtered particles for 6keV He^+ ion bombardment of molybdenum at an angle of incidence of 70° from surface normal for different oxygen partial pressures. The bombardments have been performed at ambient room temperature. The distributions are normalized to give the same maximum value.

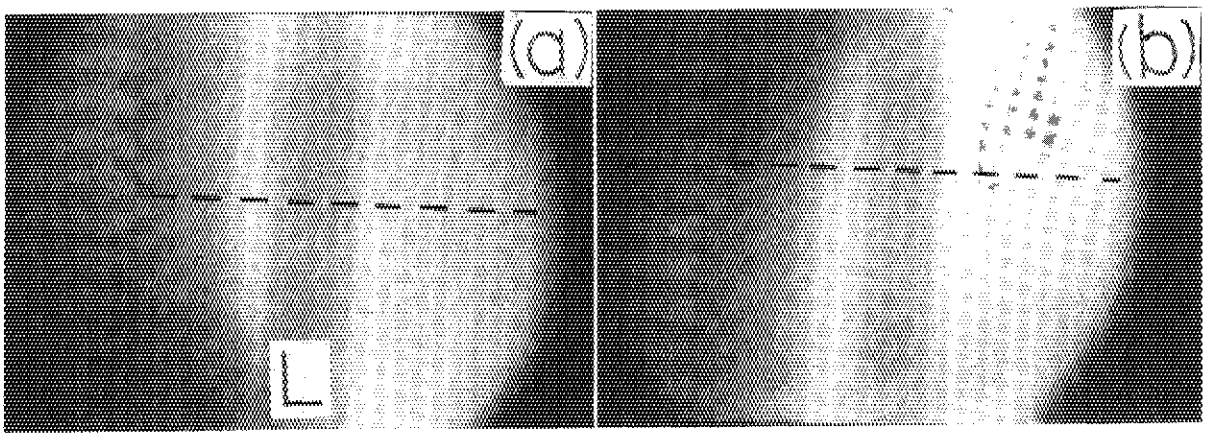

Fig. V.1-5 Light emission near the limiter; in (a) the direction of B_t is from right to left and in (b) B_t is reversed. The dashed lines indicate the position the median plane and L refers to the limiter.

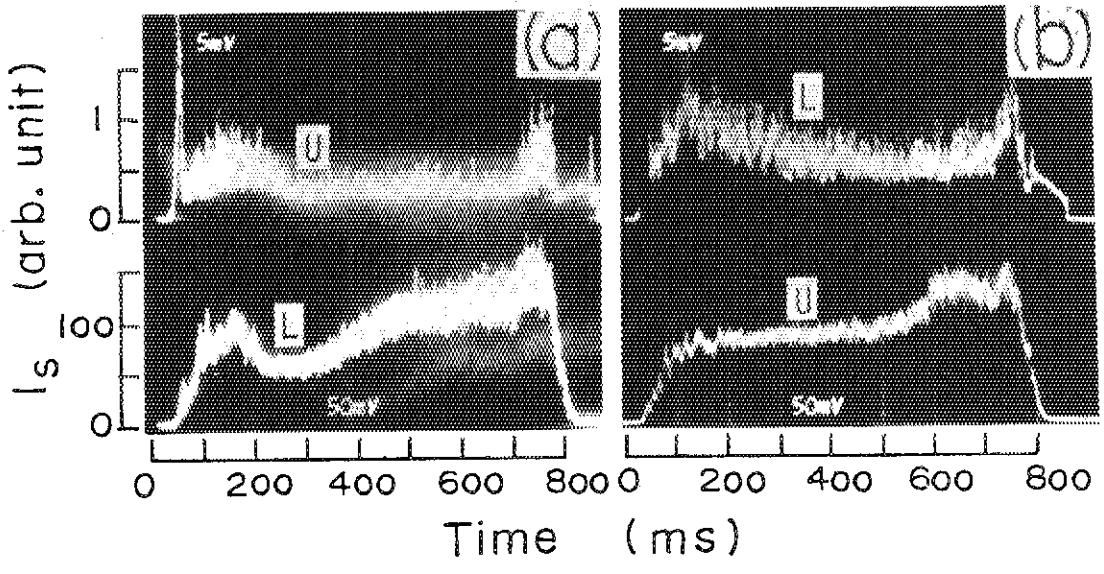

Fig. V.1-6 Probe current I_s of the upper/lower side probes designated U/L, respectively, where (a) and (b) correspond to those of Fig. V.1-5.

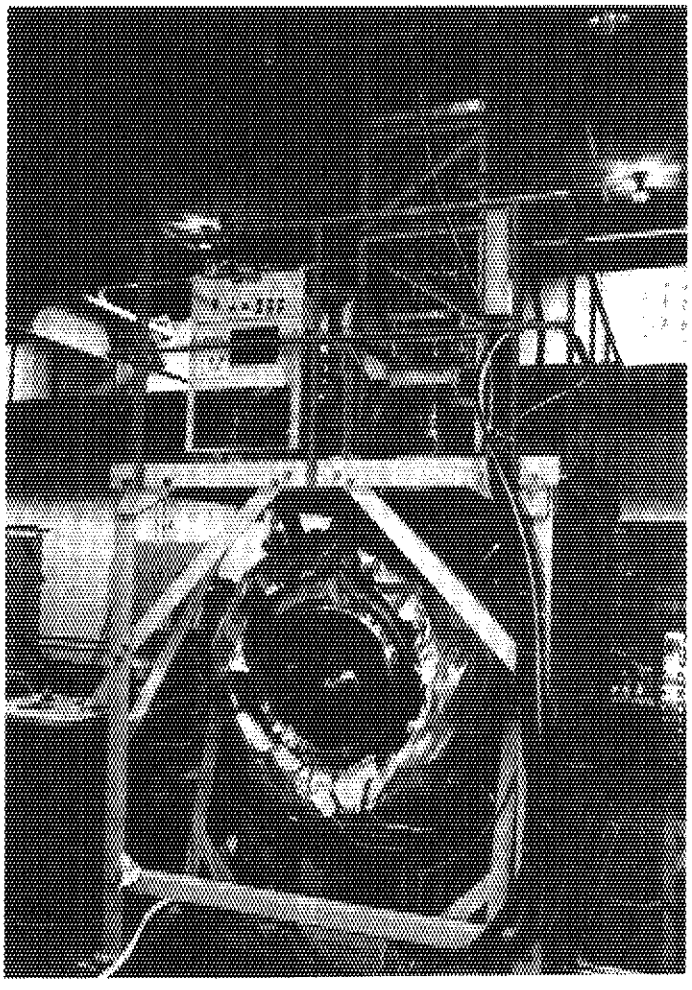

Fig. V.2-1 Prototype in-situ coating device installed in the JVX-II vacuum vessel.

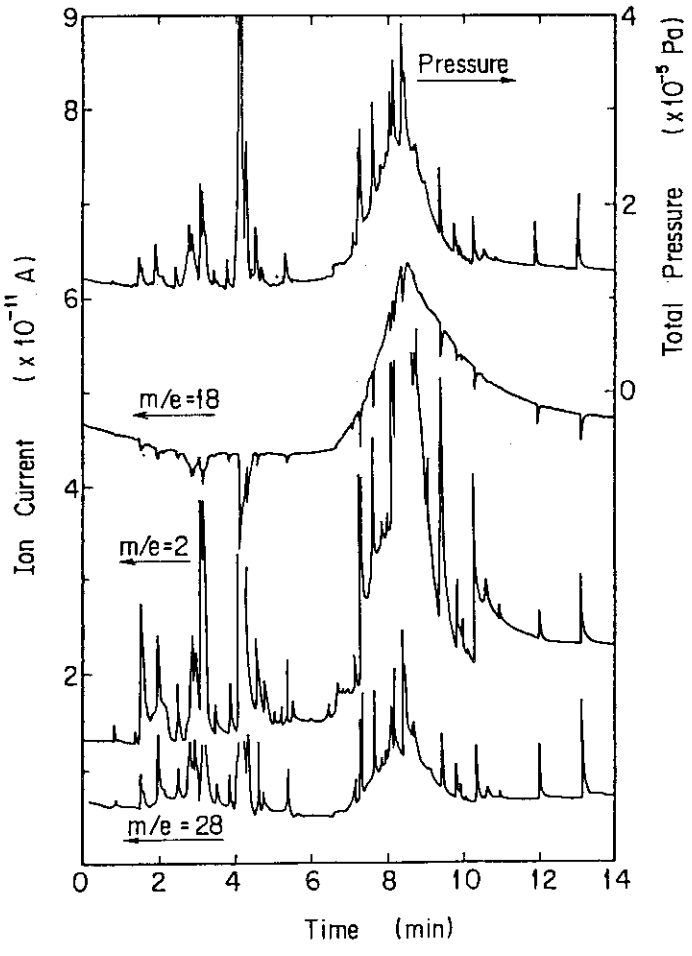

Fig.V.2-2 Variation in total pressure and mass filter signals of H_2, H_2O and CO due to the microwave-wall interaction.

VI. SUPERCONDUCTING MAGNET DEVELOPMENT

1. Introduction

The objective of superconducting magnet development in JAERI is to establish design, fabrication and operation technique for Tokamak Fusion Experimental Reactor. As toroidal coil development, two projects are being carried out. One is Cluster Test Program for high field demonstration and another is Large Coil Task, an international collaboration, for scaling-up of size. As poloidal coil development, the unit pancake program has started. Cryogenic technology and structural material are being intensively developed. The highlights in FY 1984 in JAERI Superconducting Magnet Laboratory are as follows.

1) The Japanese LCT coil was tested in 3 coil condition in Oak Ridge National Laboratory.
2) Nb_3Sn Test Module Coil was operated in 11T and cold end recovery was demonstrated with 30 A/mm^2 at 11T.
3) Fabrication of 30 kA poloidal unit pancake was started.
4) Expansion turbine test was installed.
5) New structural material development is in continuation.
6) Design of medium sized superconducting Tokamak is in continuation.

2. Cluster Test Program

2.1 Upgrading of the Cluster Test Facility and an extended test on the TMC-I[1)]

In order to study the behaviour of the TMC-I at more than 10 T, upgrading of the Cluster Test Facility (CTF-U) has been performed by installing two supplimentary coils, so called the Cluster Background Coil (CBC) in the bore of each CTC as shown in Fig. VI.2-1. Therefore, the CTF-U consists of five coils including the TMC-I. Fig. VI.2-2 shows the CBC being installed in the CTF vacuum tank. The CBC, which has a winding inner diameter of 400 mm, is composed of a pair of pool cooling coils wound with MF Nb_3Sn conductor. The cooling surface of

conductor was grooved and coated with Cu_2O to obtain a high heat fulx. A designed operating current is 2,145 A, which is the same as that of CTC because of a connection with CTC in series with one power supply. A current lead between CBC-1 and CBC-2 was directly connected with Nb_3Sn superconductor soldered on copper bar to decrease a heat load.

A total cooling weight of coil system, which is composed of five independent helium vessels, is 28 ton including the support structure of 4 ton. The cool-down time of five coils is 148 hours to 5 K with almost uniform temperature of them in parallel. This parallel cool-down technique will be usefully applied to the operation of toroidal coil system, having more than 10 coils. The current charge test of TMC-I in the CTF-U has been performed the following procedure; firstly, four background coils, connected in series, were energized to 2,145 A and next, the TMC-I was energized up to 6,000 A with a sweep rate of 300 A/mm. The maximum magnetic field on the TMC-I is 11.1 T with a background field of 4.3 T as shown at #1 point in Fig. VI.2-3. The maximum magnetic field on the CBC and the CTC are 9.6 T and 6.7 T, respectively. The measured strain on Nb_3Sn conductor due to charge-up of TMC-I to 11.1 T is 0.16 %. Therefore, the toral strain is 0.7 % of Nb_3Sn after heat treatment since bending strain during winding is 0.5 %. The total stored energy of five coils is 46 MJ.

In order to investigate the stability of TMC-I, the heater test has been carried out in two cases of TMC-I with and without the background field, using the manganin heaters embedded in Nb_3Sn conductor. Input heater power is 4.7 kW with a period of 0.2 s over a length of 192 cm, corresponding to one turn. At 6,000 A and 11 T, the normalcy returned spontaneously to superconducting state in 6.3 s after the inner most turn became normal and temperature increased over 20 K by heating. On the other hand, the heater test of TMC-I without the background field has been carried out up to 7,200 A (#2 in Fig. VI.2-3). The TMC-I recoverd to superconducting state up to 6,800 A (#3 in Fig. VI.2-3) for one turn normalcy. However, the recovery to superconducting state was not observed at 7,000 A and 7,200 A. From those results, the maximum stable current of TMC-I with the background field of 4.3 T is extrapolated on 6,300 A at 11.5 T.

This achievement shows that Nb_3Sn superconducting coil can be surely applied to toroidal coil in fusion machine.

2.2 Research and development for the TMC-II[2)]

For the second test coil (TMC-II) in the Cluster Test Program, the Segment Test Program (STEP) and FC-100M program are progressed from 1983. The STEP-I, which is the first test coil of the STEP program, has been charged up to 10 kA at 8 T without quench, in 1983. In summer of 1984, the STEP-II, the second test coil, was charged up to 20 kA at 8.7 T, and its heater test was carried out, as shown as Fig. VI.2-4. In order to test the STEP-I and STEP-II at 12 T, we started fabrication of the new split back-up coil (Spliter-15), whose maximum field and average current density were 15 T and 75 A/mm^2 respectively. For the Splitar-15, the R & D coil was fabricated and charged up to 15.25 T with average current density of 140 A/mm^2. This result is enough for the Splitar-15. The cross sectional photograph of conductor of this R & D coil is shown in Fig. VI.2-5. In the next year, STEP-I and STEP-II will be tested at 12 T by using the Splitar-15. As a forced flow conductor test, the charging test of FC-100M was carried out with 8 T back-up coil. A normal zone appeared at 3 kA and 9.6 T. As the next step, we started to fabricate the FC-150M, which will generate a magnetic field of 12 T with 8 T back-up coil. This coil will be tested in the next period.

3. Large Coil Task of IEA

3.1 General

The Large Coil Task (LCT) as an international work is being carried out under the auspice of the International Energy Agency for the purpose of fusion superconducting magnet development. Each perticipant, the United States of America, EURATOM, Switzerland and Japan, designed and fabricated an unique test coil and brought it to the International Fusion Superconducting Magnet Test Facility (IFSMTF) operated by the United States. Six test coils (US:3, Japan, EURATOM, Switzerland:1) arrayed in a compact torus will be tested. For the facility shake-down and the primary coil test before the six coil test, the three coil test was planned and carried out successfully in 1984.

The General Dynamics coil (GD coil), the Swiss coil (CH coil) and the Japanese coil (JA coil) were cooled down to 4 K, and GD and JA coils were charged up to the rated current (a little over 10 kA) in the single and the two coil conditions as planned. After the three coil test, the EURATOM coil and the General Electric coil were installed in IFSMTF. The Westinghouse coil was almost completed, and the six coil test was scheduled to be started in 1985.

3.2 Three coils test in ORNL

Three test coils (GD, JA, CH) were tested in IFSMTF constructed in Oak Ridge National Laboratory. At the time, CH coil had no current leads, so, CH coil was only cooled down. Fig. VI.3-1 shows the three test coils installed in the vacuum tank of IFSMTF.

After several inspections, the cooling down work from 300 K to 4 K was started in July, 1984. This work took about five hundred hours because the pressure drop in the gas return line from the coils was larger than designed value and the allowable temperature difference in the coil was limitted by other participants.

The charging test was performed with several troubles; miss cabling, power supply trouble, main helium tank trouble, power failure by heavy thunderstorm, etc.. JA coil was charged up to and dumped from 10.22 kA, the rated current, at the single coil test. GD coil was also single charged up to its rated current of 10.2 kA.

The two coil test (test coil:100% current, background coil:40% current) was also carried out successfully. Fig. VI.3-2 shows the result of the dumping test; JA coil was charged up to 70% current and was in persistent mode, and GD coil was dumped from 40% current. At that time, the transport current of JA coil increased 485 A. At the two coil charging state, the two coils are pulled by each other and the coil cases are bent. Fig. VII.3-3 shows the strain appeared on the corner part of JA coil case. At the two coil test, the strain value reached 550 ppm. In order to investigate the stability, a half turn of each conductor was heated and normalized. GD coil was recovered itself from normal conducting state to superconducting state at the singly 100% charging condition. JA coil was also recovered at the two coil test condition (JA 100% and GD 40% charging). Fig. VI.3-4 shows

the voltage profiles of JA coil after a half turn heating.

The coils and the facility were warmed up to the room temperature in October, 1984, and the three coil test was finished.

4. Pulsed Poloidal Coil Development

4.1 Highlights

New technology for superconducting poloidal coils has been under development for the Fusion Experimental Reactor (FER). In 1984, verification tests for both forced-flow-cooled and pool-boiling-cooled coils have been carried out. For forced-flow cooling, the maximum allowable disturbance to keep the stability of a sample coil was measured, demonstrating high feasibility of this cooling for large coils. For pool-boiling cooling, heat transfer characteristics from large-sized conductor was measured, and the perfect stability up to 116 % of the operating current was confirmed. Based on the whole results of verification tests, it has become ready to start the development of a large pulse coil, called Demo. Poloidal Coil, from 1985.

4.2 Measurement of the stability margin of a forced-flow-cooled conductor

A model coil wound with a subsized conductor of JAERI forced-flow-cooled conductor (JF-30) was fabricated and tested under the magnetic field of 7 T. So as to simulate a disturbance to this coil, this coil was heated for 20-30 ms with energy density up to 1.5 J per unit volume of helium in the conductor. Fig. VI.4-1 shows major result of this stability test. At the nominal current, it was verified that the conductor is stable against the thermal disturbance up to 0.7 J/ccHe without helium flow and up to 1.3 J/ccHe at the 1.5-g/s helium flow in the conductor. Design requirements for this stability margin is around 0.45 J/ccHe, therefore the sufficient stability of the JF-30 conductor was demonstrated.

4.3 Fabrication of 30-kA Poloidal Unit Pancake

In order to demonstrate the feasibility of a pool-boiling-cooled large-current pulsed conductor for poloidal coils, a 30-kA large-bore Poloidal Unit Pancake (PUP) is designed and under construction. PUP is wound in one double pancake with a 30-kA pulsed conductor, whose superconducting strands are supported by the inner stainless steel core. Fig. VI.4-2 shows the dimensions and testing arrangement of the PUP and two backup coils. Operating current, current density, and stored energy of the PUP are 30 kA, 18 A/mm^2, and 1.5 MJ, respectively.

In the process of the fabrication, a number of verification tests are carried out to support the design. Fig. VI.4-3 shows the experimental results of heat transfer characteristics of the conductor at various position on the subcables. In this experiment, cooling conditions were exactly simulated to that of the actual winding. As a result, the worst cooling characteristic is found at the uppermost position. Even in this position, however, equal area heat flux is 0.479 W/cm and corresponding stable current becomes up to 34.8 kA. This indicates that the PUP is designed fully cryostable at the operation current of 30 kA.

The fabrication and subsequent performance tests at 7 T will be carried out in autumn, 1985.

5. Cryogenic System Development

5.1 Introduction

A Superconducting TOKAMAK fusion machine requires the large scale helium refrigeration system which has a maximum refrigeration capacity more than 10-20 kW as a unit at 4 K. For technological realization of such a large refrigeration system, JAERI has been investigating not only the cryogenic technology but also cryogenic devices which will be applied to the system.

In this period, according to the cryogenic development plan, the experiment of the forced-cooled superconducting test loop was carried out as an advanced varsion of the previous experiment at last period.

With regard to the development of cryogenic devices, turbo-expander with mass flow rate of 100 g/s was designed and assembled, and the current leads with 15 kA was tested.

5.2 Experiment of forced-cooled superconducting test loop[3)]

Stability test of 15 kA superconducting test loop (JF-15) was carried out by using inductive heating technique which is newly developed by JAERI to initiate normal zone on the conductor. By this new heating technique, we have experimentally found the relation between stability margine of forced-cooled conductor and its operating current as a function of helium coolant conditions such as pressure, temperature, and mass flow rate. Fig. VI.5-1 shows a stability characteristics of JF-15 obtained at 6 atm and 4.8 K.

On the other hand, we have developed a stability analysis code "ALPHE-II" to theoretically calculate the stability characteristics of forced-cooled conductor. The transient behavior of helium coolant in the forced-cooled conductor can be estimated by this analysis code as shown in Fig.VI.5-2.

In these way, the design criteria of the stability margine for the forced-cooled conductor is being able to establish by both experimental and theoretical approach.

5.3 Development of helium turbo-expander

According to the cryogenic system thermal analysis code named as "CRYO" which was developed by JAERI, a large helium turbo-expander with the maximum mass flow capacity more than 1000 g/s is required to construct 10-20 kW refrigeration system for fusion TOKAMAK machine.

For this purpose, JAERI has been developing large helium turbo-expander and as a first step, the medium sized turbo-expander with 100 g/s was designed and assembled to investigate the dynamic performance and the scalability. In this turbo-expander, dynamic gas bearing was adopted to the journal bearing and static gas bearing was to the thrust bearing. The overview and the design parameters of this turbo-expander are shown in Fig. VI.5-3 and Table VI.5-1, respectively.

The performance test at cryogenic temperature will be carried out in 1985 by using the existing Superconducting Engineering Test Facility.

5.4 Development of new type of current lead[4)]

Vapor-cooled current leads with large capacity more than 20 kV and 30 kA are required for superconducting magnet for fusion. In such a large current system, the thermal performance of the current lead is extremely important since a small deviation of the coolant flow rate from the ideal value gives a significant liquefaction load to the cryogenic system.

Therefore, JAERI have been developing high-current vaporcooled current leads with cable-in-conduit configuration which can be expected to have ideal thermal performance, that is, heat leakage and coolant flow rate per 1 kA are 1 W and 0.05 g/s, respectively.

In this period, 6 kA and 15 kA current leads were fabricated and tested. Fig. VI.5-4 shows the measured thermal performance of 15 kA current lead charged up to 20 kA. We have demonstrated in these experiments that the new type of current lead has excellent thermal and electrical characteristics and then the heat leakage and the coolant flow rate are close to the ideal value. JAERI is intending to perform the verification test up to 30 kA in 1985.

6. Development of the New Cryogenic Structural Materials

We have been developing the new cryogenic structural materials, which have yield strength of more than 1,200 MPa and plane-strain fracture toughness of more than 200 MPa$\sqrt{m}$, for fusion Experimental Reactor. Several steels which had four fundamental chemical compositions as shown in Table VI.6-1 were selected from the results of tensile and Charpy impact tests at 4 K. These steels divide into three groups such as high Mn austenitic stainless steel, high Cr-Ni austenitic stainless steel, and austenitic stainless steel which chemical composition in middle of above two steels.

Elastic plastic fracture toughness Jic values of these steels

have been measured using computerized unloading compliance method. Reliability of J_{1C} measurement system was verified by comparison between results from this system and those from R-curve method according to ASTM E813. J_{1C} value is converted into K_{1C} value by following equation.

$$K_{1C} = \sqrt{E \cdot J_{1C}}$$

Fig. VI.6-1 shows relation between fracture toughness and yield strength at 4 K. NBS trend line as shown in this figure is data base of 304 grade austenitic stainless steels at 4 K. JAERI-Box, which was named by U.S.A., shows our target area. Thus, we requested high strength and high fracture toughness compared with ordinary stainless steels and our development of the new cryogenic structural materials has attracted attention of foreign countries. All data of the newly developed steels is over NBS trend line. Fracture toughness is improved compared with ordinary stainless steels which have the same yield strength. The yield strength of high Cr-Ni stainless steels is higher than that of high Mn stainless steels. Six steels are included in JAERI-Box. One of these steels, 22 Mn steel, is supplied from 15 tons production heats.

Development of base metal has almost completed and we started to develop welded part of these excellent steels. These material will be used as structural materials of Poloidal Unit Pancake and Demonstration Poloidal Coil which will be developed by us.

7. Design Study for Medium Sized Supperconducting Tokamak

For the realization of the Fusion Experimental Reactor (FER), the construction and operation of medium sized superconducting tokamak machine is necessary. For this purpose, design study of Superconducting Tokamak Test Assenbly (STTA) is under way. Major objective of the work is design and understanding of the superconducting coil system for a long-pulsed tokamak. On the STTA, the design of 12-T toloidal coil system has been carried out and current status comes to the design of poloidal coil system. Fig. VI.7-1 shows the elevation view of STTA.

In September, 1984, US/JAPAN workshop on 'Superconducting Magnet

Requirements for Intermediate-scale Long-Pulse Tokamaks' was held and nearly fifty specialists on magnet technology and plasma phyisics attended the workshop. Based on the common recognition that medium sized superconducting tokamak is indispensable for the construction of large tokamak such as FER and TFCX, the designs of STTA and ALCATOR-DCT were reviewed and a number of informations were exchange.

References

1) Ando T., et al., Proc. of the 10th International Cryogenic Engineering Coference, (1984) p.173.
2) Takahashi Y., et al., IEEE Trans. Magn. MAG-21 (1985) p.157.
3) Kato T., et al., IEEE trans. MAG-21 (1985) p.1095.
4) Tada E., et al., Advanced in Cryogenic Eng. Vol. 29 (1984) p.245.

Table VI.5-1 Design specifications of expansion turbine.

INLET PRESSURE	(ATM)	15.0
INLET TEMPERATURE	(K)	20.0
EXPANSION RATIO		6.0
FLOW RATE CAPACITY	(g/s)	100.0
DESIGNED REVOLUSION	(rpm)	214000
BRAKING METHOD		FAN-BRAKE
JOURNAL BEARING		DAYNAMIC
THRUST BEARING		STATIC

Table VI.6-1 Fundamental chemical compositions.

Fundamental Chemical Compositions
High Manganese Austenitic Stainless Steel
0.05C - 22Mn - 13Cr - 5Ni - 0.2N
0.05C - 25Mn - 15Cr - 1Ni - 0.2N
High Cr - Ni Austenitic Stainless Steel
0.02C - 25Cr - 13Ni - 0.35N
Austenitic Stainless Steel
0.02C - 12Cr - 12Ni - 10Mn - 5Mo - 0.2N

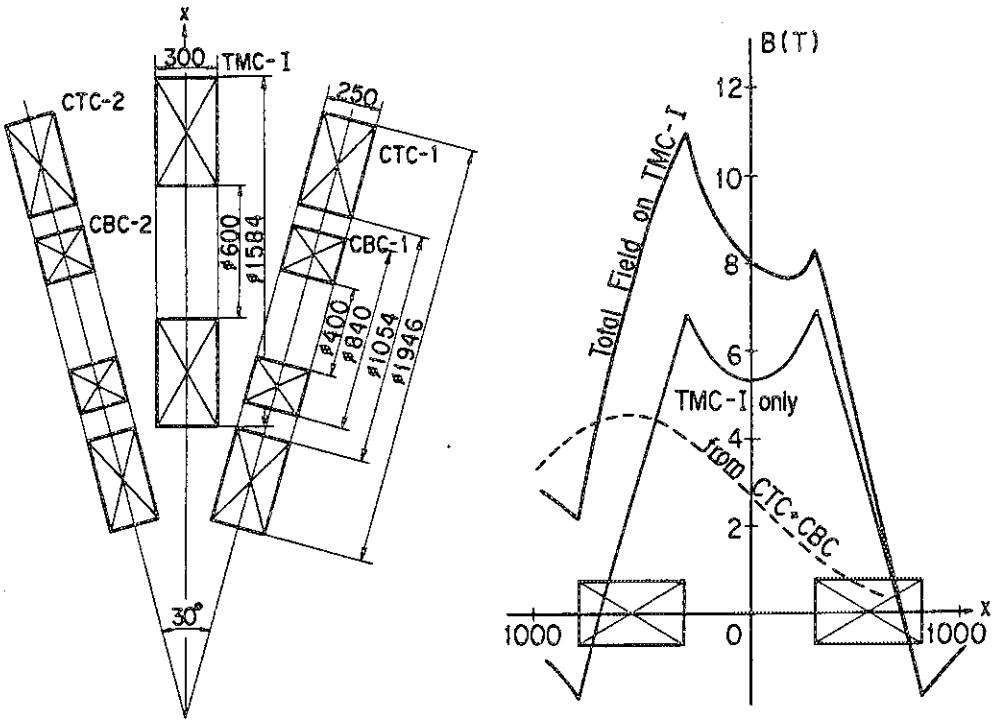

Fig. VI.2-1 Geometarical configuration of coils in the CTF-U and field distribution on the TMC-I.

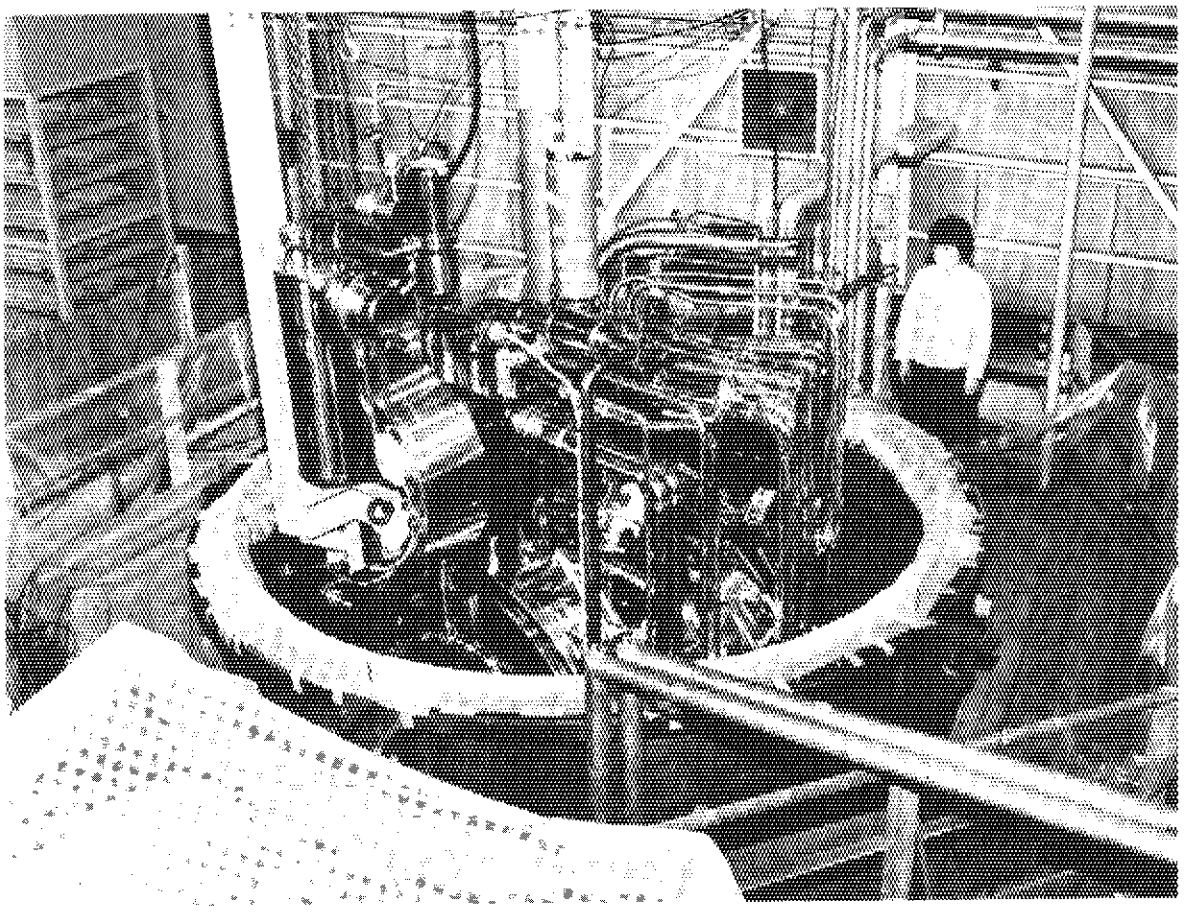

Fig. VI.2-2 CBC being installed in the CTF-U vacuum tank.

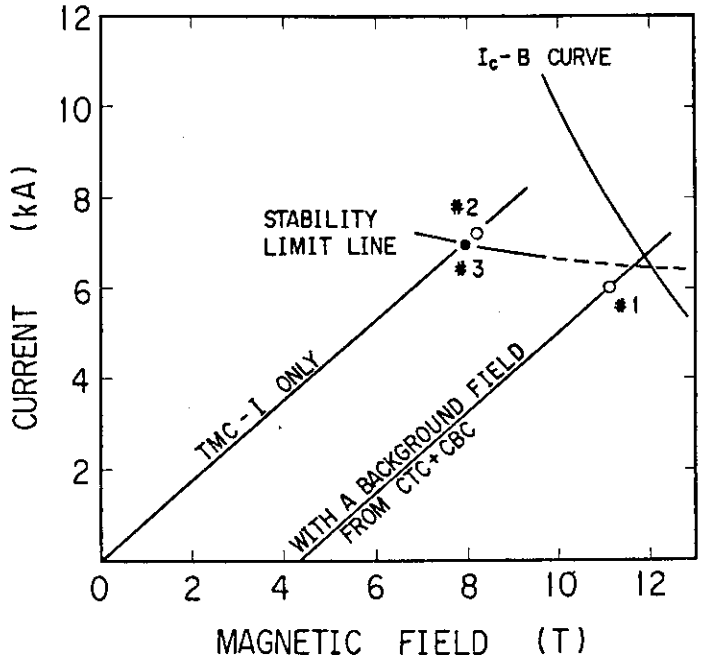

Fig. VI.2-3 Load lines and stability limit for the TMC-I.

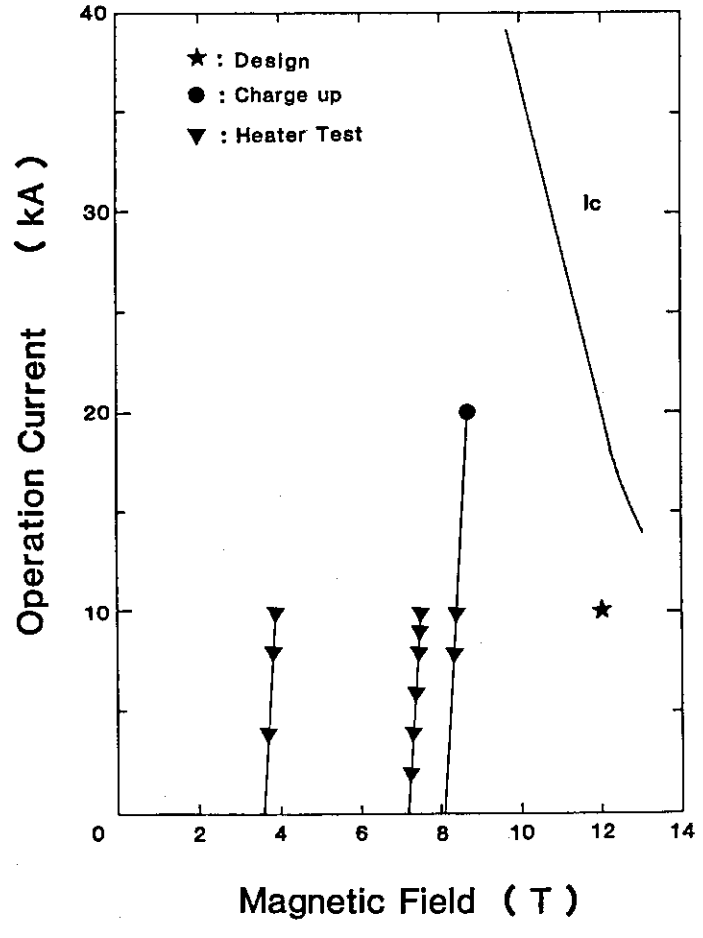

Fig. VI.2-4 The load line and Ic-B curve of STEP-II.

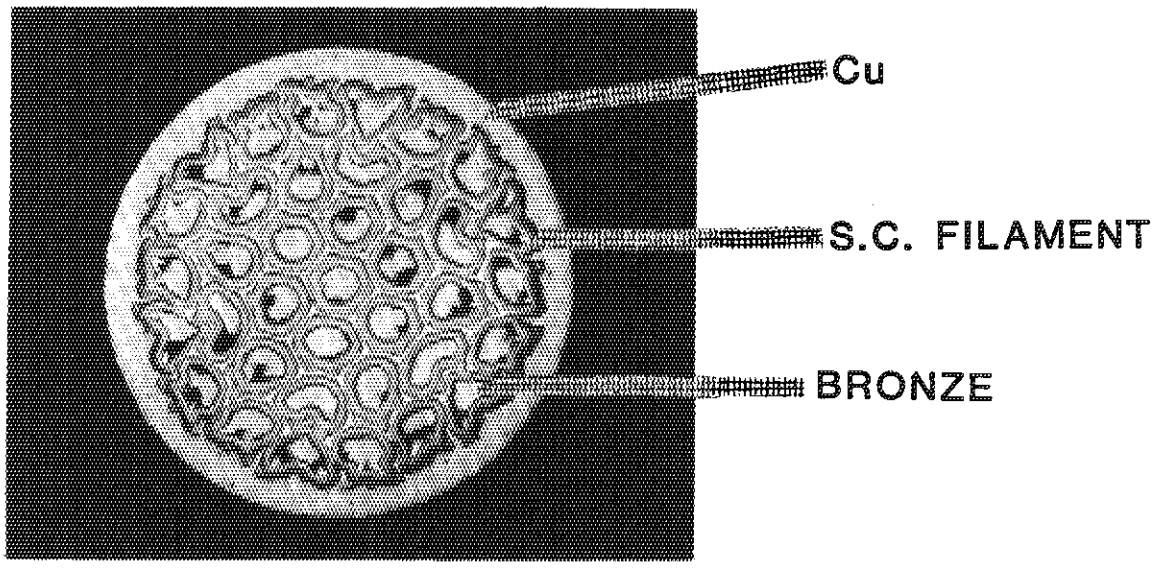

S.C. Material	$(Nb-Ti)_3Sn$
Diameter	1.1 mm
Filament Diameter	141 μm
Number of Filaments	37
Cu : non Cu	0.67 : 1

Fig. VI.2-5 The cross sectional photograph of conductor of R & D coil.

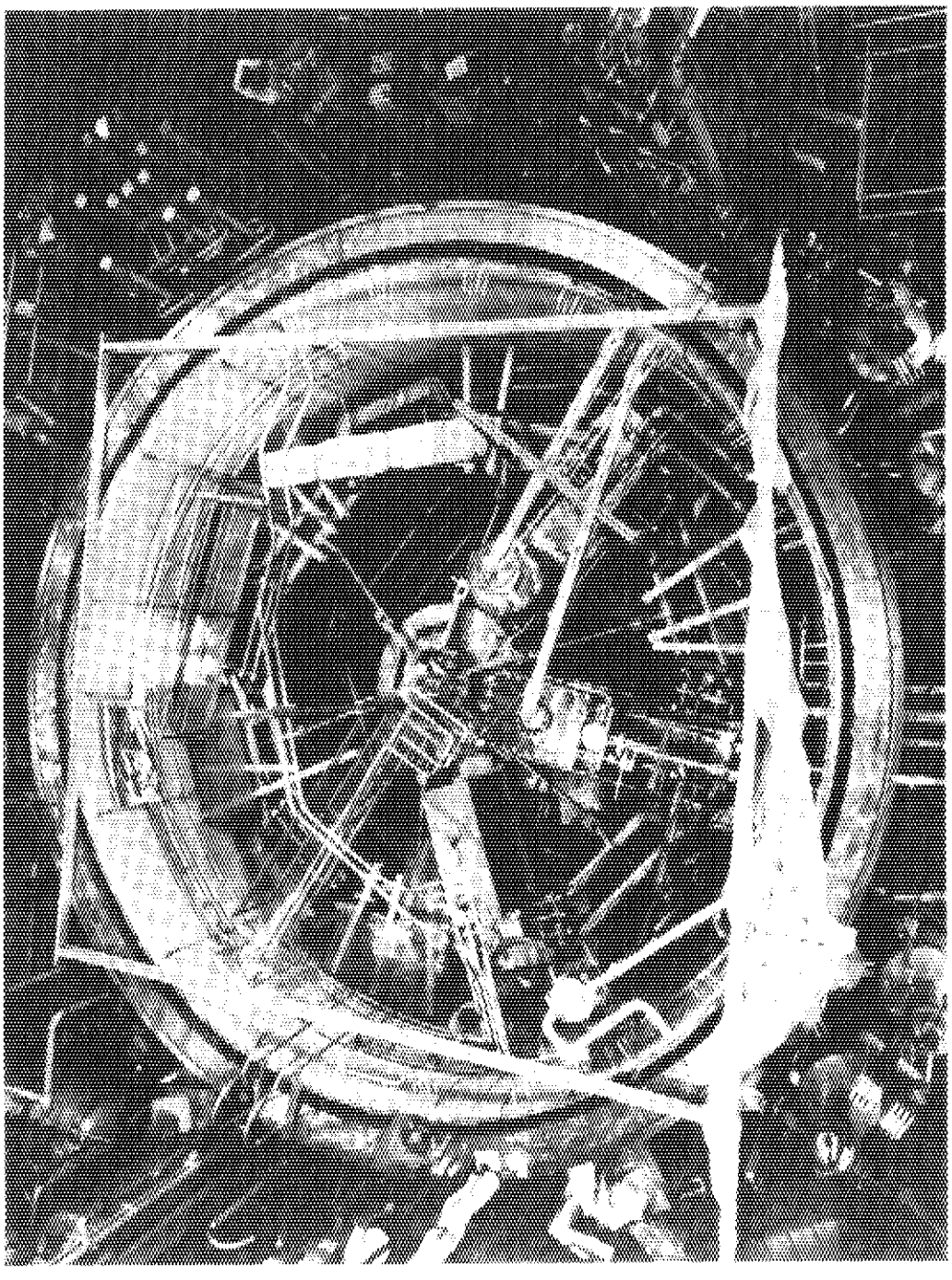

Fig. VI .3-1 A top view of the vacuum tank before three coil test: Left-Swiss coil, center Japan coil, right -General Dynamics coil.

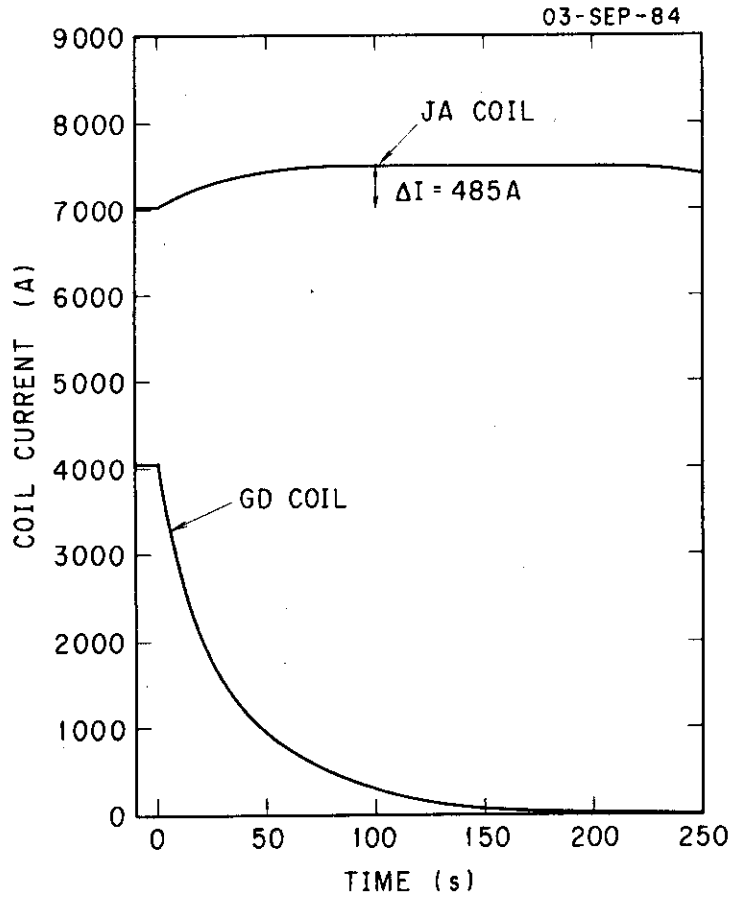

Fig. VI.3-2 JA coil and GD coil currents during JA coil 70 % current -persistent mode and GD coil 40 % current-dumping mode.

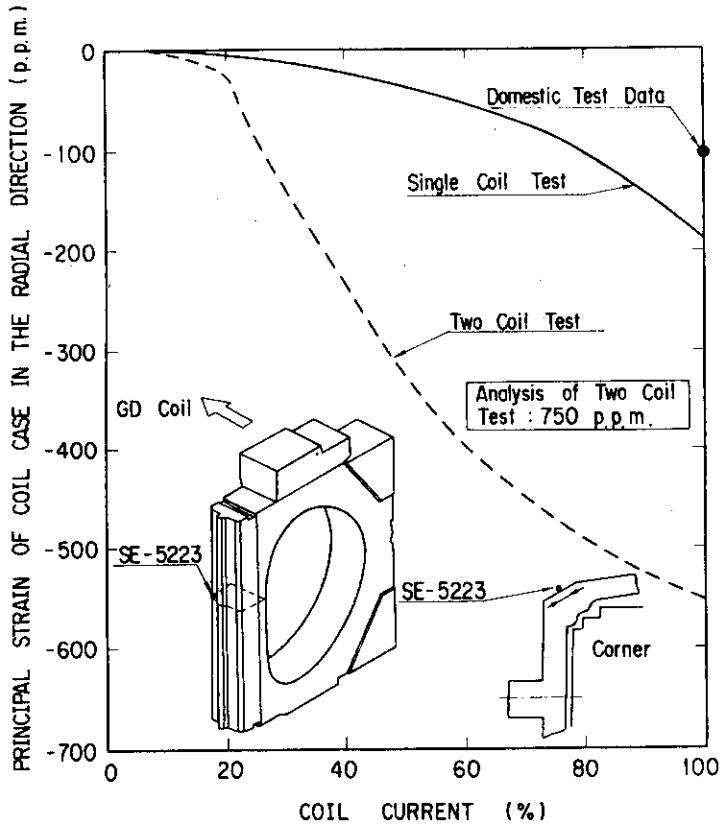

Fig. VI .3-3 Strain at the corner of JA coil case during single (JA 100 %) and two coil (JA 100 %, GD 40 %) charging mode.

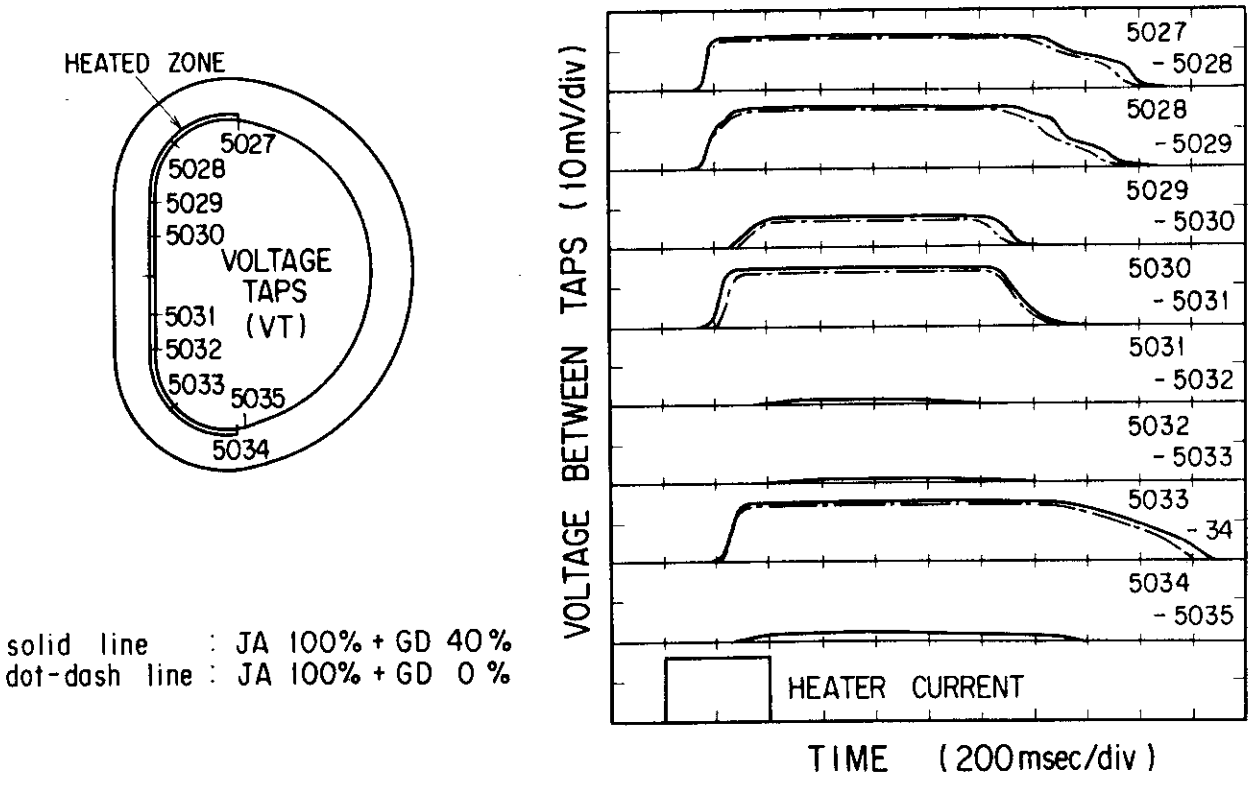

Fig. VI.3-4 JA conductor voltage profiles after a half turn heating.

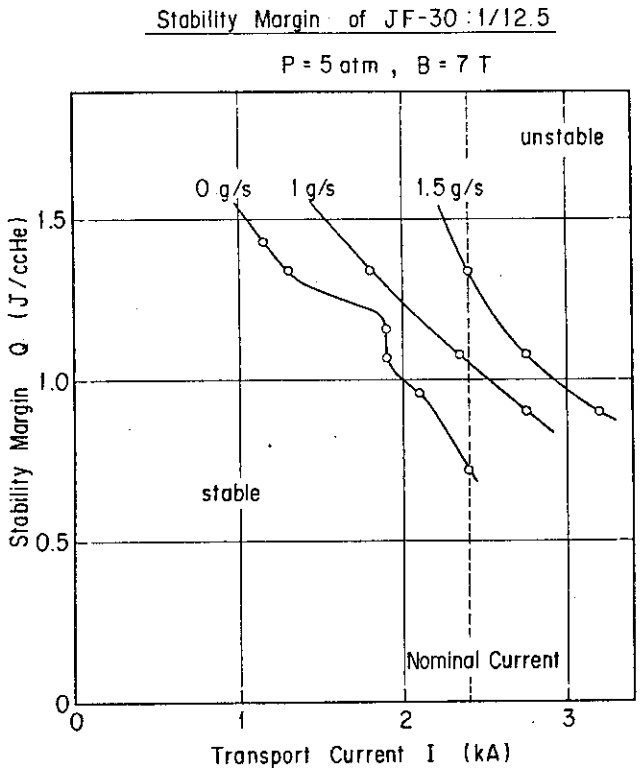

Fig. VI.4-1 Measured stability margine of JF-30 subsized conductor.

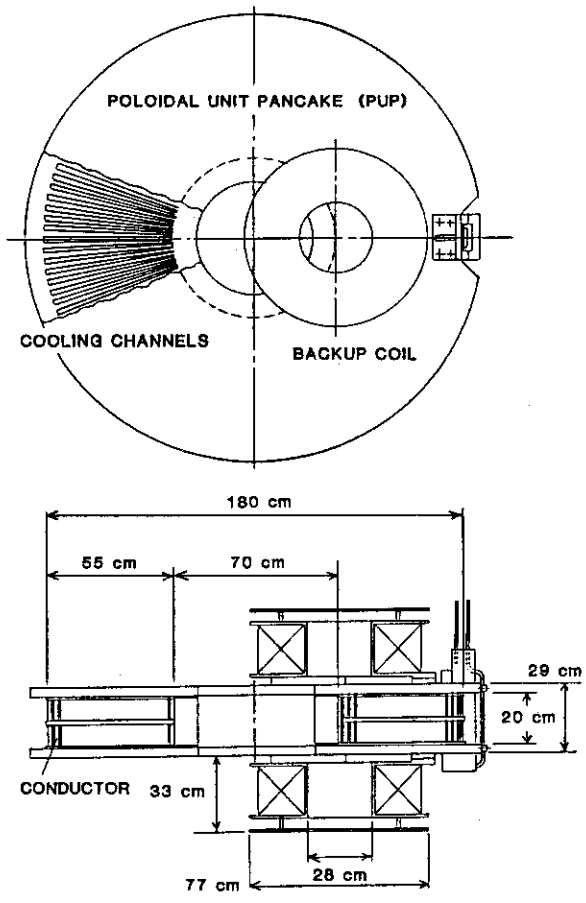

Fig. VI.4-2 Poloidal Unit Pancake (PUP) and its testing arrangement

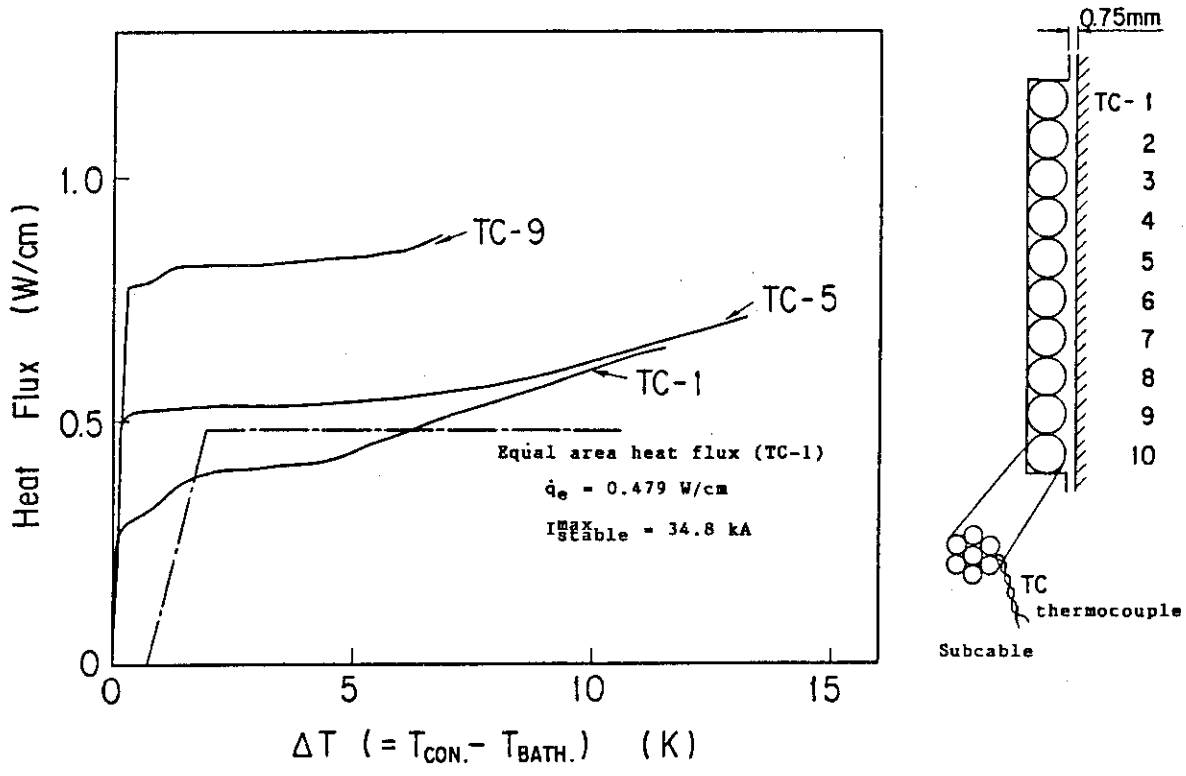

Fig. VI.4-3 Measured heat transfer characteristics of the PUP conductor. (heat flux per unit length of the subcable)

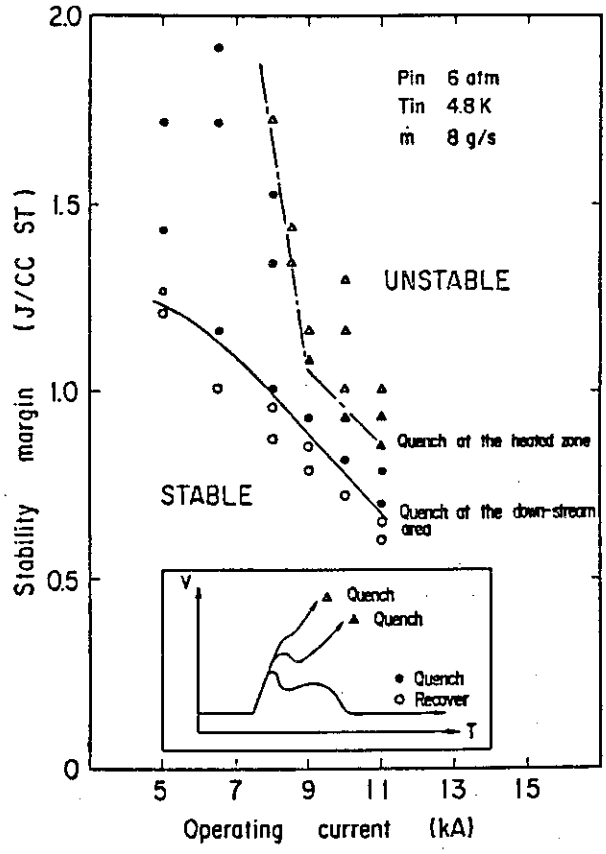

Fig. VI.5-1 Stability characteristics of JF-15.

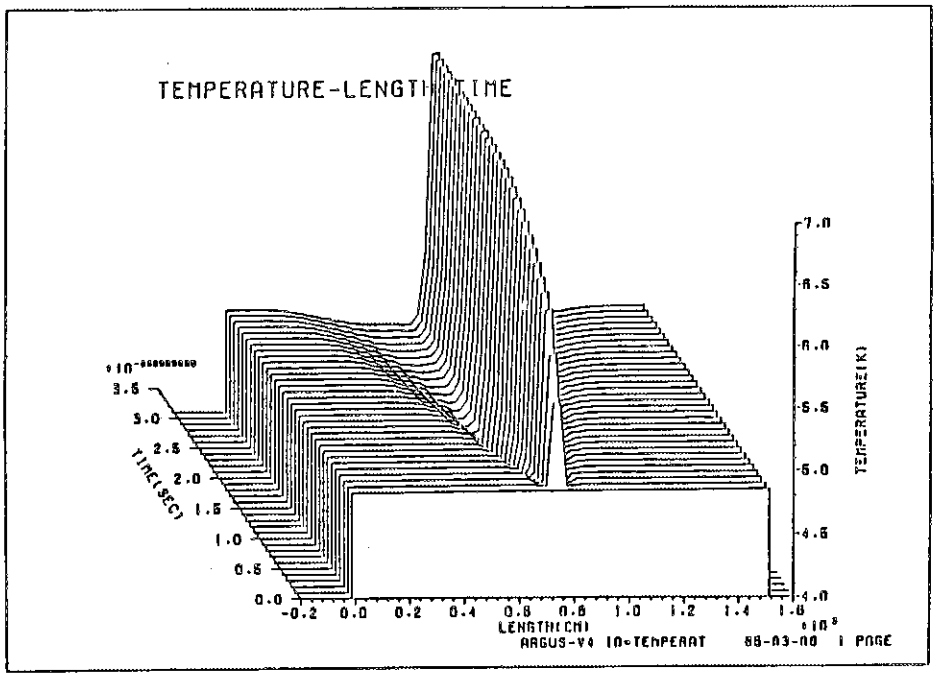

Fig. VI .5-2 Calculated stability characteristics of forced-cooled conductor obtained by "ALPHE-II".

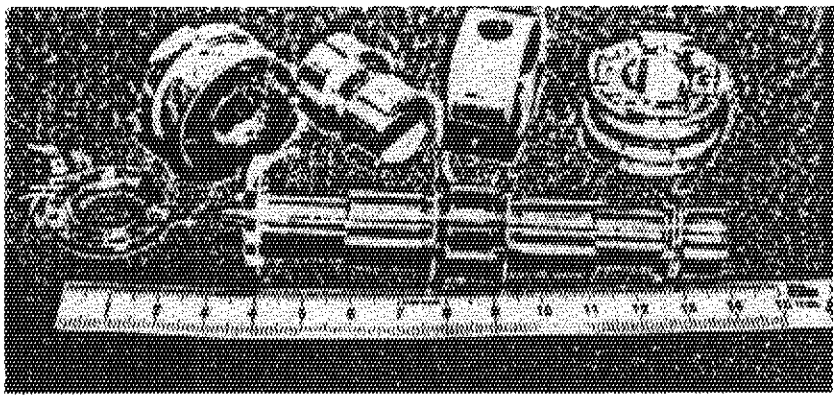

Fig. VI .5-3 The overview of turbo-expander.

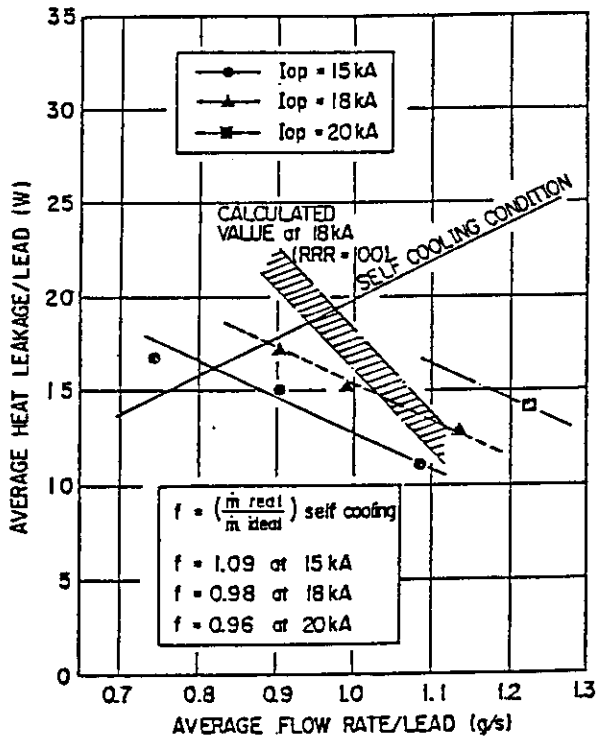

Fig. VI.5-4 Measured thermal performance of 15kA current lead charged up to 20 kA.

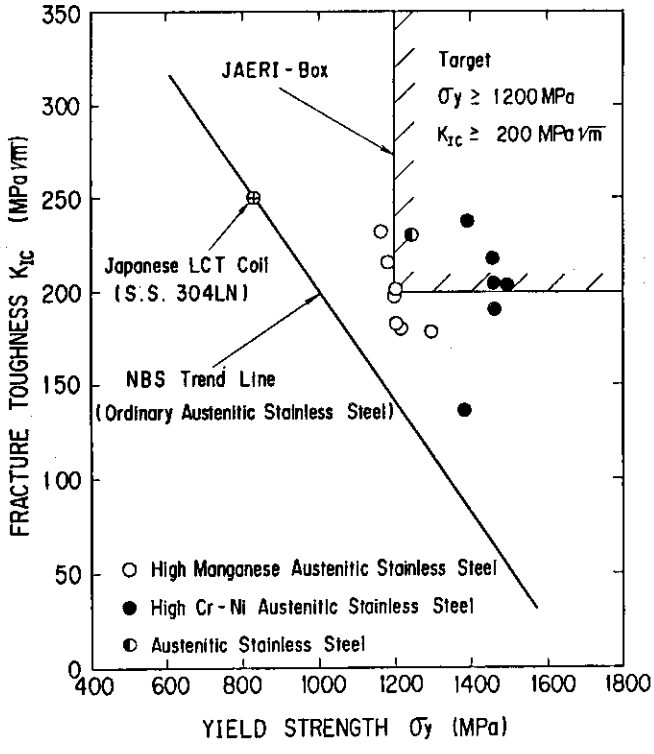

Fig. VI.6-1 Test results.

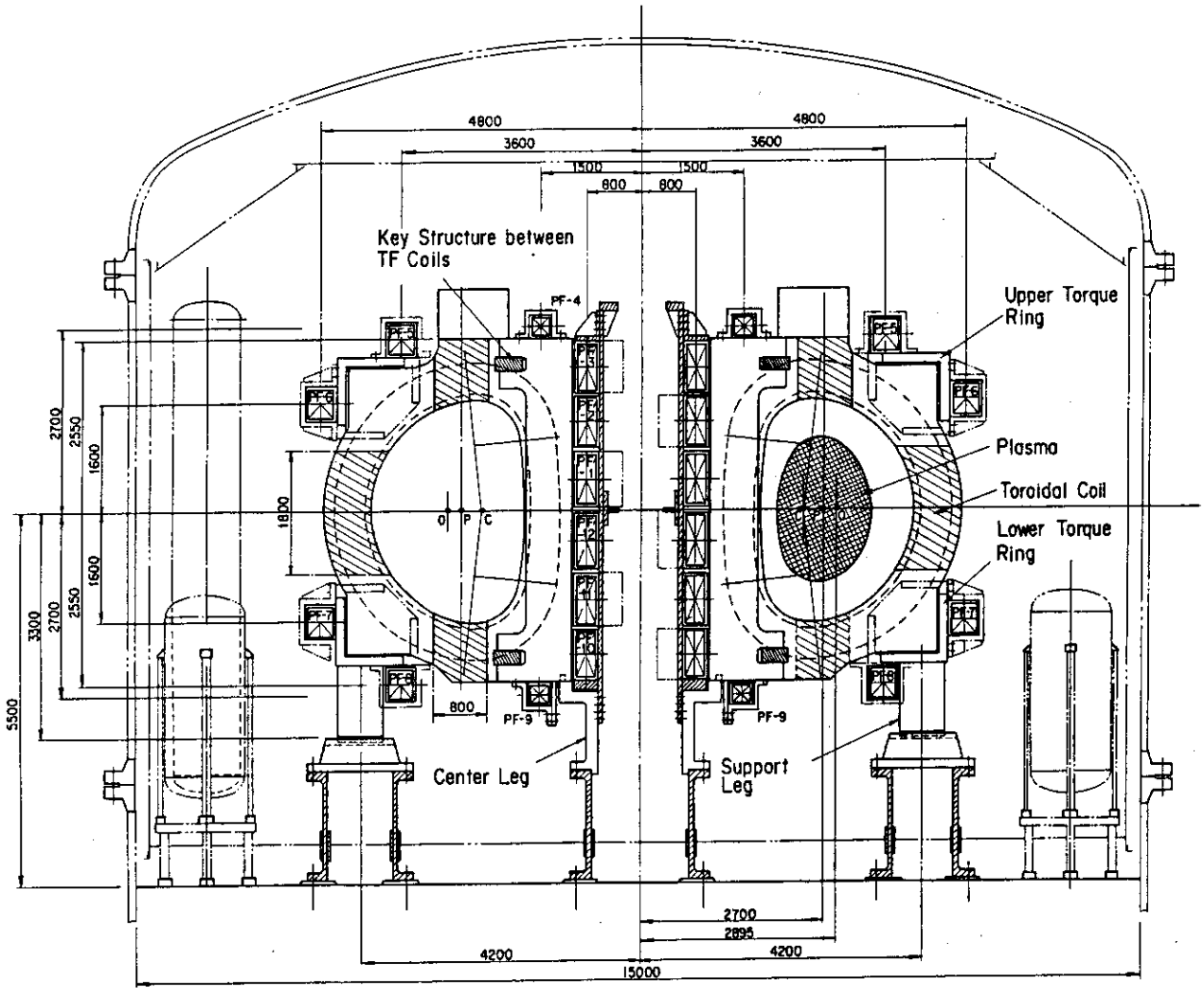

Fig. VI.7-1 Elevation view of STTA.

VII. DEVELOPMENT OF TRITIUM TECHNOLOGY

1. Tritium Processing Technology

1.1 Fuel purification

1.1.1 JAERI-LANL(DOE) fusion technology cooperation

The "Testing of Small Scale Tritium Handling Components with tritium" program(LQ3) has successfully been carried out under the Japan-US Fusion Technology Cooperation in Development of Improved Components for Fusion Fuel Cycle. As the first step of this program, a proto-type of palladium membrane diffuser (component for DT/Impurities separation) and a ceramic electrolysis cell (for conversion of DTO vapor to DT gas) has been tested with tritium to confirm their basic performance and integrity for long term operation. Table VII-1 summarizes the experimental conditions and operating performance of both components.

1.1.2 Development of components

Design and construction of the double containment type of a palladium diffuser having inner-heaters and thermal reflectors, and a electrolysis cell with multi-tube electrolite of zirconia have been carried out to meet the design criterion for the TSTA at Los Alamos National Laboratory. These components will be tested with tritium at the TSTA in the next step of JAERI-LANL(DOE) collaboration. Figures VII -1 and -2 show these components.

Material tests of the palladium alloy membrane have also been done to predict the effects of tritium gas exposure on the membrane integrity. The test items are as follows: (i) crystallographic analysis of Pd and Pd-alloy by X-ray diffraction analysis, (ii) solubility in the Pd-alloy/H_2, D_2 system, (iii) diffusivity of ^3He in the Pd-alloy membrane, (iv) implantation of ^3He with Van de Grraff accelerator, and quantitative measurement of ^3He implanted by making use of $^3He(n,p)T$ reaction, and (v) mechanical tensile tests of the Pd-alloy tubes under the hydrogen atomosphere.

1.2 Hydrogen isotope separation

1.2.1 Cryogenic distillation experiments

A series of separation experiments with N_2 and Ar have been carried out by using a cryogenic distillation column packed with various types of packings(Dixon Ring, Coil Pack, Helix and Heli-Pak). Major results obtained by these experiments are as follows: (i) the HETP value remains almost constant in a wide range of the vapor flow rate, (ii) the simulation procedure based on the stage model was verified to be useful for predicting actual column performance, (iii) Dixon Ring presented the best set of results in terms of separating performance and pressure drop across the column.

1.2.2 Hydrogen isotope separation by gas chromatographic technique

In order to establish the control system for the cryogenic distillation columns separating hydrogen isotopes, a precise and simple technique for measuring the composition of hydrogen isotope mixtures must be developed. Although the low temperature gas chromatography is expected to be reliable for this purpose, several subjects such as the sensitivity to the slight amount of isotopic species and the measurement time must further be studied.

As the first step of the development of this method, cryogenic adsorption characteristics of H_2 and D_2 on the alumina treated with various conditions were experimentally examined. The adsorption isotherms of H_2 at 77K(liquid nitrogen temperature) on the alumina treated at 200°C and 500°C are shown in Figure VII-3.

1.2.3 Design and construction of an experimental device for hydrogen isotope distillation

A design study has been performed for an experimental system separating hydrogen isotopes (H_2, HD and D_2) by cryogenic distillation. The items performed are to study the heat balance for the whole system including the refrigerator, to make design calculations for major components (packed distillation column, condenser, reboiler, vacuum jacket, heat shielding, heat exchangers, isotopic equilibrators, cryogenic adsorption columns, chemical analysis system, etc.), to determine specifications of the refrigerator, to list instrumental apparatus, to examine the control methods and operation modes, etc.

Principal subjects to be studied by using the experimental system have also been determined. Construction of a preliminary experimental apparatus based on this study has also been carried out, and its installation will be completed by next autumn.

1.3 Blanket technology

1.3.1 Tritium recovery from lithium-based materials

The chemical fate of tritium produced by the $^{6}Li(n,\alpha)T$ reaction in Li_2O have been studied with considerable attention paid to the thermal release behavior. When neutron-irradiated Li_2O was heated to 870 K under vacuum, the tritium was extracted into the gas phase in a sufficient rate. The chemical form of tritium released from the Li_2O was mainly HTO(g) and the rate-determining step of the HTO(g) release process in the crystalline powder above 570 K was found to be diffusion of tritium in the solid. The diffusion coefficient determined for the sample irradiated to 8.1×10^{16} cm^{-2} was $D=7.9\times10^{-5}\exp[-77.4(kJ/mol)/RT]$ cm^2/s. At temperature below 570 K, however, the HTO(g) release process was controlled by the thermal decomposition of LiOT at the solid surface. The first-order rate constant of the reaction $LiOT\cdot LiOH(s)\rightarrow Li_2O(s)+HTO(g)$ was expressed as $K=5.0\times10^{7}\exp[-120(kJ/mol)/RT]$ s^{-1}.

In addition, the tritium species existing in the solid phase was analyzed using a radiometric method. In Li_2O crystals irradiated with neutrons to 6.3×10^{17} cm^{-2} at ambient temperature, the tritium was distributed in T^{+}(81.1%), T^{-}(18.4%) and T°(0.6%). When the irradiated sample was subjected to the thermal annealing, the T^{+} fraction increased to nearly 100%. The results suggest that the interaction between T^{+} and O^{2-} would be involved in the course of tritium diffusion in Li_2O crystals.

In conclusion, the fundamental tritium release behavior of neutron-irradiated Li_2O crystals can be interpreted in the mechanism illastrated in Fig. VII-4 which consists of two major processes; the T^{+} diffusion in the crystal and the evolution of T_2O molecules as a result of the reaction $2LiOT(s)\rightleftarrows Li_2O(s)+T_2O(g)$.

1.3.2 In-pile experiment for tritium recovery from lithium oxide

In-pile tritium recovery experiment (VOM-21H) under the high

neutron fluence and temperature conditions has been performed at JRR-2 from May, 1984 through March, 1985. This experiment is the second step of a series of in-pile test program conducted by Fuel Property Laboratory, and is focusing to examine the feasibility of the cylindrical shape of sintered Li_2O pellet. The brief summary of the experimental conditions of VOM-21H tests is shown in Table VII-2 with the data of the first step experiment (VOM-15H) and the TRIO-01 experiment (conducted by ANL). In the VOM-21H test, effects of hydrogen addition to the He sweep gas on the tritium release characteristics (equilibrium time for steady state, chemical form of tritium), and the amount of tritium retained at various irradiation temperatures had been measured. The analytical work are now under way. Figure VII-5 shows a result of the in-line gas chromatographic analysis of gaseous tritium released from Li_2O.

2. System Analysis

2.1 Development of solution algorithm for single-stage, multicomponent, vapor-liquid flash problem

A powerful solution algorithm has been developed for single-stage, multicomponent, vapor-liquid equilibrium flash problems. The independent variables and functions to be zeroed are chosen so that the Jacobian matrix can be strongly diagonally dominant with the diagonal elements close to unity. Hence, either the identity matrix or the unit matrix can be used for all the iterations until the convergence is achieved.

2.2 Investigation of convergence characteristics of solution procedures using the Newton-Raphson methods for solving stage separation problems.

Some representative solution procedures for solving stage separation problems have critically been reviewed by a number of numerical experiments performed under various conditions. It has been clarified how the convergence characteristics of the procedures using

the Newton-Raphson methods are related with the physicochemical properties of the mixtures, types of the stage separation problems (distillation-type or absorption-type), approximate treatments in linearizing the basic equations, ways of choosing the independent variables and defining the functions to be zeroed, ways of joint use of the successive substitutions, and the input and output specifications of the separation processes. As a product from the above-mentioned study, the best solution procedure is now recognized for hydrogen isotope distillation columns that are characterized by narrow-boiling mixtures, low nonideality and presence of infinitesimal amounts of components.

2.3 Drastic reduction of computing time in dynamic simulation of hydrogen isotope distillation columns

Rather detailed reviews have been given to the integration techniques for very stiff ordinary differential equations with high dimensionality to be integrated in dynamic simulation of hydrogen isotope distillation columns. As a result, the technique developed by Ballard-Brosilow has been chosen: when applied to distillation, it requires only the solution of linear tridiagonal equations and scalar bubble point calculations at each time step. Compared to the improved Euler method, for example, it present a remarkable success: A typical numerical example simulating column dynamics from a steady state to another indicates that the calculation results can be obtained with engineering accuracy in about two orders of magnitude shorter computing time.

2.4 Design concept of cryogenic falling liquid film helium separator

The process characteristics of the cryogenic falling liquid film helium separator are greatly improved by an idea of adding an H_2 gas flow to a point near the upper end of the packed section. The flow rate of tritium lost from the top is kept extremely low (0.2 Ci/y under the flow conditions of the Tritium Systems Test Assembly) with an adequately short packed section (1.4 m), and the pressure is reduced to

1 atm.

A design procedure using the Colburn-Hougen method is developed for determining specifications for the refrigerated section. Control schemes are also proposed and compared with schemes for the cryogenic distillation column. The pressure rise that cannot readily be eliminated by adjusting input specifications of the refrigerant gas is avoided by increasing the top gas flow rate. The tritium concentration in the top gas is controlled by the H_2 gas flow rate.

Table VII-1 Long Term Operation of Proto-type Tritium Processing Components.

(i) Pd-diffuser

* Location : solid waste disposal box, TSTA
* Start data : August 15, 1984
* Stop date : August, 1985(Proposed)
* Inventory : 1400Ci-T_2
* Temperature : 550K
* Pressures : Feed gas; 200kPa, Pure gas;20kP
* Flow rates : Feed; 12.6L/h, Pure; 11.3L/h
* Scale : 1/30 TSTA-FCU flow rate

(ii)Ceramic Electrolysis Cell

* Location : Inventory Glovebox, TSTA
* Start data : Jult 30, 1984
* Stop data : January 10, 1985
* Inventory : 38Ci-T_2
* Carrier : Helium
* Temperature : 900K
* Pressure : 67kPa(97%He, 3%T_2)
* Conversion rate: 99.9%(T_2O to T_2)
* Scale : 1/10 TSTA process flow rate

Table VII-2 Brief Review of Irradiation Conditions of In-Pile Experiments.

	VOM-15H(JAERI)	VOM-21H(JAERI)	TRIO-01(ANL)
Material	Li_2O : 6.67g	Li_2O : 2.03g	$LiAlO_2$: 42.9g
Neutron Flux (thermal)	$1x10^{14}n/cm^2.sec$	$0.9x10^{14}n/cm^2.sec$	$4x10^{14}n/cm^2.sec$
Irrad. Temp.	480-760°C	350-900°C	500-700°C
Irrad. Time	990 hrs	2655 hrs	2112 hrs
Burnup	0.24%	0.85%	0.18%
Sweep Gas	He	He, 10, 100, 1000ppmD_2-He, 100ppmO_2-He	He, 1%H_2-He, 0.1%H_2-He, 0.2%O_2-He

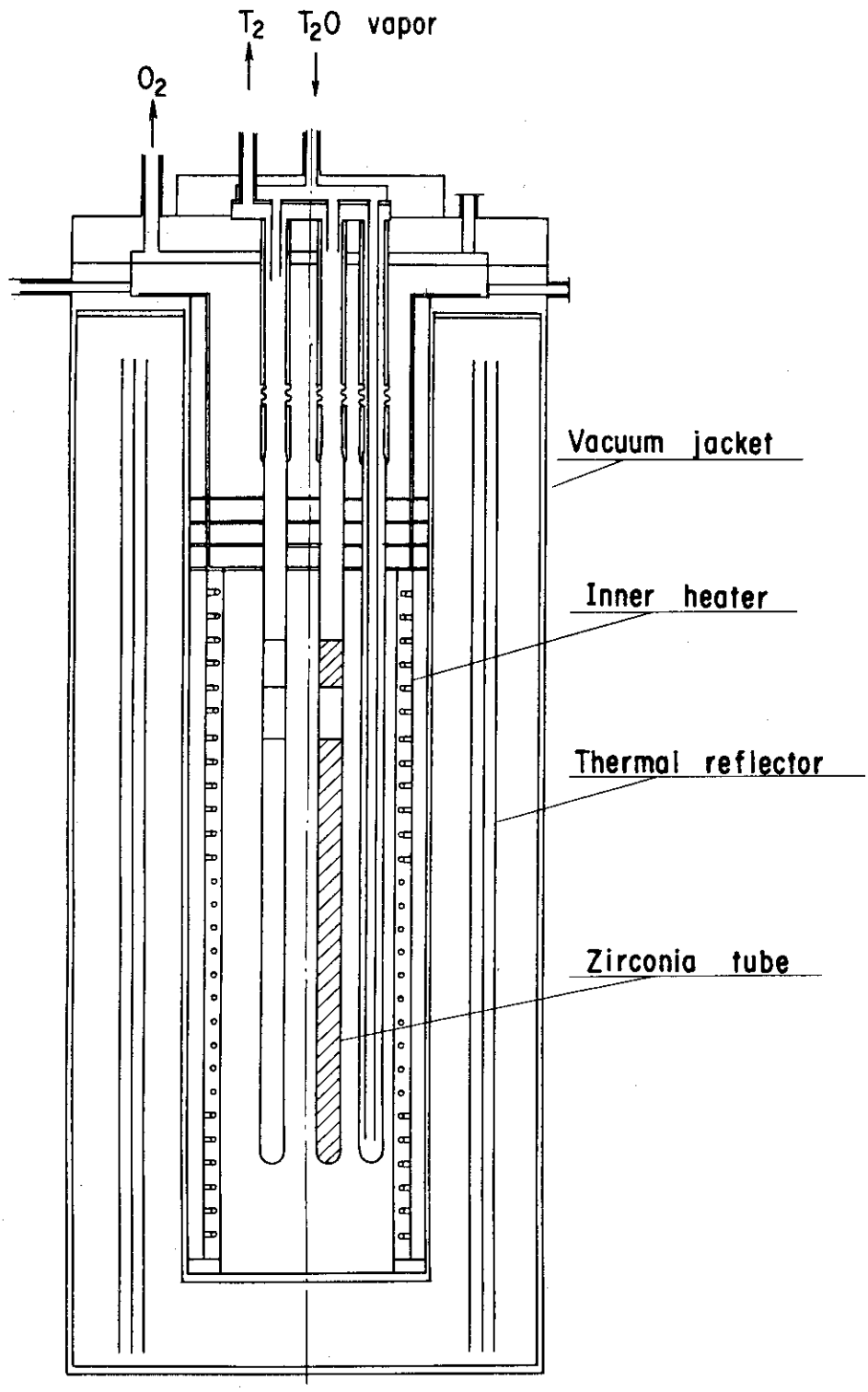

Fig. VII-1 Structure of a Multi-tube Type of Ceramic Electrolysis Cell.

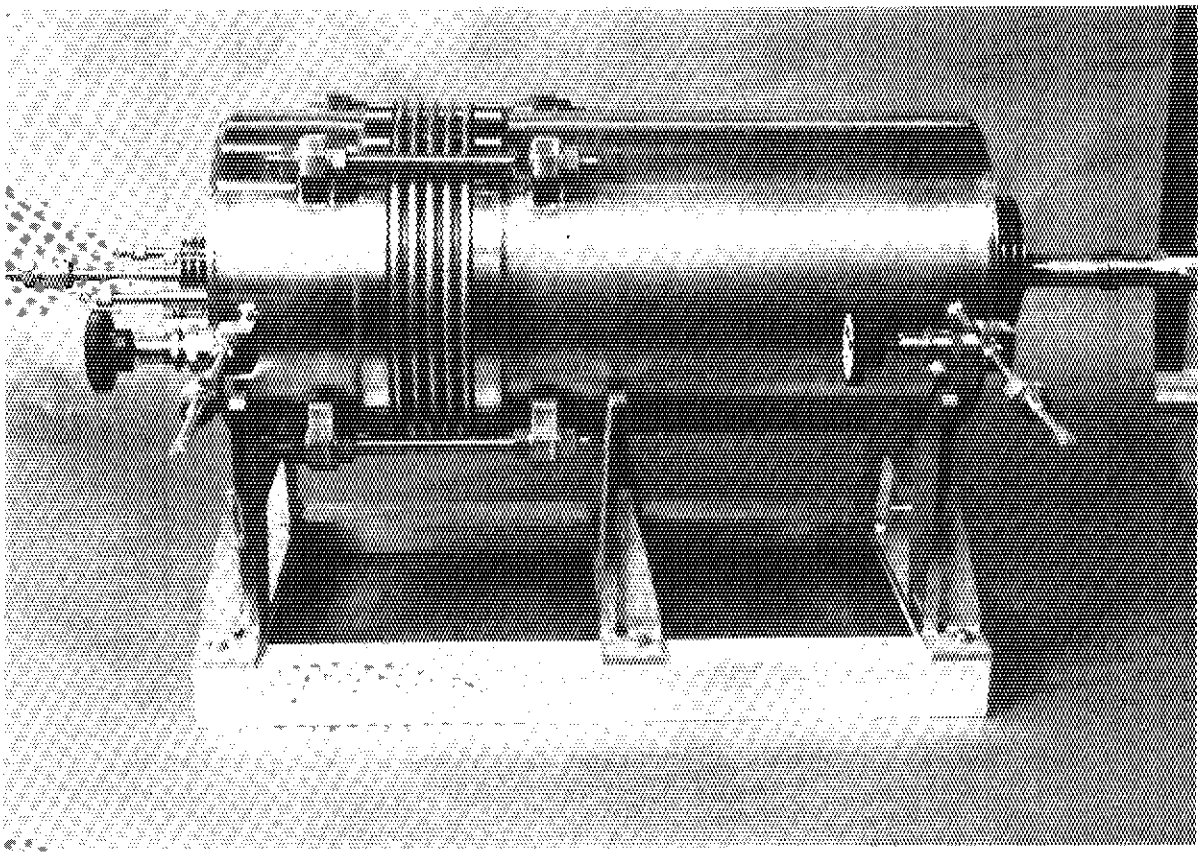

Fig. VII-2 Appearance of a Tritium Compatible Pd-diffuser.

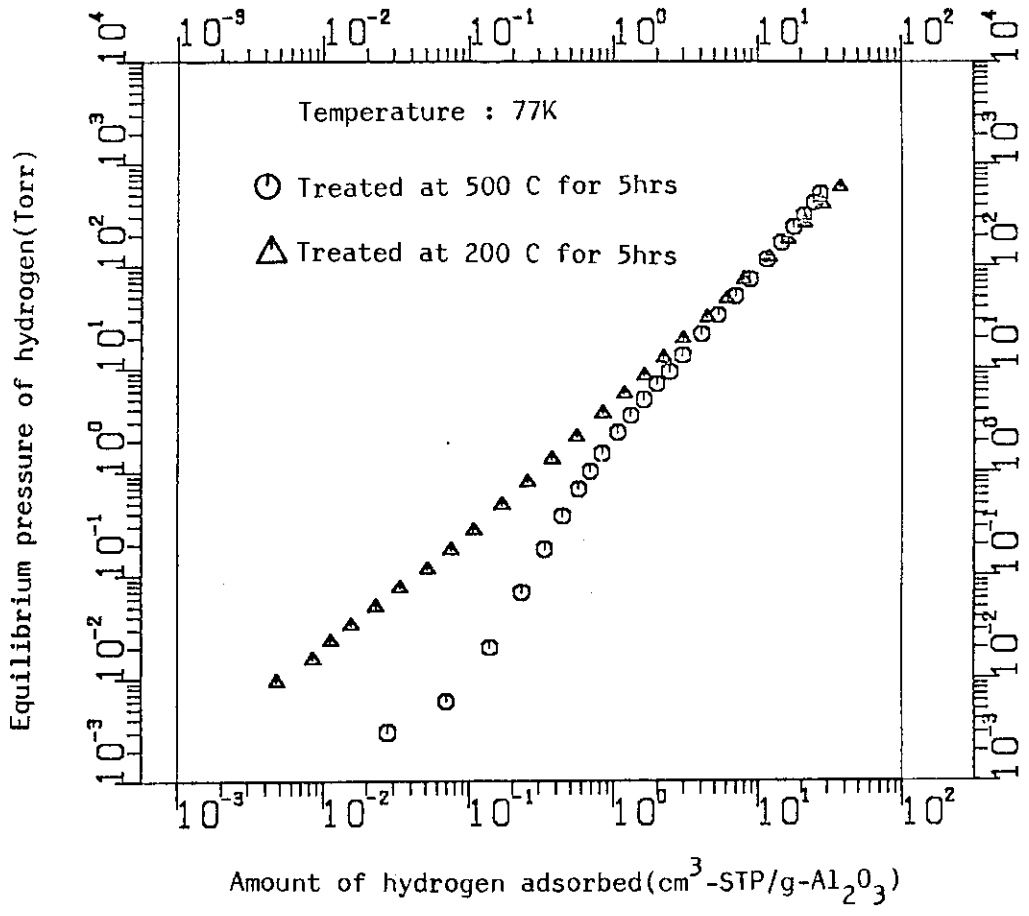

Fig. VII-3 Cryogenic Adsorption Isotherms of Alumina for H_2.

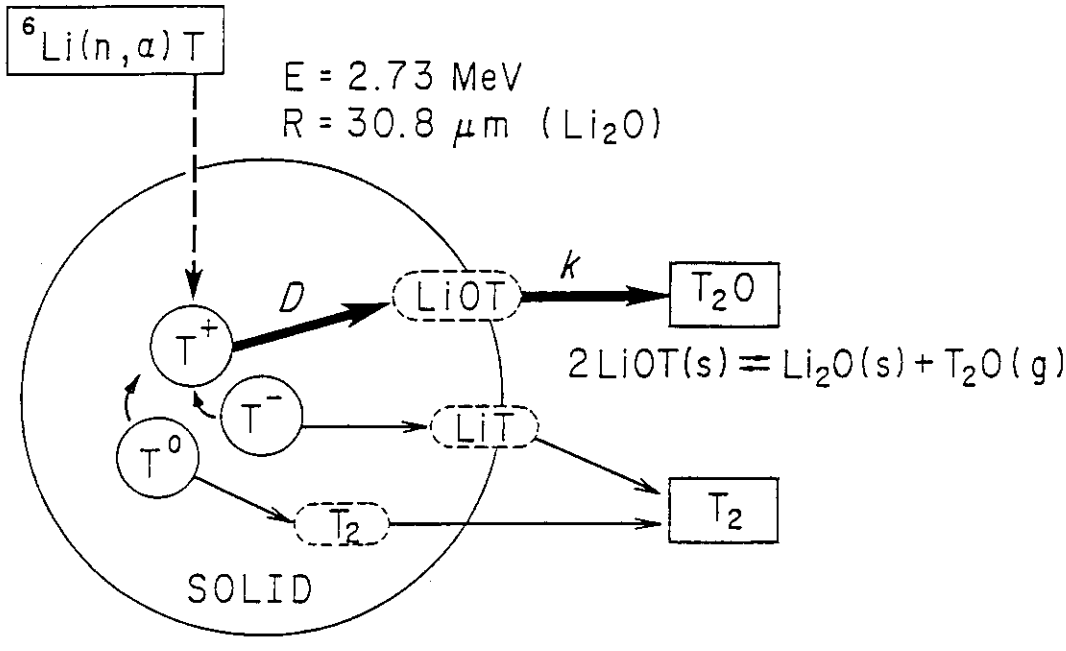

Fig. VII-4 A Mechanism of Tritium Release from Li_2O Crystalline.

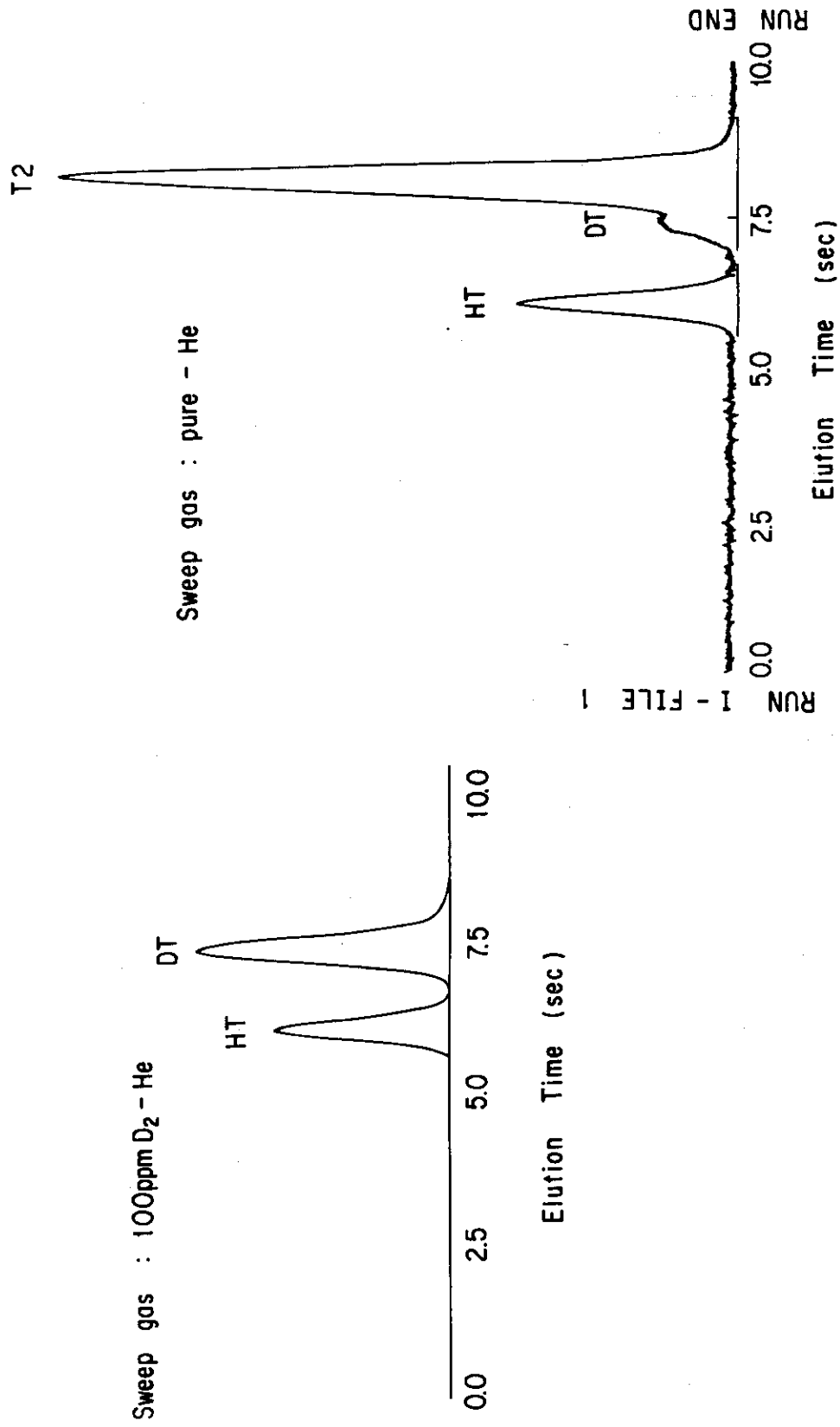

Fig. VII-5 Molecular Composition of Tritium released from Li_2O under Irradiation.

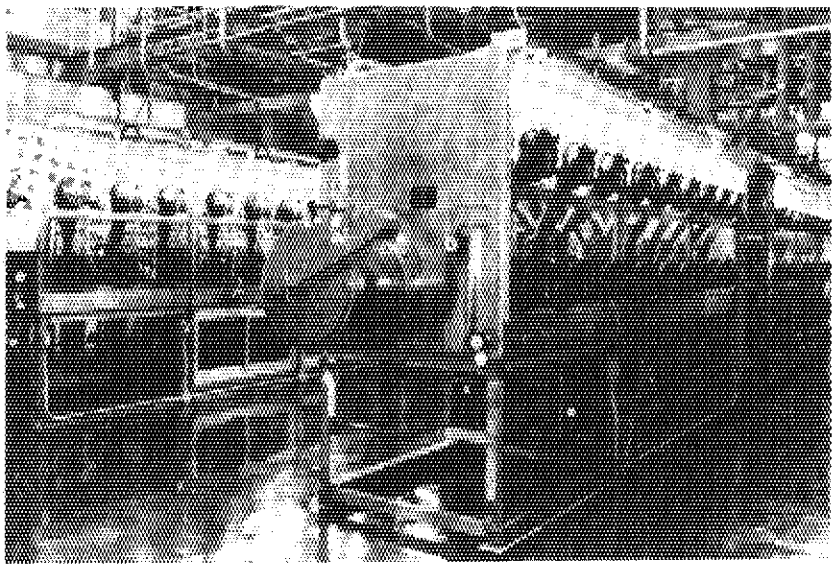

Fig. VII-6 Line-up of Gloveboxes for Tritium Processing Experiments at TPL.

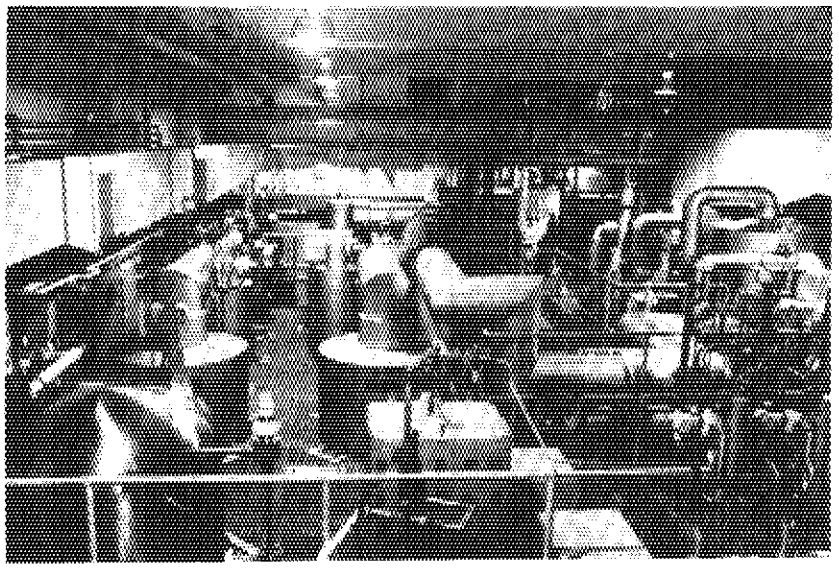

Fig. VII-7 View from the Second Floor of the Detritiation Room at TPL.

VIII. JAPAN-US RESEARCH COOPERATION IN DOUBLET-III

The original 5-year program (phase one) of the experimental study on D-shaped tokamak using the Doublet III facility at GA Tech., Inc. has been terminated in Sept. 1984. The research program as part of the US-Japan fusion research cooperation was extended for another four years until Aug. 1988. The second phase of the experiment on Big D (Large D shaped vacuum vessel, shown in Fig. VIII-1) will start in late 1985. Brief description on the results of the phase one is given here.

The highlights obtained during the first phase can be summarized as follows:

(A) High beta plasma close to the reactor relevant (volume average $\beta = 4.5$ %) was realized as a result of low q discharge optimization.

(B) High temperature plasmas of $T_i \sim T_e \sim 5 - 6$ keV at electron density of $6 - 7 \times 10^{19}$ m^{-3} and energy confinement time $\sim$70 ms were achieved with divertor operation (so called H-mode) as shown in Fig. VIII-2.

(C) By employing a pellet-injector, a high density ($\sim 10^{20}$ m^{-3}) discharge mode without confinement deterioration during beam heating in the limiter configuration was found (P-mode, shown in Fig. VII-3).

The necessary conditions for the H-mode discharge are the relatively high heating power to be deposited (above $\sim$3 MW in this case), the lower edge recycling near the main plasma and accompanied high edge temperature simultaneously. The central ion and electron temperature of H-mode discharges increases almost linearly with the absorbed power (OH + injected NBI power - calculated shine-through power) up to 7 MW and attained more than 5 keV as shown in Fig. VIII-4. The amount of kinetic energy stored in the plasma measured by the diamagnetism increases also linearly with the increase of absorbed power. The volume averaged beam component at high heating power is estimated to be 10 - 20 % in these cases. The stored energy is plotted as a function of absorbed power in Fig. VIII-5. Deuterium beam injection into deuterium plasma results in larger stored energy. The highest stored energy for deuterium case is $\sim$530 KJ. However, sufficient data were not available due to the high neutron flux. The power deposition calculated for deuterium beam shows a power density to ions higher than that for hydrogen beam in $r/a > 0.4$ and the total power to ions is larger by less than 20 %. The neutron yield with deuterium injection into deuterium plasma reached more than

10^{15} neutrons/sec. No H-mode was observed in the case of hydrogen beam into hydrogen plasma with 4 - 5 MW power level. The toroidal momentum confinement inferred from the toroidal rotation velocity measurement by the Doppler shift of a charge-exchange recombined O VIII line is also increased by a factor of $\sim$2 in H-mode.

On the plasma-wall interaction and the divertor plasma characteristics, following results were obtained:

1) The central radiation loss was reduced to a low value by strong gas puffing. Strong gas puffing resulted in smaller impurity production and more efficient suppression of backflow of impurities from the divertor.
2) The remote radiative cooling (radiative cooling of the divertor plasma) increased with electron density of the main plasma. The radiative power of the main plasma was constant for the whole electron density range investigated. The remote radiative cooling power in high density divertor discharge was 24 % of the total absorbed power (4.5 MW).
3) The electron temperature at the divertor plate became lower with high electron densities in the main plasma. An electron temperature of 8 eV was observed with an absorbed power of 4.5 MW, which suggests that unacceptably high erosion of the divertor plate can be avoided by operating the divertor at high densities.
4) The ion saturation current increased with main electron density. An electron density of 3×10^{20} m^{-3} was observed with an absorbed power of 4.5 MW. This suggests that the pumping requirements of fusion reactors can be relaxed in high density divertor operation.
5) Though complicated by the perturbations made to the main and divertor plasmas by the probe insertion, the measurements of the electrostatic potential in the divertor plasma suggest that there is a possibility of a significant difference in the electrostatic potential between good-heating modes and poor-heating modes.
6) Experiments of divertor configuration with a small mirror ratio suggest that the magnetic mirror might not be important in H-mode physics.

References

1) KITSUNEZAKI, A., et al., in Plasma Physics and Controlled Nuclear Fusion Research (Proc. 10th Int. Conf. London, 1984) Vol.1, IAEA Vienna (1985) 57.
2) SENGOKU, S., et al., ibid 405.
3) SHIMADA, M., et al., ibid 281.

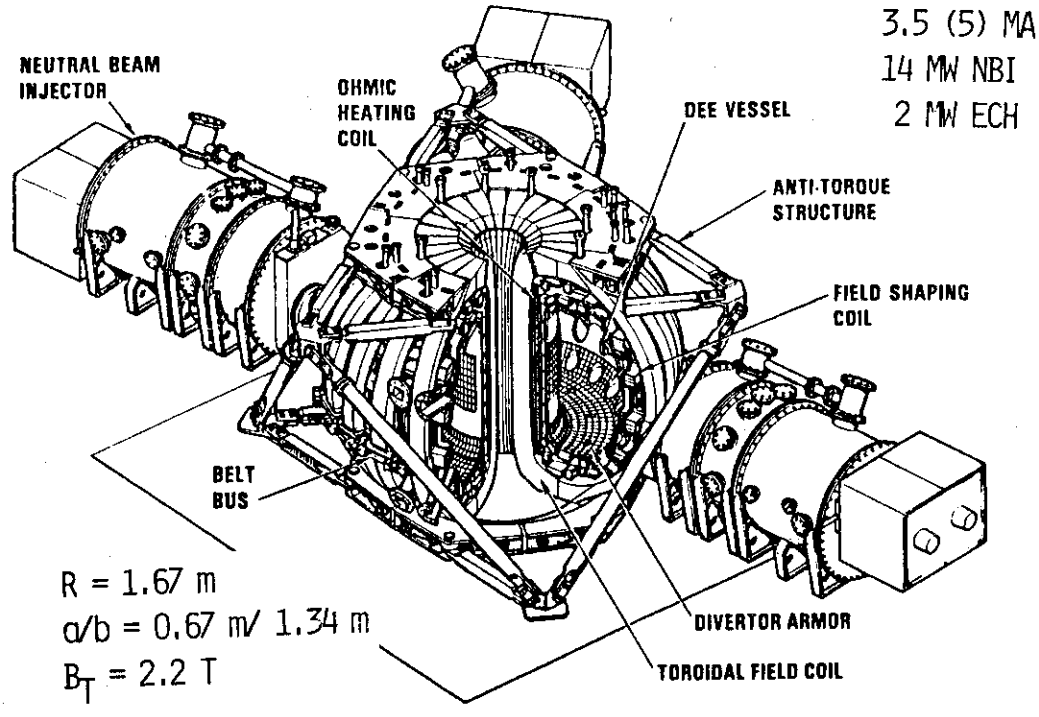

Fig. VIII-1 Cutaway isometric of DIII-D with one neutral beamline removed.

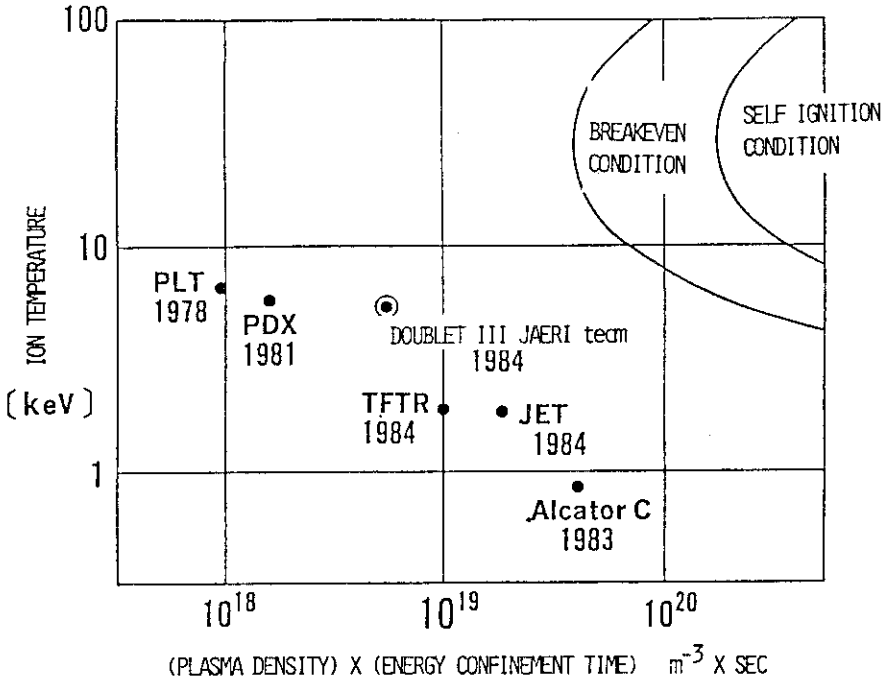

Fig. VIII-2 Lawson diagram.

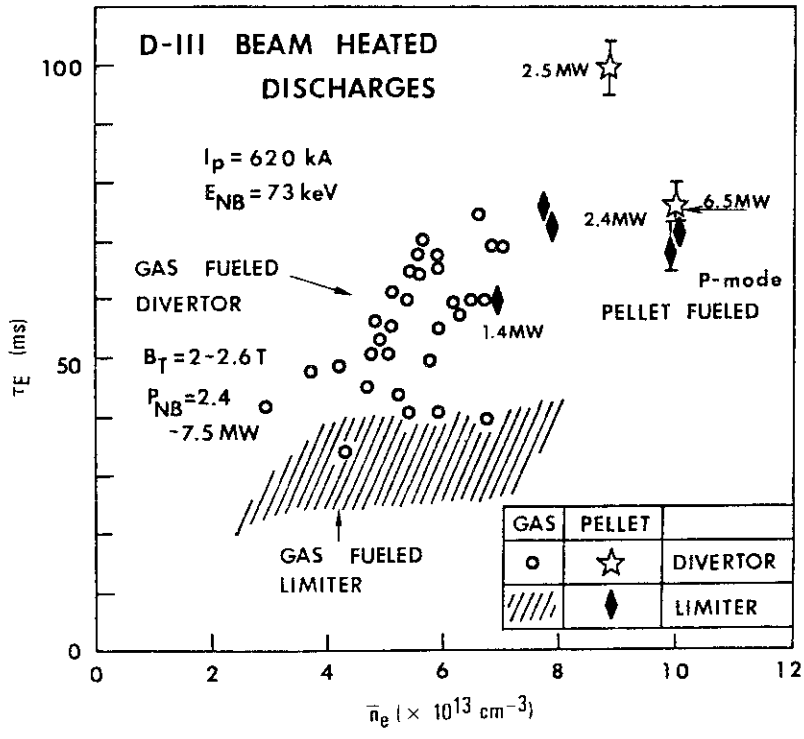

Fig. VIII-3 Comparison of $\bar{n}_e$, τ_E plot between pellet and gas fueled discharges for both limiter and divertor configurations with continuous beams. The upper envelope of open circles corresponds to D-III H-mode discharges. For gas fueled discharges, τ_E is calculated when dW/dt = 0.

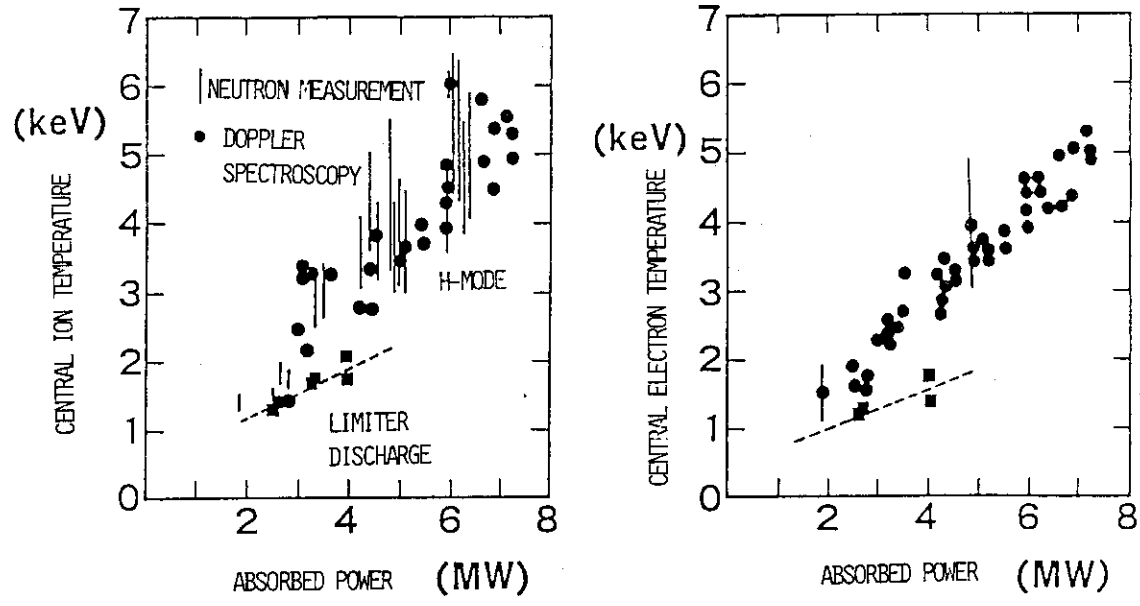

Fig. VIII-4 Central temperatures vs. absorbed power.

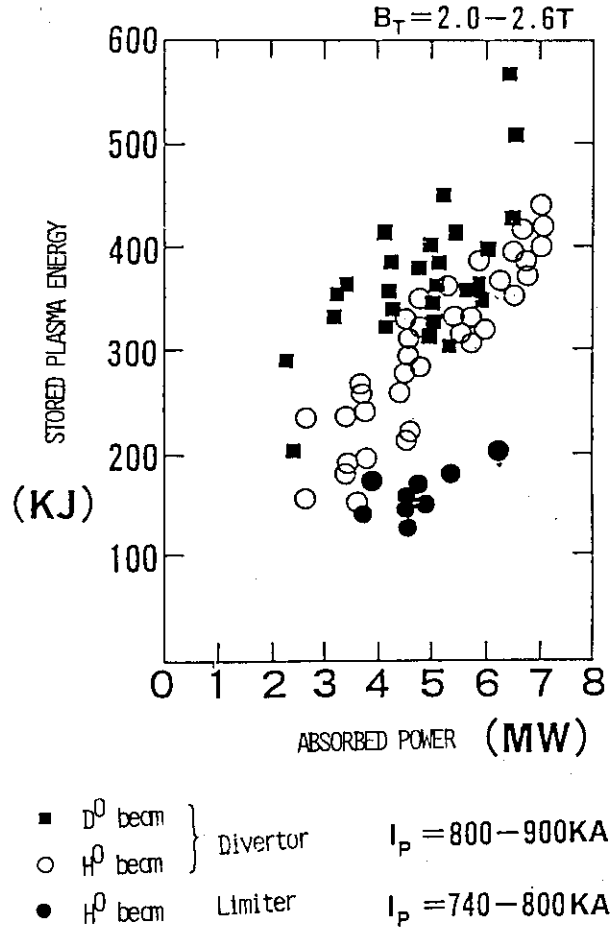

Fig. VIII-5 Stored energy vs. absorbed power.

IX. DEVELOPMENT OF LARGE TOKAMAK JT-60

1. Introduction

A great effort made by JAERI and industry for the JT-60 project was rewarded by successful progress and completion of installation and tests of the JT-60 device. The contractual completion is expected in April 1985, to be immediately followed by the initiation of experiments.

The fabrication of the heating and diagnostic devices has progressed as planned. Emphasis during this year was also placed on preparing for the experiment and device operation in the coming year.

2. Outline of the Progress of JT-60

Construction of JT-60 except heating devices and diagnostic system was completed at the top of FY 1985 after its full performance test in FY 1984. The commissioning activities feature this fiscal year. Control system integration test was carried out from June to November of 1984 after linkage tests between the subsystem controllers in the previous fiscal year. During this test, the JT-60 hardwares and softwares were checked and reviewed by the task force team which consisted of the members of JAERI and industries. About 600 items were pointed to be improved or modified for the coming system integlated test and the operation. Installation of tokamak machine continued day and night for 20 months was completed on October 1984. The vacuum tests of the vacuum vessel at the room temperature as well as a baking one of 350°C followed installation. Tokamak machine was subjected to the power test from December 1984 to the end of February 1985. The integrated performance test was continued during March. These tests were successfully performed at the full power ratings. Technical problems were solved each time then they appeared. Reliability and performance of the JT-60 system were fully certified as the result of the these test.

The operation aiming at the first plasma formation in JT-60 was expected successfully. On the other hand, construction of the heating

devices, *i*,*e*., NBI and RF, and the diagnostic system progressed in this fiscal year. The diagnostics equipments required for the initial OH experiment were assembled. Beamlines for NBI and klystrons as well as launchers for RF were continued assembling and preconstruction tests. They are expected to be installed around the Tokamak machine after the initial OH experiment. Construction of the NBI and RF power supplies building and the high pressure gas and compressors building was completed in this fiscal year. Installation of the NBI and RF power supplies was started. Construction of JT-60 made significant progress in this fiscal year along the project schedule shown in Fig. IX.2-1.

3. Status of Tokamak Machine

3.1 Assembly

Assembling and installation work of JT-60 tokamak machine were started in February 1983 and progressed to complete the assembling of most of its major components such as the toroidal and poloidal field coils, the vacuum vessel, the mechanical support structure and the vacuum pumping system. Following the progress achieved in the last year, assembling and installation work were continued in this year.

During the first four months efforts were focussed on welding works of the poloidal field coils (including the magnetic limiter coils and casing) and the vacuum vessel at the split section, through which eighteen toroidal field coils had been inserted. As the poloidal field coils were consisted of 188 turns of conductors and the space for welding work was limited, strict inspection was carried out about the dimension and integrity of the welded joint such as the penetrant testing, ultrasonic testing and withstand voltage test. As the welded joint of the vacuum vessel and magnetic limiter casing constitute the vacuum boundary, emphasis of inspection was laid on helium leak test as well as the dimensional check and the welded joint integrity test mentioned above.

Installation of the first walls was carried out together with the welding work of the poloidal field coils and the vacuum vessel. First walls are consisted of the fixed limiters, liners and so on, amounting

up to around 10,000 pieces. In this work, attention was paid to minimizing the dimensional dispersion and the contamination of the surfaces of the vacuum vessel and the first walls themselves. Specical care was directed to the radial dimension of the fixed limiters, whose dispersion was limited within ±1.5 mm.

87 sets of the gate-valves were installed at the edge of the ports after installation of the first walls. Installation work was carried out in the temporary dust free room not to degrade the vacuum sealing property of the gate valve by dust.

Outside the vacuum vessel carried out were a huge amount of piping work of the coolant channels and wiring work of the electric heaters and several kinds of sensors such as thermocouples, strain gauges and so on, which required a long period over half a year. Assembling and installation work of the tokamak machine were completed in November 1984.

Gas injection and pre-ionization systems were also installed in September 1984, followed by their performance tests. Performance tests of the other components such as vacuum system, primary cooling system, heating and cooling systems of the vacuum vessel were also started from September 1984 one by one after completion of installation and completed in November, followed by the power tests. Outline of the performance tests is summarized in the following section.

3.2 Test

3.2.1 Vacuum system test

JT-60 vacuum vessel is a toroidal chamber made from Inconel 625 with a large volume of around 200 m^3 and inner surface of about 2750 m^2. It consists of rigid rings and bellows welded together into a torus and is bakable at a temperature over 350°C. It is required to satisfy the vacuum properties listed in Table IX.3-1 from physical requirements, and extensive effort was made to meet them throughout fabrication and installation processes.

Helium leak detection was carried out at any welding seal and bolt-jointed flange, so far as it constitutes the vacuum boundary, which amounted to 1500 locations. Several leakages were observed at the electromagnetic probes and thermocouples installed inside the vacuum vessel and port flanges. Some of the leaked electromagnetic probes

were backed up by differential pumping, and others were repaired by re-welding or re-fastening the bolts. Finally no leakages were observed within the sensitivity of the detector.

Each component including vacuum vessel itself was carefully cleaned and baked out in the factory, and strict attention was also paid to the installation work and inspection at the site so as to minimize the contamination of the vacuum vessel inner surface. After completion of installation the vacuum vessel was washed internally again with Aceton rinse and Freon jet spray, followed by two cycles of baking at the temperature over 350°C and for the hold time over 24 hrs per cycle. And finally vacuum properties listed in Table IX.3-1 were obtained, which were far below the specifications.

3.2.2 Baking test

Following completion of vacuum vessel installation, baking test was carried out to confirm temperature control characteristics by heating and cooling systems and also to confirm structural integrity of the vacuum vessel and its support system.

JT-60 vacuum vessel is heated by electric heaters attached on its outer surface and cooled down by nitrogen gas and water (possible under the condition of the vacuum vessel temperature less than 200°C) flowing through the square pipes fastened on the outer surface of the vacuum vessel with cleats and stud bolts. Major specifications of heating and cooling systems are summarized in Table IX.3-2.

Baking test was classified into temperature control characteristics test, vacuum pressure measurement and displacement measurement due to thermal expansion. The results of the former two tests are shown in Fig. IX.3-1 and Table IX.3-2. As shown, all of the specifications conserning temperature control characteristics were satisfied. In the present test, baking temperature was suppressed in the vicinity of the lower limit of the specification taking necessary baking effect and machine security into consideration. Change of the cooling from nitrogen gas to water was carried out without any problem at the vacuum vessel temperature of 200°C.

Time evolution of the vacuum pressure is also shown in Fig. XI.3-1. Vacuum pressure was reduced from 2×10^{-5} Pa (before baking) to 4×10^{-6} Pa (after baking) by a cycle of baking shown in Fig. IX.3-1. After another cycle of baking the pressure less than the specification, which

is listed in Table IX.3-1, was achieved.

Each rigid ring of JT-60 vacuum vessel is supported from outside by two support arms, one of which has one pin-joint and the other has two. When the rigid ring expands due to the temperature rise, the former corresponds to the fixed point and the latter movable point. Figure IX.3-2 shows the relation between the mean temperature of the vacuum vessel and the displacements of the movable points of two 60°-sectorical rigid ring named #1 and #5. Solid and broken lines denote the designed displacement and blank circle and triangle the measured ones. They showed good agreements with an error less than 1 mm. And it was concluded that pin-joint structure fulfilled its function expected in the design without sticking even at elevated temperature and thermal expansion of the rigid ring was not restrained excessively.

3.2.3 Cooling system test

Cooling system of JT-60 tokamak machine is consisted of the primary cooling system and gas cooling system. The former is utilized to cool down the toroidal and poloidal field coils and the vacuum vessel with water, and the latter to cool down the vacuum vessel and the magnetic limiter plate with nitrogen gas.

The primary water cooling system is composed of four pumps, four heat exchangers, five filters, a strage tank, pipings and many valves including three flow requlation valves. Four pumps are designed to have a capacity of the total flow rate of 2500 m^3/hr and the outlet pressure of 1.6 MPa. In addition, the system is provided with a purification subsystem capable of maintaining the extremely pure water with the electric resistivity more than 10^3 Ω·m. This system is controllable both in the primary cooling system room and in the center control room. After the cooling loop had been flushed with water in order to remove all dusts left inside the pipes, the cooling system test began in October 1984. The purposes of the test are to adjust the regulation valves, to confirm the effect of the water temperature rise on the flow rate and to confirm the functions of the instrumentation and safety interlock system.

The results of the regulation valves adjustment are listed in Table IX.3-3 and an example of the relationship between the flow rate and the valve opening is shown in Fig. IX.3-4. From the above results, it is clear that the regulation valves can control the flow rate of the

JT-60 coil cooling water with sufficient accuracy. Instrumentations such as the flow meters and interlock system fulfilled their function as expected in the design.

For the gas cooling system which is composed of the vacuum vessel cooling system and the magnetic limiter plate cooling system, similar tests were carried out and sufficient characteristics were confirmed. Natural and forced drain operations functioned well in the exchange stage of the coolant from water to nitrogen gas, though several times of repetition was found to be necessary to remove water in the piping line.

3.2.4 Gas injection system test

(1) Fundamental test

The primary purposes of the fundamental test are to verify the throughout equation, to examine the throughput characteristics and to obtain the response time of the PEV gas injection system. Setup for the fundamental test is shown in Fig. IX.3-4. Relation between the throughput rate and impressed voltage of the crystal was determined by the pressure buildup in the vacuum vessel of around 1.0 m^3. For the injection gas, hydrogen and nitrogen were used to examine the applicability of throughput equation to various gases.

Comparison between the calculated throughput and the measured one is shown in Fig. IX.3-5. Throughput was observed at the impressed voltage over 60 V, though 25 V was expected by throughput equation. Measured throughput was larger than the calculated one at the impressed voltage over 110 V. The discrepancy between them was thought to be caused by neglecting the arresting force of the spring, which might reduce the throughput area and then make impressed voltage larger. It was concluded that the throughput equation was applicable at the impressed voltage over 110 V with an error less than 20%.

Response time of 2,5 msec from open to completely closed was obtained, which was less than the designed one. And seat leakage rate less than 1.33×10^{-8} Pa·m^3/sec was obtained with the helium gas at the pressure of 0.2 MPa.

(2) Performance test

Performance test was carried out during power tests to verify the reliability of PEV gas injection system under the strong magnetic field and at the elevated temperature.

Seat leakage rate less than 1.33×10^{-8} Pa·m^3/sec was achieved before baking using helium gas at the pressure of 0.2 MPa. After baking seat leakage rate over the designed value by a factor of 10 was found at three small valves, which were exchanged with spare ones.

Typical examples of throughput rate is shown in Fig. IX.3-6. The maximum throughputs of 53.7 Pa·m^3/sec and 5.33 Pa·m^3/sec were obtained under the inlet pressure of 0.2 MPa for large and small flow rate type PEVs, respectively, which showed good agreement with the injection CAMAC command of 53.3 Pa·m^3/sec and 5.33 Pa·m^3/sec, respectively.

Dependence of the throughput rate on the toroidal and vertical magnetic fields is typically shown in Fig. IX.3-7. Throughput rate of the large flow rate type PEV was increased by 7% and 5% under the maximum toroidal and vertical magnetic fields, respectively. And that of the small flow rate type PEV was increased by 10% under the maximum toroidal field. As the PEV has virtually an error of throughput rate of around 6% because of the inaccuracy of the inlet pressure, dependence of throughput rate on the magnetic fields is negligible.

3.2.5 Power test of tokamak machine

Following the completion of the tokamak machine, JT-60 power tests were carried out from Dec. 10, 1984 to Feb. 20, 1985 to demonstrate, in advance of actual plasma operation, satisfactory performance of tokamak machine, power suppliers and control system in combination. The tests began with low-power tests of individual coil systems and progressed to full-power tests and tests of all coil systems in combination. At the final stage of the power tests the vacuum vessel temperature was raised up to 350°C and full-power tests of all coil systems in combination were demonstrated. The coil current was raised step by step, monitoring the mechanical, thermal, electrical and vacuum data.

Power tests were concluded almost on schedule with successful results. All of the coil systems were raised up to full-power operation in combination and verified was the system performance including the structural integrity of tokamak machine.

Principal results are shown in Figs. IX.3-8, IX.3-9 and IX.3-10. Figure IX.3-8 shows the comparison between measured circumferential strain of the toroidal field coil casing and designed one. Strain was measured at the location indicated in the figure for nine toroidal field coils and expressed by the average and standard deviation of nine

measurements. As revealed in this figure, measured strain, which had a linear relationship with the square of toroidal field coil current, was less than the designed one. This might be caused by the presence of the gap between the conductor and the casing. In the design of toroidal field coil, it was assumed that there was no gap between the conductor and the casing, and electromagnetic force and thermal stress acting on the conductor were directly transferred to the casing. However, fabricated toroidal field coils had actually the gap between the conductor and the casing to some extent and the loads shared by the casing might be reduced. Accordingly, the strain observed in the casing was less than that expected in the design. Increase of strain in the conductor, which was afraid with increase of loads shared by the conductor, was proved to be negligible small by FEM analysis.

In the case of combined operation of toroidal and poloidal field coils, overturning moment of toroidal field coils up to 140 MN·m was supported by the wall of the building through the upper support structure and trusses. And the maximum displacement of 3.0 mm was expected at the periphery of the upper support structure. Figure IX.3-9 shows the comparison between the designed displacement of the upper support structure and that measured by transit. Abscissa represents an electromagnetic force parameter f defined by the following equation,

$$f \equiv T \times \frac{F + 3V}{4} \quad ,$$

where T, F and V denote the ratios of the toroidal field, ohmic heating and vertical field coil currents to their full-power ones, respectively. Measured displacement showed a linear relationship with f and a good agreement with the designed one over the whole range of f.

Noticeable vibration of the vacuum vessel was observed in case of combined operation of toroidal and poloidal field coils. Acceleration and displacement observed at the gate-valve attached on the lateral port named P14S1U, whose location is indicated in the figure, is shown in Fig. IX.3-10. They also showed a linear relationship with the electromagnetic force parameter f and reached the maximum of 50 m^2/sec in acceleration and 0.5 mm in displacement at full power operation. As the vibration observed at the lateral port gate-valve was excessive over the permissible level of the gate-valve, vacuum leakages were observed at the gate-valve flanges of ten out of twenty lateral ports

during power tests. As larger acceleration was afraid to be observed in case of rapid plasma disruption, it was necessary to take measures such as structural modification of gate-valve.

The results obtained in the power tests are summarized as follows from the mechanical and thermal viewpoints of JT-60 tokamak machine;

(1) All of the coil systems were raised up to full power operation in combination and system performance was verified including thermal and structural integrity of tokamak machine.

(2) Measured strain and deflection showed good agreements with those predicted in the design, which was an evidence that electromagnetic loads were supported adequately as expected in the design.

(3) Vibration of lateral port was found to be large up to 50 m/sec^2 and caused excessive vibration of gate-valves. It was found to be necessary to take measures such as structural modification of gate-valve.

(4) A few limitations to machine operation was made clear quantitatively. Allowable period of continuous TDC operation was limited by temperature rise of the vacuum vessel bellows, and rapid start-up caused excessive vibration of the lateral port gate-valves attached to the vacuum vessel directly.

(5) It was found that the existing detectors were insufficient to monitor the machine integrity and a few kinds of detectors were necessary to be installed, e.g. the deflection detector of the magnetic limiter coil feeder and the vibration monitor of the lateral port gate-valves.

3.3 Construction of auxiliary devices

3.3.1 Glow discharge cleaning system

Glow discharge cleaning is a effective cleaning method of the surface of internal components attached inside the vacuum vessel. The JT-60 glow discharge cleaning system is composed of a main cleaning device and a sub cleaning device.

The main cleaning device is attached to the upper slow movable limiter port. The head of the device is made of molybdenum tiles coated with titanium carbide. The device is also designed to function as a pumped limiter to study density control in the fixed limiter operation.

Therefore, the head is provided with the exhaust throat and duct. The exhausted gas is pumped out by the Zr/Al getter pump with a pumping rate of 7.5 m^3/s for hydrogen at 20 deg C. Langmuir probes, H_α and HeI light detectors, thermocouples, fast vacuum gauges and a fast residual gas analyser are installed in the device. The measured data are transferred to the data acquisition system using CAMAC and processed by personal computers.

The sub discharge cleaning device is attached to one of the 14 neutral injection ports to reduce gaseous impurity inside the port and thus to improve the heating power deposited in the plasma.

The contract for the design, fabrication and installation of the glow discharge cleaning system was placed in March 1985. The installation and testings will be finished in December 1985.

3.3.2 Pumping system in divertor chamber

Particle pumping is required in a long pulse operation to avoid a serious density build up by the neutral beam injection and to get a stable discharge termination [1]. High density in the divertor chamber can be obtained in the divertor operation by reducing the conductance from the divertor chamber to the main chamber. This effect makes it easy to pump out the particles enough to control the plasma density. The divertor pumping system is installed in the JT-60 machine from this point of view.

The JT-60 divertor pumping system is composed of 4 Zr/Al getter pumps, each of which consists of 3 cartridges of SORBAC C-500. The getter pumps are placed in the space close to the divertor chamber and connected through the duct. The total effective pumping rate in the divertor chamber is 20 m^3/s for hydrogen at 20 deg C including the pumping rate of the torus vacuum pumping system. Pressure gauges are installed to measure the pressure in the getter pumps during discharges. The data are also transferred to the data acquisition system mentioned in 3.3.1.

Buffle plates are installed inside the vacuum vessel by welding in order to reduce the conductance between the divertor chamber and the main chamber.

The contract of the divertor pumping system was placed in March 1985. The completion of its installation and testings is scheduled for December 1985.

Reference

1) Y. Shimomura, et al. : J. Nucl. Mater. 128 & 129, 19-25 (1984).

4. Status of Power Supplies

4.1 General status

The assembling and installation of all JT-60 power supplies have been completed and tests of the all power supplies have been continued.

Although the load tests for poloidal field power supply have been carried out by the end of last fiscal year, the size and complexity of the poloidal field power supply would make it necessary to carry on sub-system test in accordance with the ZENKEI(main control system) test. Moreover the test using the dummy coil to examine the soundness of power supplies have been carried out on occasion prior to the JT-60 coil load test. Especially, the test of protective interlock with the rated current level was intended to establish a safety of JT-60 machine.

The connection test to ZENKEI system was started from the beginning of the June of 1984 and continued for six monthes, and load test with JT-60 machine was started from the December of 1984. These tests have been carried out really at full load level involving the protection performance test such as the over current, ground fail protection. All the preoperational testing activities, had to be completed before a first plasma operation was finished till the end of March of 1985. These load tests with JT-60 machine were an acceptance test of power supplies that served the training of JT-60 operation and maintenance personnel, thus JT-60 power supplies were given official approval by JAERI at the end of March 1985.

All the construction effort of power supplies was finished and finally the sufficient performance of it has been comformed.

4.2 Poloidal field power supply

The several component tests of PFPS closed in itself were completed on March 1984. According to JT-60 project program, the PFPS joined in

system integration test which related to the all JT-60 facilities. And the required various PFPS performances were finally comformed through those tests.

The scheme of PFPS is illustrated in Fig. IX.4-1. The energy storage M-G set has ratings of 500 MVA, 18 KV, and 1.3 GJ available energy in 70 - 100% revolution speed. OH-PS has capacity to generate about 25 volt-sec. V-PS can generate the vartical field of about 3.3K-Gauss. In the dummy coil test, we tested each PS in the rated voltage and the rated current independently. But we could not test with all field coil PS. Therefore the most interresting item under the system integration test for PFPS was Power Test.

At first, the Power Test started for only one PS and field coil, and the other field coil and PS were added to the test step by step. Finally all PFPS powered each field coil at a same time. The typical current pattern of the each coil are illustrated in photograph 2-6 of Fig. IX.4-2.

In this case, the OH-PS generated about 75% volt-sec of rating by swinging from maximum premagnetized current (92KA) to -46KA. The peak current value of V-PS reached to 45KA at IP flat top period from permagnetized current -8.7KA. The current of H-PS, Q-PS and M-PS were reached to the rated current 20KA, 25KA, 95KA respectively.

PFPS were completed at the end of March 1985 successfully. Through the long period of installat-on and test, it was lucky and happy to be no accident.

4.3 Toroidal field power supply

Each component of the toroidal field power supply (TFPS) was reviewed by checking its soundness after installation. The construction of TFPS was completed by the end of last fiscal year, and no-load tests of TFPS were started in March 1984. They included open- and short-circuit tests and control system simulation tests.

Open- and short-circuit tests served to examine the electrical reliability of the hardware with the DC output terminals of TFPS being open and shorted respectively. The open-circuit test was a full voltage test to check the all the 24-pulse diode convertor banks output voltage up to the maximum value. In the short-circuit test, the equivalent

maximum DC current (53kA-38sec) operation at intervals of 10 minutes for about 7 hours was carried out. It was confirmed that the rise of the temperature at any point in TFPS was within the reasonable level according to the design value. Fig. IX.4-1 shows the DC current and the temperature rise of DC aluminum bus in the equivalent maximum DC current operation.

A dummy load and a simulator, instead of the toroidal field (TF) coil and/or the motor-generator of TFPS, were adopted for the control system simulation tests to check over the control and operation sequence of TFPS. The dummy load was a resistor of 7kV-5A connected to the DC output terminals, and the simulator was a electronic circuit to simulate TF coil's and/or MG's electrical characteristics. It was also examined that all the AVR (Automatic Voltage Regulator) computer programs of MG were available for TFPS's operations.

TFPS was under system integration tests from June 1984 to March 1985. After no-load tests and control system integration tests were finished, tests of applying the rating current to TF coil were carried out in power tests of coils from December 1984. TFPS could generate continuous or pulse TF coil current successfully in the overall setting range. Fig. IX.4-2 shows TF coil voltage and current in the maximum rating current operation of TFPS. On the same conditions, the harmonic current from TFPS to the utility power network was measured and proved to be lower than the allowable level.

All the tests of TFPS were finished by the end of this fiscal year. TFPS will be in operation from April 1985.

4.4 Motor generator for plasma heating system

The assembly and installation of the motor generator with flywheel (MGF) has been completed in August 1984. In September 1984, the rotation test was started to check the dynamic balance. The static Scherbius system was tested in combination with MGF. It controls the rotational speed of MGF from 406.5 rpm to 582 rpm.

In February 1985, the three-phase sudden short-circuit tests were carried out to examine the electrical characteristics of the generator (Fig. IX.4-5). Maximum terminal voltage before the short-circuit was 50%.

The combination test with the plasma heating systems (Neutral Beam Injection System and Radio Frequency Heating System) will be done in next fiscal year.

5. Status of Control System

5.1 General status

The performance testing of the control system at the site was continued according to the test schedule prepared by the JT-60 coordination engineering program, and it was completed in March 1985.

Moreover, a feedback control algorithm for divertor plasmas was additionally developed and its program installed in the feedback control computer of the JT-60 central control system, "ZENKEI". It enables the position of separatrix surface at the divertor throat to be controlled by magnetic limiter coil current with the signals from a set of the magnetic probes near the divertor region.

On the other hand, quality assurance (QA) activities for improving the softwares in the control system have been started in order to cope with development of JT-60 operation and plasma experiments in the near future.

The JT-60 control system has a hierarchical structure with "ZENKEI" and subsystem controllers. Therefore, the performance of the control system was confirmed by the following three steps: the individual test of each controller, the linkage performance test between "ZENKEI" and each subsystem controller and the system integration test with all subsystems.

The linkage performance test that spent about one year was completed in May 1984. Succeedingly, the control system integration test with "ZENKEI" and the subsystem controllers of tokamak machine, gas injection and preionization system, toroidal field coil power supply, poloidal field coil power supply, secondary cooling system, power distribution system and emergency power supply, and diagnostic system was started for evaluating the total performance of the JT-60 control system prior to the power tests of tokamak system.

The electromagnetic measurement system for plasma control and

monitoring was totally evaluated at the power tests of tokamak machine. The JT-60 integration performance test was carried out as the preoperational testing to verify the total performance of the JT-60 operation from starting up all of the subsystems to executing the full discharge sequence including the protective interlock functions without plasmas.

5.2 ZENKEI, the JT-60 central control system

The performance testing of "ZENKEI" after completion of its individual test was carried out according to the total plan for the system integration test.

At the final stage of the linkage performance test, operational characteristics of the feedback control computer system in "ZENKEI" was evaluated in combination with the direct digital control (DDC) CAMAC system in the poloidal field power supply (PFPS) by excitation of the dummy coil. It was demonstrated that the feedback control computer system located at the power supply control room runs without trouble under the environment of the electromagnetic noise induced by high commutation current in the DC circuit breaker operation in the ohmic heating coil power supply. Figure IX.5-1(a) shows that a result of linkage performance between the feedback control computer system in "ZENKEI" and the DDC CAMAC system in PFPS at the power test with the dummy coil. It was also proved that the time required from the data input to the command output in the feedback control computer satisfies the control cycle of 1 msec as shown in Fig. IX.5-1(b).

At the control system integration test it was verified for the first time that "ZENKEI" is able to supervise all of the subsystem controllers. Its test procedures and results are described in section IX.7-1.

The electromagnetic measurement system for plasma control was totally evaluated at the power tests of tokamak system. The outputs of the Rogowski coils for plasma current measurement were calibrated by excitation of the primary magnetic limiter coil in the vacuum vessel. The effects of the external magnetic field to the output signals of the magnetic probes and their setting errors were also examined by exciting separately the toroidal and each poloidal field coil. It was proved that the signal processing system including the newly developed

integration method is very useful. (See Fig. IX.5-2.)

At the JT-60 integration performance test "ZENKEI" was fully used and finally tuned in consideration of the actuator performance. Its test procedures and results are described in section IX.7-3. The main functions and performance of "ZENKEI" finally obtained are summarized in Table IX.5-1.

6. Status of Auxiliary Systems

The construction of the secondary cooling system and the power distribution system/emergency power supply was finished in October 1983 as scheduled. These auxiliary systems are now in operation for various tests of other JT-60 subsystems and JT-60 integrated performance test.

6.1 Secondary cooling system

The outline of this system is as follows.

(i) Total circulation of water ; 10,070 m^3/hr

(ii) Outlet temperature of cooling water ; 31 °C

(iii) Inlet temperature of cooling water ; 37 °C

(iv) Constitution of cooling system ; four separate cooling lines (tokamak secondary cooling line, power supplies secondary cooling line, heating system secondary cooling line and auxiliary equipment cooling line)

(v) Water treatment ; the quality of water is maintained through scale prevention, slime prevention and corrosion prevention treatments.

Total time of operation at fiscal year (from April 1984 March 1985) is as follows.

Tokamak secondary cooling line : 1,920 hour

Power supplies secondary cooling line : 1,734 hour

Heating system secondary cooling line : 826 hour

Auxiliary equipment cooling line : 2,137 hour

6.2 Power distribution system/emergency power supply.

6.2.1 Power distribution system

The outline of this system is as follows.

(i) the capability of the system : 13 MVA
(ii) 6.6 kV M/C : 19 lines
(iii) 400 V P/C : 3 banks
(iv) 200 V P/C : 3 banks

capacity of electric power at fiscal year (from April 1984 to March 1985) used about 5000 MWH.

6.2.2 Emergency power supply

The outline of this power supply is as follows.

(i) the capability of the power supply : 8.3 MVA
(ii) 6.6 kV M/C : 11 lines
(iii) 400 V P/C : 3 banks
(iv) 200 V P/C : 2 banks
(v) the AC no break power supply static type invertor (CVCF) 500 kVA, 4 sets
(vi) battery (HS-2500) 2500 AH, 2 sets
(vii) the DC no break power supply rectifier device : 250 kVA, 2 sets
(viii) battery (HS-500) 500 AH, 2 sets

capacity of electric power at fiscal year (from April 1984 to March 1985) used about 3,600 MWH.

7. System Integration Tests

7.1 Control system integration test

7.1.1 Planning of the control system integration test

Objectives of the control system integration test are the improvement of reliability and the final check of JT-60 control system design under the condition that the test should be done without energizing the tokamak device. The test plan was made according to the following procedures:

(a) To classify the functions and usage of control system.

(b) To decide the testing items according to the functions.
(c) To understand the testing boundary conditions.
(d) To decide how to simulate the actuators and sensors.
(In principle, software simulation should be made at minimum).
(e) To select the abnormal conditions for checking the treatment of the abnormal events.
(f) To decide the methods of data processing load test.

As a result, the conceptual contents of the test become as follows:

(1) Safety interlock system test

This test aims at checking, (a) whether proper protections are executed when many abnormal events occur at the same time, (b) whether certain switches of the emergency power distribution system are sequentially turned on according to the preset program when the power of commercial line fails.

(2) Plant monitoring system test

This test aims at checking, (a) whether various plant monitoring data of all subsystem are acquired, (b) whether the treatments of the illegal data are properly performed even if all subsystems send them.

(3) Discharge control system test

This test aims at checking, (a) whether the proper discharge sequence normally runs even if abnormal events occur before, after and during discharges, (b) the transfer of the discharge conditions and the result data, (c) whether the real time control is performed within the cycle of 10 msec/1 msec even if many events interrupt the real time control computer, (d) whether the treatment of the illegal data is properly performed, (e) whether the computer can received and send the full data at the definite cycle, (f) whether the plasma control phase is properly shifted according to the programmed schedule and the events.

In order that the normal sequence might go forth, the dummy coil for the poloidal field power supply, the toroidal field coil simulator, the motor generator simulator, the movable limiter simulator, etc. were used.

7.1.2 Result of the control system integration test

The test needed about 250 hours with 60 personnels in total and 163 problems were pointed out. As is shown in Fig. IX.7-1, half of the problems are related to software which can be classified to 2 causes; illegal design and illegal logic including careless bugs. An example

of illegal design is that the meaning of the message in discharge sequences was misunderstood by a certain subsystem. The illegal logics including careless bugs are unavoidable mistakes in producing a software. Since every control system communicates with each other according to the sequence, values of timers counted in the computers were able to be fixed. Hardware problems were soon solved because most of the causes were very simple such as insufficient electrical contacts, etc. Simulation/operation and documents prepared incorrectly, occupy not so small percentage in total problems. It is likely because the system is very complicated and the personnel had not yet practiced to operate this system. Thus, this test contributed the practice of operators as well as the integration of JT-60 control system.

7.2 Power tests of tokamak system

The schedule of the JT-60 integrated system test is shown in Fig. IX.7-2. The power tests of tokamak system were performed after obtaining the complete assembly of tokamak machine. The tests were devided in following four steps.

1st ----- toroidal field (TF) coil excitation
2nd ----- poloidal field (PF) coil excitation
3rd ----- simultaneous excitation of toroidal and poloidal field coils with room temperature vacuum vessel
4th ----- simultaneous excitation of toroidal and poloidal field coils with baked vacuum vessel

In the 1st and 2nd steps, we raised the coil current step by step, according as monitoring the temperature of cooling water, the stress forces of coil supports, the circumstanical temperature of DC feeders, the signals of pick-up loops, the current and voltage waveforms of coils, effects to the commercial power line.

In the 3rd step, after the coil current reached the designed maximum value in each coil, we made tests on simultaneous excitation of more than 2 coils. At the last stage of this combined excitation test, we excited simultaneously all of the coils with careful caution not to produce plasma. In the final step, we raised the temperature of vacuum vessel up to 250°C and excited all the coils up to the maximum current levels, with the safety and protection system working and with the

inter-rock system not to produce plasma.

The test required 53 days with 680 shots in total. Toroidal and poloidal field coils were able to be excited up to the full rates of currents and voltage. The tokamak machine could stand the stress forces with the designed conditions. The power supply systems worked with the expected controlability. Fig. IX.7-3 shows the typical current patterns of each coil with the maximum current. In this power test, 212 technical problems were pointed out. Some major items were as follows;

- air leak in vacuum vessel under pulsed magnetic field
- damage in the filaments of electron gun under strong toroidal magnetic field
- effect of eddy currents.

Most of problems were solved untill the integrated performance test. Some of these problems were checked again in the integrated performance test.

7.3 Integrated performance test

At the final construction stage, the JT-60 integrated performance tests were conducted from 27 February to 20 March, 1985 as shown in Fig. IX.7-4 succeeding to the power tests.

The purpose of this tests was to check the integrity of overall system in JT-60 facilities and to verify the operational response sufficient for plasma operation. This test was implemented without plasma production by making the gas injection system dumb.

The test were conducted in seven parts as follows;

(1) preparation for tests

Prior to conducting the test sequence the machine verification of preparatory works was performed.

(2) test of operational mode transition

JT-60 has nine modes according to its operational stage including the suspension mode for all subsystems. The mode transition test was performed for each mode.

(3) preoperational test of discharge cleaning and experimental discharge

Discharge cleaning shots and experimental shots were performed with no plasma. The poloidal coils and toroidal coil were energized

at the same time up to the full rating as the typical plasma discharge shots.

(4) test of safeguard

These tests ensured the integrity of the following major safeguard items; 1) PF/TF coil ground fault safety verification test, ii) test of emergency shutdown function works, iii) protective action test in an electricity failure, iv) secondary cooling water flow protective action test, v) protective action test of vacuum vessel gas cooling system.

(5) test of plasma controllabilities

The real time plasma controllabilities with feedback loop were checked in experimental discharge shots.

(6) checking of data monitoring

We checked whether all the monitoring items indicate the ordinary values in every step of operational modes.

(7) recovery from simulation

Recovering related to the hardware and software was implemented and checked for all modifications which were requested in plasma simulation and setting up for dummy signals.

The number of shots and the technical problems are summarized in Table IX.7-1. Major problems denoted with i) leak under high pulsed magnetic field, ii) trouble in the thyristor static startor of TFC-MG, iii) deterioration of insulation of vacuum vessel were worked out for each case and it was proved that JT-60 had excellent performance through these most strict examinations.

8. Status of Diagnostic System

8.1 General status

Fabrication and installation of Group A diagnostic instruments have been continued for the last fiscal year.

8.2 Electron density measuring system (A-1)

FIR laser device (λ = 118.8 μm) of (A-1-a) submm wave interferometer subsystem has been installed in the laser room I, and accomplished the outstanding performance as it did in the firm: single mode, $\Delta\lambda$ Beat/$\lambda \leq 10^{-9}$ for 240 hours without maintenance. The development of the vacuum window sealing technique and the flexible light-guide was pursued as well, which brought forth new engineering devices: permeation-less repetitively bakable vacuum window sealing material up to 250°C, and the beam axis stabilizer that depresses the deviation angle within 100 μrad when the incident beam is deflected up to 5 degrees in 2 Hz.

2 mm wave interferometer subsystem (A-1-b) has been installed in the Torus Hall, and finished final adjustment with the performance of SNR 30 dB, fringe resolution 0.02, and the fringe counter responce 0.67 fringes/μs. The measurement of the vibration of Diagnostic Platform was successfully carried out during the integrated performance test of JT-60.

8.3 Electron temperature measuring system (A-2)

The main components of the Fourier transformed interferometer subsystem (A-2-a) had been fabricated last year and the initial test had been carried out in the laser room II. The soft ware controlling the whole of this subsystem has been tested under the condition co-operating with the data-processing system (A-7). The interferometer has been installed to the JT-60 and is waiting the completion of the light pipe connection.

The detail design of a multipulse thomson scattering subsystem (A-2-c) has been completed and the components is now under construction in the firm. A high repetition 100 Hz of YAG laser has been achieved with the output power of more than 100 mJ per pulse. This output power will be increased up to 1 J per pulse. The construction and also the installation will be completed in the fiscal year of 1985.

8.4 Ion temperature measuring system (A-3)

The construction of the neutral particle energy analyzer subsystem (A-3-a) has been continued. The performance test of mass and energy neutral particle analyzer subsystem (A-3-b) has been completed in the testing room and the analyzer with be installed to the JT-60 in the next fiscal year,

The active beam probing apparatus subsystem (A-3-c) has been successfully developed with the performance of 3.5A at 200 keV by plasma heating laboratory I. The performance test of the whole subsystem including detectors has been completed.

The detector of neutron counter subsystem (A-3-b) has been calibrated with the monochromatic neutrons generated by Van de Groff accelerator and the energy resolutions of 9.8, 8.8, 5.6 and 8.3% have been obtained at the energies 1.8, 2.4, 3.3 and 4.3 MeV respectively.

8.5 Impurity measuring system (A-4)

The two unit type spectrometers with 512 and 1024 channels array detectors of light impurity spectrometer subsystem (A-4-a) have been fabricated and the calibration of each spectrometer has been carried out in the testing room. The energy resolving power ($\lambda/\Delta\lambda$) with 512 channel array detector was 40 - 150 over the wavelength region of 0.5 - 5 nm and the resolving power with 1024 channel array detector was 10 - 230 over 0.5 - 50 nm.

The calibration of grazing incidence spectrometer (A-4-f) has been carried out and the resolving power of 6500 at 52.2 nm has been obtained.

In addition to the performance test of each subsystems, the linkage test of whole A-4 system to the data processing system (A-7) has been completed.

8.6 Radiation flux measuring system (A-5)

High speed counting PHA subsystem (A-5-a) was tested for calibration, and linkage test with A-7 system was completed in December 1984. This system was installed in January 1985 and will participate in the

first OH experiment in April 1985. Design of high speed counting PHA array subsystem (A-5-b) have been continued. PIN diode array and Bolometer array subsystems (A-5-c, A-5-d) have been fabricated in the firm.

8.7 Peripheral plasma measuring system (A-6)

IR IV subsystem (A-6-a) has been completed with the performance of 1 dB/m transmission of 3 - 5 μm IR region image guide fiber.

Electromagnetic probes subsystem (A-6-c) has been installed and accomplished the performance as it did in the firm: gain flatness of 60 dB ± 0.3 dB over the frequency range DC-10 kHz, below 20 μV input noise amplitude. And linkage test with A-7 system has been completed.

A-6-d subsystem (spectrometer for periphery) has been fabricated in the firm, and will be installed in the next fiscal year.

8.8 Data processing system (A-7)

Constraction of A-7 data processing system was completed in September 1984. This system consists of one general purpose computer, three mini-computers, about 40 micro-computers, mass data recorder and I/O terminals connected to them.

The test of A-7 data processing system in JAERI was carried put from June 1984 to March 1985. The linkage test with A-8-h diagnostic optical communication subsystem was started in June 1984 and 5 MB/sec data transfer rate in CAMAC serial highway was realized. The linkage test with Zenkei JT-60's central control system was carried out from July to September 1984. A-7 data processing system was certained to work following to the JT-60's discharge sequence created by Zenkei system. The test of real time data transfer rate of A-7-c real time processing system was carried out and about 30 W/msec transfer rate was obtained. The linkage test with A-1 - A-6 diagnostic systems was started in October 1984 and 15 of 23 diagnostic subsystems were successfully linked with A-7 data processing system until March 1985. A-7-a2 diagnostic vacuum control CAMAC system was tested to control A-8-a, b diagnostic vacuum pumping system.

A-7 data processing system was ready to operate for the JT-60's first plasma discharge in April 1985.

8.9 Diagnostic support system (A-8)

Most of design and fabrication of A-8 diagnostic support system has been completed at industries. Three A-8 subsystems (Carriers & Crance, Optical Data Communication subsystem, Calibration subsystem) were supplied in 1985, March. Necessary parts of A-8 system for JT-60 ohmic heating experiment I, such as Vacuum, Compressor, Power supply, Cooling Water supply, were installed within March. Construction and installation of A-8 diagnostic support system has been continued and it will be completed in 1985, December.

9. Status of Heating System

9.1 Construction of Neutral Beam Injector (NBI) for JT-60

Neutral beam injection of 20 MW will be required to achive reactor grade plasma in JT-60. The JT-60 NBI system consists of 14 beam line units. Each unit is designed to deliver 1.43 MW of neutral beams at energy of 75 to 100 keV for 10 seconds using two ion sources with a capacity of 35 A ion beam extraction. A cross sectional view of lower and upper beam line units is shown in Fig. IX.9-1. The performance characteristics of the JT-60 NBI are tabulated in Table IX.9-1.

The significant features of JT-60 NBI are following.

1) Long pulse operation of up to 10 seconds. This is a longest pulse in the injectors for the large tokamaks.
2) Beam energy can be changed during a beam pulse for the purpose of matching the beam energy to the plasma density at any instance.
3) High proton ratio (more than 90%) and low impurities in the beam.

The whole system consists of systems of power supply, cryogenic, cooling water, vacuum pump, control and operation, and diagnostic, in addition to the beamline units. The control system supervises the whole NBI system including 28 ion sources. Therefore this system

consists of a computer which manages a large amount of the operation data and a high speed hard wired interlock circuits.

Construction of the NBI system started in autumn of 1983. The inspection and performance test, including actual beam extraction of each beam line unit was started on April 1984. This test was conducted on the test stand into which the prototype injector facility was altered. Tested beam line units will be installed on the JT-60 from July 1985 with completion of the whole system scheduled for the middle of 1986.

1) Y. Okumura et al., "Development of high performance neutral beam injectors at JAERI", 10th International conference on plasma physics and controlled nuclear fusion research, London UK, 12-19 September 1984, IAEA-CN-44/H-I-5-2

9.2 Radio frequency heating system

In JT-60, the RF heating of 10 MW for 10 sec is planned together with neutral beam injection (NBI) heating of 20 MW.[1] The RF heating system has three units of lower hybrid range of frequencies (LHRF) and one unit of ion cyclotron range of frequencies (ICRF) systems. The main specification of the system is shown in Table 9.2-1. The RF system is composed of power supply system, high power RF amplifier system, RF power transmission system, coupling system, pumping system, primarily water cooling system and control system. The overview of the system in illustrated in Fig. 9.2-1. The high RF power amplifier system has 8 high power electron tubes per one unit, i.e. 1 MW krystrons developed in JAERI for LHRF heating and high power tetrodes whose cavity is newly designed for JT-60. The frequency of krystron can be changed from 1.7GHz to 2.25GHz by moving the cavity using stepping motor. The phased array waveguide launcher is adopted for the coupling system of LHRF system. The launcher has 8 columns × 4 rows-waveguide array. We can carry out the efficient plasma heating and current drive by controlling the phase difference of RF in toroidal direction. On the other hand, the launcher of ICRF is composed of 2 columns × 2 rows-loop antennas. The phase difference among loop antennas can also be controlled. The view of launchers installed on the tokamak is illustrated in Fig. 9.2-2. The RF input power, phase difference and RF frequency (frequency is only in

the LHRF case) can be controlled in real time and the best heating of the plasma or current drive is possible by selecting the optimum values corresponding to the plasma parameters which sometimes change during plasma discharge.

The RF parameters for launcher conditioning or remote control of the system are programmed at the mini computer of RF system (RF computer) and are sent to the RF components in every 10 msec via CAMAC system. The data from the system are collected by the A/D converter or digital input (D/I) of the CAMAC system in the amplifier room and are sent to the RF computer. The data are processed by the computer and displayed by the CRT of each unit and stored by the magnetic tape. Moreover, RF computer is linked with ZENKEI computer system. In the case of heating experiment, RF parameters are sent from ZENKEI computer system so that the RF system is feed back controlled.

The construction of the system starts in 1983 and the supporting structure of RF power transmission system and coupling system in JT-60 hall has been equiped. Design and manufacturing of the system has been continued.

Reference

1) Annual Report of April 1, 1983 to March, 1984, JAERI-M 85-006 (1985).

10. JT-60 Experimental Planning, Plasma Consideration and Operation Program

10.1 Experimental program and schedule

The experimental schedule was kept as shown in Fig. IX.10-1. The objective of JT-60 is the study of a reactor grade plasma including plasma-machine interface phenomena. In other words, technology to generate and maintain a reactor grade plasma has to be investigated in JT-60 and it is necessary to show how we can build up and control a reactor core plasma with realistic methods. The experimental program is indicated in Fig. IX.10-1 and is briefly summarized as follows:

1. Preliminary Experiment

2.7 MA discharge with and without divertor

NBI, ICRF and LHF heatings

RF current drive

2. Reactor Like Plasma Experiment

$\bar{n}\tau_E = (2 - 6) \times 10^{19}$ $m^{-3}s$

$\bar{T} = 5 - 10$ keV

$P_h = 30$ MW

$t = 5 - 10$ s

$V_p = 50$ m^3

3. R & D for Reactor Core Plasma Experiment

a) Impurity control with a High Power & Long Pulse Heating

simple poloidal divertor

boundary plasma control

first wall material

b) Long Pulse & High Power Heating

NBI (20 MW/75 - 100 keV/10 s)

LHRF (7.5 MW/1.7 - 2.3 GHz/10 s) → Modification

ICRF (2.5 MW/phase array antenna)

c) Tokamak Plasma Improvement

RF current drive

high β (with $B_t = 4.5$ T, profile control)

disruption control

4. Advanced Experiment

10.2 Plasma control

In a large tokamak, careful plasma control is essential not only for production of a high quality plasma but also for safety and machine protection. From this point of view, as well as for the position and shape control of a plasma, the real time control system is employed for other important features, e.g. heating power, gas influx and disruption. All diagnostic instruments can be used as sensors. Disruption control and soft plasma quenching will be intensively investigated as well as control of conventional plasma parameters. The compact poloidal divertor

is one of the most essential characteristics of JT-60. The divertor is the promissing method for controlling plasma-wall interactions and for optimizing main plasma parameters. Divertor plasma parameters, neutral pressure in the divertor and heat flux on the divertor plate as well as the divertor configuration will be controlled.

A typical magnetic configuration with the divertor is shown in Fig. IX.10-2. In this configuration, the separatrix magnetic surface does not intersect any material except the divertor plate, and the following geometrical factors have to be controlled.

R_p : plasma center position,

δ_{30} : the minimum clearance between the separatrix magnetic surface and toroidal limiter,

δ_t : clearance between the separatrix magnetic surface and the main divertor coil,

x_p : position of the separatrix magnetic surface on the divertor plate.

$$x_p = 4.2(\delta_t - 4.7) \pm 0.8.$$

State equation against these control objectives is obtained from the numerical results of Grad-Shafranov equation (see Fig. IX.10-3).

Control characteristics of above control objectives are analyzed by using the matrix transfer function analysis code and the simulation code. Recommended gains, maximum response frequency, responses to plasma parameter variations and mutual interactions between controllers are qualitatively determined.

For getting the optimum divertor-plasma, it is necessary to control adequately the magnetic configuration both in the main chamber and in the divertor chamber. JT-60 has five types of poloidal magnetic field coil with each power supply in order to regulate the control objectives. However, if we control each objective by each coil current independently, there must inevitably occur large interaction between control objectives. This situation may be the same with a fusion reactor device. For making it possible to control each objective independently without causing large interaction, we adopt the noninteracting control algorithm. This algerithm is effective to suppress the interaction between control objectives and is strong against the β_p disturbance.

10.3 Plasma consideration

10.3.1 Numerical analysis of divertor discharge

In order to study the plasma characteristics of the divertor discharge in JT-60, the two-point divertor model has been developed and combined with the one dimensional tokamak transport code. In this model, the relation between plasma parameters in the scrape-off layer and at the divertor plate are expressed by the simple analytic forms with the particle multiplication factor at the divertor plate, which is a function of the ionization mean free path of the neutral particles and is evaluated by using the one fluid divertor code. By using this code, the dependence of the electron temperature and plasma density at the divertor plate on the average density in the main plasma has been studied for different scaling laws of energy confinement time. For the standard operation of JT-60 with heating power of 30 MW, the relatively high value of the average main plasma density, $\bar{n}_e = 10^{20}$ m^{-3}, is required for the cold and dense divertor plasma. The improvement of the particle confinement in the main plasma increases this threshold density because of the reduction of the particle flux into the divertor chamber. In order to prevent the high temperature plasma at the divertor plate, the additional heating power is required to increase consistently with the density increasing rate in the main plasma. These simulation results show that the ideal divertor-tokamak plasma with reactor-grade parameters can be obtained in JT-60 under an appropriate control of the plasma density and the additional heating power.

10.3.2 Numerical analysis of limiter discharge

The influence of radiation cooling on the plasma-wall interaction and the self-limitation of impurity contents have been numerically studied for typical plasma parameters and different wall/limiter materials in JT-60. Impurity transport equations are solved in combination with the main plasma transport. These equations describe ionization, recombination and anomalous diffusion for each charge state and sputtering by charged particles and charge-exchanged neutrals are taken into account as impurity source. The other production mechanism such as arcing and evaporation are neglected.

In the case of wall/limiter materials with medium-Z values (Fe and TiC), the main plasma is heavily contaminated by these metal impurities

and more than 80 percent of heating power is lost by radiation. Saturation levels of impurity contents are determined from the condition that the effective self-sputtering yield is unity. The average ion temperatures in the steady state are 4.0 and 4.6 keV for Fe and TiC, respectively, and these values decrease with anomalous inward flow velocity.

In the case of carbon limiter, chemical sputtering is much larger than physical sputtering. Because sputtering yield of this process depends on the limiter temperature and the time history, we simply assume it as 0.05 in the Joule phase and 0.1 in the additional heating phase of 30 MW. The carbon content in the steady state is 3 to 5 percent, depending on the inward flow velocity, and the radiation loss is about 10 MW. This result show that the low-Z material is required for reactor grade plasmas in the divertor discharge.

10.3.3 Tearing mode analysis during the current rise-up phase

The dependence of the magnetic island width on the plasma current rise-up rate has been studied by using the tokamak transport code incorporated with the island code, which evaluates the magnetic island width on the basis of Δ' analysis. The rapid increase of the plasma current up to 2.7 MA with toroidal magnetic field of 4.5 T results in the contact of the magnetic island with the limiter and may cause the disruption, even if the tearing mode is stable in the steady state. The critical value of the current rise-up rate in the Joule heating phase is $I_p = 0.7$ MA/sec both for INTOR and neo-Alcator scaling laws of the energy confinement time.

10.3.4 Positional stability of JT-60

JT-60 has the poloidal divertor outside of the torus and the n-index has the strong radial dependence in the plasma region. Therefore, the positional stability of the JT-60 divertor configuration has been studied by using the ideal MHD stability code ERATO. Results show that JT-60 configurations are stable against positional mode in the range of $-0.2 \leq n_{z0} \leq 1.2$ for $\beta_p = 1.0$ and $Rj = 1 - \psi^2$, even without the conducting shell, where n_{z0} is the n-index value at the plasma center. Detail analysis of the stability range of n_{z0} is now under investigation for wide region of plasma parameters and configurations.

10.4 Operation program

The JT-60 operation program for the initial Ohmic heating experiments was studied and a complete plan shown in Fig. IX.10-4 was obtained.

The first operation cycle aims at cleaning of the vacuum vessel wall by discharge cleaning, while the following operation cycles are assigned to Ohmic heating experiment with a daily discharge cleaning. A complete specification for the contract of JT-60 operation and maintenance was prepared.

The initial draft of the safety rule was made and the final design of the operational procedures and manuals was completed in April 1985.

Table IX.3-1 Vacuum properties of JT-60 vacuum vessel

Item (Unit)	Specification	Achieved
Ultimate pressure (Pa)	$<1.33 \times 10^{-6}$	4.2×10^{-7}
Helium leak rate ($Pa \cdot m^3/sec$)	$<6.65 \times 10^{-8}$	$<7.1 \times 10^{-9}$*
Outgassing rate ($Pa \cdot m^3/sec \cdot m^2$)	$<1.33 \times 10^{-8}$	6.82×10^{-10}

* less than the sensitivity of detector

Table IX.3-2 Major specifications of heating and cooling systems for vacuum vessel and results obtained in baking test

Item	Unit	Specification	Achieved
Baking Temperature range of Rigid Ring and Bellows	°C	500^{+20}_{-200}	500^{-86}_{-200}
Baking Temperature of Port	°C	≥ 250	≥ 250
Heating Time from R.T. to Baking Temperature	hrs	≤ 70	66
Hold Time of Baking	hrs	48	50
Difference Between Max. Temp. and Min. Temp. on Vacuum Vessel	°C	≤ 150	< 113
Heater Temperature	°C	≤ 750	< 505
Cooling Time from Baking Temperature to 80°C	hrs	≤ 60	38

Table IX.3-3 Results of regulation valve adjustment

Operation mode	Flow Rate (m^3/hr)			Valve Opening (%)		
	T coil	P coil	M coil	T coil	P coil	M coil
1	1050	65	13	48	37	29
2	545	65	13	25	44	30
3	545	43	13	25	21	30

Table IX.5-1(a) Functions of JT-60 Control System (1/2)

	Items	Contents
Plant Support and Monitoring	Management of JT-60 Operation Mode	○ Check before mode transition ○ Check of deviation from the mode
	Device Operation Management	○ Operator's support function for permission/inhibition of deivce operation
	Acquisition, Logging & Display of Plant Data	○ Acquisition items: Process data, Statistics data, Event data ○ Monitoring points: 7500 analog inputs, 9000 Digital Inputs (every 10 sec and 1 minute) ○ Logging: Periodic, Daily, Monthly, Statistic, Treud, Operation ○ Display: Numerical, Semi-graphic, Trend
	Alarm Monitoring	○ Treatments corresponding to five alarm levels
Discharge Control	Setting Discharge Conditions	○ Number of items: 2800 discharge conditions ○ Reasonability check on discharge conditions
	Discharge Sequence Control	○ 9 patterns of experiment, discharge cleaning, etc. ○ Standard cycle of discharge: 10 minutes (experiment) ○ Pre-shot and post-shot checks ○ Stop sequence with computers and hardwired interlock: Soft landing, Control stop, Normal stop, etc.
	Acquisition, Logging and Display of Discharge Result Data	○ Data amount: 1.5 Mword/shot (Experiment) ○ Acquisition time: 3 minutes ○ Data saving in MT, Transfer to Data Processing System ○ Discharge control trend and management logging

Table IX.5-1(b) Functions of JT-60 Control System (2/2)

	Items	Contents
Plasma Control	Feedback Control of MHD Equilibrium	○ Plasma current: Minor loop control with DDC in ohmic heating coil heating coil power supply ○ Horizontal and vertical position, Shape (n-index value), Position of the separatrix surface at the divertor throat: Feedback computer and DDC's in V,H,Q,M power supplies, Control cycle: 1 msec
	Plasma Parameter Contorl and Interlick Function	○ Real time control for gas injection (4 systems), neutral beam injection heating (14 units) and radio frequency wave heating (4 units), Control cycle: 10 msec/1 msec ○ Phase control: Soft landing, Disruption recovery, etc.
Safety and Protection	Protective Interlock	○ Method: Hard-wired relay logic, 100 protection items ○ Stop sequence corresponding to 5 emergency levels
	Failure Diagnosis and Prediction	○ Cause identification of failure and indication of check points (Support function to operators)

Table IX.7-1 Number of shots and Technical Problems

Item of tests		No. of shots	No. of Tech. Problems
(1)	preparation	——	0
(2)	mode transition	——	3
(3)	Taylor D.C	~90,000	11
	short pulse D.C	345	11
	long pulse D.C	20	6
	50% rating discharge	31	3
	full rating discharge	119	29
(4)	safeguard	——	3
(5)	plasma controllability	——	0
(6)	data monitoring	——	0
(7)	recovery	——	0

Table IX.9-1 Basic performance of the JT-60 NBI

Beam Energy; 75-100 keV
Ion Beam Current; 70 A x 14
Beam Duration Time; 10 sec
Cold Gas Flow to the Torus ; 0.84 Pa m3/s

Table IX.9.2-1 Specifications of the JT-60 RF heating system

	LHRF	ICRF
Number of unit	3	1
Frequency	1.7 - 2.3 GHz	110 - 130 MHz
Injection power	10 MW	
RF pulse length	10 sec	
Duty	1/60	
High power amplifier	klystron (8 tubes/unit)	tetrode (8 tubes/unit)
Launcher	Phased array of waveguides (4 rows × 8 columns)	Phased array of loop antennas (2 rows × 2 columns)

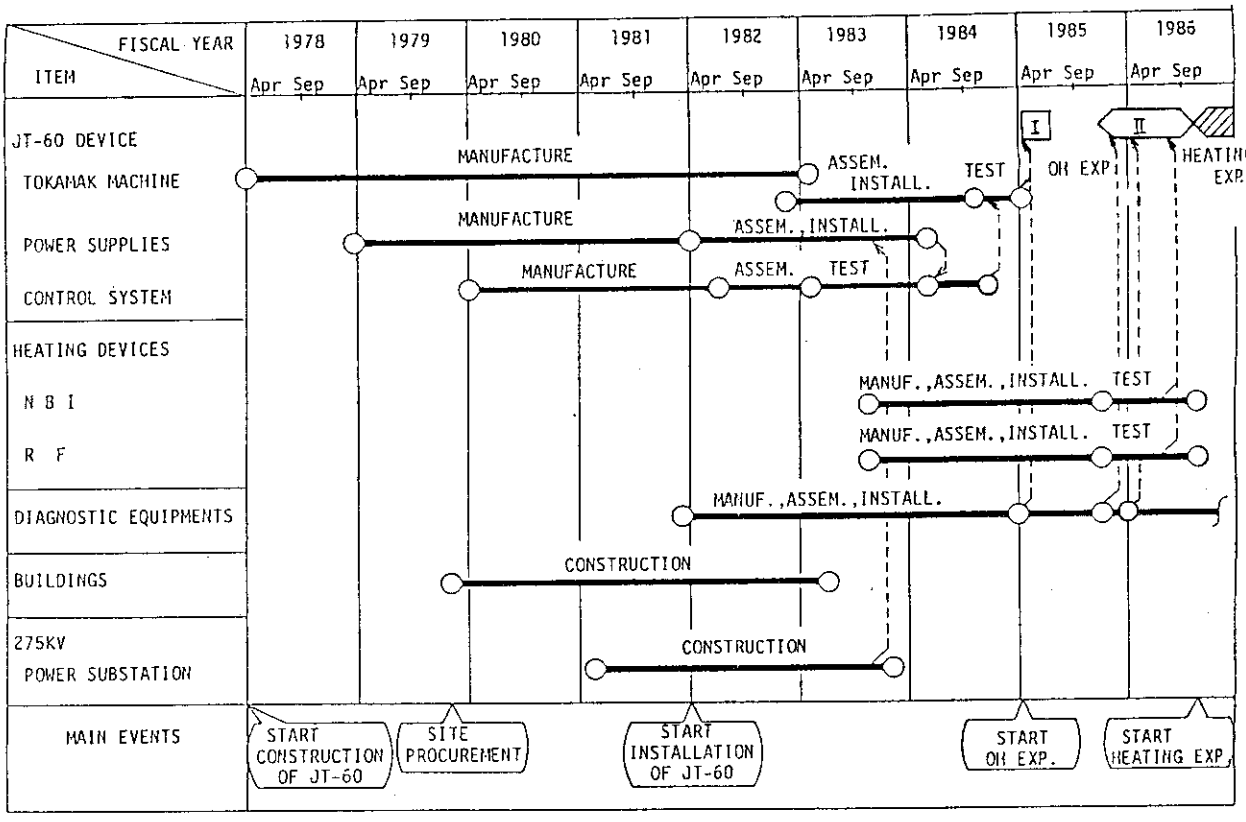

Fig. IX.2-1 JT-60 project schedule.

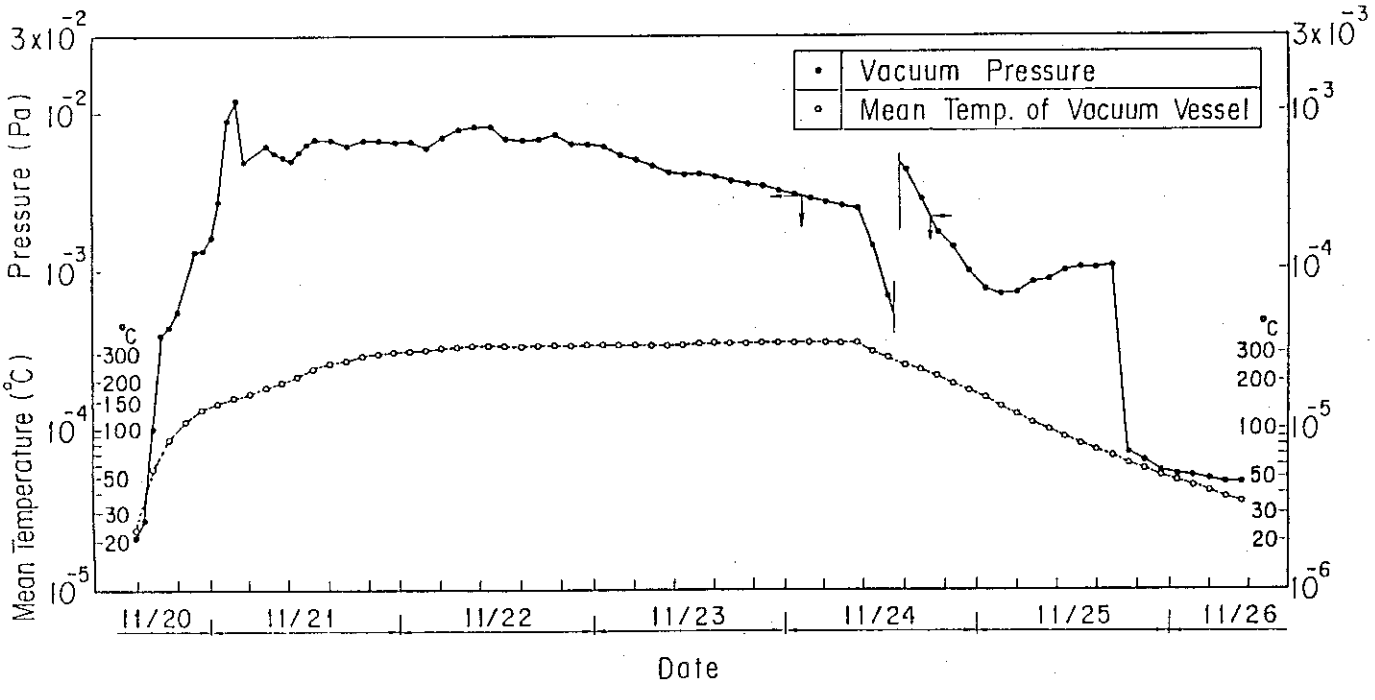

Fig. IX.3-1 Time evolution of mean temperature of vaccum vessel and vacuum pressure during the second cycle of baking.

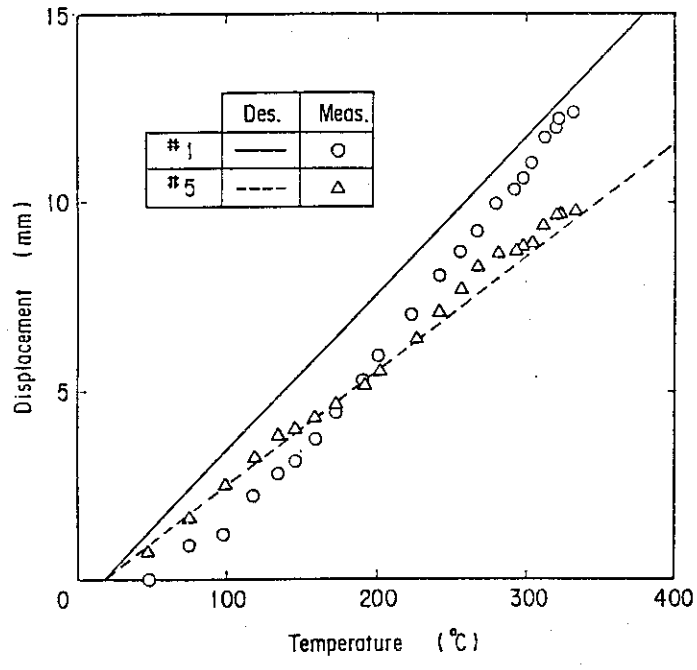

Fig. IX.3-2 Relation between mean temperature of vacuum vessel and displacement of movable pin-joint of vaccum vessel support arm.

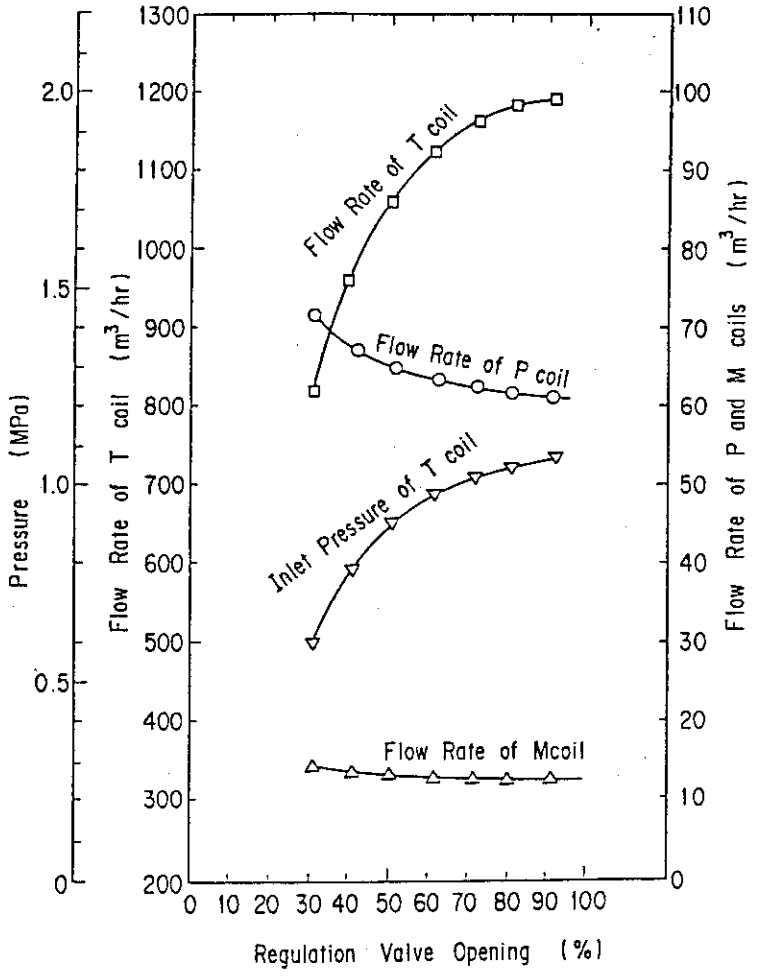

Fig. IX.3-3 Relation between valve opening and flow rate for primary cooling system.

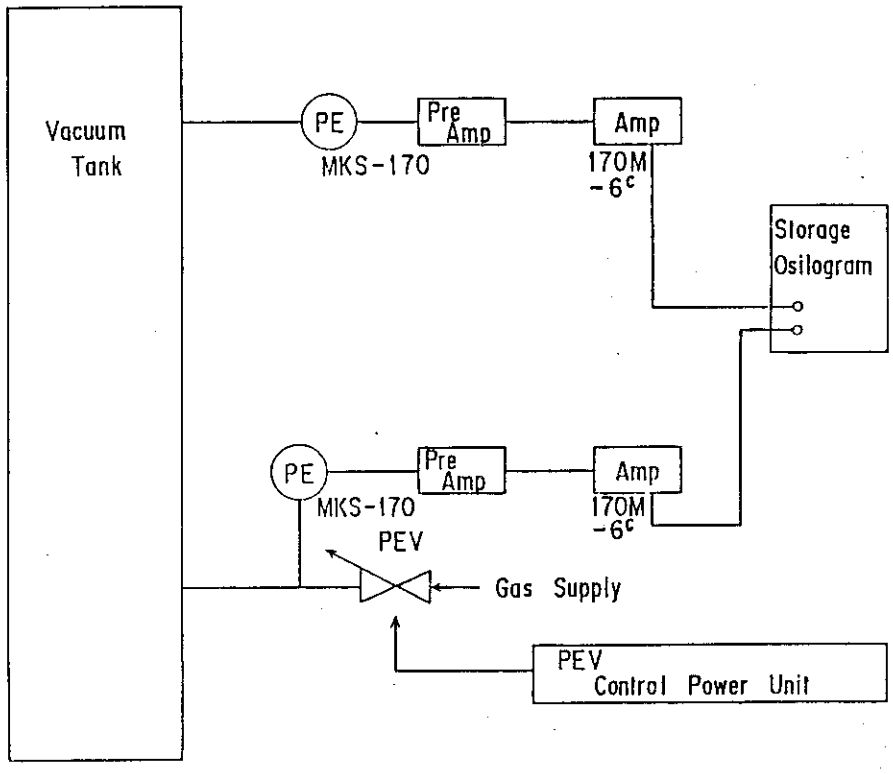

Fig. IX.3-4 Diagram of setup for PEV gas injection system fundamental test.

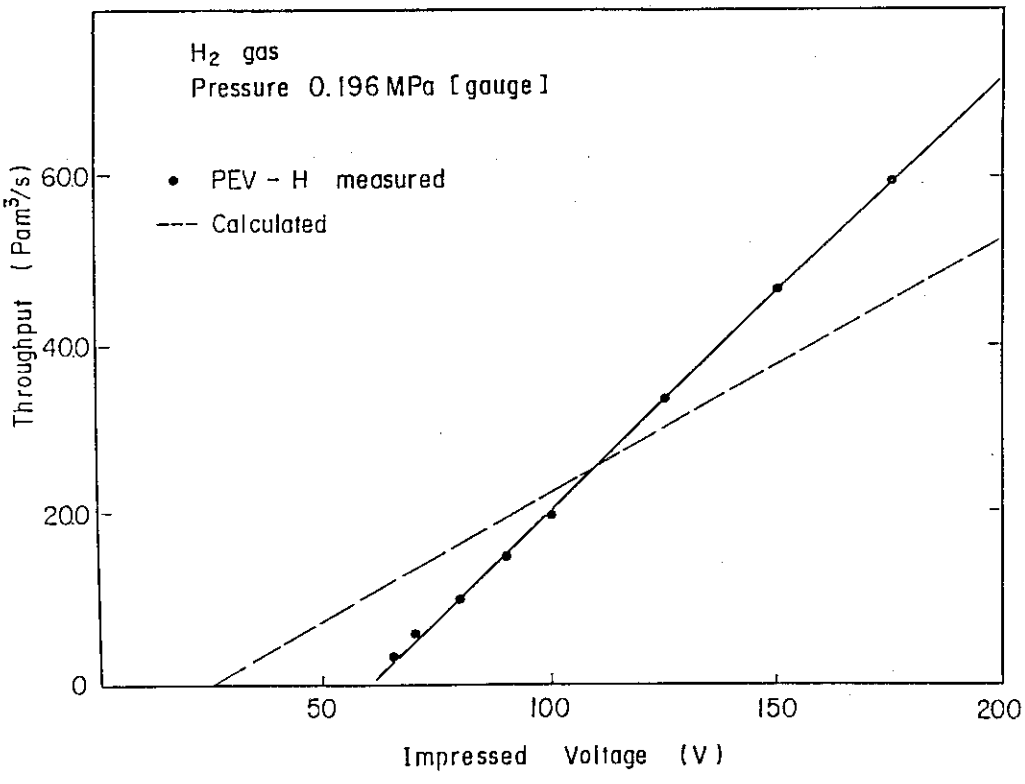

Fig. IX.3-5 Comparison between calculated throughput and measured one for large flow rate type PEV.

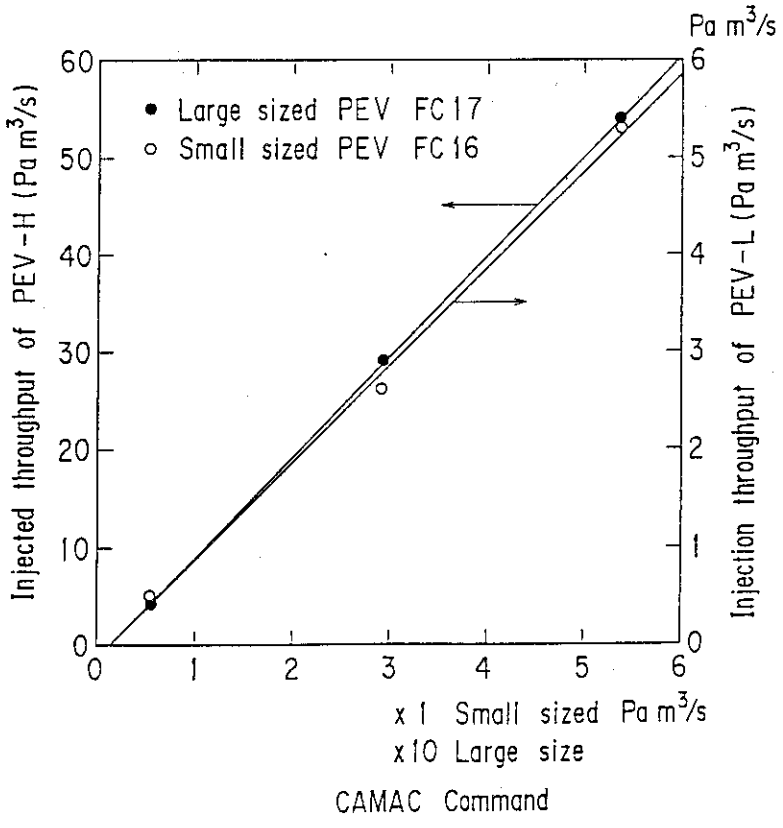

Fig. IX.3-6 Relation between injection CAMAC command and obtained throughput for large and small flow rate type PEVs.

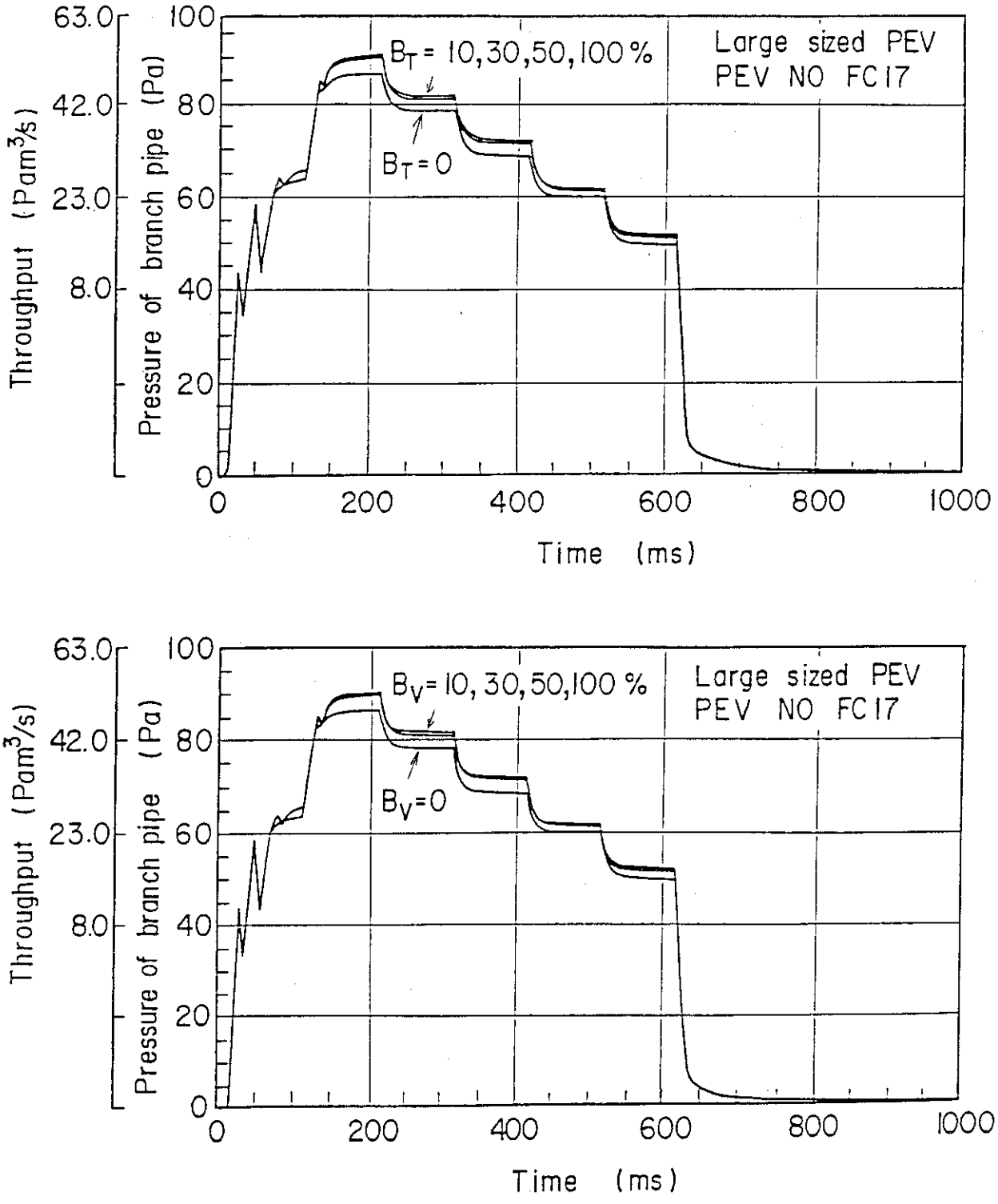

Fig. IX.3-7 Dependence of throughput rate on toroidal and vertical magnetic fields for large flow rate type PEV.

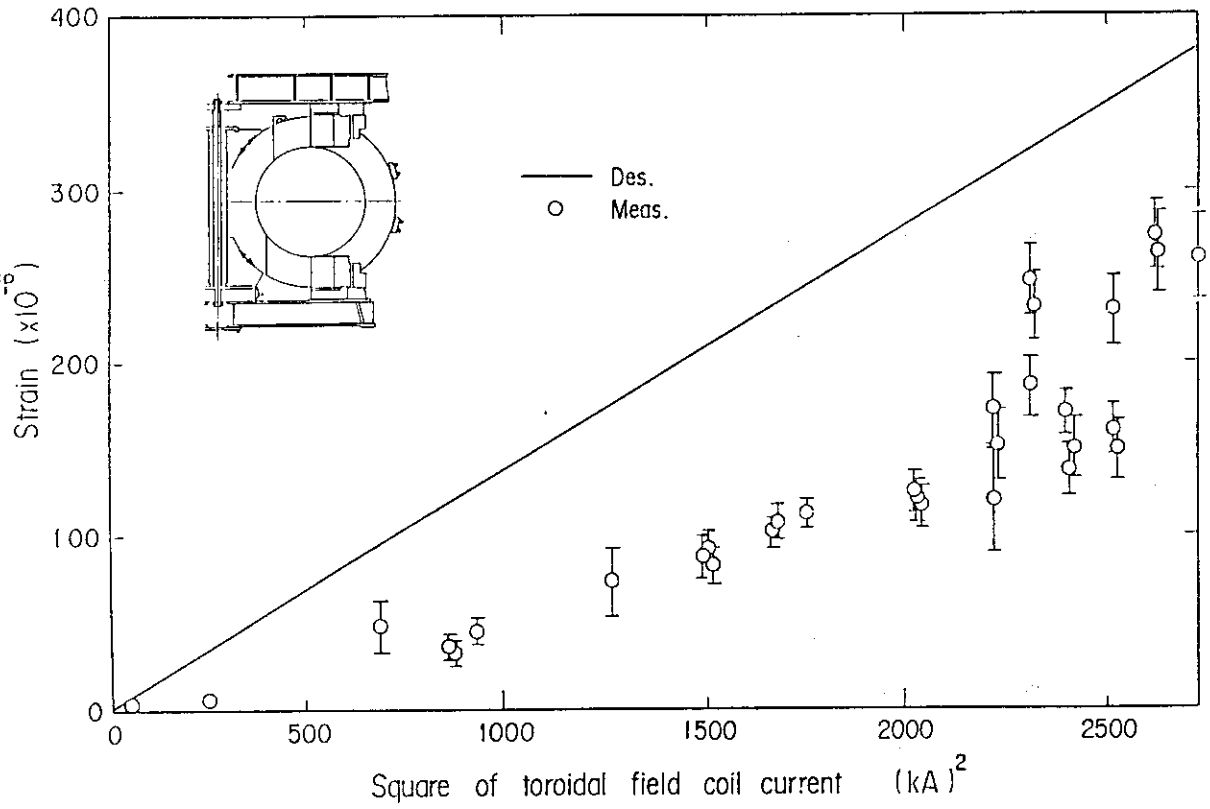

Fig. IX.3-8 Comparison between measured strain of toroidal field coil casing and designed one.

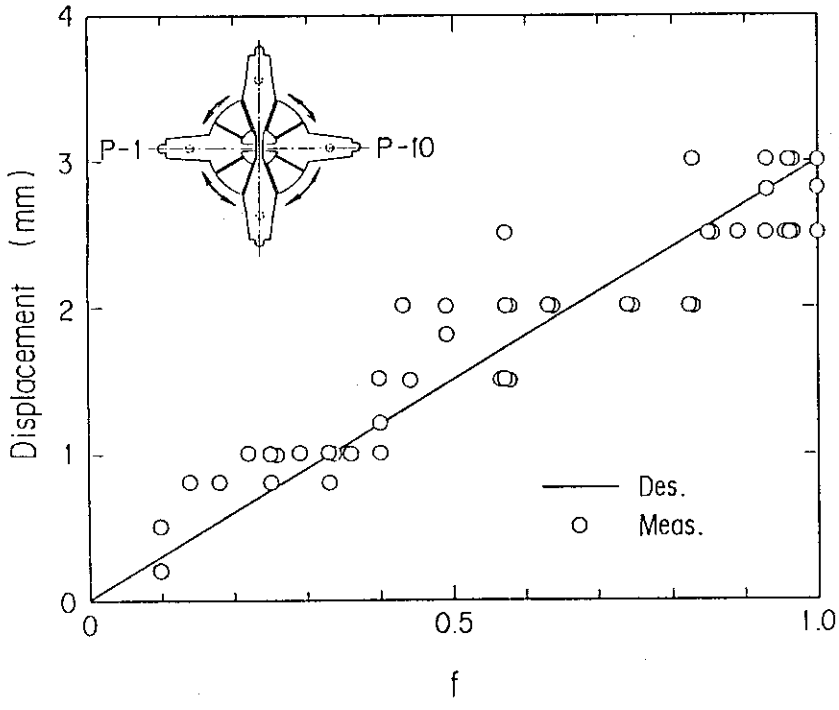

Fig. IX.3-9 Time evolution of maximum temperature difference in vacuum vessel during continuous TDC operation with parameters of ohmic heating coil terminal voltage.

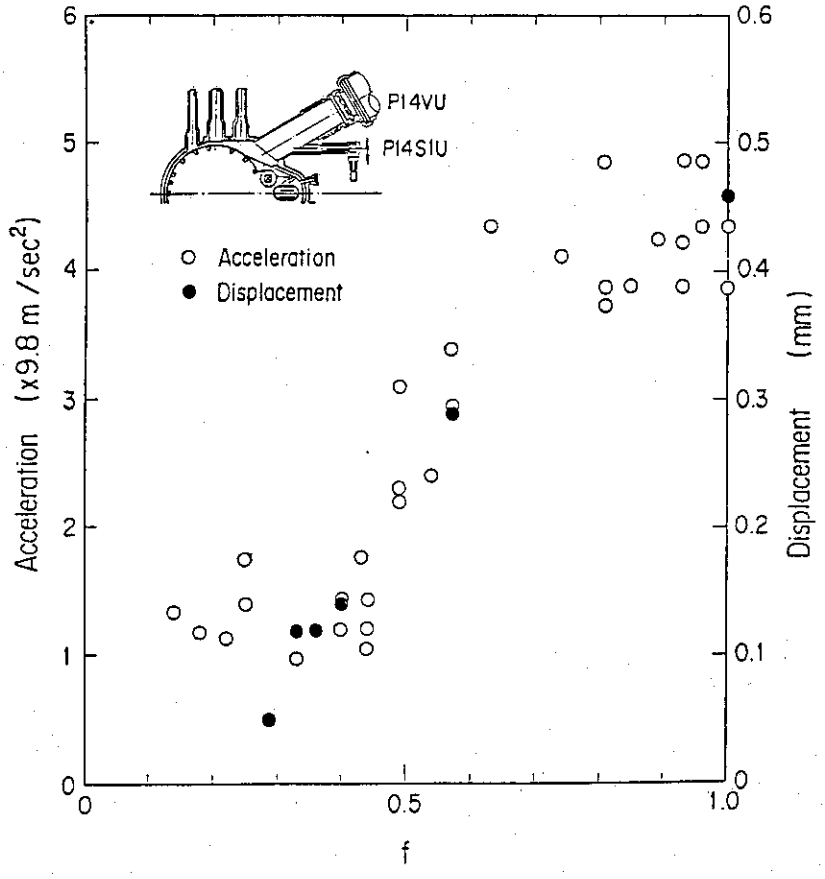

Fig. IX.3-10 Comparison between designed displacement of upper support structure and measured one.

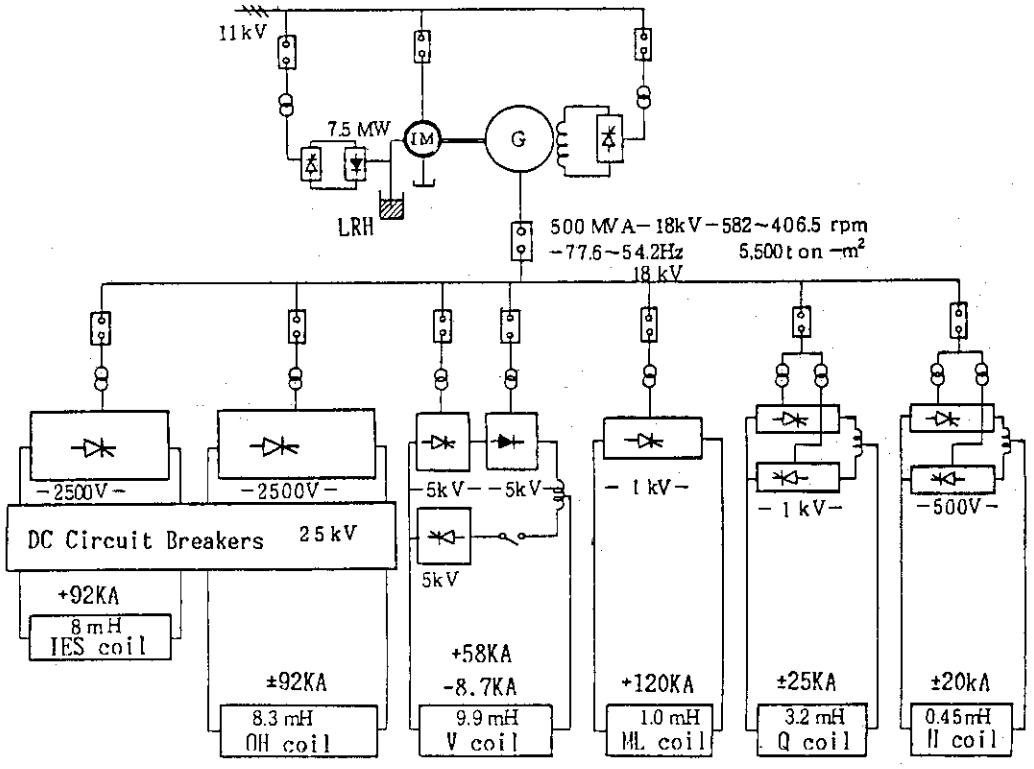

Fig. IX.4-1 Schematic diagram of the JT-60 poloidal field power supply System.

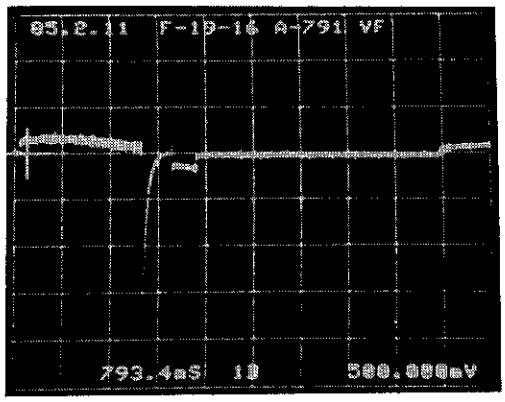

OH-COIL VOLTAGE 5KV/DIV
PHOTO.1 793.4ms/DIV

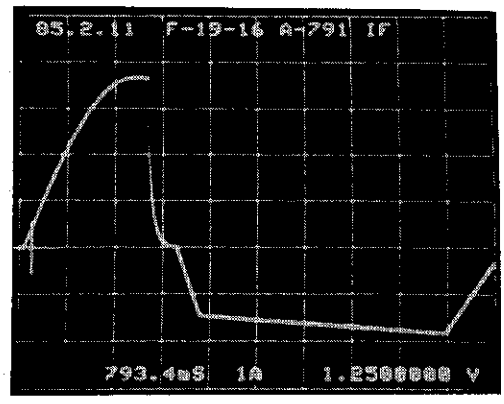

OH-COIL CURRENT 25.0KA/DIV
PHOTO.2 793.4ms/DIV

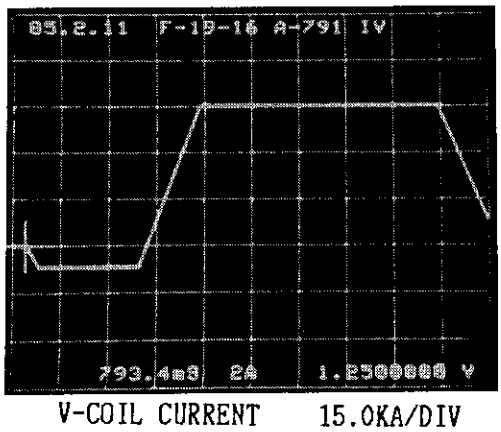

V-COIL CURRENT 15.0KA/DIV
PHOTO.3 793.4ms/DIV

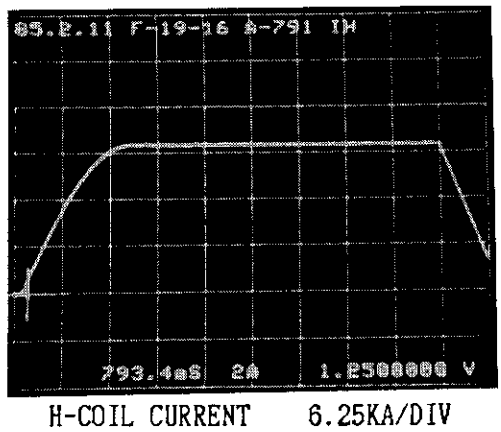

H-COIL CURRENT 6.25KA/DIV
PHOTO.4 793.4ms/DIV

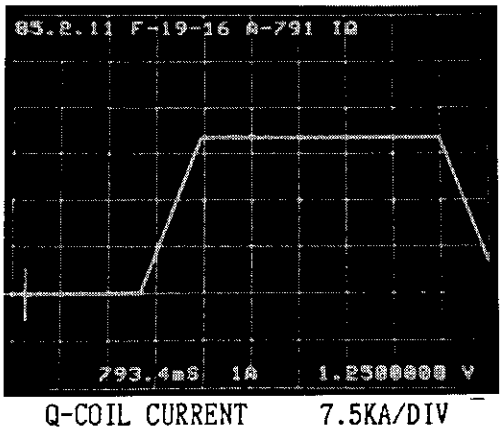

Q-COIL CURRENT 7.5KA/DIV
PHOTO.5 793.4ms/DIV

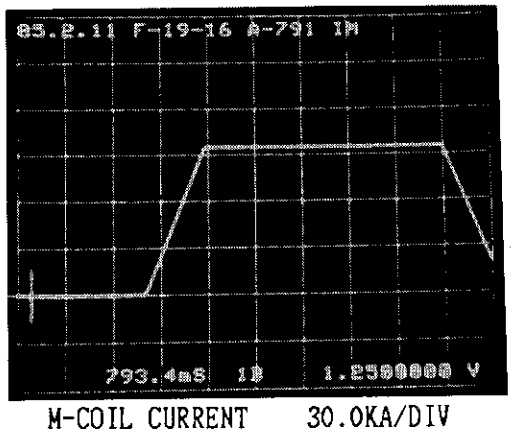

M-COIL CURRENT 30.0KA/DIV
PHOTO.6 793.4ms/DIV

Fig. IX.4-2 Test results of typical power test of PEPS.

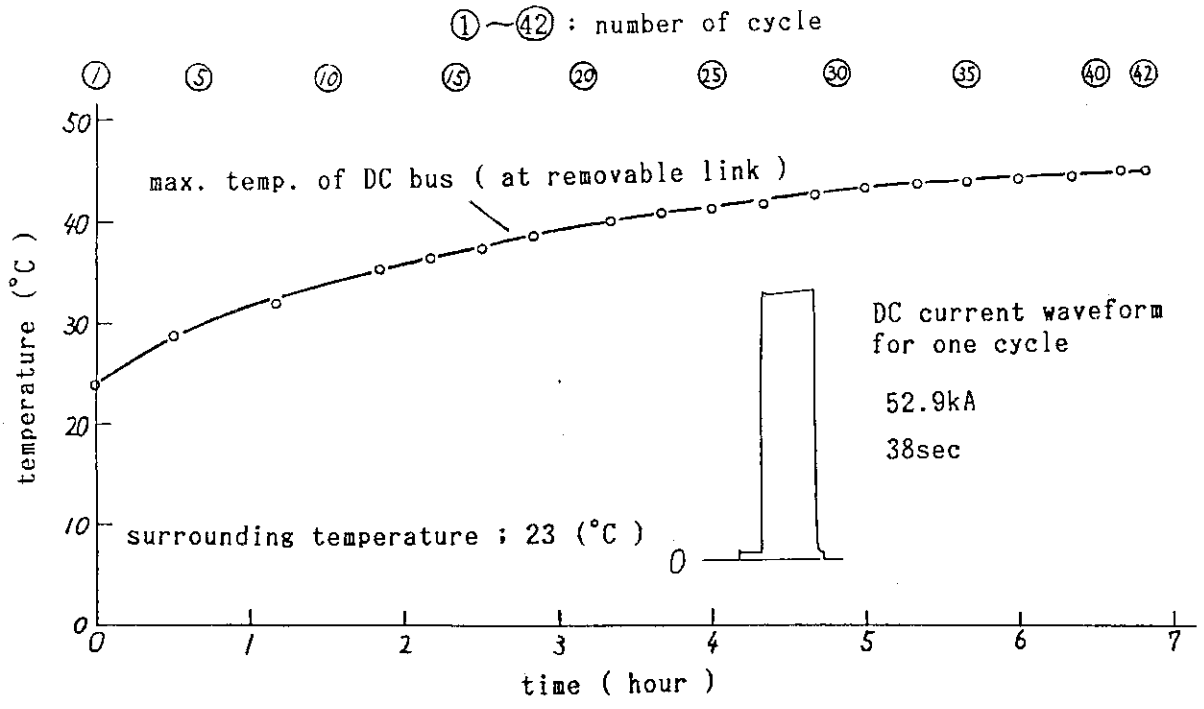

Fig. IX.4-3 The rise of the temperature of DC bus in the equivalent maximum current operation.

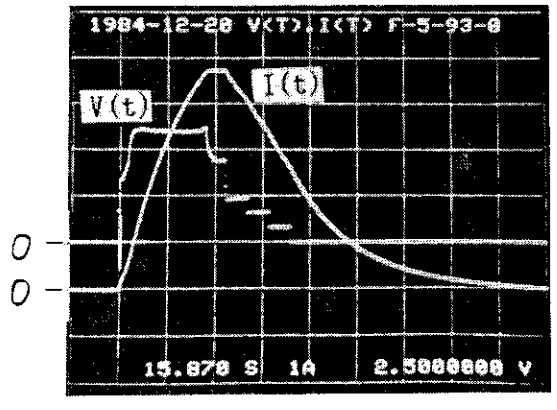

V(t) : TF coil voltage, 2.5 kV/div.
I(t) : TF coil current, 11 kA/div.
hor. axis : time, 15.9 sec/div.

Fig. IX.4-4 TF coil voltage and current of the maximum rating current operation.

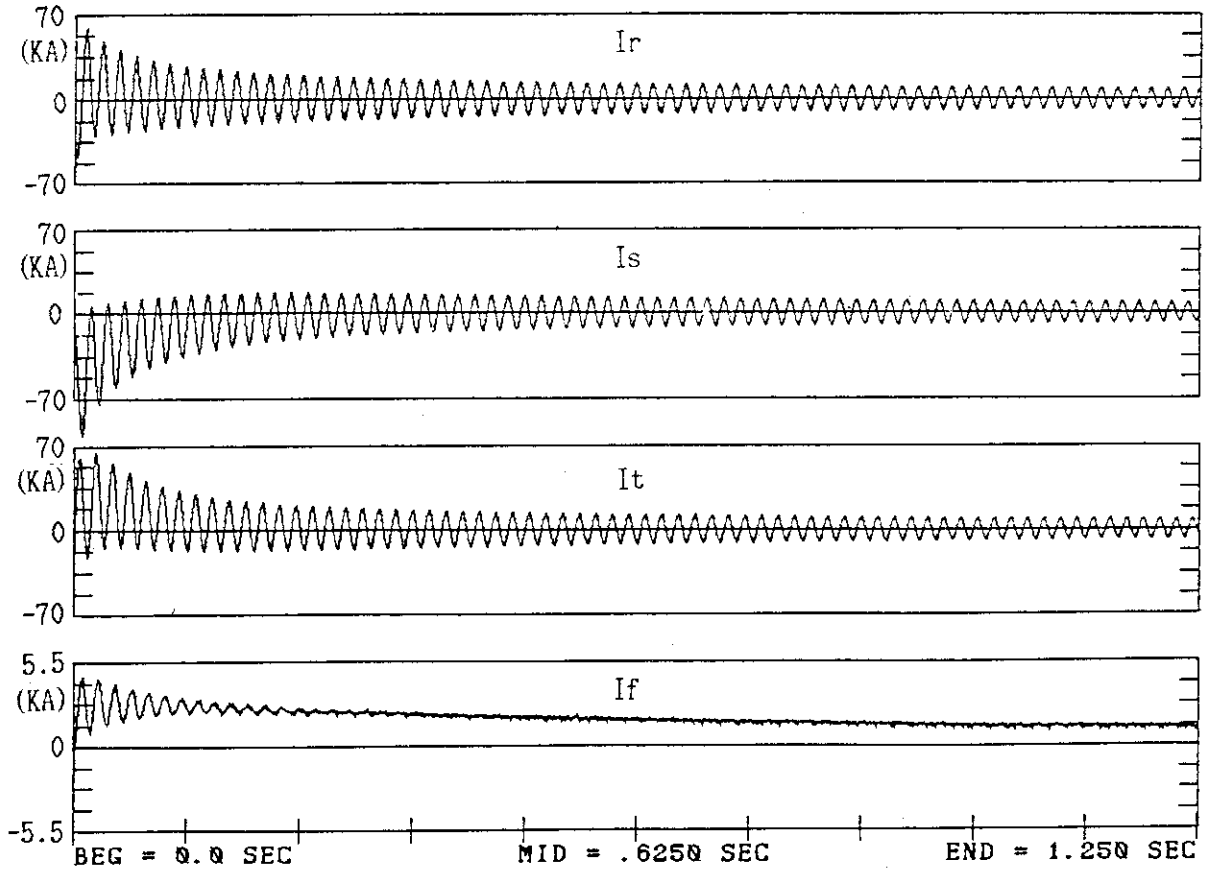

Fig. IX.4-5 Currents in the three-phase sudden short-circuit test (terminal voltage 31%, 406.5rpm)

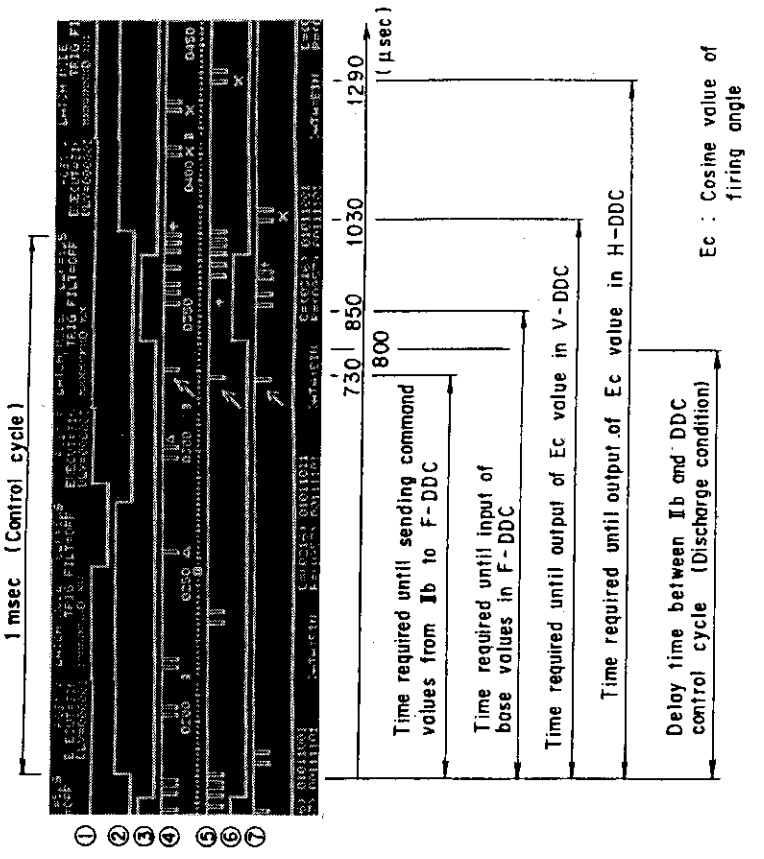

Fig. IX.5-1(b) Timing chart between the feedback control computer (IIb) and DDC CAMAC system in PFPS.

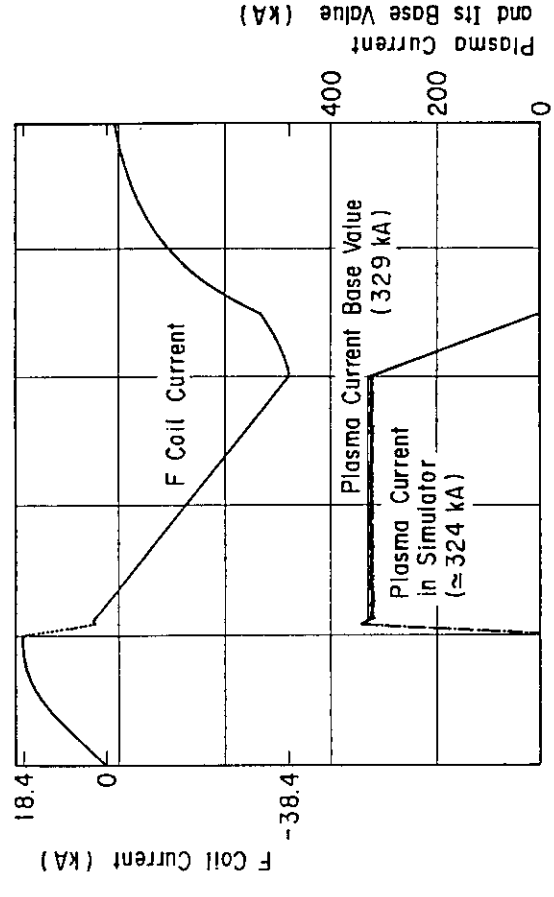

Fig. IX.5-1(a) A result of linkage performance between the feedback control computer (IIb) in "ZENKEI" and DDC system in PFPS at the power test with the dummy coil.

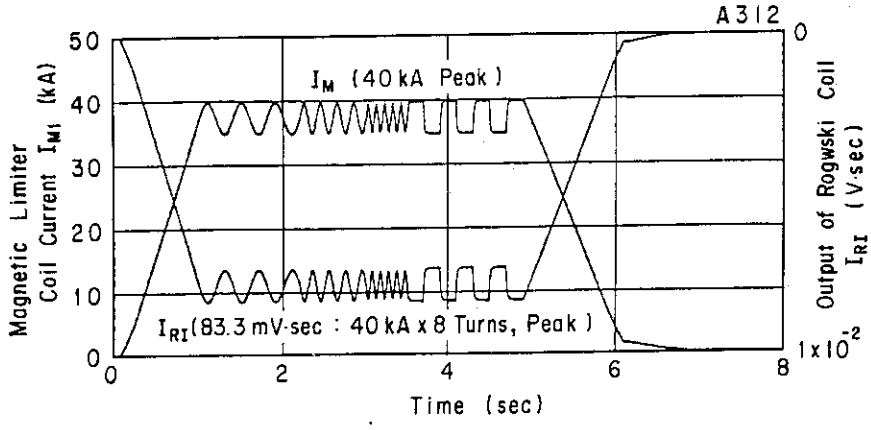

Fig. IX.5-2(a) Output signal of the Rogowski coil by exciting the primary magnetic limiter coil.

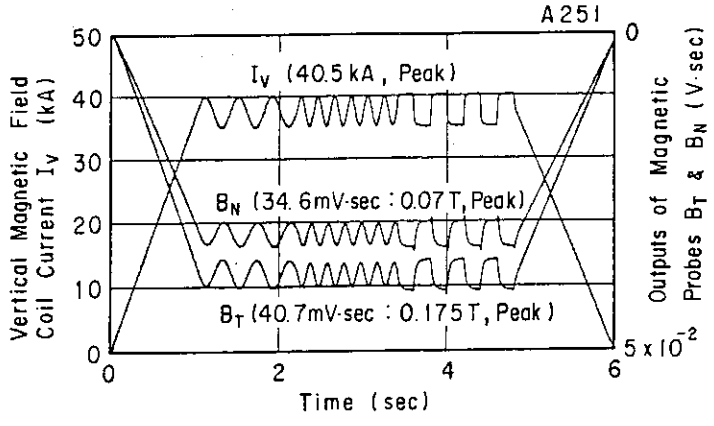

Fig. IX.5-2(b) Output signals of magnetic propes by exciting the vertical magnetic field coil.

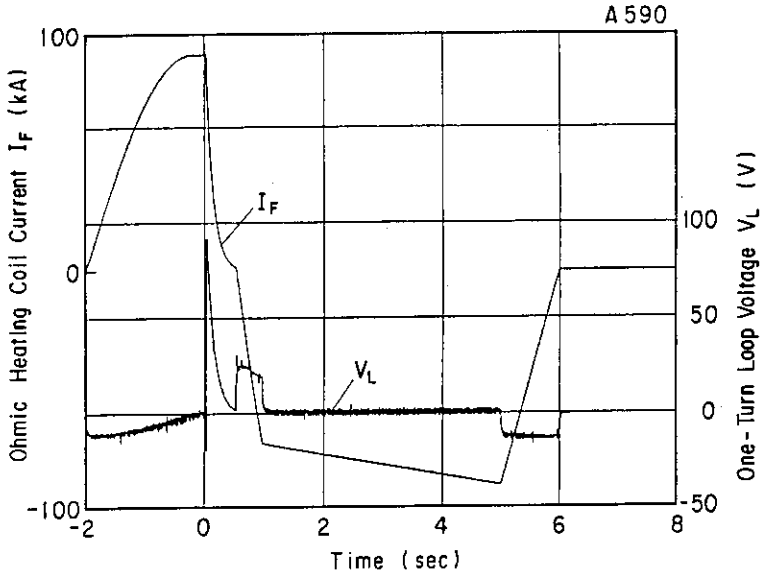

Fig. IX.5-2(c) One-turn loop output by exciting the ohmic heating coil.

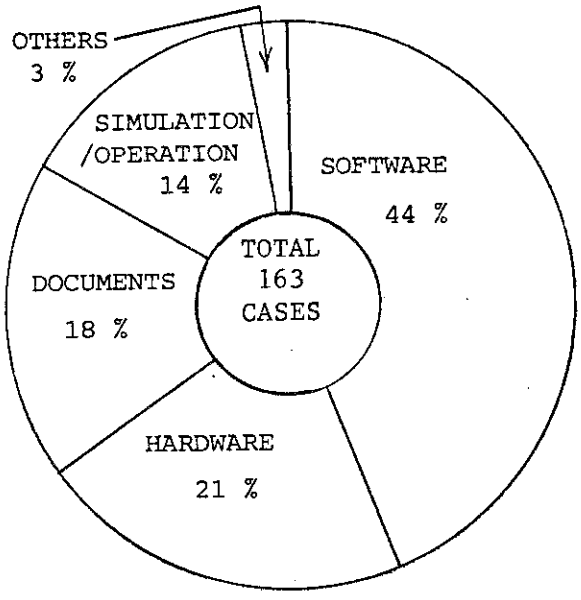

Fig. IX.7-1 Contents of problems appeared in the control system integration test.

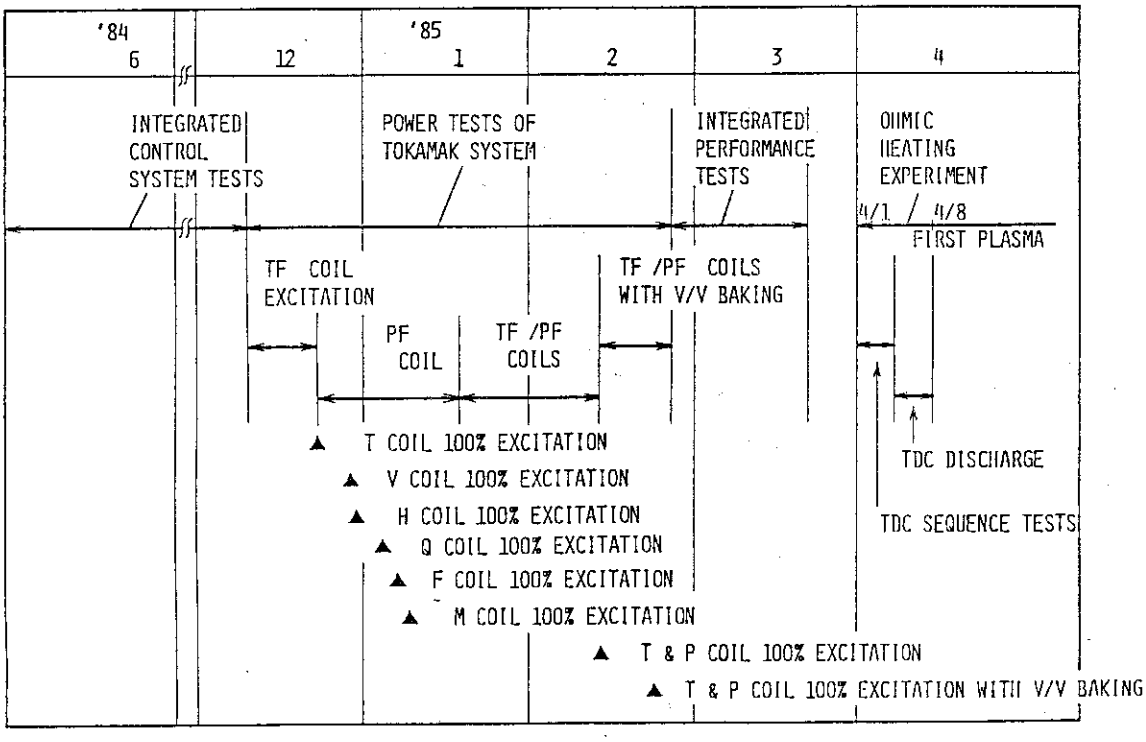

Fig. IX.7-2 JT-60 integrated system tests schedule.

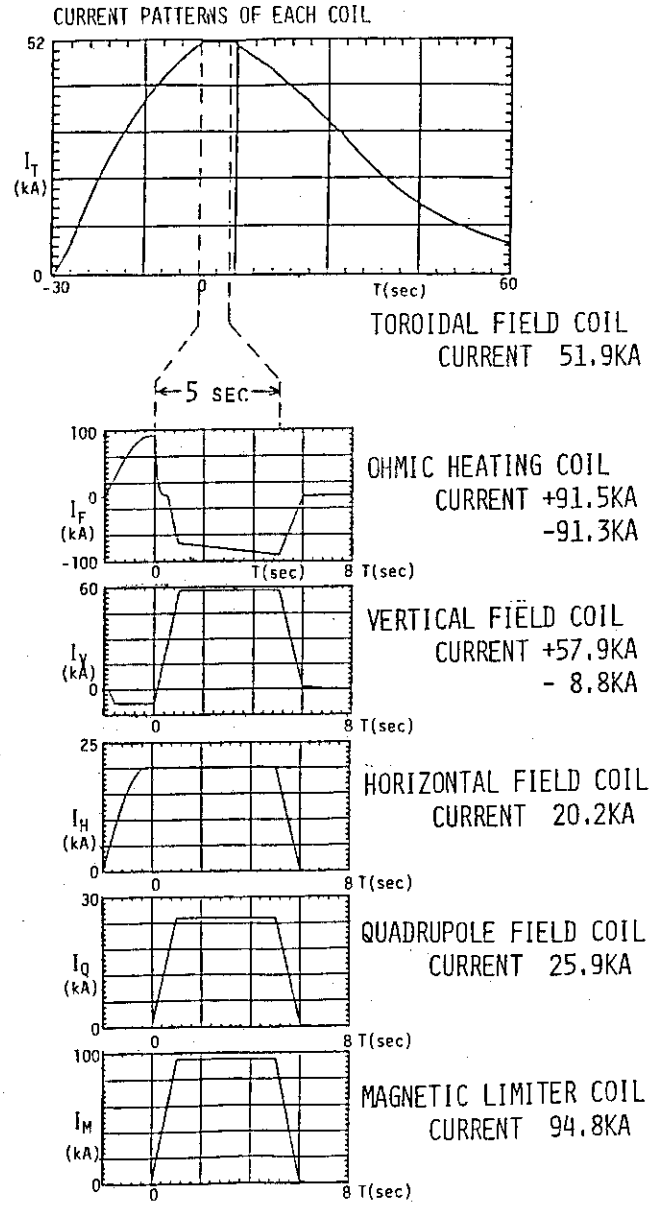

Fig. IX.7-3 Current waveforms of each coil.

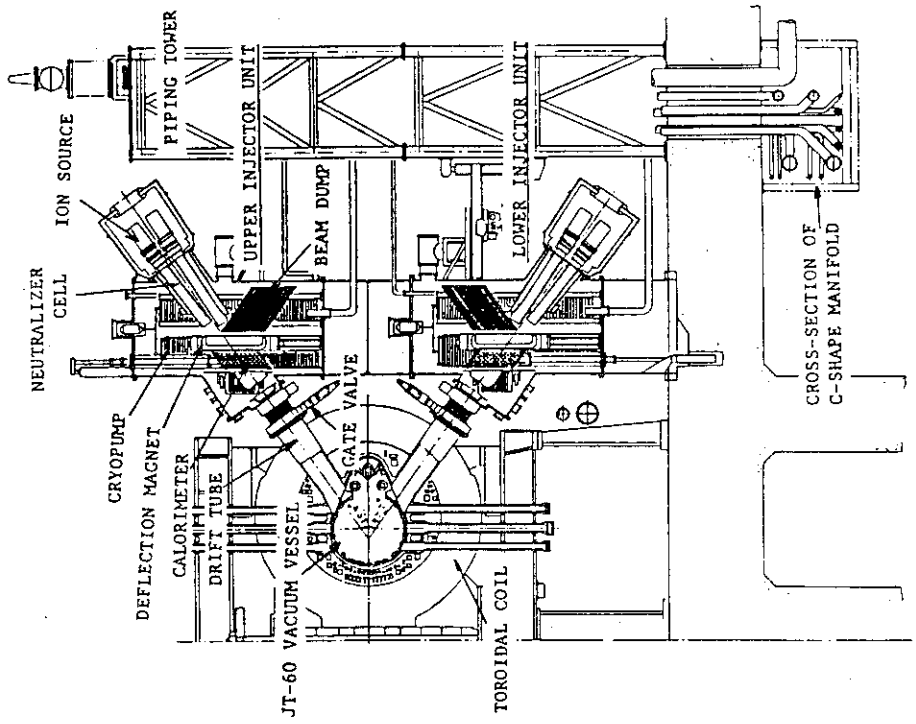

Fig. IX.9-1 Cross sectional view of the JT-60 NBI.

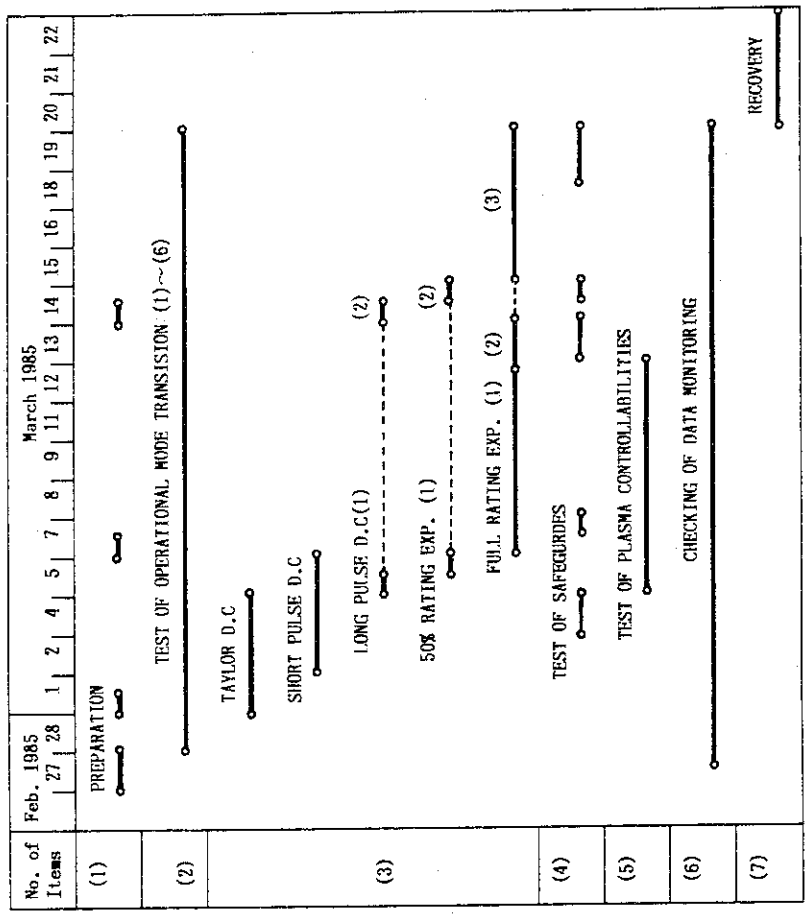

Fig. IX.7-4 Schedule of the integrated performance test.

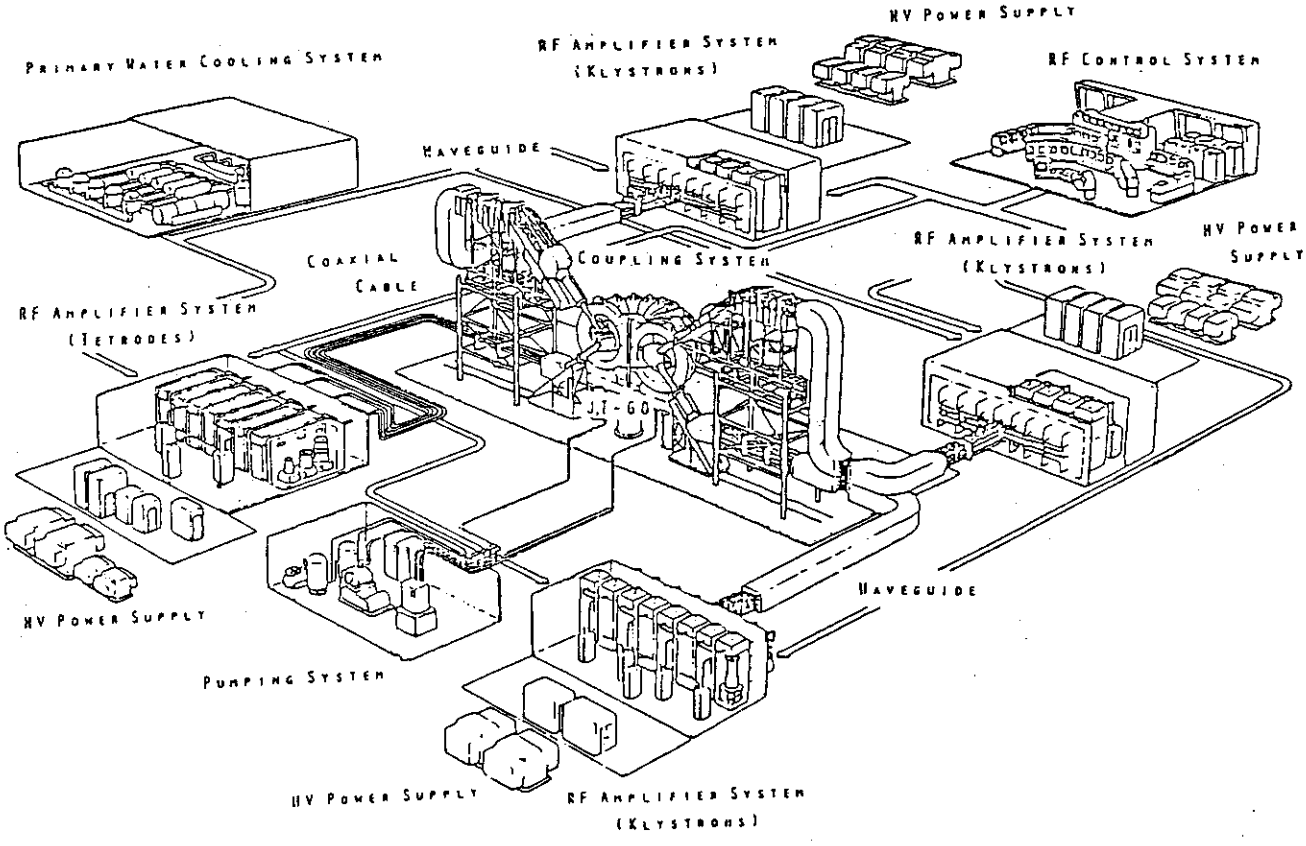

Fig. IX.9-2.1 Overview of JT-60 RF heating system.

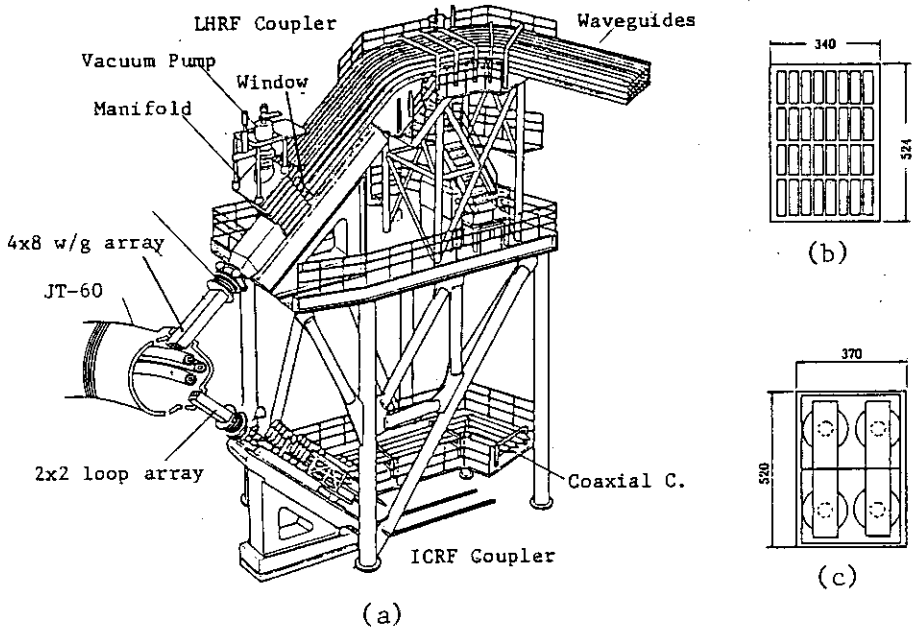

Fig. IX.9-2.2 Launchers of RF heating system.
(a) overview of the coupling system.
(b) top view of LHRF launcher.
(c) top view of ICRF launcher.

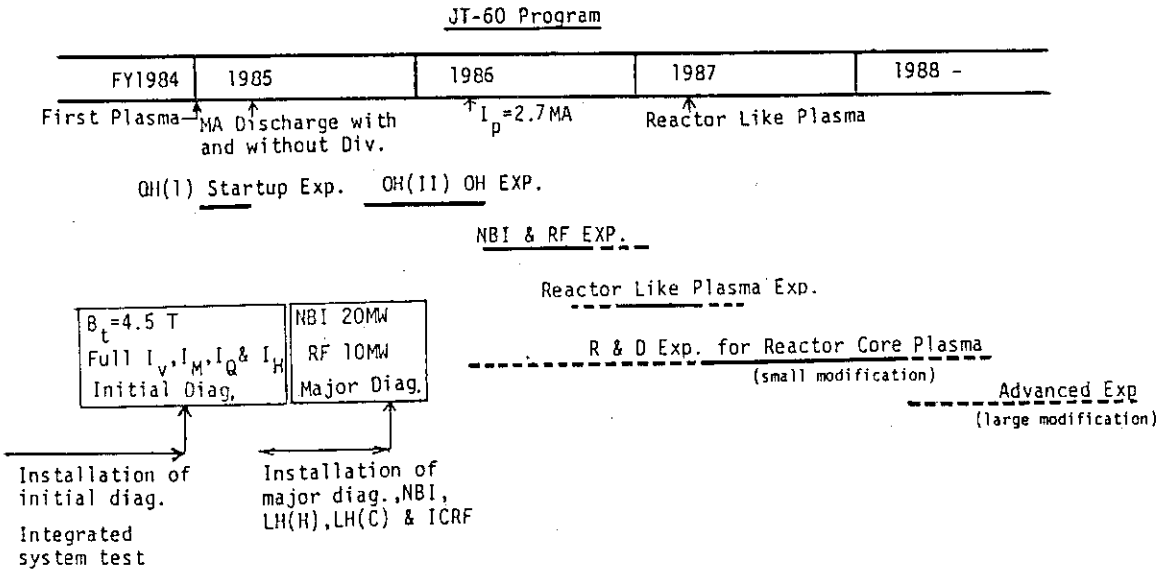

Fig. IX.10-1 Experimental program and schedule of JT-60.

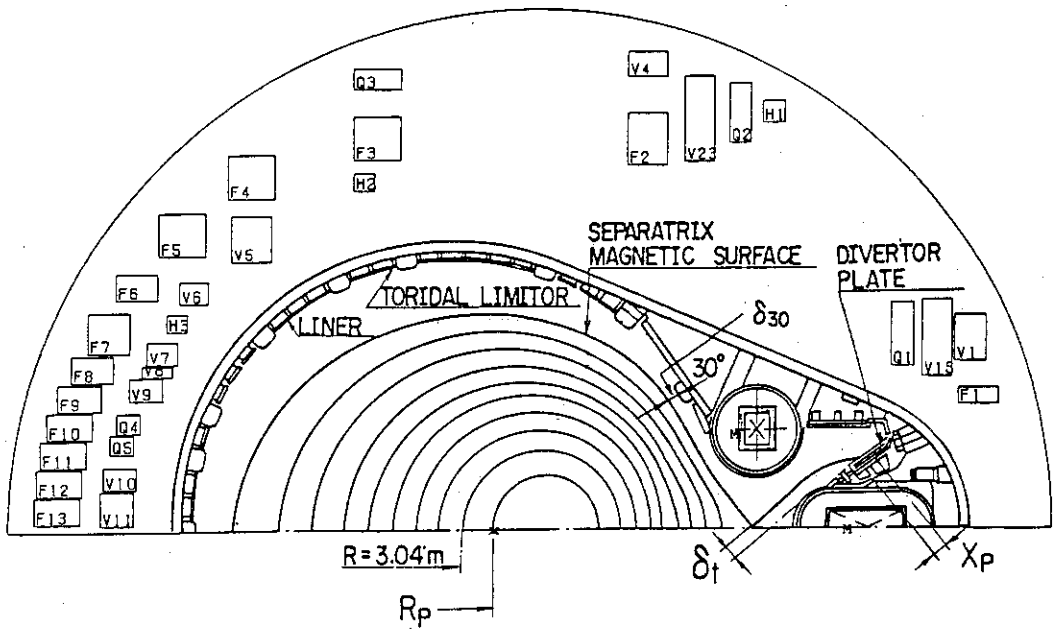

Fig. IX.10-2 Cross sectional view of JT-60. F: OH-field coil, V: vertical field coil, Q: quadrapole field coil, H: horizontal field coil, and M: magnetic limiter field coil.

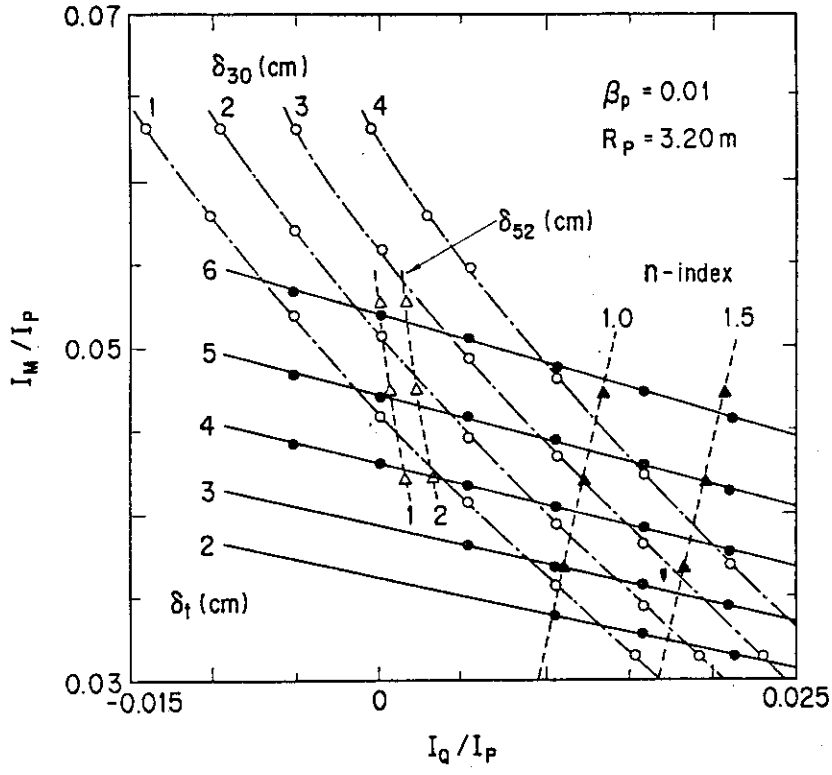

Fig. IX.10-3 δ_{30} (open circles) and δ_t (dotes) in the $I_Q/I_p - I_M/I_p$ plane. These are the numerical results of Grad-Shafranov eq. In this case R_p = 3.10 m, β_p = 1.00, and ℓ_i = 1.0.

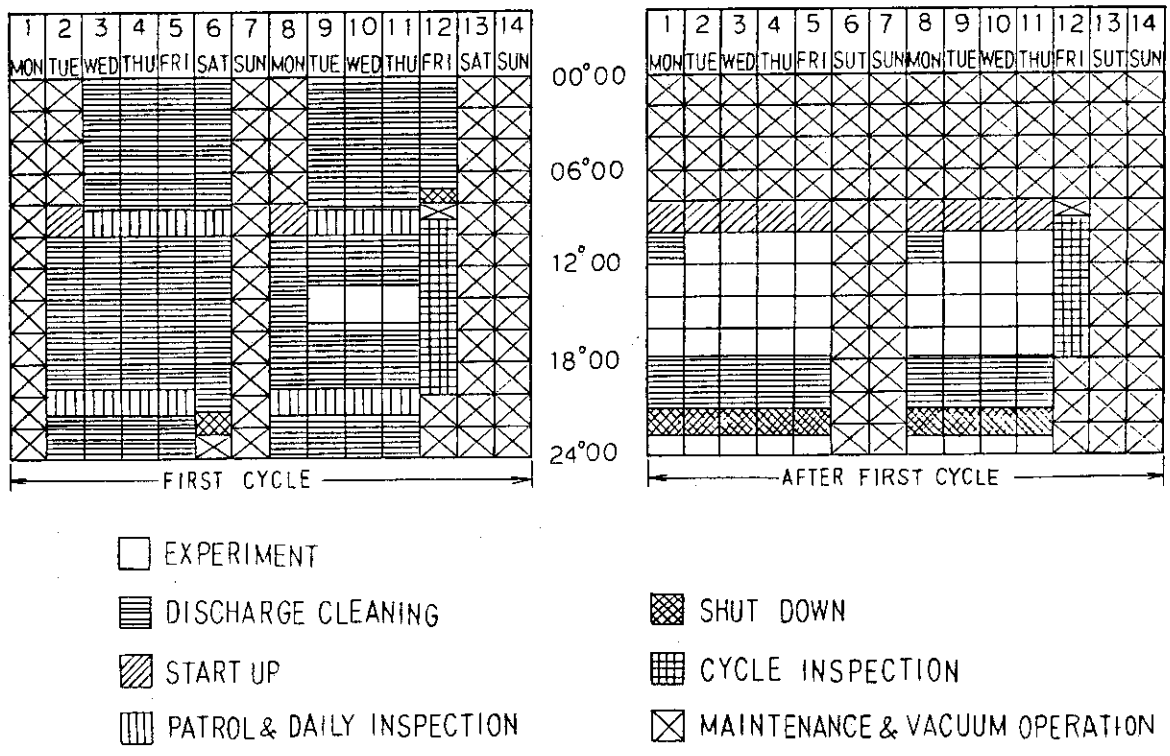

Fig. IX.10-4 Operation program of JT-60.

X. DESIGN STUDY OF THE NEXT GENERATION DEVICE AND FUSION REACTOR SYSTEM

1. Fusion Experimental Reactor (FER)

1.1 Introduction

Table X.1-1 shows parameters and specifications of FER reference design for FY 1984. The primary features of 1984 design are the following.

1) Long burn operation and reduction of the machine size as well as power supply capacity were achieved by means of RF current drive scenario.
2) Remote maintenance procedure is greatly simplified in such a way that sectors of the reactor core components such as the removable shield and the divertor will be withdrawn and inserted with a single straight motion in radial direction.

For the reference design in FY 1984, the following selections of parameters and specifications were made.

1) A neutron fluence of 0.3 MWY/m^2 was selected, considering required fluences for various test objectives and associated cost performance as well as test periods.
2) Shielding type blanket is employed in order to get more reliable reactor structure, and blanket test modules of tritium breeding type are installed to get sufficient engineering data.
3) As for the impurity control system, single null poloidal divertor is employed, taking account of reality of the plasma concept and simplification of the remote maintenance procedure.

1.2 Design of reactor plasma and operating scenario

For the design FY 1984, current research activities primarily based on recent tokamak experiments were evaluated. In addition to this evaluation, near term experimental results expected on JT-60, JFT-2M, Doublet-III and so forth were also taken into account for the design. Design parameters of the reactor plasma are shown in Table X.1-1. In this table, it should be noted in particular that quasi-steady state

operating scenario is used. This operating scenario is schematically shown in Fig. X.1-1, and consists of alternating cycles of high density plasma burn with the plasma current being driven by flux swing which are followed by RF driven low density plasma phases. During the low density plasma phase which follows each plasma burn, the ohmic heating coils are recharged by the RF power. Since the plasma current will be kept almost constant and rate of the plasma current ramp up will be fairly low, this operating scenario gives the reactor design significant benefit such as mitigation of fatigue design as well as reduction of helium refrigeration capacity.

1.3 Reactor structure concept

Reactor structure design for FY 1984 was performed based on the plasma concept described in section X.1-2. Fig. X.1-2 shows the elevation view of FER of FY 1984 version. Device and plasma parameters were optimized, meeting the requirements from the FER objectives under available physics data base and the engineering restrictions such as confinement scaling, beta limit, divertor configuration and maximum magnetic fields on superconducting coils. All the superconducting coils system is contained in a common cryostat(bell-jar type) and the PF coils are placed external to the TF coils. The single null-poloidal divertor configuration is employed, and the remote maintenance procedure for the shielding structure and the divertor is greatly eased as mentioned in section X.1-1. As for the cooling system of the superconducting coils, forced flow cooling is employed both for TF and RF coils, considering potential advantages of higher mechanical integrity and insulation withstand ability. In addition, Nb_3Sn superconductors are used for PF coils similarly to those of TF coils, in order to make the reactor inboard size more compact and get better cost performance for conductor development.

2. INTOR

The INTOR workshop of Phase Two A, Part 2 started in August 1983,

and will be completed in July 1985. Major objectives of the Part 2 are to study critical technical issues, and to assess scientific and technical data bases, and to finally upgrade the INTOR design concept.

To study critical technical issues that affect the feasibility or practicability of the INTOR design concept, the following five groups are organized.

A : Impurity control and first wall
B : RF heating and current drive
C : Transient electromagnetics
D : Maintainability
E : Technical benefit

In addition to those groups, the three disciplinary groups are organized to assess the worldwide scientific and technical data bases that exist now and will exist in 4 - 5 years to support the detailed design and construction of an INTOR-like machine, and to identify additional R & D that is required.

F : Physics
G : Engineering
H : Nuclear

In assessment of data base, discussions have been focussed on a beta value limit. The present beta value of 5.6%, which was assumed in the conceptual design in Phase One, has been found to significantly exceed the value from the beta scaling law established recently, $(3\text{-}4)I_p[MA]/a[m]B_T[T]$. To keep the beta value within the beta scaling limit, design modification is ongoing, in which a major radius is reduced by saving spaces for poloidal and toroidal coils and shield, and a safety factor is reduced as well. Those reductions lead to increase in the beta value limit. The major parameters of modified INTOR are listed in Table X.2-1, and the cross section is illustrated in Fig. X.2-1.

3. Studies on Fusion Reactor System

3.1 Design study of power-producing breeding blanket

For a tokamak power reactor a comparison design study of

power-producing breeding blankets has been weighted in view of material and coolant selection.

Considering the current data base and the perspective of its further improvement, the selection of titanium modified austenitic stainless steel as first wall and blanket structural material is realistic. In addition to the stainless steel with water coolant, molybdenum alloys have been selected as a structural material among refractory metals to realize the advantage of a helium coolant. The major concerns associated with the use of molybdenum alloys as the structural material are the loss of ductility due to neutron irradiation and the weldability. The new molybdenum alloys being developed in JAERI, to which are added small amounts of rhenium, vanadium and niobium to control interstitial impurities such as oxygen, nitrogen and carbon in grain boundaries, show better ductility after neutron irradiation and welding.

The solid lithium oxide Li_2O was selected as a reference breeding material for both water-cooled and helium-cooled blankets in view of its high breeding and tritium release performances. The mass transport feature of Li_2O due to the enhanced vaporization at high temperature in the presence of moisture will not permit direct helium cooling of the breeder. In addition a solid breeding material α-$LiAlO_2$ was chosen for the reference blanket design for the helium-directly-cooled breeder in terms of its operating temperatures compatible for use of the helium coolant.

Major design parameters of first-wall/blanket are shown in Table 3.1.1. In case of water coolant, the operating coolant conditions employed are similar to those of pressurized water fission reactors. The maximum coolant temperature of 320°C is consistent with the temperature limit on stainless steel ($\lesssim$ 450°C). The helium outlet temperature of 700°C is determined with consideration for providing steam conditions of latest steam-power plants and for the molybdenum alloy temperature limit of $\sim$1000°C because of recrystalization. The helium inlet temperature is set to 400°C to keep breeder temperatures above 400°C from the viewpoint of continuous tritium recovery.

Figure 3.1.1 shows the blanket design concept in which helium cools directly the breeding material ($LiAlO_2$ of 3 mm-dia, pebble) located inside the coolant tube. The operating temperature range of the breeder is narrower (400 $\sim$ 700°C) than that for the concept of breeder outside

coolant tube since the temperature change in a pebble is small. The first wall is structurally integral with the blanket to enhance the tritium breeding ratio and simplify the support structure in front of the blanket. Circular cross sections are selected for the first wall coolant channels in terms of reliable pressure boundaries and manufacturing feasibility.

3.2 Development of tokamak system code

There is a growing demand for system analyses of various tokamaks in order to improve tokamak designs in wide parameter range, and a few computer codes[1,2,3,4,5] have been developed with these points as background. Although these computer codes have been developed for the sensitivity study or the cost evaluation, they seem to be not necessarily satisfactory for producing a new design concept. Then the computer code is indispensable for producing a new design concept without the expenditure of large amount of professional staff design time.

The tokamak design code under development has the function of an automatic design optimization according to the certain design objective, and it is named "TORDEC" (Tokamak Reactor Design Code). The design calculations are basically performed from inside (plasma side) to outside (coil side) so that all components can be consistently designed. Especially the consistency between the plasma power balance, the radiation shield criteria, the plasma MHD equilibrium, the PF coil current distribution and the operation scenario is considered. The flow diagram of "TORDEC" is shown in Fig. X.3-2.

References

1) R.L. Reid and D. Steiner, Nuclear Technology/Fusion 4 (1983) 120.
2) R.L. Reid and K.F. Wu, "FTF SYSTEM CODE-COMPOSITION AND APPLICATIONS CONF-801011-5.
3) D.A. Sink and E.M. Iwinski, "A COMPUTER CODE FOR THE COSTING AND SIZING OF TNS TOKAMAKS", Proceedings of the 7th Symposium on Engineering Problems of Fusion Research, IEEE Pub. No.77CH1267-4NPS.
4) L.M. Waganer, L.A. Carosella and D.A. Defreece, "ESTABLISHMENT OF DESIGN AND PERFORMANCE REQUIREMENTS USING COST AND SYSTEM ANALYSIS",

Proceedings of the 7th Symposium on Engineering Problems of Fusion Research, IEEE Pub. No.77CH1267-4NPS.

5) M. Kasai, M. Nishikawa, A. Kameari, I. Yanagisawa, N. Ueda, T. Tone, T. Hiraoka, 9th Symposium on Engineering Problems of Fusion Research (Oct. 26-29, 1981, Chicago).

3.3 Safety analysis

Failure modes of components in a fusion experimental reactor were identified and accident sequences following the failure were systematically investigated. Taking the amount of radioactive material release to the environment as the measuring indicator, the accident consequences were compared to identify the most important accidents. As a result, the accidents leading to the release of the tritium inventory of the main vacuum pump were found to be most important.

As the first step for the analysis of the important accidents, a nuclear-thermal coupled calculation system was developed. The calculational flow in the system is shown in Fig. X.3-3. This system tests not only steady state problems but also non-steady problems in two-dimensional geometry. At first the neutron and gamma-ray fluxes are calculated using the two-dimensional radiation transport code DOT-3.5[1], and then nuclear heating rate is calculated using the APPLE-2 code[2]. The nuclear heating distribution is input to the nonlinear heat transfer calculation code DOT/DETECT[3] to obtain the temperature distribution based on the finite element method. The above procedures are followed automatically and the outputs are shown graphically. The distributions of nuclear heating rate and resulting temperature are shown in Figs. X.3-4 and X.3-5 for the first wall and blanket vessel of the fusion experimental reactor designed in 1983[4]. These results are for the steady state operation but non-steady temperature distributions caused by the decay heat may be calculated by the use of the induced activity calculation system THIDA-2[5] in obtaining the decay heat.

As regards the calculation system THIDA-2, the following two improvements have been incorporated:

(i) In the calculation of decay heat, the transport of the delayed gamma-rays are taken into consideration.

(ii) Using the Evaluated Nuclear Structure Data File (ENSDF)[6], the

libraries for the decay chain data and the delayed gamma-ray data as the input for the THIDA-2 system, can now be generated automatically.

References

1) RHOADES, W.A. and MYNATT, F.R., "The DOT-III Two Dimensional Discrete Ordinates Transport Code", ORNL/TM-4280 (1973).
2) KAWASAKI, H. and SEKI, Y., "APPLE-2; An Improved Version of APPLE Code for Plotting Neutron and Gamma Ray Spectra and Reaction Rates", JAERI-M 82-091 (1982).
3) POLIVKA, R.M. and WILSON, E.L., "DOT/DETECT", University of California Berklay (1976).
4) Fusion Reactor System Laboratory, "Conceptual Design of Fusion Experimental Reactor (FER) (FY 1983 Report)", JAERI-M 84-212 (1985).
5) SEKI, Y. et al., to be published.
6) EWBANK, W.B. et al., "Evaluated Nuclear Structure Data File, A Manual Preparation of Data Sets", ORNL-5054/RI (1978).

Table X.1-1 Design parameters and specifications of FER (FY 1984)

Fusion power	(MW)	385
Operating mode		Quasi-steady (RF current ramp up)
Burn time	(Sec)	2000
Neutron fluence	(MWY/m^2)	0.3
Neutron wall loading	(MW/m^2)	0.88
Plasma major/minor radius	(m)	5.2/1.12
Plasma elongation		1.5
Average ion temperature	(keV)	10
Average ion density	(m^{-3})	1.32×10^{20}
Plasma current	(MA)	5.7
Beta	(%)	4.56
Toroidal field on axis	(T)	5.3
Plasma heating		
Refernce		RF power (ICRF / LHRF)
Alternative		Neutral beam injection
Injected power	(MW)	60
Impurity control		Single null poloidal divertor
Blanket		Shielding type
TF coils		
Number of coils		12
Superconductor		$(NbTi)_3Sn$ (Max. 12T)
PF coils		
Superconductor		Nb_3Sn/NbTi (Max. 10T)

Table X.2-1 Major deisgn parameters of INTOR

Plasma major radius (m)	5.0
Plasma minor radius (m)	1.2
Plasma elongation	1.6
Plasma volume (m^3)	227
Axial toroidal field (T)	5.5
Plasma current (MA)	8.0
Average ion temperature (keV)	10
Average ion density ($10^{20}/m^3$)	1.4
Energy confinement time (s)	1.4
Average beta (%)	4.9
Q value	ignition
Peak fusion power (MW)	585
RF heating power (MW)	
ICRF (85 MHz)	50
ECRF (140 GHz)	10
Burn time (s)	150
Duty cycle (%)/Availability (%)	67/25
Neutron wall load (MW/m^2)	1.3
Toroidal magnetic field coil	superconducting
Poloidal magnetic field coil	superconducting
Divertor	yes
Tritium consumption (kg/year)	6.1
Initial tritium inventory (kg)	3.1-4.6
Tritium breeding ratio	0.65

Table X.3-1 Major Design Parameters of Blankets and Primary Coolant Operating Conditions

Blanket type	Water Cooling	Indiect He Cooling	Direct He Cooling
Thermal power/gross electric power (MW)	3900/1340	3790/1790	3580/1690
Neutron wall loading (MW/m^2)	3.3	3.3	3.3
Coolant (pressure: MPa)	H_2O (15.5)	He (9)	He (9)
Inlet/Outlet temperatures (°C)	280/320	400/700	400/700
Coolant flow direction	Poloidal	Poloidal	Toroidal
Number of primary cooling loops	4	7	7
Heat flux on the first wall(MW/m^2)	0.9	0.9	0.9
Nuclear heating in the first wall (MW/m^3)	43	27	27
Structural material	Ti-modified SS	Molybdenum alloy	Molybdenum alloy
Breeder/neutron multiplier	Li_2O/Be	Li_2O/Be	α-$LiAlO_2$/Be
Breeder configuration	Outside tube	Outside tube	Inside dube
Temperature range of breeder(°C)	450 ~ 950	400 ~ 950	400 ~ 730
Tritium recovery	He purge stream	He purge stream	He coolant
Net/local breeding ratio (^6Li enricled: %)	1.05/1.20(30)	1.21/1.37(30)	1.08/1.24(95)

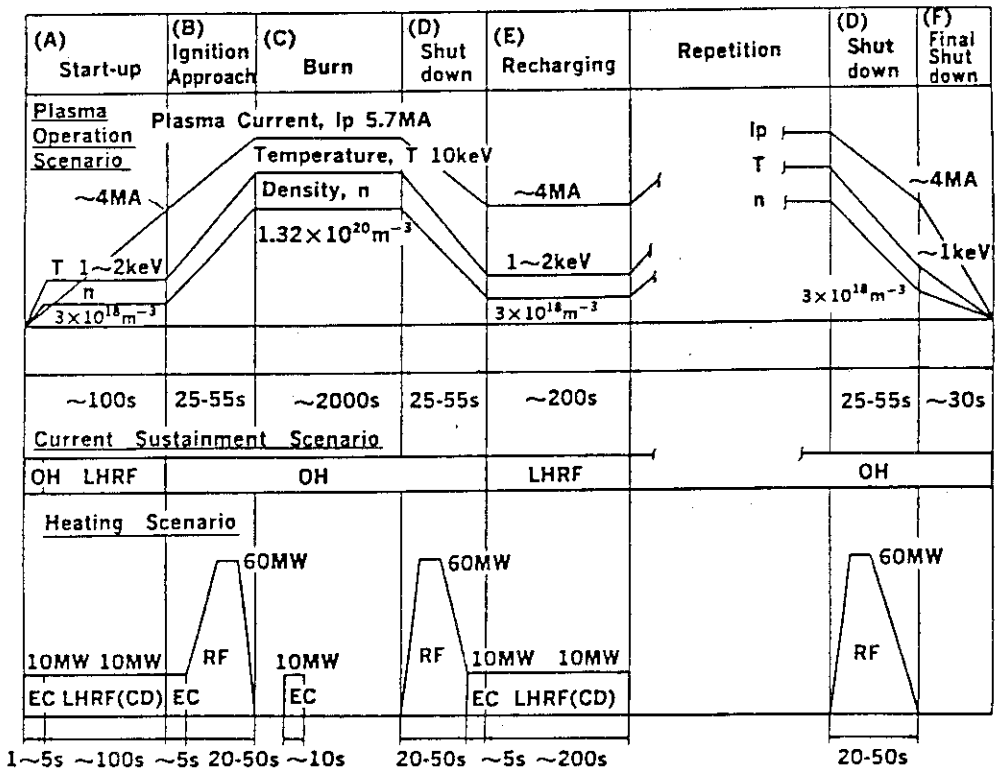

Fig. X.1-1 Schematic drawing of FER quasi-steady operation.

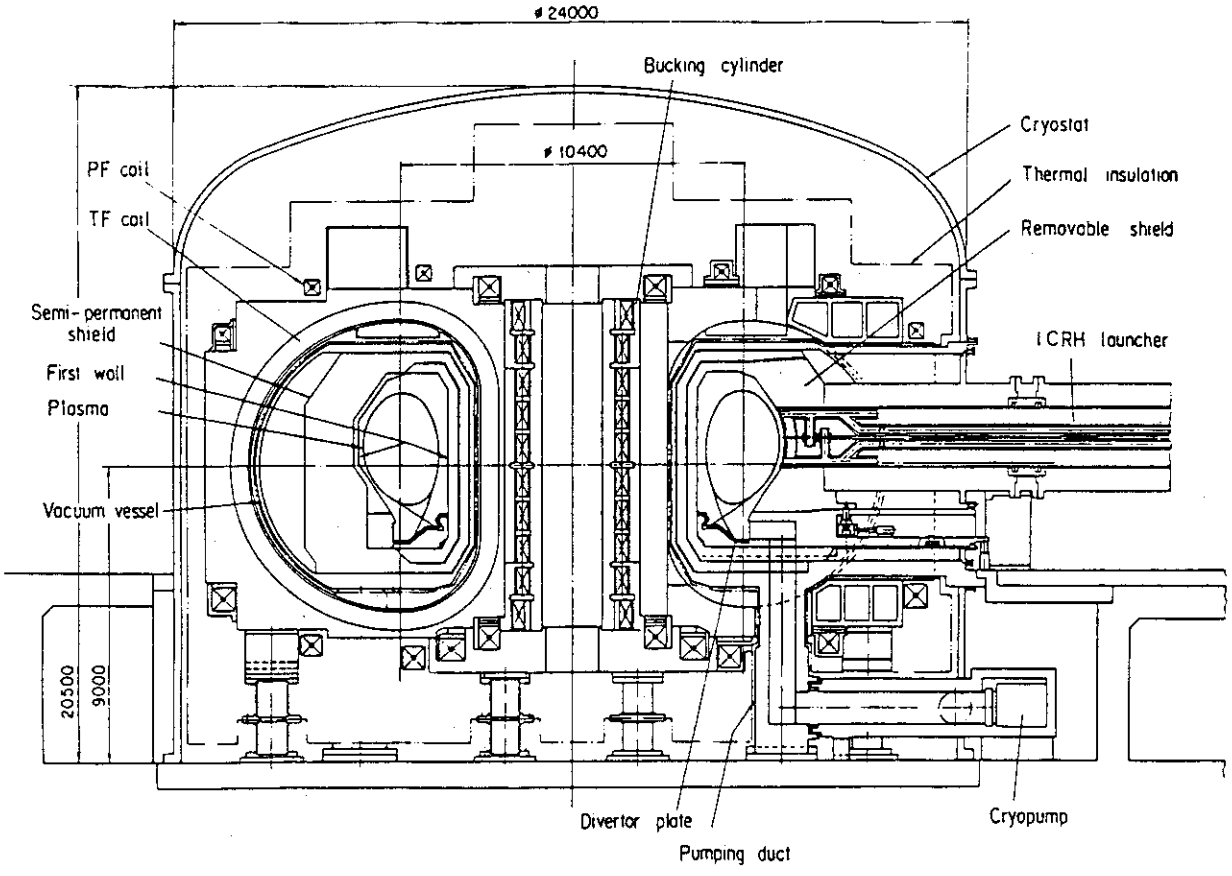

Fig. X.1-2 Elevation view of FER.

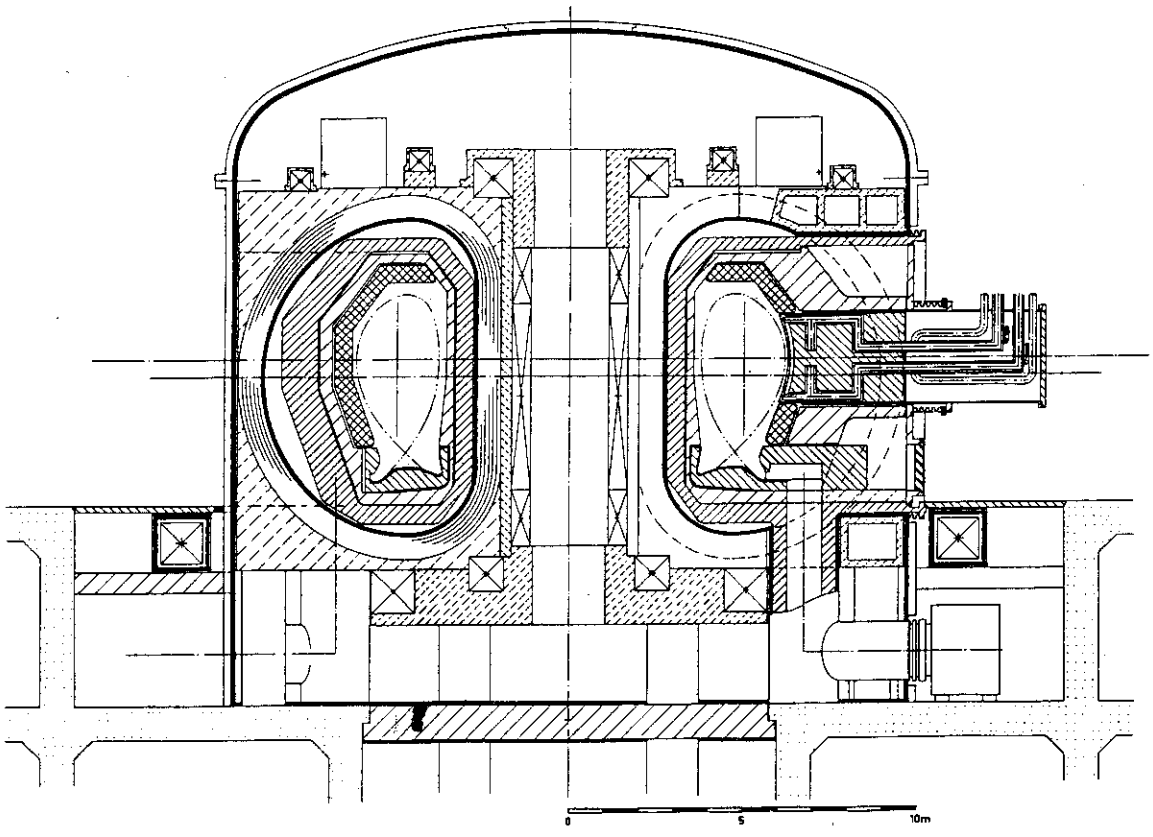

Fig. X.2-1 INTOR elevation view.

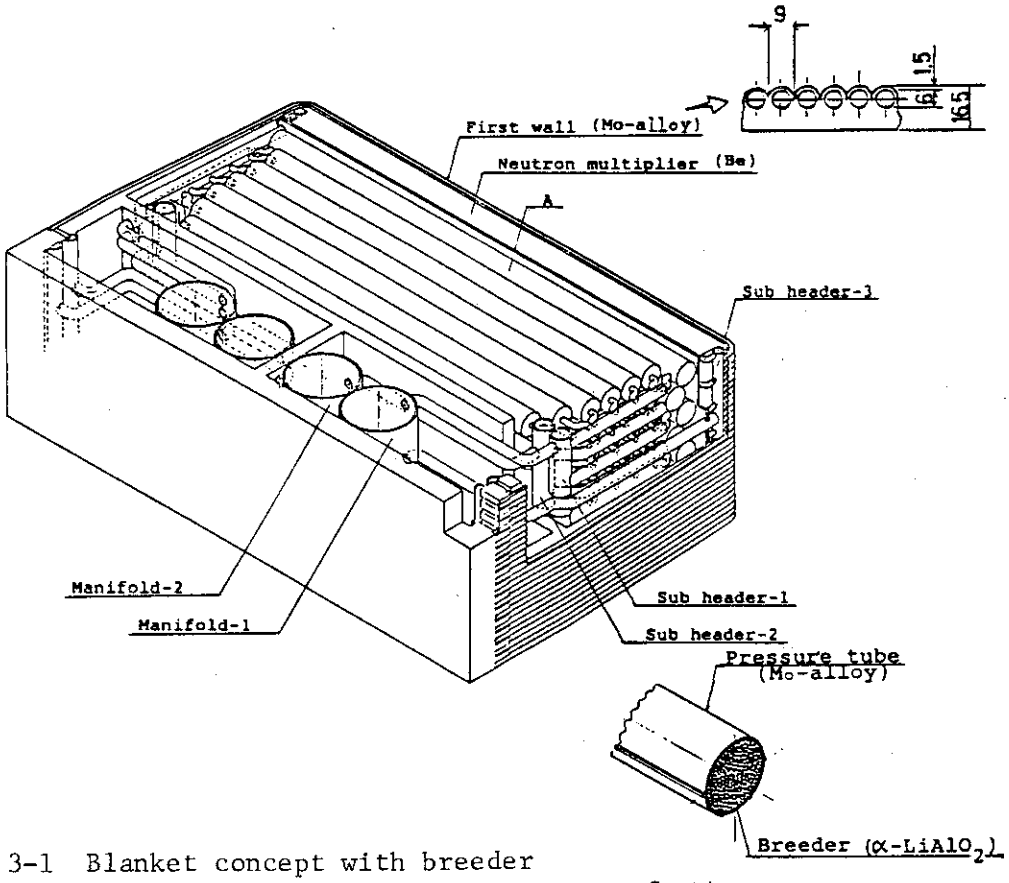

Fig. X.3-1 Blanket concept with breeder inside coolant tube.

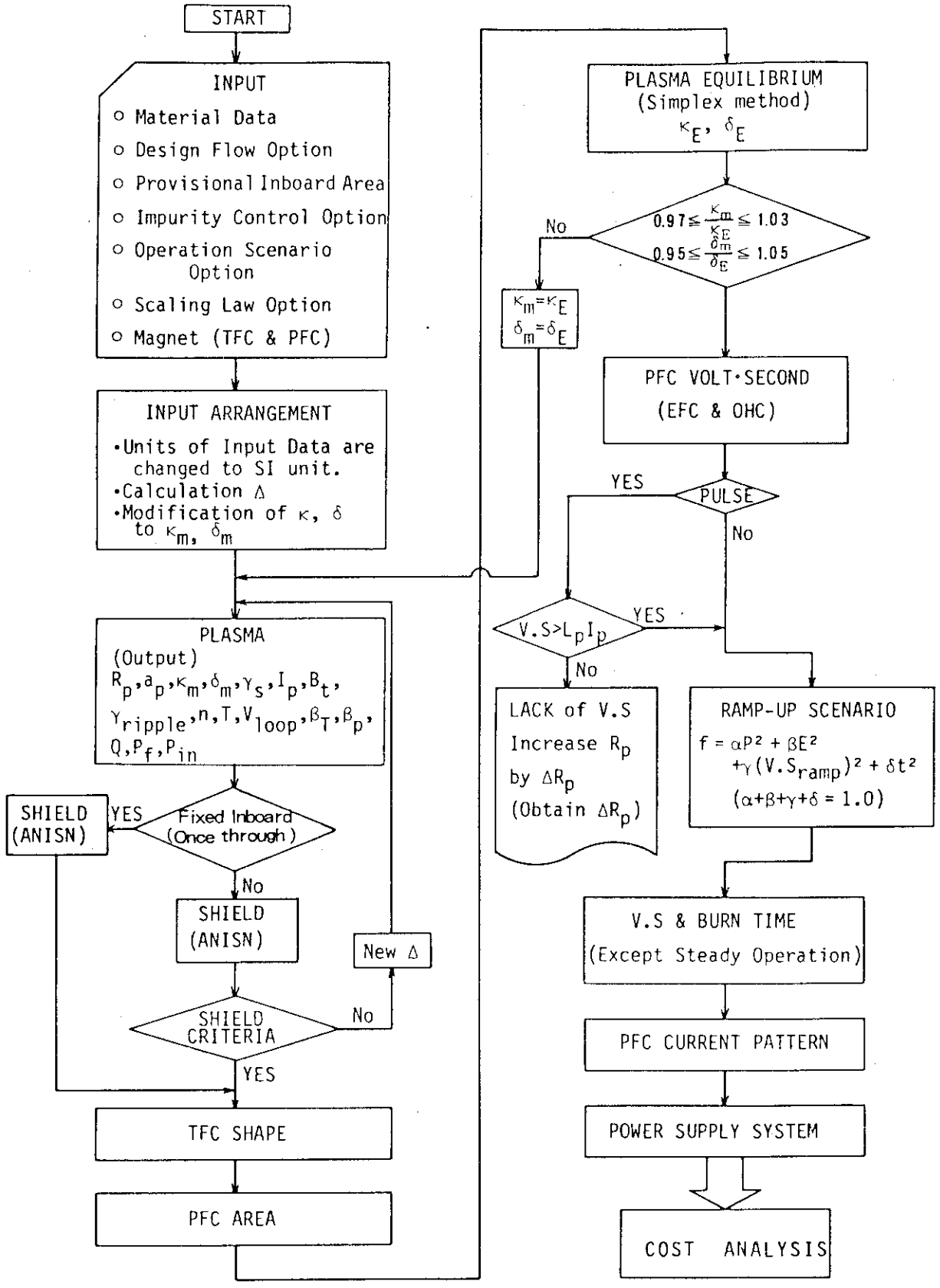

Fig. X.3-2 Flow Diagram of TORDEC.

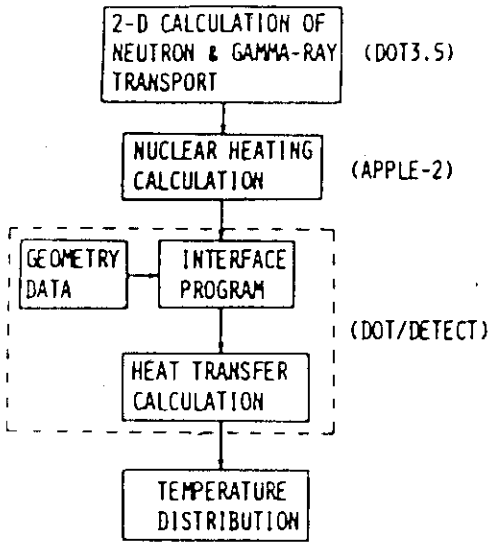

Fig. X.3-3 Calculation System Flow.

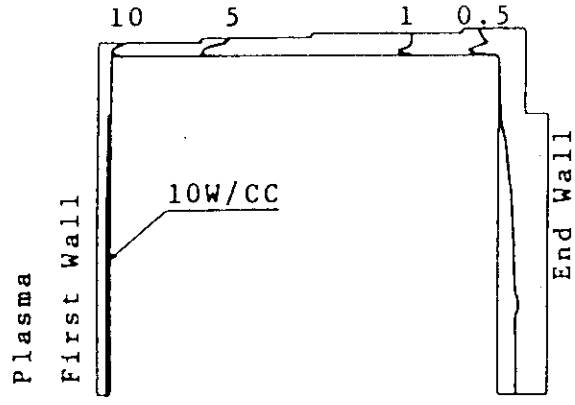

Fig. X.3-4 Nuclear Heating Rate in First Wall and Blanket Vessel.

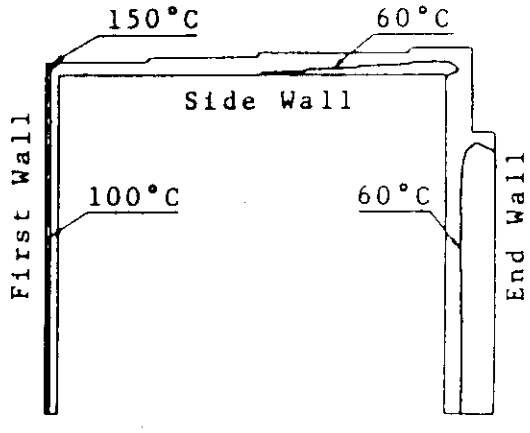

Fig. 3.5 Temperature Distribution.

APPENDIX

A.1 Publication List

A.1.1 List of JAERI-M reports

1) Nagamine, K.[**5] : "Review of Studies of the Muon Catalyzed Nuclear Fusion", JAERI-M 84-115 (June 1984) (in Japanese).
2) Tsunematsu T., Naraoka K.[*1], Adachi M.[*1], Takeda T.: "Software Information Sorting Code PLUTO-R", JAERI-M 84-185 (October 1984) (in Japanese).
3) Tanaka, Y.[*1]: "Numerical Analyses of Disruptive Instabilities in a Tokamak Plasma", JAERI-M 84-225 (December 1984) (in Japanese).
4) Ohtsuka H., Yamamoto S., Maeno M., Matsuda T., Miura Y., Suzuki, N., Mori M., Shoji T.: "Observation of ICRF Wave during Neutral Beam Injection in Tokamaks", JAERI-M 84-150 (Sep. 1984)
5) Yanagisawa I.[*3], Yamauchi T.: "Relative Sensitivity Calibration of Thomson Scattering Device using LED Lamp", JAERI-M 84-186 (Sep. 1984) (in Japanese).
6) Yamauchi T., Yanagisawa I.[*3], Odajima K., Matsumoto H., Shoji T., Mori M., Tamai H., Ogawa T., Matsuda T., Suzuki N., Yamamoto S., Kasai S., Miura Y., Ogawa H., Matoba T., Maeno K., Yamamoto T., Hoshino K., Uesugi Y., Kawashima H., Kawakami T., Ochiai K., Ohta K.[*11], Kimura H.: "Electron Temperature and Density Profiles in JFT-2M Tokamak Plasma Measured by Thomson Scattering Apparatus", JAERI-M 84-206 (Oct. 1984) (in Japanese).
7) Matoba T., Kawashima H., Tamai H.: "Evaluation Method of Electron Velocity Distribution from Soft-X Ray Radiation Spectrum in Lower Hybrid Current Drive Experiment", JAERI-M 84-207 (Oct. 1984) (in Japanese)
8) Kawashima H., Matoba T., Ogawa T., Kawakami T.: "The Development of 128 ch Fast Multi-Channel Pulse Height Analyzer for a Tokamak Plasma", JAERI-M 85-005 (Jan. 1985) (in Japanese).
9) Matsuoka M., Kawai M., Komata M., Kitamura S., Matsuda S., Mizuhashi K., Nagamura H.[*2], Ohara Y., Watanabe K.: "100 kV, 80 A, 10 s Power Supply for a Neutral Beam Injector Using a Series of Gate Turn Off Thyristors as a Regulator Switch Valve", JAERI-M 84-112 (June 1984).
10) Okumura Y., Ohara Y., Horiike H., Shibata T.: "Development of H Ion Source for Neutral Beam Injector", JAERI-M 84-98 (May 1984).

11) Saigusa M., Kimura H., Fujii T., Ikeda Y., Samamoto K., Imai T., Uehara K., Nagashima T.: "Coupling Characteristic of Ridge Waveguide Launcher for ICRF Heating". JAERI-M 84-187 (Oct. 1, 1984) (in Japanese).

12) Ikeda Y., Kimura H., Fujii T., Saigusa M., Imai T., Sakamoto K., Uehara K., Nagashima T.: "Calculation of Coupling of Loop Antenna for ICRF Heating on JT-60", JAERI-M 84-191, 1984 (Oct. 1984) (in Japanese).

13) Kurasawa T., Yoshida H., Watanabe H., Takeshita H., Miyauchi T., Matsui T.: "In-pile Test of Tritium Recovery from Lithium Oxide --- Tritium Release Behabior ---", JAERI-M 84-087 (May 1984) (in Japanese)

14) Kinoshita M.: "Studies on Cryogenic Distillation Columns for Hydrogen Isotope Separation", JAERI-M 84-016 (Aug. 1984).

15) Tanaka K.: "Conceptual Design of Fusion Experimental Reactor", Chapter 17, JAERI-M 84-212 (Jan. 1985) (in Japanese).

16) Kikuchi M., Ninomiya H., Yoshino R., Yoshida H., Hosogane N., Tsuji S., Seki S.: "Matrix Transfer Function Analysis of JT-60 Plasma Equilibrium Control", JAERI-M 84-095 (April 1984) (in Japanese).

17) Aoyagi T., Ninomiya H., Tani K.: "PFD User Exit Routine for Graphic Terminal D-SCAN", JAERI-M 84-240 (Dec. 1984) (in Japanese).

18) Tani K., Osame T.*32, Kihara K.*38: "Handling Manual of Computer Aided Tracing System "CATS" (Version I)", JAERI-M 84-078 (March 1984) (in Japanese).

19) Yoshino R., Ninomiya H., Seki S., Kikuchi M., Yoshida H., Hosogane N., Tsuji S.: "Noninteracting Control of JT-60 Equilibrium Configuration", JAERI-M 84-120 (June 1984) (in Japanese).

20) Yokomizo H.: "Positional Stability Experimental and Analysis of Elongated plasmas in Doublet III JAERI-M 84-077

21) Ando T., Watanabe Y.*38: "Wall Heat Flux from Radiative Heat Sources Distributed in a Toroidal Spaces", JAERI-M 84-072 (April, 1984) (in Japanese).

22) Horie T., Kawasaki K., Hiratsuka H., Yasumitsu N.*10: "Throughput Calibration Methods for Piezoelectric Valves of JT-60", JAERI-M 84-097 (May, 1984) (in Japanese).

23) Nakamura H., Shimizu M., Makino T.[**9], Kunitomo T.[**9]: "Measurement of Emissivities on JT-60 First Wall Materials", JAERI-M 85-007 (February, 1985) (in Japanese).

24) Nakamura H., Ogiwara N., Inagawa K.[*21], Takahashi Y.[*21], Itoh A[*21]: "R & D Results of Carbon and Titanium Carbide Coating on Molybdenum Substrate for JT-60 First Wall", JAERI-M 85-022 (March, 1985) (in Japanese).

25) Horie T., Kawasaki K., Noshiroya S.[*21], Koizumi J.[*33]: "Development of the Vacuum System Pressure Response Analysis Code PRAC", JAERI-M 85-033 (March, 1985) (in Japanese).

26) Robert. A. Ellis., Yokomizo H.: "Design of Viewing Damps for JT-60 Thomson Scattering System", JAERI-M 24-157

27) Seki Y., Ikeda Y., Oyama Y., Nakamura T., Maekawa H., Kawasaki H.[*25], Yamada K.[*25]: "Monte Carlo Calculation of the characteristics of Source Neutrons and Irradiation Field of the FNS Rotating Target," JAERI-M 84-193 (1984).

28) Fusion Reactor System Laboratory: "Conceptual Design of Fusion Experimental Reactor (FER), FY1983 Report" (in Japanese), JAERI-M 84-212 (1985).

29) Tone T., Iida H., Sugihara M., Kasahara T.[*4], Nishikawa M.[*3], Kitamura K.[*2], Kuroda T.[*18]: "Japanese Contributions to the Japan-US Workshop on FER/ETR Design", JAERI-M 84-107 (1984).

A.1.2 Papers published in JOURNALs

1) Itoh K., Fukuyama A.[**3], Itoh S.-I.[**1]: Numerical calculation of ICRF waves in tokamak plasma", Comput. Phys. Commun. 32 (1984) 35.

2) Tsunematsu T.: "MHD instabilities and stability control", Kakuyugo Kenkyu 51 (1984) no.2, p.101 (in Japanese).

3) Seki S., Takizuka T., Saitoh S.[**4], Ninomiya H., Yoshida H., Tani K., Azumi M., Andoh T., Sugihara M., Shimomura Y.: "Experimental program of JT-60 and its relevance with the research of divertors", J. Nucl. Mater. 121 (1984) 422.

4) Itoh K., Itoh S.-I[**1], Tuda T., Tokuda S.: "Kinetic theory of global n=1 instabilities in toroidal plasmas", J. Phys. Soc. Japan 53 (1984) 1759.

5) Itoh K., Itoh S.-I.[**1], Fukuyama A.[**3]: "Study of ICRF wave propagation and absorption in INTOR tokamak plasma", Jpn. J.

Appl. Phys. 23 (1984) 889.

6) Takeda T., Tsunematsu T., Tokuda S.: "Integrative graphic subroutine package ARGUS-V4", Comput. Phys. Commun. 34 (1984) 15.

7) Itoh S.-I[**1], Itoh K., Fukuyama A.[**3]: "Beam-driven ICRF instability and associated nonclassical transport in tokamak", Plasma Phys. Controlled Fusion 26 (1984) 1311.

8) Takizuka T., Itoh K., Azumi M.: "Motion of electrons due to high-mode-number electrostatic waves in tokamak", Comments Plasma Phys. Controlled Fusion 9 (1984) 1.

9) Takizuka T., Tani K., Azumi M., Shimizu K.: "Particle simulation of divertor plasma", J. Nucl. Mater. 128 & 129 (1984) 104.

10) Miura Y., Matsumoto H., Kimura H., Odajima K., Mori M., Matsuda T., Takeuchi T., Hoshino K., Kasai S., Kawashima H., Kawakami T., Konoshima S., Maeno M., Matoba T., Ohasa K., Ohtsuka H., Ogawa T., Sengoku S., Shoji T., Sugie T., Suzuki N., Uesugi Y., Yamauchi T., Yamamoto S., Yamamoto T.: "Analysis of Charge Exchanged Spectra during ICRF Heating in the JFT-2 Tokamak", Nucl. Fusion 2 (1984) 211.

11) Matsumoto H., Kimura H., Odajima K., Hoshino K., Kasai S., Kawakami T., Kawashima H., Konoshima S., Maeno M., Matoba T., Matsuda T., Miura Y., Nakamura H., Mori M., Ohasa K., Ohtsuka H., Ogawa T., Sengoku S., Shoji T., Sugie T., Suzuki N., Takeuchi H., Uesugi Y., Yamauchi T., Yamamoto S., Yamamoto T.: "Power Balance Analysis of ICRF Heating Experiments in JFT-2 Tokamak", Nucl. Fusion 24 (1984) 238.

12) Maeno M., Sengoku S., Yamamoto S., Suzuki N., Yamauchi T., Kawashima H., Miura Y.: "Diamagnetic Measurement of JFT-2 Plasma Heated by Neutral Beam Injection", Jpn. J. Appl. Phys. 23 (1984) 1236.

13) Yamauchi T., Yanagisawa I., Kawashima H.: "Thomson Scattering Device Calibrated by Rotational Raman Scattering of Hydrogen", Jpn. J. Appl. Phys. 23 (1984) 1435.

14) Matsuzaki Y., Tani T.: J × B gun pre-ionization equipment in JFT-2 tokamak", Jpn. J. Appl. Phys. 23 (1984) 941.

15) Horiike H., Akiba M., Araki M., Dairaku M., Itoh T., Kawai M., Kuriyama M., Kitamura S., Matsuda S., Matsuoka M., Mizuhashi K., Oguchi Y.[*19], Ohara Y., Ohga T., Okumura Y., Shibanuma K., Shibata T., Shigematsu H.[*8], Shirakata H., Sugawara T.[*4], Tanaka S., Watanabe K.: "100 keV TEST of the Prototype Neutral Beam Injector for JT-60", Rev. Sci. Instrum. 55(3) (1984) 332.

16) Tanaka S., Akiba M., Mizuhashi K., Ohara Y., Okumura Y.: "Characteristics of a Hollow Cathode Ion Source with Magnetic Multipole Semicylindrical Arc Chamber", Rev. Sci. Instrum. 55 (1984) 1069.

17) Matsuoka M., Matsuda S., Nagamura H.*2, Watanabe K.: "A New Method of protecting Ion Source Accelerators Against Deterioration Due to Source Breakdown", IEEE Trans. on Plasma Science PS-12, No.3 (1984) 231.

18) Tanaka S., Ohara Y.: "Tapered Tungsten Filament for a Long Life Cathode", Rev. Sci. Instrum. 55 (1984) 1625.

19) Shibata T., Matsuoka M., Ohara Y., Okumura Y., Shibanuma K.: "Hydrogen Gas Reemission from Beam Target Bombarded by Intense Neutral Hydrogen Baam of 75-100 keV, 1.4 MW at the Prototype JT-60 Injector", J. Nuclear Materials 128 & 129 (1984) 713.

20) Okumura Y., Akiba M., Mizuhashi K.: "Application of a Solid-state Image Sensor to Optical Profile Measurement of Intense Neutral Beams", Rev. Sci. Instrum. 55, 12 (1984) 2027.

21) Minami M.*8, Morita H.*8, Nagashima T., Imai T.: "Study on Development of Doublet Metal-Sealed Valve for JT-60 Radio Frequency Heating System", Fusion Technology 6 (1984) 516.

22) Yamada R., Sone K.: "Chemical Erosion Yield of Graphite Simultaneously Bombarded with Energetic Protons and Thermal Atomic Hydrogens", J. Nucl. Mater. 120 (1984) 119.

23) Sone K., Murakami K.: "The Effect of Wall Materials on Hydrogen Recycling in JT-60", J. Nucl. Mater. 121 (1984) 254.

24) Saidoh M.: "Sputter-Erosion of Molybdenum and Tungsten Due to Ion Bombardnent at Temperatures Up to 1500°C", J. Nucl. Mater. 128&129 (1984) 540.

25) Sone K.: "The Effect of Chemical Sputtering on Hydrogen Recycling at TiC Wall Surface", J. Nucl. Mater. 128 & 129 (1984) 589.

26) Yamada R., Bay H.L.*, Schweer B.**32: "Measurements of Neutral Ti Atoms from TiC and Ti Targets Sputtered by Low Energy H^+ and Ar^+ Ions Using Laser Induced Fluorescence", J. Nucl. Mater. 128&129 (1984) 583.

27) Fujimori N.*37, Yashiki T.*37, Abe T., Murakami Y., Mizoguchi Y.*4, Itou Y.*4: "Preparation and characterization of TiC-coated molybdenum wall for the JT-60 reactor", Thin Solid Films 118 (1984) 5.

28) Inagawa K.[*21], Watanabe K.[*21], Tanaka I.[*21], Itoh A.[*21], Abe T., Murakami Y., Mizoguchi T.[*4], Itou Y.[*4]: "Titanium carbide coating on Inconel 625 liner for JT-60 by HCD-ARE", J. Nucl. Mater. 128&129 (1984) 925.

29) Murakami Y., Shimomura Y., Abe T., Obara K.: "A new helium sniffing device for locating very fine leaks", J. Vac. Sci. Technol. A2 (1984) 1589.

30) Inagawa K.[*21], Abe T., Hiroki S., Obara K., Murakami Y.: "Preformance test of twisted-wired titanium evaporators for in-situ TiC deposition", JAERI-M 84-105.

31) Murakami Y.: "Surface science and technology relating to tokamak fusion devices", Hyomen-Kagaku 5 (1984) 96,

32) Kudo H., Okuno K.: "Thermal Release of Tritim from Neutron-Irradiated Li_2C_2", Radiochemica Acta. 33 (1984) 223.

33) Yamanishi T., Kinoshita M.: "Preliminary Experimental Study for Cryogenic Distillation Column with a Small Inner Diameter (II)", J. Nucl. Sci. & Technol., 21 (1984) 853.

34) Kudo H., Okuno K., Sugai H., Nagame Y.: "Chemical States in Solid Lithium Compounds Irradiated with Neutrons", J. Radioanal. Nucl. Chem., Letters 93 (1985) 55.

35) Takamatsu T., Hashimoto I., Kinoshita M.: "A New Simulation Procedure for Multistage Water/Hydrogen Exchange Column for Heavy Water Enrichment", J. Chem. Eng. Japan 17 (1984) 255.

36) Kinoshita M.: "Effects of Helium on Separation Characteristics of Cryogenic Distillation Column Cascade for Fusion Reactor", Fusion Technol. 6 (1984) 564.

37) Kinoshita M.: "An Efficient Simulation Procedure Especially Developed for Hydrogen Isotope Distillation Column", 6 (1984) 574.

38) Takamatsu T., Kinoshita M.: "A Simulation Procedure for Multicomponent Distillation Columns Incorporating Plate Efficiencies", J. Chem. Eng. Japan 17 (1985) 78.

39) Nagami M., Kasai M.[*3], Kitsunezaki A., Kobayashi T.[*4], Konoshima S., Matsuda T., Miya N., Ninomiya H., Sengoku S., Shimada M., Yokomizo H., Angel T.[*5], Armentrout C.[*5], Blau F.[*5], Bramson G.[*5], Brooks N.[*5], Chase R.[*5], Colleraine A.[*5], Fairbanks E.[*5], Fasolo J.[*5], Fisher R.[*5], Groebner R.[*5], Hino T.[*5], Hong R.[*5], Jahns G.[*5], Kamperschroer J.[*5], Kim J.[*5], Lieber A.[*5], Lohr J.[*5], McColl D.[*5], Rottler L.[*5], Seraydarian R.[*5], Silagi R.[*5], Smith J.[*5], Snider R.[*5], Taylor T.[*5], Tooker J.[*5], Vaslow D.[*5],

Wojtowicz S.[*5]: "Energy Confinement of Beam-Heated Divertor and Limiter Discharges in DOUBLET III"; Nucl. Fusion 24 (1984) 183

40) Sengoku S., Shimada M., Miya N., Kasai M.[*3], Aikawa H., Azumi M., Hoshino K., Kitsunezaki A., Kobayashi T.[*4], Konoshima S., Matsuda T., Nagami M., Ninomiya H., Nishikawa M.[*3], Tokutake T., Yamauchi T., Yokomizo H., Burrell K.H.[*5], Kahn C.L.[*5]: "Observation of Very Dense and Cold Divertor Plasma in the Beam-Heated DOUBLET III Tokamak with Single-Null Poloidal Divertor", Nucl. Fusion 24 (1984) 415.

41) Yokomizo H., Konoshima S., Aikawa H., Kasai M.[*3], Ninomiya H., Kobayashi T.[*4], Matsuda T., Miya N., Nagami M., Shimada M., Kitsunezaki A.: "Plasma Shapes for Achieving High Heating Efficiency during Neutral Beam Injection in Doublet III", Jpn. J. Appl. Phys 23 (1984) L316.

42) Kobayashi T., Shimada M., Sengoku S., Miya S., Kasai M., Aikawa H., Kitsunezaki A., Konoshima S., Matsuda T., Nagami M., Ninomiya H., Yokomizo H., Kahn C.L.[*5]: "Langmuir Probe Measurements in Beam-Heated Divertor Discharges in D-III", N. Nucl. Mater. 121 (1984) 17.

43) Nagami M. Kasai M.[*3], Kitsunezaki A., Kobayashi T.[*4], Konoshima S., Matsuda T., Miya N., Ninomiya H., Shimada M., Yokomizo H., Angel T.[*5], Armentrout C.[*5], Blau F.[*5], Bramson G.[*5], Brooks N.[*5], Chase R.[*5], Colleraine A.[*5], Fairbanks E.[*5], Fasolo J.[*5], Groebner R.[*5], Hino T.[*5], Hong R.[*5], Jahns G.[*5], Kamperschroer J.[*5], Kim J.[*5], Lieber A.[*5], Lohr J.[*5], McColl D.[*5], Rottler L.[*5], Seraydarian R.[*5], Silagi R.[*5], Smith J.[*5], Snider R.[*5], Taylor T.S.[*5], Tooker J.[*5], Vaslow D.[*5], Wojtowicz S.[*5]: "Production of High Temperature and High Density Plasmas by Controlling Edge Particle Recycling in D-III Divertor Equilibria", J. Nucl. Mater. 121 (1984) 114.

44) Miya N., Shimada M., Kasai M., Kobayashi T., Sengoku S., Aikawa H., Kameari A., Kitsunezaki A., Konoshima S., Matsuda T., Nagami M., Ninomiya H., Yokomizo H.: "Heat Load Reduction of the Divertor Plate by Remote Radiative Cooling in D-III Beam-Heated Divertor Discharges", J. Nucl. Mater. 121 (1984) 126.

45) Shimomura Y., Shimizu K., Hirayama T., Azumi M., Ninomiya H.: "JT-60 Program", J. Nucl. Mater. 128 & 129 (1984) 19.

46) Kahn C.[*5], Burrell K.H.[*5], Fairbanks E.[*5], Petrie T.[*5], Shimada M., Washizu M.[*2], Sengoku S.: "The Scaling of Edge Properties with

Main Plasma Parameters in Doublet III Discharges", J. Nucl. Mater. 128 & 129 (1984) 172.

47) Hirayama T., Takizuka T., Shimada M., Nagami M., Konoshima S., Abe M.*4, Kameari A.*3, Kitsunezaki A., Kodama K., Sengoku S., Washizhi M.*2, Yamamoto T. Burrell K.H.*5, Zawadski G.*5, Brooks N.*5, Groebner R.*5: "Trace Impurity Transport in DOUBLET III Beam Heated Plasma: Comparison of Numerical Simulations with Decay Time of Titanium Line Emission in L- and H-Mode Discharges", J. Nucl. Mater. 128 & 129 (1984) 271.

48) Shimada M., Washizu M., Sengoku S., Suzuki N., Nagami M., Konoshima S., Matoba T., Miya N., Kobayashi T., Kasai M., Kameari A., Abe M., Hirayama T., Kodama K., Yamamoto T., Kitsunezaki A., Kahn C.L.*5, Hsieh C.L.*5, Snider R.*5, Groebner R.*5, Brooks N.H.*5, Burrell K.H*5, GA Doublet III Groups: "Divertor Studies in High-Power Beam Heated Discharges in DOUBLET III", J. Nucl. Mater. 128 & 129 (1984) 340.

49) Nishikawa M.*3, Yokomizo H., Kitsunezaki A., JAERI Team, McKelvey T.E.*5, Taylor T.S.*5, Doll D.*5, Brook N.*5, Seraydarian R.*5: Graphite Limiter Damage due to Runway Electrons and Abrupt I_p Termination in DOUBLET III", J. Nucl. Mater. 128 & 129 (1984) 493.

50) Yokomizo H., Kasai M.*3, Aikawa H., Callis R.*5, Doll D.*5, Kitsunezaki A., Konoshima S., Matsuda T., Nagami M., Shimada M., Taylor T.*5: "Thermal Heat Load onto Primary Limiter for Three Plasma Configurations in DOUBLET III", J. Nucl. Mater. 128 & 129 (1984) 812.

51) Shimada M., JAERI Team: "Modelling of Dense and Cold Divertor Plasma in D-III", J. Nucl. Mater. 121 (1984) 184.

52) Seki S., Takizuka T., Saito S.*4, Ninomiya H., Yoshida H., Tani K., Azumi M., Ando T., Sugihara M., Shimomura Y.: "Experimental Program of JT-60 and its Relevance with the Research of Divertors", J. Nucl. Mater. 121 (1984) 422.

53) Takatsu H., Yamamoto M., Shimizu M., Suzuki K.*4, Sonobe T.*4, Hayashi Y.*27, Mizuno G.*27: "Experimental Evaluation of Torsional Fatigue Strength of Welded Bellows and Application to Design of Fusion Device", 21 (1984) 341.

54) Ando T., Ohta M., Sanokawa K.: "Present Status of Research and Development of Heat Transfer in Fusion Technology at JAERI", J. At. Energy Soc. Japan 26 (1984) 1020 (in Japanese).

55) Shimada R.: "Tokamak Plasma Equilibrium and Positional stability Analysis by Energy Function", Trans. IEE of Japan, 105-A (1985) 113, (in Japanese).

56) Seki Y., Yamauchi I.*34, Yamada K.*25, Kawasaki H.*25: "Radioactivation of Structural Material of the Superconducting Magnet for a Fusion Reactor", J. Fusion Energy, Vol. 3, 4 (1983) 241.

57) Seki Y., Kawasaki H.*25, Mori S.*18: "Radiation Shielding Considerations for the Repair and Maintenance of a Swimming Pool-Type Tokamak Reactor", Nucl. Eng. Design/Fusion, 1 (1984) 243.

58) Seki Y., Yamada K.*25, Kawasaki H.*25: "Evaluation of Decay Heat in Fusion Experimental Reactor", J. Nucl. Sci. Technol., 21 [10] (1982) 727.

59) Ogawa M., Minato A., Seki M.: "Preliminary Thermal Cycling Test of Tungsten-Copper Duplex Structure for Use as Divertor Plate"., J. Nucl. Sci. Technol., 21 [8] (1984) 642.

A.1.3 Papers published in Conference Proceedings

1) Itoh S.-I.**1, Itoh K., Fukuyama A.**3: "Beam-driven ICRF instability and nonclassical transport in tokamak", 1984 International Conf. on Plasma Phys., June 27 - July 3, Lausanne, P5-2, p.56.

2) Fukuyama A.**3, Itoh K., Itoh S.-I.**1: "Kinetic analysis of ICRF waves in tokamak", 1984 International Conf. on Plasma Phys., June 27 - July 3, Lausanne, P5-7, p.61.

3) Takizuka T., Tsunematsu T., Tokuda S., Azumi M., Kurita G., Watanabe M.*32, Takeda T.: "Equilibria of anisotropic pressure tokamak with high-energy alpha particles", 1984 International Conf. on Plasma Phys., June 27 - July 3, Lausanne, P9-5, p.111.

4) Azumi M., Takizuka T., Tsunematsu T., Kurita G., Tokuda S., Takeda T.: "Scaling of beta limit in a tokamak for infinite-n ballooning modes", 1984 International Conf. on Plasma Phys., June 27 - July 3, Lausanne, P16-5, p.200.

5) Tuda T., Tokuda S., Itoh K., Takizuka T.: "Nonlinear model equation of ballooning instability", 1984 International Conf. on Plasma Phys., June 27 - July 3, Lausanne, P16-7, p.202.

6) Azumi M., Shimizu K., Hirayama T., Takizuka T., Sugihara M., Saitoh S.*4, Tani K., Nakanishi M., Kimura H., Imai T., Shimomura Y.: "Performance analysis of JT-60 plasma with poloidal divertor",

Proc. 10th International Conf. on Plasma Phys. and Controlled Nuclear Fusion (London 1984), IAEA-CN-44/E-II-5-4.

7) Tuda T., Azumi M., Itoh K., Kurita G., Takeda T., Takizuka T., Tokuda S., Tsunematsu T., Adachi M.[*1], Tanaka Y.[*1], Watanabe M.[*32], Itoh S.-I.[**1]: "Accessible beta value of tokamaks", Proc. 10th International Conf. on Plasma Phys. and Controlled Nuclear Fusion (London 1984), IAEA-CN-44/E-III-4.

8) Itoh S.-I.[**1], Fukuyama A.[**3], Gotoh A.[**3], Itoh K.: "Propagation and coupling efficiency of ICRF waves in tokamaks", Proc. 10th International Conf. on Plasma Phys. and Controlled Nuclear Fusion (London 1984), IAEA-CN-44/F-III-4-1.

9) Kurita G., Azumi M., Tuda T., Tsunematsu T., Takizuka T., Tanaka Y.[*1], Takeda T.: "Bubble formation due to surface tearing mode", Proc. US-Japan Workshop Magnetic Reconnection December 10-13, 1984, Austine Texas, DOE/ET/53088-182, (IFSR 1982) p.325.

10) Odajima K., Matsumoto H., Kimura H., Tamamoto T., Hoshino K., Kasai S., Kawakami T., Kawashima H., Ogawa H., Ohta K.[*11], Ohtsuka H., Sengoku S., Shoji T., Suzuki N., Tamai H.[**29], Uesugi Y., Yamamoto S., Yamauchi T., Yanagisawa H., Katagiri M.[*40]: "Second Harmonic ICRF Heating Experiment in the JFT-2M Tokamak", 4th International Symposium on Heating in Toroidal Plasma (Rome, Italy, Mar. 1984)

11) Ogawa H., Odajima K., Ohtsuka H., Matsumoto H., Kimura H., Hoshino K., Kasai S., Kawakami T., Kawashima H., Maeno M., Matoba T., Matsuda T., Miura Y., Mori M., Ogawa T., Ohta K.[*11], Shoji T., Suzuki N., Tamai H., Uesugi Y., Yamamoto S., Yamamoto T., Yamauchi T., Yanagisawa T.[*3], Nakamura H., Katagiri M.[*40]: "Impurity Behavior during ICRF Heating in JFT-2M", 6th Int. Conf. on Plasma Surface Interactions in Controlled Fusion Devices, Nagoya, (May 1984).

12) Miura Y., Takeuchi H., Ohara Y., Konagai C.[*2], Kimura H.[*2]: "Application of Silicon Surface Barrier Detector for Fast Neutral Particles", 5th Topical Conf. on High Temperature Plasma Diagnostics, (APS-Meeting, Tahoe) (Sep. 1984).

13) Miura Y.: "Plasma Ion Temperature Measurements with Hydrogen Beam Scattering in JFT-2 Tokamak", Joint US-Japan Workshop on Local Plasma Potential and Magnetic Field Measurements, LLNL (Sep. 1984)

14) Mori M., Hasegawa K., Honda A., Hoshino K., Ishibori I., Kasai S., Kashimura T., Kashiwa Y., Kawakami T., Kawashima H., Kazawa M., Katagiri M., Kikuchi K., Kimura H., Koide Y., Kunieda T., Maeno M., Matoba T., Matsuda T., Matsumoto H., Matsuzaki Y., Muira Y., Nakamura H., Ochiai I.[**5], Odajima K., Ogawa H., Ogawa T., Ohta K.[*11], Ohtsuka H., Ohuchi K., Okano F., Shibata T., Shibuya T., Shiina T., Shoji T., Suzuki K., Suzuki N., Tamai H., Tsugi S., Uesugi Y., Yamamoto S., Yamamoto T., Yamauchi T., Yanagisawa I.[*3], Yokoyama K.: "High Power ICRF Heating Experiments in the JFT-2M Tokamak", 10th Int. Conf. on Plasma Physics and Controlled Nuclear Fusion Research, London (Sep. 1984).

15) Yamamoto S., Experiment Group, Operation and Engineering Group, Itoh K., Theory Group, Fukuyama A.[**3], Itoh S.-I.[**1]: "Plasma Heating by Multiple-Short-Pulse Neutral Beams", ibid.

16) Uesugi Y., Matoba T., JFT-2M Group: "Far Infrared Laser Interferometer in the JFT-2M Tokamak", 9th International Conference on Infrared and Millimeter Waves (Takarazuka, Japan, Oct. 1984).

17) Odajima K.: "ICRF Heating Result of the JFT-2M Tokamak", U.S.-Japan Workshop on RF Heating and Current Drive (Tokai, Japan, Oct. 1984).

18) Yamamoto T.: "LHD Results and Ongoing Current Drive Program of the JFT-2M Tokamak", ibid.

19) Tanaka S., Akiba M.: "Development of Long Life Filament Cathode for Ion Sources of Neutral Beam Injectors", Proc. 8th Symp. Ion Sources and Ion Assisted Technology (Tokyo, Japan, June, 1984)

20) Matsuoka M., Akiba M., Kawai M., Kitamura S., Matsuda S., Nagamura H.[*2], Ohara Y., Ohga T., Watanabe K.: "The JT-60 NBI Power Supply System", 13th Symp. Fusion Tech. Soft (Varese, Italy, September 1984)

21) Ohara Y., Akiba M., Araki M., Dairaku M., Horiike H., Itoh T., Kawai M., Kuriyama M., Kitamura S., Matsuda S., Matsuoka M., Mizuhashi K., Nagamura H.[*2], Ohga T., Ohuchi U., Okumura Y., Shibanuma K., Shibata T., Shigematsu H.[*8], Shirakata H., Sugawara T.[*4], Suzuki Y.[*9], Tanaka S., Terakado T.[*9], Usui K., Watanabe K.: "Construction of the JT-60 NBI System", ibid.

22) Tanaka S., Akiba M., Araki M., Dairaku M., Horiike H., Itoh T., Kawai M., Komata M., Kuriyama M., Kitamura S., Matsuda S.,

Matsuoka M., Mizuhashi K., Nagamura H.[*2], Ohga T., Ohuchi U., Ohara Y., Okumura Y., Shibanuma K., Shibata T., Shigematsu H.[*8], Shirakata H., Sugawara T.[*4], Watanabe K., Wells R.[**28]: "Performance of the Prototype JT-60 Injector Unit in the Presence of a Simulated Stray Magnetic Field", IEEE Inter. Conf. Plasma Science (St. Louis, USA, May, 1984)

23) Okumura Y., Akiba M., Horiike H., Itoh T., Kawai M., Kuriyama M., Matsuda S., Matsuoka M., Ohara Y., Shibata T., Shimizu M., Tanaka S., Tani K., Watanabe K.: "Development of High Performance Neutral Beam Injector at JAERI", IAEA 10th International Conference on Plasma Physics and Controlled Nuclear Fusion Research (London, England , Sep. 1984)

24) Shibata T., Horiike H., Inami H.[*19], Matsuda S., Ohara Y., Okumura Y., Tanaka S.: "H Production in Large Bucket Source at JAERI", IAEA Technical Committee Meeting on Negative Ion Beam Heating (Grenoble, French, Mar. 1985).

25) Miyake S.[*2], Ohno H.[*2], Ishihara H.[*2], Hosoi M.[*2], Okamoto T.[*2], Nagashima T., Uehara K., Imai T., Fujii T., Sakamoto K., Ikeda Y., Saigusa M.: "Development of 2 GHz, 1 MW klystron for Plasma Heating", 1984 IEEE Int. Elect. Device Meeting. (San Fransisco, U.S.A. 1984).

26) Okamoto T.[*2], Miyake S.[*2], Ohno H.[*2], Hosoi M.[*2], Ishihara H.[*2], Nagashima T., Uehara K., Imai T., Fujii T., Sakamoto K., Ikeda Y., Saigusa M.: "Super Power Klystron for Fusion Plasma Heating", Proc. of 19th Annual Symp. on Inter Microwave Power Institute. (Minneapolise, U.S.A.) 11.

27) Sone K.: "Surface Physics", IEA Mini Workshop on Plasma Materials Interactions (Tokyo, Dec. 1984).

28) Takahashi Y., Tada E., Okuno K., Tsuji H., Ando T., Hiyama T., Koizumi K., Nishi M., Nakahima H., Yoshida K., Kato T., Kawano K., Oshikiri M., Hattori Y., Takahashi R., Kamiya S., Shimamoto S.: "Experimental Results of JF-15 Forced-cooled Superconducting Test Loop", Tenth International Cryogenic Engineering Conference (Helsinki, Finland, July 1984).

29) Ando T., Hiyama T., Tsuji H., Takahashi Y., Nishi M., Tada E., Yoshida K., Okuno K., Koizumi K., Nakajima H., Kato T., Oshikiri M., Kawano K., Takahashi R., Hattori Y., Kamiya S., Yamaguchi T., Shimamoto S., Yasukochi K.: "Upgrading of the Cluster Test Facility and an Extended Test on the MTC-I", ibid.

30) Nakagawa S., Haraguchi K., Kamiya S., Iwata A., Yoshiwa M., Tada E., Kato T., Okuno K., Shimamoto S.: "Pressure Drop and Heat Transfer in Helium Two-phase Flow", ibid.

31) Shimamoto S.: "Status Report on the Japanese Large-coil-task Coil for Fusion Development", ibid.

32) Takahashi Y., Ando T., Hiyama T., Tsuji H., Tada E., Nishi M., Yoshida K., Okuno K., Nakajima H., Kato T., Kawano K., Oshikiri M., Hattori Y., Takahashi R., Kamiya S., Ohgane Y., Shimamoto S.: "Development of 12 T-10 kA Al-Stabilized Nb_3Sn conductor for TMC-II", 1984 Applied Superconductivity Conference (San Diego, USA, Sept. 1984).

33) Ando T., Takahashi Y., Nishi M., Tada E., Okuno K., Shimamoto S.: "Effect of the Thermal Barrier on the Stability of Cable-in-conduit Conductor", ibid.

34) Kato T., Tada E., Takahashi Y., Okuno K., Tsuji H., Ando T., Hiyama T., Koizumi K., Nakajima H., Takahashi O., Kawano K., Oshikiri M., Nishi M., Yoshida Y., Hattori Y., Takahashi R., Kamiya S., Shimamoto S.: "Cryogenic System Development and Helium Behavior Study for Forced-flow Superconducting Coils", ibid.

35) Shimamoto S.: "STTA/FER", US-Japan Workshop on Superconducting Magnet Requirements for Intermediate-scale, Long-pulse Tokamaks (Boston, USA, Sept. 1984).

36) Okuno K.: "Specified Parameters of STTA", ibid.

37) Koizumi K.: "Overview of STTA Coil System", ibid.

38) Shimamoto S.: "Cryogenic System of STTA", ibid.

39) Shimamoto S.: "11 T Generation in Cluster Test Facility", ibid.

40) Okuno K.: "Large Current Poloidal Conductor Experiment", ibid.

41) Koizumi K.: "Structure Material Development", ibid.

42) Shimamoto S.: "Cryogenic Technology Development", ibid.

43) Shimamoto S.: "JAERI Future Plans", ibid.

44) Shimamoto S.: "High Field Superconducting Coil Development Work for Fusion Machine at JAERI", Japan-US Workshop on High-field Superconducting Materials for Fusion (Tsukuba, Japan, Dec. 1984).

45) Takahashi Y., Ando T., Hiyama T., Tsuji H., Tada E., Nishi M., Yoshida K., Okuno K., Koizumi K., Nakajima H., Kawano K., Kato T., Oshikiri M., Hattori Y., Takahashi R., Kamiya S., Ohgane Y., Yamaguchi T., Shimamoto S.: "Design and R & D of a 12 T Forced Flow Coil (TMC-II) in the Cluster Test Program", ibid.

46) Ando T., Hiyama T., Tsuji H., Takahashi Y., Nishi M., Tada E., Yoshida K., Okuno K., Koizumi K., Nakajima H., Kato T., Oshikiri M., Kawano K., Takahashi R., Hattori Y., Kamiya S., Ohgane Y., Yamaguchi T., Shimamoto S.: "Test Results of a 60 sm-bore Nb_3Sn Coil (TMC-I) in the Cluster Test Program", ibid.

47) Konishi S., Ohno H., Yoshida H., Katsuta H., Naruse Y.: "Solid oxide Electrolysis Cell for Decomposition of Tritiated Water", Proceeding on World Hydrogen Energy Conference V, Toronto (1984).

48) Kudo H., Okuno K.: "Kinetics and Mechanism of Triitum Release from Neutron-Irradiated Li_2O", Proceeding on First International Conference on Fusion Reactor Materials (Tokyo, Japan, Dec. 1984).

49) Kurasawa T., Yoshida H., Takeshita H., Watanabe H.: "In-situ Tritium Recovery Experiment from Lithium Oxide under High Neutron Flux", Proceeding on First International Conference on Fusion Reactor Materials (Tokyo, Japan, Dec. 1984).

50) Yoshikawa M.: "Present Status of JT-60", Proceeding on First International Conference on Fusion Reactor Materials (Tokyo, Japan, Dec. 1984).

51) Yoshikawa M.: "JT-60 Final Construction and Initial Operation", 6th Topical Meeting on Technology of Fusion Energy (Mar. 1985).

52) Washizu M.[*2], Shimada M., Sengoku S., Kahn C.[*5], Petrie T.[*5], Fairbanks E.[*5], Kobayashi T.[*4], Miya N., Kasai M.[*3], Abe M.[*4], Kameari A.[*4], Kitsunezaki A., Konoshima S., Nagami M., Szuki N., Yamamoto T., GA D-III Group: "Observation of Edge Plasma Properties in Doublet III by a Combination of Langumuir Probes, Thermocouples and IR-Camera", Proc. IEEE International Conf. on Plasma Science, St. Louis (1984).

53) Kitsunezaki A., Abe M.[*4], Hirayama T., Hoshino K., Kameari A.[*3], Kodama K., Koike T., Konoshima S., Matoba T., Nagami M., Ohga T., Oikawa A., Sengoku S., Suzuki N., Takahashi S., Takizuka T., Tani K., Yamamoto T., Washizu M.[*2], Angel T.[*5], Armentrout C.[*5], Baur J.[*5], Blau F.[*5], Bramson G.[*5], Brooks N.[*5], Burrell K.[*5], Callis R.[*5], Chase R.[*5], Colleraine A.[*5], Fairbanks E.[*5], Fasolo J.[*5], Groebner R.[*5], Hohg R.[*5], Hsieh C.[*5], Jahns G.[*5], Kahn C.[*5], Kellman A.[*5], Kim J.[*5], LEE P.[*5], Lieber A.[*5], Lohr J.[*5], McColl D.[*5], Petersen P.[*5], Petrie T.[*5], Phillips J.[*5], Rottler L.[*5], Scoville T.[*5], Seraydarian R.[*5], Silagi R.[*5], Sleaford B.[*5], Smith J.[*5], Snider R.[*5], Stav R.[*5], Stockdale R.[*5], Strait E.[*5], Tooker J.[*5], Wojtowicz S.[*5]: "High-Pressure Plasma

with High-Power NBI Heating in DOUBLET III", Proc. 10th IAEA Conf. on Plasma physics and Controlled Nuclear Fusion Research Vol. I P.57 1984.

54) Shimada M., Washizu M.[*2], Kameari A.[*3], Sengoku S., Itoh K., Nagami M., Konoshima S., Abe M.[*4], Ohga T., Koike T., Kitsunezaki A., Kahn C.[*5], Fairbanks E.[*5], GA DOUBLET-III Groups[*5], Itoh S.-I.[**1]: "Divertor and Edge Plasma Characteristics of Beam-Heated D-III Discharges", ibid. 281

55) Sengoku S., Abe M.[*3], Hoshino K., Itoh K., Kameari A.[*3], Kitsunezaki T., Koike T., Konoshima S., Matoba T., Nagami M., Oikawa A., Ohga T., Shimada M., Suzuki N., Takahashi H., Tani K., Washizu M.[**2], Foster C.A.[*14], Milora S.L.[*14], Attenberger S.E.[*14], Stockdale R.[*5], Itoh S.-I.[*1], Wojtowicz S.[*5], Angel T.[*5], Burrell K.[*5], Blau F.[*5], Callis R.W.[*5], Colleraine A.F.[*5], Fairbanks E.[*5], Fasolo J.[*5], Groebner R.[*5], Hong R.-M.[*5], Kim J.[*5], McColl D.B.[*5], Peterson P.I.[*5], Phillips J.C.[*5], Schissel R.[*5], Scoville T.J.[*5], Silagi R.[*5], Sleaford B.[*5], Smith J.[*5], Stan R.[*5], Tooker J.F.[*5], GA DOUBLET III Group[*5]: "Improvement of Beam-Heated Limiter Discharges by Continuous Pellet Fuelling in DOUBLET III", ibid. 405

56) Yoshino R., Kikuchi H., Ninomiya H., Yoshida H., Tsuji S., Hosogane N., Seki S.: "Control of Divertor Configuration in JT-60", 13th Symp. on Fusion Technology, (Varese, Italy, 1984).

57) Effthimion P.C.[**19], Bretz N.[**19], Bell M.[**19], Bitter M.[**19], Blanchard W.R.[**19], Boody F.[**19], Boyd D.[**34], Bush C.[**14], Cecchi J.L.[**19], Coonrod J.[**19], Davis S.[**19], Dimock D.[**19], Dylla H.F.[**19], von Goeler S.[**19], Goldston R.J.[**19], Grek B.[**19], Grove D.J.[**19], Hawryluk R.J.[**19], Hendel H.[**19], Hill K.W.[**19], Hulse R.[**19], Johnson D.[**19], Johnson L.C.[**19], Kaita R.[**19], Kaye S.[**19], Kikuchi M., Kilpatrick S.[**19], Kiraly J.[*34], Knize R.[**19], LaMarche P.[**19], Little R.[**19], Manos D.[**19], McCarthy M.[**19], McCune D.[**19], McGuire K.[**19], Meade D.M.[**19], Medley S.S.[**19], Mikkelsen D.R.[**19], Mueller D.[**19], Murakami M.[**14], Nieschmidt E.B.[*39], Owens D.K.[**19], Ramsey A.T.[**19], Roquemore A.L.[**19], Sauthoff N.R.[**19], Schivell J.[**19], Schwob J.-L.[**19], SCOTT S.[**14], Sesnic S.[**19], Sinnis J.[**19], Stauffer F.[**33], Strachan J.D.[**19], Suckewer S.[**19], Tait G.D.[**19], Tavernier M.[**35], Taylor G.[**19], Tenney F.[**19], Towner H.[**19], Ulrickson M.[**19], Wong K.-L.[**19], Wouters A.[**19], Yamada H.[**9], Young K.M.[**19], Zarnstorff M.[**19]: "Confinement Studies of Ohmically Heated Plasmas in TFTR", 10th

Int. Conf. on Plasma Physics and Controlled Nuclear Fusion Research (London, Sep. 1984). 29

58) Eubank H.P.[**19], Bell J.[**14], Bell M.G.[**19], Bitter M.[**19], Blanchard W.R.[**19], Boody F.[**19], Boyd D.[**33], Bretz N.[**19], Bush C.[**14], Cecchi J.L.[**19], Coonrod J.[**19], Davis S.L.[**19], Dimock D.[**19], Dylla H.F.[**19], Efthimion P.C.[**19], England A.C.[**14], Fonck R.[**19], Fredrickson E.[**19], Furth H.P.[**19], Grisham L.R.[**19], von Goeler S.[**19], Goldston R.J.[**19], Grek B.[**19], Grove D.J.[**19], Hawryluk R.J.[**19], Hendel H.[*41], Hill K.W.[**19], Hillis D.L.[**14], Hulse R.[**19], Johnson D.[*19], Johnson L.C.[**19], LaMarche P.[**19], Kaita R.[**19], Kamperschroer J.[**19], Kaye S.M.[**19], Kikuchi M., Kilpatrick S.[**19], Kiraly J.[**19], Knize R.[**19], Kugel H.[**19], Little R.[**19], Manos D.[**19], McCarthy M.[**19], McCann R.T.[**19], McCune D.C.[**19], McGuire K.[**19], Meade D.M.[**19], Medley S.S.[**19], Mikkelsen D.R.[**19], Mueller D.[**19], Murakami M.[**14], Nieschmidt E.[**31], Owens D.K.[**19], Pare V.[**19], Prichard B.[**19], Ramsey A.[**19], Rasmussen D.[**19], Redi M.H.[**19], Roquemore A.L.[**19], Rutherford P.H.[**19], Sauthoff N.R.[**19], Schivell J.[**19], Schwob J.-L.[**37], Scott S.[**33], Sesnic S.[**19], Sinnis J.[**19], Stauffer F.[**14], Strachan J.D.[**19], Suckweer S.[**19], Tait G.[**19], Tavernier M.[**35], Taylor G.[**19], Tenney F.[**19], Towner H.H.[**19], Ulrickson M.[**19], Wieland R.[**19], Williams M.[**19], Wong K.-L.[**19], Wouters A.[**19], Yamada H.[**5], Young K.M.[**19], Zarnstorff M.C.[**19]: "Neutral-Beam Heating in TFTR-Projections and Initial Results", ibid. 303

59) Tait G.[**19], Bell J.[**14], Bell M.G.[**19], Bitter M.[**19], Blanchard W.R.[**19], Boody F.[**19], Boyd D.[**33], Bretz N.[**19], Bush C.[**14], Cecchi J.L.[**19], Cohen S.[**19], Coonrod J.[**19], Davis S.L.[**19], Dimock D.[**19], Dylla H.F.[**19], Efthimion P.C.[**19], England A.C.[**14], Fonck R.[**19], Fredrickson E.[**19], Furth H.P.[**19], von Goeler S.[**19], Goldston R.J.[**19], Grek B.[**19], Grove D.J.[**19], Hawryluk R.J.[**19], Hendel H.[**41], Hill K.W.[**19], Hillis D.[**14], Hulse R.[**19], Johnson D.[**19], Johnson L.C.[**19], Kaita R.[**19], Kaye S.M.[**19], Kikuchi M., Kilpatrick S.[**19], Kiraly J.[**19], Knize R.[**19], LaMarche P.[**19], Little R.[**19], Manos D.[**19], McCarthy M.[**19], McCune D.C.[**19], McGuire K.[**19], Meade D.M.[**19], Medley S.S.[**19], Mikkelsen D.R.[**19], Mueller D.[**19], Murakami M.[**14], Nieschmidt E.[**36], Owens D.K.[**19], Pare V.K.[**14], Ramsey A.[**19], Rasmussen D.[**14], Redi M.[**19], Roquemore A.L.[**19], Sauthoff N.R.[**19], Schivell J.[**19], Schwob J.-L.[**37], Scott S.[**14], Sesnic S.[**19], Sinnis J.[**19], Stauffer F.[**33], Stangeby P.[**19], Strachan J.D.[**19],

Suckewer S.[**19], Tavernier M.[**35], Taylor G.[**35], Tenney F.[**19], Timberlake J.[**19], Towner H.H.[**19], Ulrickson M.[**19], Wong K.-L.[**19], Wouters A.[**19], Yamada H.[**5], Young K.M.[**19], Zarnstorff M.C.[**19]: "Adiabatic Toroidal Compression and Free-Expansion Experiments in TFTR", ibid 141.

60) Ando T., Ohkubo M., Nakao K., Ohta M., Takizawa T.[*4], Kiuchi T.[*4], Kamiya H.[*4], Hoashi R.[*4], Sasajima H.[*4], Teruyama K.[*4], Kohda T.[*4], Itoh Y.[*4]: "Design and Fabrication of JT-60 Magnetic Limiter Cois", 13th Symposium on Fusion Technology (Varese, Italy, September, 1984).

61) Ogiwara N., Arai T., Shimizu M., Takizawa T.[*4], Kimijima F.[*21]: "JT-60 Torus Vacuum Pumping System", ibid.

62) Takatsu H., Yamamoto M., Shimizu M., Suzuki K.[*4], Sonobe T.[*4], Hayashi Y.[*27], Mizuno G.[*27]: "Type Test of Welded Bellows for Ports of JT-60 Vacuum Vessel", ibid.

63) Shimada R., Shirahama H., Ishigaki Y.: "Control Method for Coil Currents of Hybrid Poloidal Field Coil System in a Tokamak Reactor", Proc. 13th Symposium on Fusion Technology (Varese, 1984).

64) Shimada R., Aoyagi T., Matsukawa M., Miya N., Arakawa K., Ieta Y., Igarashi J.: "Test of JT-60 Poloidal Field Coil Power Supply using Dummy Coil", ibid.

65) Kimura T., Takahashi M., Hosogane N., Anno K., Kondo I.: "Design and Test of Plasma Monitor System for JT-60 Control", 13th Symposium on Fusion Technology at Varese (September, 1984).

66) Kurihara K., Kimura K., Yonekawa I., Kondo I.: "System Design for JT-60 Computer Aided Production of Preprogrammed Wave from", 13th Symposium on Fusion Technology at Varese (September, 1984).

67) Kondo I., Kimura T., Yonekawa I., Kurihara K.: "Construction and Test of ZENKEI, the Central Control System of JT-60", 13th Symposium on Fusion Technology at Varese (September, 1984).

68) Fukuda T., Nagashima A.: "Multichannel CH_3OH/2mm waves Interferometer for electron density measurement in JT-60", 9th International Conference on IR & MM waves Digest P.258-259.

69) Sukegawa O.[*16], Hoshi K.[*16], Isobe K.[*16], Fukuda T., Nagashima A.: "A Highly Reliable Twin FIR Laser System", 9th International Conference on IR & MM waves Digest P260-261.

70) Aoki S.[*16], Kondo H.[*16], Shiratama K.[*16], Kunitsugu M.[*16], Fukuda T., Nagashima A.: "Application of a FIR Interferometer Large Tokamak

Devices", 9th International Conference on IR & MM Waves Digest P.262-261.

71) Inoue A.*16, Senba S.*16, Horiguchi Y.*16, Kajiura S.*4, Fukuda T., Nagashima A.: "Design and Performance of Wave Guides for JT-60 2 mm Interferometer", 9th International Conference on IR&MM Waves Digest P.264-265.

72) Sukegawa O.*16, Hoshi K.*16, Isobe K.*16, Fukuda T., Nagashima A.: "A Stable Low Noise CW CH_3OH Laser", 9th International Conference on IR & MM Waves Digest P.396-397.

73) Sato M., Nagashima A., Maeda H., Suzuki Y., Muramatsu T.*16, Miyamoto K.*16, Satake K.*16, Inoue A.*16, Hata K.*16: "Calibration of Fourier Transform Spectrometer", 9th International Conference on IR & MM Waves Digest P.417-418.

74) Tone T., Fujisawa N., Seki Y., Iida H., Iida H., Tachikawa k., Sugihara M., Minato A., Nishio S., Seki M., Shimada R., Iijima T., Yoshikawa M., Tomabechi K.: "Conceptual Design of the Fusion Experimental Reactor (FER) Based on an Advanced Scenario of Plasma Operation and Control", 10th Int. Conf. on Plasma Physics and Controlled Nuclear Fusion Research, London, 12 - 19 September 1984, IAEA-CN-44/H-I-2.

A.1.4. List of other reports

1) Kerner W.**27, Lerbinger K.**27, Gruber R.** , Tsunematsu T.: "Normal mode analysis for linear resistive magnetohydrodynamics", IPP 6/235 (October, 1984).

2) Itoh K., Itoh S.-I.**1, Cross-field transport in plasma disruption", HIFT-109 (February 1985).

A.2.2 List of scientific staff and officers during FY 1984

Fusion Research Center

ISO Yasuhiko (Director General)
TOMABECHI Ken (Director)
INOUE Kenji (General Manager)

(A) Department of Thermonuclear Fusion Research

OBATA Yukio (Director)
TANAKA Masatoshi (Deputy Director)
TSUDA Nobuyoshi (Administrative Manager)

Plasma Theory Laboratory

TAKEDA Tatsuoki (Principal Scientist, General Manager)
ADACHI Masao*1
AZUMI Masafumi (Senior Scientist)
ITOH Kimitaka
KURITA Gen-Ichi
MIZUNO Nobuo**6 (Scholarship Fellow)
TAKIZUKA Tomonori
TANAKA Yukio*1
TOKUDA Shinji
TSUNEMATSU Toshihide (Senior Scientist)
TUDA Takashi (Senior Scientist)
WATANABE Masami*32

Experimental Plasma Physics Laboratory

TANAKA Yuji (General Manager)
HOSHINO Katsumichi
KASAI Satoshi (Senior Scientist)
KAWAKAMI Tomohide
KAWASHIMA Hisato
MAENO Masaki (Senior Scientist)
MATOBA Tohru (Senior Scientist)
MATSUDA Toshiaki
MIURA Yukitoshi

MORI Masahiro
OCHIAI Isao**5 (Scholarship Fellow)
ODAJIMA Kazuo (Senior Scientist)
OGAWA Hiroaki
OGAWA Toshihide
OTA Kanji*11
SENGOKU Seio
SHOJI Teruaki
SUZUKI Norio (Senior Scientist)
TAMAI Hiroshi
UESUGI Yoshihiko
YANAGISAWA Ichiro*3
YAMAMOTO Shin (Senior Scientist)
YAMAMOTO Takumi
YAMAUCHI Toshihiko

Facility Operation and Engineering Division

SUZUKI Kihachiro (General Manager)
HASEGAWA Kōichi
HONDA Atsushi
ISHIBORI Ikuo
KASHIMURA Takanori
KASHIWA Yoshitoshi
KAZAWA Minoru
KIKUCHI Kazuo
MATSUZAKI Yoshimi
OKANO Fuminori
OHUCHI Katsuji
SHIBATA Takatoshi
SHIBUYA Toshihiro
SHIINA Tomio
TANI Takashi
YOKOYAMA Kenji

Plasma Heating Laboratory I

MATSUDA Shinzaburo (General Manager)
AKIBA Masato
DAIRAKU Masayuki
HORIIKE Hiroshi
ITHO Takao
KOMATA Masao
MATSUOKA Mamoru
MIZUHASHI Kiyoshi
OHARA Yoshihiro
OKUMURA Yoshikazu
SHIBANUMA Kiyoshi
SHIBATA Takemasa (Senior Scientist)
SUZUKI Yoshimi*9
TANAKA Shigeru
TERAKADO Takuya*9
WATANABE Kazuhiro

Plasma Heating Laboratory II

NAGASHIMA Takashi (General Maneger)
FUJII Tuneyuki
HIRASHIMA Teruhisa*2
HARA Mitsuru*16
IIDA Kazuhiro*9
IMAI Tsuyoshi
KATO Tsuguo*16
SAGAWA Junki*4
SAIGUSA Mikio
SAKAMOTO Keishi
SAWAHATA Masayuki

Plasma Engineering Laboratory

MURAKAMI Yoshio (General Manager)
ABE Tetsuya (Senior Scientist)
HIROKI Seiji
NAKAMURA Kazuyuki
OBARA Kenjiro

OHTSUKA Hideo
SAIDOH Masahiro (Senior Scientist)
SONE Kazuho (Senior Scientist)
TAKEMORI Makoto**5 (Scholarship Fellow)
YAMADA Rayji

Superconducting Magnet Laboratory

SHIMAMOTO Susumu (General Manager)
ANDO Toshinari
HATTORI Yasuhide*11
HIYAMA Tadao
KATO Takeshi
KAMIYA Shoji*18
KAWANO Katumi
KOIZUMI Koichi
NAKAJIMA Hideo
NISHI Masataka
OHGANE Yasuo*38
OKUNO Kiyoshi
OSHIKIRI Masayuki
TADA Eisuke
TAKAHASHI Ryukichi*4
TAKAHASHI Yoshikazu
TSUJI Hiroshi
YOSHIDA Kiyoshi

Tritium Engineering Laboratory

NARUSE Yuji (General Manager)
AISAWA Takeshi*8
HIRATA Shingo*18
HONMA Takashi
KINOSHITA Masahiro
KONISHI Sataoshi
MATSUDA Yuji
MUNEMOTO Iwao*10
OKUNO Kenji
TANAKA Kichizo (Senoir Scientist)

SUZUKI Takumi
YAMADA Masayuki
YAMANISHI Toshihiko
YOSHIDA Hiroshi (Senior Scientist)

(B) Division of Large Tokamak Development

YOSHIKAWA Masaji (Director)
IIJIMA Tsutomu (Deputy Director)
SAWADA Yoshio
SAKO Jun (Principal Scientist)
SAITO Ryota
ITOH Hiroshi

Large Tokamak Adminstration System

NARUI Masao (Administrative Manager)

JT-60 Program Office

TAMURA Sanae (General Manager)
KISHIMOTO Hiroshi (Deputy General Manager)

* Planning and Coordination Group

AIKAWA Hiroshi (Senior Scientist)
MIYA Naoyuki
OIKAWA Akira
OZEKI Takahisa
SUZUKI Kunihiro

* Experimental Planning Group

HAYASHI Kazuo*12
HOSOGANE Nobuyuki
KIKUCHI Mitsuru
KOIDE Yoshihiko
KONOSHIMA Shigeru
NAGAMI Masayuki
NIIKURA Satsuo*11
NINOMIYA Hiromasa
SEKI Shogo (Senior Scientist)

SHIMOMURA Yasuo (Principal Scientist)
TSUJI Shunji
USHIGUSA Kenkichi (Scholarship Fellow)
YAMADA Kimio*4
YOSHIDA Hidetoshi
YOSHINO Ryuji

* Plasma Analysis Group
HIRAYAMA Toshio
SHIRAI Hiroshi
SHIMIZU Katsuhiro
SHINTANI Kiyomori*31
TANI Keiji

* Doublet-III Experiment Group
SHIMADA Michiya

* Operation Planning Group
KITSUNEZAKI Akio (Senior Scientist)
KODAMA Kozo
KOIKE Tsuneyuki
SEIMIYA Munetaka
TAKEDA Takashi
TOKUTAKE Toshikuni

JT-60 Project Office I
OHTA Mitsuru (General Manager)
AKINO Noboru
ANDO Toshiro
ARAI Takashi
HARA Yasuhiro
HIRATSUKA Hajime
INOUE Hiromi
ISAKA Masayoshi
KANEKO Makoto
KAWASAKI Kozo
KURODA Takeshi

NAKAMURA Hiroo
NAKAO Keizo
NISHIYAMA Takeji*4
NOSHIROYA Syoji*21
OGIWARA Norio
OHKUBO Minoru (Senior Scientist)
OTSU Kazuyoshi
SERIZAWA Yasunori
SHIMIZU Masatsugu (Senior Scientist)
SHIMIZU Tohru
SUNAOSHI Hidenori
TAKATSU Hideyuki
TANAKA Takejiro
TOMIYAMA Yoshimi
TOYOSHIMA Noboru
URAKAWA Hiroshi
YAMAMOTO Masahiro
YANAI Munetoshi

JT-60 Project Office II

TAMURA Sanae (General Manager)
KONDO Ikuo (Dupaty General Manager)

* Power supply Group

AOYAGI Tetsuo
ARAKAWA Kiyotsugu
ICHIGE Hisashi
IKEDA Yukiharu
MATSUKAWA Makoto
MATSUKAWA Tatsuya
MIYA Naoyuki
MIZUNO Makoto
OHMORI Ken-ichiro
SHIINA Minoru
SHIMADA Ryuichi (Senior Scientist)
TAKAHASHI Shunji
TANAKA Emi

TERAKADO Tsunehisa
TSUNEOKA Masaki
UJIIE Keiichi
YAGYU Jun-ichi

* Control Group
AKASAKA Hiromi
ANNO Katsuto
ISAJI Nobuaki*39
ITOH Yasuhiro*39
KAWAMATA Yoichi
KIMURA Toyoaki
KURIHARA Kenichi
MIYACHI Kengo
MUTOH Mitsugu
SAKATA Shinya
TAKAHASHI Minoru
TOSUKA Toshiyuki
YONEKAWA Izuru

JT-60 Project Office III
SUZUKI Yasuo (General Manager)
AKAOKA Nobuo
FUKUDA Takeshi
HARUE Morihiko*1
IIDA Yukio
KITAHARA Katsumi
KUBO Hirotaka
MAEDA Hikosuke (Senior Scientist)
NAGASHIMA Akira
NAKAMURA Yukiharu
NEYATANI Yuzuru
NISHITANI Takeo
NOMATA Hideyuki
OHASA Kazumi
OHSATO Yukio*24
OHSHIMA Takayuki

SATO Masayasu
SHIHO Makoto (Senior Scientist)
SHITOMI Morimasa
SUGIE Tatsuo
TAHIRA Shigeo
TAKAHASHI Toranosuke
TAKAYASU Toshio
TAKEUCHI Hiroshi (Senior Scientist)
TOBITA Kenji
TSUGITA Tomonori
URAMOTO Yasuyuki
YAMASHITA Osamu
YOKOMIZO Hideaki
YOKOUCHI Shigeru*23

JT-60 Project Office IV

SHIRAKATA Hirofumi (General Manager)

* NBI Group

ARAKI Masanori
EBISAWA Noboru
INAMI Hiroshi*9
KANAI Takeo*2
KAWAI Kikito
KITAMURA Shigeru
KURIYAMA Masaaki (Senior Scientist)
OHGA Tokumichi
OHUCHI Yutaka
SHIGEMATSU Hirotsugu*8
SUGAWARA Tadayoshi*4
USUI Katsutomi

* RF group

HONDA Masao
IKEDA Yoshitaka
KIHARA Yoshihiko*10
KIMURA Haruyuki
KIYONO Kimihiro

SEKI Masami
SUGANUMA Kazuaki
SUZUKI Norio
UEHARA Kazuya (Senior Scientist)
YOKOKURA Kenji

JT-60 Operation Division

KUNIEDA Shunsuke (General Manager)
FURUKAWA Hiroshi
HIRUTA Kazuharu
HOSODA Ryujiro
IMAHASHI Koichi
ISHIHARA Masaru
NAGAYA Susumu
OHMORI Shunzo
SUZUKI Sadaaki

Fusion Reactor System Laboratory

IIJIMA Tsutomu (General Manager)
FUJISAWA Noboru (Principal Scientist)
HITOKI Shigehisa*11
IIDA Hiromasa (Senior Scientist)
KITAMURA Kazunori*2
KURODA Hideo
MINATO Akio*18
MIZOGUCHI Tadanori*4
MORI Seiji*18
NISHIO Satoshi
OKAZAKI Takashi*4
SEKI Yasushi (Senior Scientist)
SUGIHARA Masayoshi
TONE Tatsuzo (Principal Scientist)
TACHIKAWA Katsuhiro
TACHIKAWA Nobuo*2
TSUJIMURA Seiichi*8
YAMAMOTO Takashi*6
YAMANAKA Toshiyuki*8

**1 Hiroshima University
**2 Nagoya University
**3 Okayama University
**4 Tohoku University
**5 The University of Tokyo
**6 Nihon University
**7 Osaka University
**8 Tokyo Institute of Technology
**9 Kyoto University
**10 National Research Institute for Metals
**11 National Laboratory for High Energy Physics
**12 Power Reactor and Nuclear Fuel Development
**13 Confédération Suisse, Ecole Polytechnique Fédérale de Lausanne
**14 Oak Ridge National Laboratory
**15 Culham Laboratory
**16 FB-National Magnetic Laboratory
**17 Argonne National Laboratory
**18 University of Wisconsin
**19 Princeton Plasma Physics Laboratory
**20 Max-Planck Institute für Plasmaphysik
**21 Centre d'Etude Nucléaires, Fontenay-aux-Rose
**22 Bell Laboratories
**23 JET Joint Undertaking
**24 Institute für Angewandte Physik II, Universitäte Heidelberg
**25 Academia Sinica, Peking, The Peoples Republic of China
**26 The Institute of Fundamental Technological Research, Warsaw/Poland
**27 Institut für Plasmaphysik (Garching)
**28 Lawrence Berkely Laboratory, Univ. of California
**29 Tsukuba University
**30 Toho University
**31 Los Alamas National Laboratory
**32 FKA-IPP, Jülich
**33 University of Maryland
**34 Institute of Isotopes of the Hungarian Academy of Science
**35 Institut Curie, Université de Paris
**36 Idaho National Engineering Laboratory
**37 Hebrew University of Jernsalem

*1 Fujitsu Ltd.
*2 Toshiba Corp.
*3 Mitsubishi Atomic Power Industry Inc.
*4 Hitachi Ltd.
*5 GA Technologies Inc.
*6 Fuji Electric Co., Ltd.
*7 Kaihatsu Denki Co., Ltd.
*8 Mitsubishi Heavy Indu., Ltd.
*9 Nuclear Engineering Co., Ltd.
*10 Sumitomo Heavy Ind., Ltd.
*11 Mitsubishi Electric Co., Ltd.
*12 Japan Steel Works Ltd.
*13 Nippon Atomic Industry Group
*14 Kobe Steel Ltd.
*15 Saginomiya Johnson Controls Co., Ltd.
*16 Nippon Electric Co., Ltd.
*17 Hitachi Cable Co.
*18 Kawasaki Heavy Ind., Ltd.
*19 Nissin Electric Co., Ltd.
*20 Touyo Information System Co., Ltd.
*21 ULVAC Co.
*22 Nippon Kogaku Co., Ltd.
*23 Osaka Vacuum Ltd.
*24 Nissei Sangyo Co., Ltd.
*25 Century Research Center Co.
*26 Yokokawa Electric Works Ltd.
*27 Irie Koken Co., Ltd.
*28 Ishikawajima-Harima Heavy Ind. Co., Ltd.
*29 Kishikawa Special Valve Co., Ltd.
*30 Mitsui Engineering & Shipbuilding Co.
*31 Japan Information Service Ltd.
*32 Nuclear Data Corporation
*33 Nuclear Energy Data Center
*34 Nippon Steel Co.
*35 Hazama-Gumi, Ltd.
*36 Kanazawa Computor Service
*37 Sumitomo Electric Ind. Ltd.

*38 Nihon Software Kaihatsu Inc.

*39 IBS DATA Center Corporation

*40 Denki Kogyo Ltd.

*41 RCA David Darnoff Research Center

A.2 Personnel of the Center

A.2.1 Number of the Staff of the Departments

	FY1982	FY1983	FY1984
Regular staff	220	250	275*1
Staff on loan	30	31	34*2
Guest scientist	3	3	2*3
Scholarship fellow	1	2	5

*1 Including scientists, technicians and secretaries

*2 From industry

*3 From University of Tokyo and Kogakuin University

A.3 Budget of the Center

	FY 1982*1	FY 1983*1	FY 1984*1
JT-60 Construction*2	28,936	26,020	28,346
Research & Development*3	3,117	3,348	3,058
Japan-US Cooperation	3,042	1,436	1,672
Site Construction	5,633	7,771	1,199

(unit : Million ¥)

*1 From April to March

*2 Including cashing of the financial obligation in each FY

*3 Excluding fusion-related R&D in other divisions than the Center